EUROPEAN COMMISSION

Community Research

SEVENTH FRAMEWORK PROGRAMME

CARBOWASTE

Treatment and Disposal of Irradiated Graphite and Other Carbonaceous Waste

Grant Agreement Number: FP7-211333

Technical Report (T-4.2.1-a)

Investigations on High Temperature Thermal Treatments of Virgin AVR Graphite

Author(s): **Corrado Rizzato**

Forschungszentrum Juelich

Reporting period: 01/03/2011 – 30/06/2012

Date of issue of this report : 30/03/2013

Start date of project : **01/04/2008** Duration : **48 Months**

Project co-funded by the European Commission under the Seventh Framework Programme (2007 to 2011) of the European Atomic Energy Community (EURATOM) for nuclear research and training activities		
Dissemination Level		
PU	Public	
RE	Restricted to the partners of the CARBOWASTE project	
CO	Confidential, only for specific distribution list defined on this document	**X**

Distribution list

Person and organisation name and/or group	Comments
WP3 & WP4 Partners	
Coordinator	
European Commission	

CARBOWASTE		
Work package: 4 **Task: :** 4.2	**CARBOWASTE document no:** CARBOWASTE-1303-D-4.2.1-a (e.g. May 2008 as date of issue: 0805)	**Document type:** D=Deliverable
Issued by: FZJ **Internal no.:** CW1303-D-4.2.1-a		**Document status:** Final

Document title

Investigation on High Temperature Thermal Treatments of Virgin AVR Graphite

Executive summary

The present deliverable aims to reporting on:

- Measurements of gaseous emissions from virgin massive graphite samples during thermal treatment
- Evaluation of the effects of high temperature thermal treatments under inert gases on AVR graphite
- Pre- and post-treatment characterization via XPS, SEM, SIMS
- Parallelisms among irradiated and un-irradiated (virgin) graphite and previous thermal treatments
- Analysis of the different radionuclide precursors (e.g. coming from manufacture and storage)

Revisions

Rev.	Date	Short description	Author	Internal Review	Task Leader	WP Leader
00	30/03/2013	Issue	Rizzato, FZJ	Von Lensa, FZJ	Vulpius, FZJ	Vulpius, FZJ

TO MY BELOVED PARENTS
GIANNI AND LUISA

Index

Introduction **1**

The Carbowaste Project **4**

1. AVR Reactor **6**

1.1 Reactor Category 6

1.2 Concept 6

1.3 Structure 7

1.4 Fuel 11

1.5 Major Problems and Accidents 12

1.6 The Dismantling Plan of the AVR 14

2. Graphite: Overview on Structure, Properties and Nuclear Applications **19**

2.1 Graphite: Structure and General Properties 19

2.2 Nuclear Applications 23

3. Manufacture of Nuclear Graphite **23**

3.1 Raw Materials 25

3.1.1 Petroleum Coke 25

3.1.2 Coal Tar Pitch 26

3.2 The General Manufacture Process 28

3.2.1 Calcination 28

3.2.2 Crushing and Sizing 29

3.2.3. Mixing 29

3.2.4. Extrusion 29

3.2.5 Molding 30

3.2.6 Baking 31

3.2.7 Impregnations 33

3.2.8 Graphitization 34

3.2.9 The Final Product 38

3.3 AVR Graphite: Original Receipt 40

3.4 AVR Carbon Brick: Original Formulation 42

4. Radionuclides in i-Graphite : Inventory and Creation Mechanisms 45

4.1 Radionuclide Inventory and Distribution inside the AVR 45

4.2 Radionuclides: Formation Mechanisms 52

4.2.1 Carbon-14 52

4.2.2 Tritium 56

4.2.3 Chlorine-36 60

4.2.3 Calcium-41 61

5. Graphite: Chemical Reactions, Gas Desorption and Radionuclide Release Mechanisms 71

5.1 Reactions occurring with Graphite 72

5.2 Gas Adsorption and Desorption in Graphite: Effects of Temperature on Release 77

5.3 Overview on the Release Mechanisms of Radionuclides 80

5.3.1 Carbon-14 80

5.3.2 Hydrogen-3 84

5.3.3 Chlorine-36 88

6. Decontamination Methods for i-Graphite 91

6.1 Waste Classification 91

6.2 Options for the Disposal of Irradiated Graphite in Germany 93

6.2.1 Repository Konrad 93

6.2.2 Konrad Acceptance Requirements and CarboDISP Project 94

6.3 Purification Methods 96

6.3.1 Purification Methods Developed in the Carbon Industry 96

6.3.2 Comparison among some Purification Methods 98

6.3.3 Off-gas Reprocessing: some Options to precipitate Radiocarbon 101

6.3.3.1 Obtaining Carbon in Solid Form 101

6.3.3.2 A more Complex Solid: Conversion of CO_2 in Alkaline Earth Carbonate 103

6.3.3.3 Conversion in Silicon Carbide 103

6.3.3.4 Isotopic Separation 104

7. Experimental Choices **105**

7.1 Virgin Materials: Separation of Different Histories 105

7.2 Treatment Parameters and Sample Selection on the basis of former experiments 107

8. High Temperature Thermal Treatment Experiments **111**

8.1 Equipment Used 111

8.1.1 Induction Oven facility 111

8.1.2 Mass Spectrometer 117

8.1.3 Thermo Gravimetric Oven (TGA) 118

8.2 Sample Preparation 121

8.3 Performance of Experiments 123

8.3.1 Experiments with the Induction Oven 123

8.3.1.1 Experiment "Massive AVR 1" in Argon atmosphere 112

8.3.1.2 Experiment "Massive AVR 2" in Argon atmosphere 126

8.3.1.3 Experiment "Massive AVR 3" in Argon atmosphere 128

8.3.1.4 Experiment "Massive AVR 3T" in Argon atmosphere 130

8.3.1.5 Experiment "Massive AVR FT" in Argon atmosphere 132

8.3.2Discussion of the Experimental Results obtained with the Induction Oven 134

8.3.3Discussion of the Results from the Experiment "Massive AVR 3T" 153

8.4 Experiments with the TGA Equipment 162

8.4.1 Experiment "AVR Square 1" under Argon atmosphere 162

8.4.1.1 Interpretation of the Results 164

8.4.2 Experiment "AVR Heat Step 1" under Argon atmosphere 166

8.4.2.1 Interpretation of the Results 168

8.4.3 Experiment "AVR Heat Step 2" under Argon atmosphere 170

8.4.3.1 Interpretation of the Results 172

9. SIMS Analyses before and after Thermal Treatment 175

9.1 Generalities on Secondary Ion Mass Spectrometry 175

9.2 Results and Discussion 176

9.2.1 Sulphur before and after Thermal Treatment 179

9.2.2 Chlorine before and after Thermal Treatment 181

9.2.3 Nitrogen before and after Thermal Treatment 189

9.2.4 Oxygen before and after Thermal Treatment 191

9.2.5 Hydrogen before and after Thermal Treatment 193

9.2.6 Lithium Oxide before and after Thermal Treatment 195

9.2.7 Calcium as CaO- and CCa- before and after Thermal Treatment 196

10. XPS Analyses before and after Thermal Treatment 201

10.1 Generalities on X-Ray Photoelectron Spectroscopy 201

10.2 Results and Discussion 202

11. Scanning Electron Microscope Investigations 209

11.1 Generalities on Scanning Electron Microscope 209

11.2 Investigations on the Superficial Morphology of AVR graphite, before and after Thermal Treatment 210

11.3 Investigations on the Sample Holder 218

Summary and Outlook 223

A1 Appendix 227

A.1.1 Temperature calibration of the Induction Oven 227

A.1.2 Delay Time corrections of the Measured Values 228

A.1.3 Purification/Regeneration of the Al2O3 sample holder 229

A.1.4 Mass Calculations from the on-line Gaseous Measurements 231

A.1.5 Calibration of the Mass Spectrometer 232

A.1.6 Design of the new Sample Holder 234

References 241

List of Tables 247

List of Figures 249

Acknowledgements 257

INTRODUCTION

The first material successfully used as moderator and reflector in nuclear reactors was graphite, due to its chemical, physical, structural and especially nuclear properties, together with the possibility of the manufacturer to produce a high degree of purity with regards to neutron poisons. Over the years, graphite, along with various carbonaceous materials, was used in many types of nuclear reactors. Although a number of graphite-moderated test and research reactors have been decommissioned in various EU Member States, the quantity of irradiated graphite (i-graphite) and size of those reactors were relatively small (experimental reactors) in comparison to the future amounts associated with commercial reactors, which are scheduled for decommissioning. A worldwide estimation of the involved graphite is of the order of 250.000 Mg, most of which resides in EU and Russian reactors.

The AVR (Arbeitsgemeinschaft Versuchsreaktor) reactor was an experimental graphite-moderated high temperature reactor of pebble bed type located at the research center in Jülich, Germany. It was helium cooled and operated at nominal temperatures of 950 °C. It started working in 1967 and its final shut-down dates to 1988. The electrical power output was 15 MW_e (46 MW_{th}).

After many decades of operation the permanent reactor core materials, consisting of nuclear grade graphite and non-graphitized carbon brick, have accumulated significant amounts of radionuclides, originating both from neutron activation of impurities and diffusion of fission products. Thus, at the end of reactor's life, arises the necessity to dismantle the contaminated components and an appropriate strategy for waste management is required. The simplest and widely adopted choice in the past for all nuclear reactors had been the "safe enclosure" of materials within the existing nuclear facilities; the reasons of that are related to the decay of radioactive short-lived species and to personnel safety in handling, transporting, processing and storing vast amounts of radioactive material. For irradiated graphite , effective treatment and conditioning processes haven't been standardized yet and various methods are under study.

Difficulties in handling such materials are underlined by the involved volumes and the presence of significant amounts of volatile and/or leachable species, such as short-lived (e.g. ^{3}H), and long-lived radionuclides (^{14}C, ^{36}Cl, etc.). Since the costs of disposal are bound to the waste volume and e.g. the volatility of ^{14}C compounds, according to the waste acceptance criteria for the German Konrad waste repository, it is necessary to determine the release mechanisms and chemical bonds of the radioisotopes. These information would lead to substantial savings, considering that the waste may be classified in a different category. The

knowledge in the location and chemical bonds of radionuclides can also be used to establish purification and decontamination processes for irradiated graphite. It is assumed that pre-treated graphite waste will show an improved leaching behaviour under repository conditions. Moreover, the resulting treated carbon materials, purified from radionuclides, might be stored normally or even reused in the nuclear field.

Starting from that, the idea of studying virgin materials of the same type involved in the reactor leads to accelerate the development of an industrial purification process. The basic hypothesis is that governing physical-chemical mechanisms, in particular the ones occurring during thermal treatments, are mainly the same both for virgin and activated graphite.

A first trial treatment of radioactive carbon materials could be gasification, which would separate the volatile radionuclides from the non-volatile ones, but unfortunately it is known that isotopes, such as ^{14}C and ^{12}C, are not chemically separable, so an isotope separation would be necessary. A more promising decontamination process concerns high temperature treatment, in argon or in water vapor atmosphere, which showed a higher release rate of volatile radionuclides compared to the case of simple oxidation[1]. A central role for the development of a separation process that follows this line is the impurities location in the carbonaceous matrix and their chemical bonds: it is important to know the materials history in the way to understand how the primary impurities came inside the graphite and how the successive activation products can be released through a particular processing.

Up to now, only small samples have been studied, mostly within a limited temperature of 1060 °C.[2] Due to the availability of an induction oven and a thermo gravimetric equipment, together with a quadrupole mass spectrometer (QMS), it was possible to undertake some studies on thermal treatments effect and measuring gaseous emissions from virgin AVR reflector graphite. Because of radioprotection concerns it was not possible to run radioactive samples in the oven under the given circumstances.

The main objective of this study is to investigate the influence of high temperature thermal treatments on nuclear virgin graphite, assuming that the governing physical-chemical mechanisms are the same than the ones taking place in the activated graphite at the end of the reactor's life, under the same conditions. In particular the on-line emissions during thermal treatment under inert gas of virgin AVR reflector graphite will be investigated, with

[1] T. Podruzhina, "Graphite as radioactive waste: corrosion behaviour under final repository conditions and thermal treatment", Juel 4166, 2004

[2] Idem

the purpose of proving the existence of oxidizing species originally embedded in the graphite structure. Moreover, concentration gradients and migration of many chemical elements (as Sulfur, Oxygen, Nitrogen, Chlorine and Calcium) from and also to the sample surface will be studied with several SIMS and XPS analyses before and after a well defined thermal treatment cycle. Changes in the superficial graphite structure will be examined with SEM pictures before and after thermal treatment.

Further studies are going on in the European CARBOWASTE project (GA N° 211333) and the German CarboDISP project (02S8790) for a deeper understanding of the basic mechanisms, which will make it possible getting closer to an effective purification treatment on a larger scale.

The Carbowaste Project

In April 2008 the five-years European project “Treatment and Disposal of Irradiated Graphite and other Carbonaceous Waste (CARBOWASTE)", under the 7th EURATOM framework Programme (FP7-211333), has been launched.

The objective of this project is the development of best practices in the retrieval, treatment and disposal of irradiated graphite & carbonaceous waste, like structural material e.g. non-graphitized carbon bricks and fuel coatings (pyrocarbon, silicon carbide). It addresses both legacy waste as well as waste from future generations of graphite-based nuclear fuel.

After having defined the targets for an integrated waste management, analysis of the key-stages from the in-reactor storage to final disposal have been undertaken, considering the most economic, environmental and sustainable options. A characterization program to localize the contamination in the microstructure of the irradiated graphite, their origin and release mechanisms during treatment and disposal, is supporting the strategy analysis.

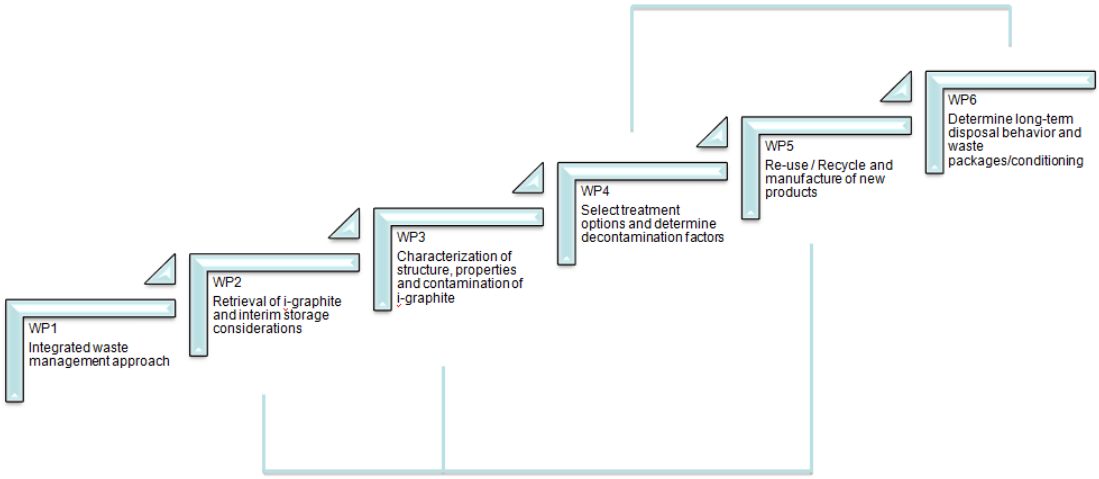

Figure 0.1: Carbowaste Project's Work Package Scheme

It has been discovered that a significant part of the contamination (including ^{14}C) can be removed by thermal, chemical or even microbiological treatment. The feasibility of the associated processes are being experimentally investigated to determine and optimize the decontamination factors. Reuse of the purified material will also be addressed to close the "Graphite Cycle" for future graphite moderated reactors. The disposal behaviour of graphite

and carbonaceous wastes and the improvement of suitable waste packages are another focus of the programme.[3]

This work is in line with the Carbowaste Project Work Package 3 and 4, related to the characterization of graphites' structure, properties and contamination and to the best suitable treatment for removal of volatile and long-lived radioactive contaminants.

[3] www.carbowaste.eu

1. AVR Reactor

As the sample material for the investigations are mainly taken from unirradiated graphite of the AVR (Arbeitsgemeinschaft VersuchsReaktor), some short information is provided on this special type of reactor.

1.1 Reactor Category

The VHTR (Very High Temperature Reactor), also known as HTGR (High Temperature Gas-cooled Reactors) or HTR, represent a particular branch of 4th generation thermal nuclear reactors. HTGR are graphite-moderated, gas-cooled nuclear reactors with once-through uranium fuel cycle, able to reach outlet temperatures up to 1000 °C. The core structure can be of two types: prismatic core (PMR) and pebble bed core (PBR).

1.2 Concept

Passive safety and high coolant temperatures are the concept keys of the PBR. The high outlet temperatures allow high plant efficiencies, usually reached in fossil-fueled steam power plants. Core physics, together with technical and economical aspects, has led to the choice of ceramic fuel and graphite as fuel element cladding and core structure material, able to bear high core temperatures.

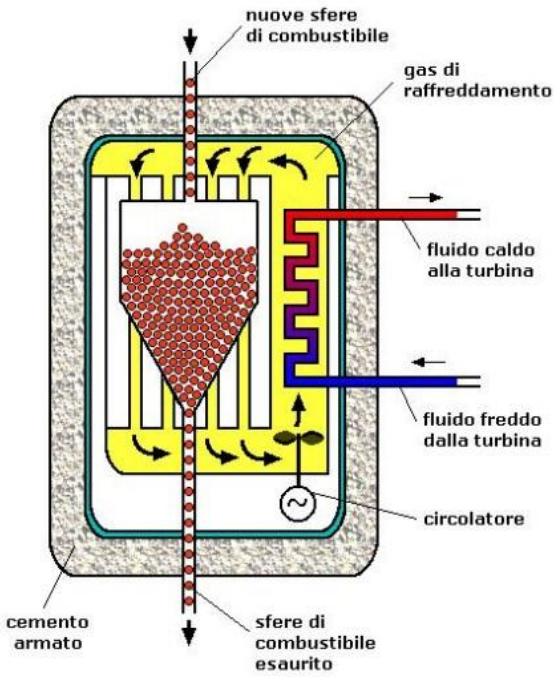

Figure 1.1: Scheme of a Pebble Bed Nuclear Reactor

The development of coated particles has given an essential contribution to the reactor safety due to the higher retention capacity of fission products.

1.3 Structure

The AVR was the first experimental high temperature reactor of pebble bed type worldwide on industrial scale. Main aim of this experimental reactor was the test of the pebble bed core concept and the test of many different types of pebble shaped fuel elements. It was helium cooled and high-purity graphite was used both as moderator and reflector. It started working in 1967 and its definitive shut-down dates back to 1988. The electrical power output was 15 MW_e (46 MW_{th}). The electrical power was generated throw a steam cycle, with a steam generator (73 bar), which was inside the primary reactor vessel, on top of the core. AVR was equipped with a double wall pressure vessel and a gas tight containment, in order to avoid leakage of radioactivity due to the fact that coated-particle fuel was not yet invented when the reactor was designed. Thus, no major retention of fission products was possible in the early fuel element types.

The pebble bed core has a diameter of 3.0 m and an average height of 2.8 m.[4] This, together with the helium circulation system and the steam generator, is integrated in the reactor vessel, surrounded in turn by the confinement vessel. The former consists itself of two concentric vessels. Between the first and the second reactor vessel the first biological shield (iron ore granulate) is installed and the space in-between is kept at a slightly higher pressure than in the inner one.[5] The confinement vessel is the second gas-tight barrier to ensure no radioactivity release to the environment, even in accident scenarios. This vessel was accessible to personnel through several air locks. At last, the cylindrical reactor building, a concrete tower of 40 m height, 21 m diameter with 1.5 m wall thickness, forms the second biological shield.

Two cooling blowers, placed on the bottom part of the reactor, ensured the recirculation of cooling helium, from the bottom to the top, with a pressure of about 10.8 bar and a flow rate of 13-15.5 kg/s depending on the outlet temperature desired (9 m/s of maximum velocity to prevent erosion by graphite dust) [4,5]. The outlet temperature of helium was initially maximum 850 °C but, after 02/1974, it was increased at maximum of 950-990 °C, with an inlet

[4] Association of German Engineers (VDI) - The society for energy technologies (PUBL.), "AVR - Experimental High Temperature Reactor 21 years of successful operation for a future energy technology", VDI Verlag, Düsseldorf 1990

[5] Proceedings of the 11th International Conference on environmental Remediation and Radioactive waste Management, ICEM2007, The AVR (HTGR) decommissioning project with new strategy

temperature of 270 °C [6]. After 4 years, inadmissible high core temperatures were detected, so the maximum allowed temperature became 750 °C till the end of the reactor's life.

The bottom, side and top reflectors as well as the so-called "reflector noses" consisted of polycrystalline graphite (needle-coke graphite, ARS/AMT grade made by SIGRI-Elektrographit), chosen due to its chemical and physical properties and behavior under fast neutron irradiation (see chapter 2). The graphite reflector wall of 50 cm thickness surrounded the reactor core containing the spherical fuel elements. The 4 absorber rods were fed into the "reflector noses" and their aim was to control the neutron flux and the reactor shutdown.

To insulate the external metal structures from high temperatures present in the core, the reflector in turn was enclosed in an insulating carbon brick layer, manufactured with a similar process used to produce graphite but not exceeding about 1200°C to avoid graphitization of the material. This insulating material was less pure and less expensive than nuclear grade graphite, with the advantage of having low thermal conductivity. The thickness of the carbon bricks insulation amounted to 50 cm. Both bottom and top graphite reflectors and carbon brick layers contained cooling gas channels.
The total mass of the graphite used in the reflector amounted to 67 tons and, concerning the carbon bricks, to 158 tons[7].
The choice of the materials for the primary system was taken with utmost conservativeness, to ensure a maximum level of operational safety. At the time of AVR construction there were no sufficient computational results neither sufficient information available on all materials parameters. Luckily the loads were determined taking into account the thermal and radiation-induced effects rather than the pure mechanical ones. So the ceramic structure (see fig. 1.3) was composed of the maximum possible number of small blocks respecting defined expansion gaps. An accurate machining of the blocks ensured the leak tightness of this structure. As a result of that, after many years of operation, a visual inspection of the top and upper side reflector (the most neutron and thermal stressed parts) in 1984 confirmed the reflector good conditions, without cracks neither evidences of corrosion found.

In table 1.1 are summarized the most important parameters of the AVR reactor.

[6] R. Moormann, "A safety Re-Evaluation of the AVR", ForschungszentrumJülich, Jül-4275
[7] Idem

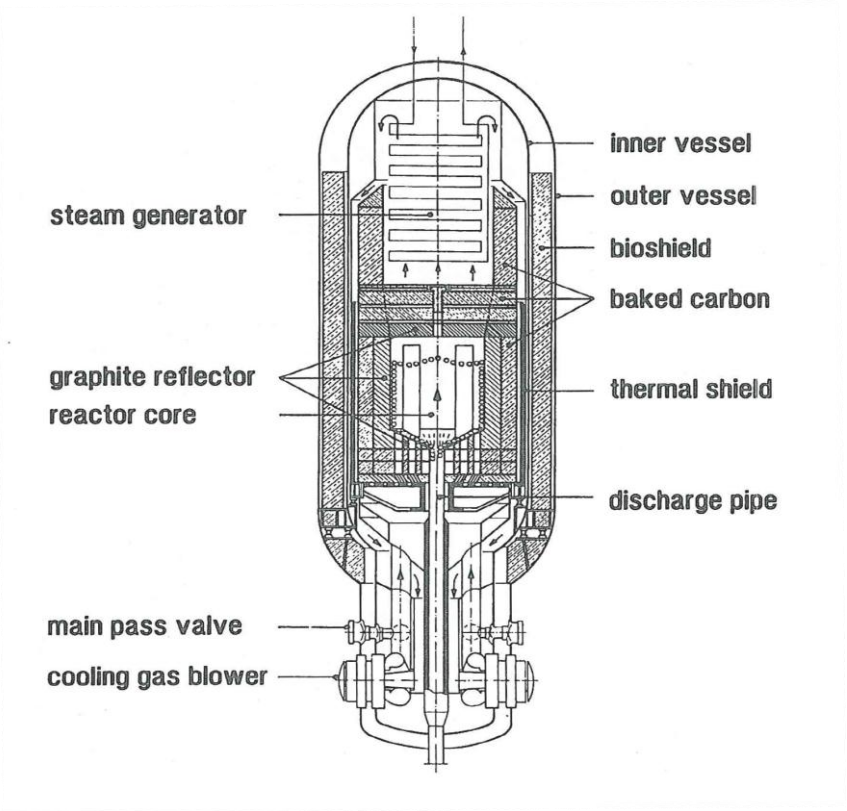

Figure 1.2: View of the reactor vessel and its internal structure

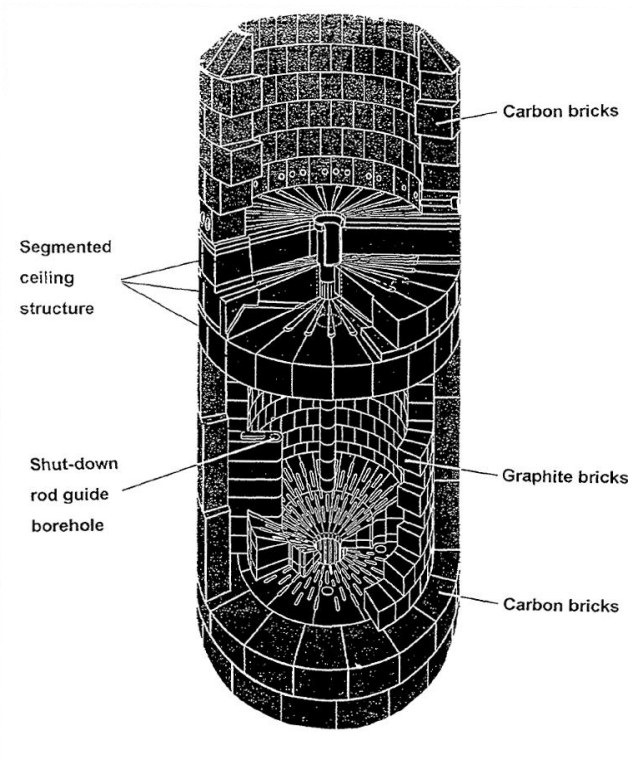

Figure 1.3: Internal structure of the core and heat exchanger's chamber

Core and vessel		
Thermal power	46,0 (2,6)	MW (MW/m^3)
Electrical Power (gross/net)	15/13	MW
Diameter	3,0	m
Average height	2,8	m
Number of fuel elements	100.000	
Pressure of helium	10,8	Bar
Average inlet temperature of coolant gas	275	°C
Average outlet temperature of coolant gas	950	°C
Main steam temperature	505	°C
Reactor pressure vessel material	steel	
Reactor pressure vessel (inner/outer) height	24.9/26	m
Reactor pressure vessel (inner/outer) diameter	5.8/7.6	m
Total reactor vessel weight	1600	Mg
Total reactor vessel weight with concrete	2100	Mg
Number of shut down rods	4	
Fuel Elements		
Diameter of a fuel element	6,0	cm
Fuel	U+Th	
Uranium 235 mass per fuel element	1	g
Enrichment	10; 16,7; 93	%
Thorium mass per fuel element	0; 5; 10	g

Table 1.1: Main parameters of AVR reactor[8,9]

To ensure no radioactivity escaping the AVR was provided with a double reactor vessel, a steel vessel and two barrier gas zones in the middle, with a higher pressure in the outer zone than in the inner (see fig 1.4).

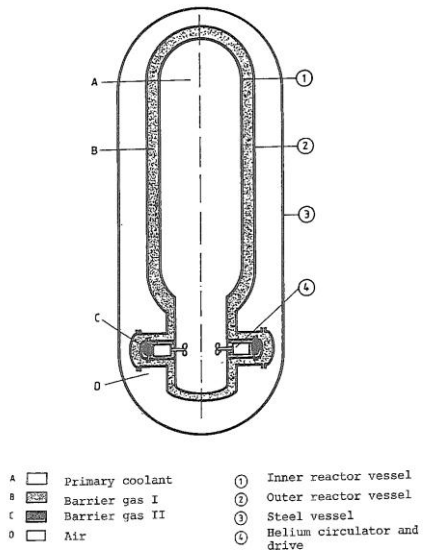

Figure 1.4: Barriers structure of AVR

[8] Ref. [4]

[9] Ref. [6]

1.4 Fuel

Many types of fuel have been tested in the AVR. The main pursued concepts[10] for fuel design have been:

- Prevent radioactivity from escaping in any situation;
- Limit transients by low power density;
- Allow passive safety of the reactor;
- Employ higher temperatures than other reactors type;

The AVR pebble bed core consists of 100000 graphite pebbles[11], which each contain up to 40000 multicoated fuel particles. Different fuel types were used as part of the fuel development programme ending with improved TRISO fuel. The fuel particles are incorporated in a graphite matrix to form 6 cm diameter spheres, including a 5 mm graphite layer surrounding. All fuel pebbles contained 1 g ^{235}U and different quantities of ^{232}Th and ^{238}U (6-11 g total HM) [5]. A porous carbon buffer, to allow gas diffusion inside the pebble without pressure build-up during the operation, surrounds the cores of these particles. In addition, several layers of pyrolitically-precipitated carbon and silicon carbide are implied to give thermo-mechanical resistance and to prevent fission products from escaping. During reactor operation the pebbles are re-circulated continuously (about 500 pebble/hour [5]), taken from the core bottom and re-fed into the core top, until the final burn-up is reached and the fuel element is replaced with a fresh one (average of 50 fuel elements replaced per equivalent full-power day [5]). In order to achieve a more even radial temperature profile, low power fuels were fed into the core center and fresh ones into the outer regions. Pebble flow velocities were higher in the inner than in the outer core region.

The discharged fuel elements are now stored in cast iron containers (CASTOR), at the Jülich site, awaiting transport to the intermediate storage at Ahaus, in Germany.

[10] Association of German Engineers (VDI) - The society for energy technologies (PUBL.), "AVR - Experimental High Temperature Reactor 21 years of successful operation for a future energy technology", VDI Verlag, Düsseldorf 1990

[11] R. Moormann, "A safety Re-Evaluation of the AVR", Forschungszentrum Jülich, Jül-4275

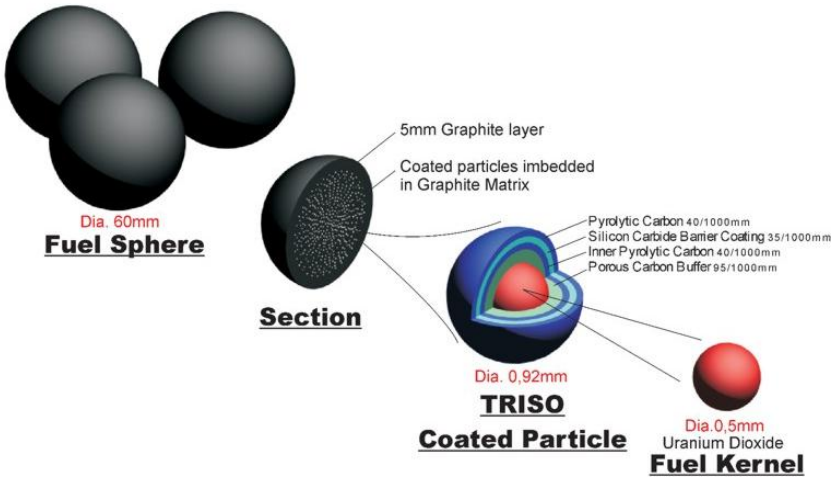

Figure 1.5: Fuel structure and TRISO particles

1.5 Major Problems and Accidents

One of the most important features of the AVR showed to be one of the biggest problems during operation: the steam generator was placed inside the inner vessel, above the core and the slight shielding of the top reflector (only three bridge layers of graphite and carbon brick). That choice was taken to have a simple and small hot gas chamber to obtain the desired high outlet temperatures even with a small heat exchanger. The great disadvantage of that choice was to have the bottom part of the steam generator's tubes to be activated: part of these activated corrosion products were entrained in the steam/water cycle and accumulated in places where the flow was small enough.

Moreover, because of the bad-dimensioned instrumentation, the steam generator leakage in 1978 was not identified in time, resulting in about 27 tons of water penetrating into the core and accumulating at the vessel bottom. [12]After 72000 hours of operation without any faults a leak developed in one of the superheater tubes. The hole's cross section was about 3 mm^2 and the leakage lasted 3 days before being recognized, so that 27 tons of water penetrated into the primary system, flowed through the core and collected in the bottom part of the vessel. The location and blanking off of the defective pipe was performed without major difficulties, but the removal of the water which had penetrated into the primary circuit and the drying of the system required a great deal of time. If the volume of water which had entered the reactor vessel had been displayed the incident would have been earlier recognized and the consequences would have progressed more favourably. The incident was one of the most challenging for a high temperature reactor, considering the positive effect of the water on reactivity and considering the possible chemical reaction of water with the graphite with the

[12] R. Moormann, "A safety Re-Evaluation of the AVR", Forschungszentrum Jülich, Jül-4275

formation of explosive gases (CO, H_2). Fortunately, the incident had no immediate consequences due to the low temperature of the core (500 °C), since the reactor was operating at low power (independently of the leakage since it was not immediately recognized) [13]. The incident resulted in a strong contamination of the surrounding environment: the water washed out 1500 GBq of Sr-90 and 10^5 GBq of H-3 and went partially in the reactor grounding, reaching so the surrounding soil.

The AVR suffered of high uncertainties on real core temperatures: there is no way to measure directly (and rapidly) the temperatures in a pebble-bed core, so core temperatures were based only on calculations.[14] It was calculated a core maximum temperature of about 1070 °C to obtain 950 °C at the gas outlet. Coated particles of the latest-design fuel elements were supposed to operate at T<1250 °C, which showed to be too optimistic: many test pebbles measured maximum surface temperatures higher than 1280 °C, which meant to have coated particles temperatures roughly up to 1420°C. A direct measurement of fission products collected in the hot gas filters showed a significant increase of Sr-90 and Cs-137, released in the primary circuit, after the outlet temperature was increased till 950 °C average: the inadmissible high core temperatures may have caused the release (even from TRISO fuel) of many fission products, which accumulated in the primary circuit.

Considering the friction occurring during the pebble movement among them and with the reflector walls, together with the presence of defective pebbles, a significant graphite dust formation takes place[15]. It was found in the AVR about 150-200 kg of dust.[16] Such dust is heavily contaminated by fission products (as Sr-90, Cs-137), but also by small quantities of actinides (^{241}Pu, ^{241}Am), coming from coated particle failures and the uranium contamination of the fuel matrix.

Taking the AVR experience as a reference to better understand many problems occurring in different situations, successively-built reactors modified some of these design features:
- THTR 300 (Thorium High Temperature Reactor) with 750 MW_{th} and 300 MW_{el} which unfortunately suffered from some pebble bed specific problems (mechanics) and operated only for 1.2 full power years;

---

[13] R. Priggen, "Die beinahe Atom-Katastrophe in inhaerent sicheren Reaktor in Juelich"

[14] R. Moormann, "A safety Re-Evaluation of the AVR", Forschungszentrum Jülich, Jül-4275

[15] In the THTR it was observed a large amount of pebble rupture compared to AVR, partially explainable with the rod movement inside the core

[16] R. Moorman, Fission product transport and source terms in HTRs: Experience from AVR pebble bed reactor (2008)

- HTR-10 (High Temperature Reactor), more recent than the former, with 700°C nominal outlet Helium temperature with a thermal power of 10 MW, built in China. It showed to be safer after many tests[17] and led to the large-scale project of the HTR-PM with 2x250 MW of thermal power and an outlet Helium temperature of 750 °C [18].

In spite of the observed problems, AVR showed with success the feasibility of high temperature gas cooled reactors with many reached targets:
- High outlet temperature (even though the design temperature was limited to 750 °C due to fuel design)
- High level of fuel utilization
- High fission products retention capability of the fuel (TRISO) when temperature does not exceed the maximum designed one
- Good safety based on the high temperature resistance of the fuel encasing and of the ceramic core

1.6 The Dismantling Plan of the AVR

The dismantling of the AVR reactor is more complex, work intensive and risky compared to GCR and LWR with the same power.[19] The reasons of that are mainly due to three operational and design factors:

- High dust production due to inferior test fuel pebbles
- Very high core temperatures during fuel testing
- High impurity level of tritium due to lithium impurities in the carbon bricks

These factors can explain the fission product contamination (Sr-90 and Cs-137 as mentioned before) due to fuel failures during tests of different fuels and the high level of activation products, as H-3, C-14 and Co-60 originating from impurities.
In addition, other factors influenced the decommissioning strategy:

- The steam generator leak in 1978 which led to flooding of the reactor and a contamination of the lower building structures and of the ground below the reactor building

- The secondary loop which resulted to be contaminated

[17] Hu, Shouyin; Wang, Ruipian; Gao, Zuying (2004), "Safety Demonstration Tests on HTR-10", proceedings of the conference on High Temperature Reactors (Beijing, China)
[18] IAEA TWG-GCR-22, HTR-PM “Project Status and Test Program”
[19] Sterner H., Cross M.T. and Rodriguez A., “Decommissioning of gas-cooled reactors”. Kerntechnik 70 (2005)

- Free space available is very limited in the confinement vessel (reactor vessel is not accessible)

Considering the above-described reasons, the chosen strategy was the so-called "Safe Enclosure": the fuel was unloaded (this step lasted 4 years), all contaminated systems outside the building were dismantled and the systems inside the reactor building started to be dismantled too. At a certain point, the decommissioning strategy changed (2003), considering also the contaminated ground, recently discovered, due to the 1978's accident. The preferred decommissioning strategy resulted in the direct complete dismantling (the remote one in situ would have been more expensive, in addition to the radiological situation and the waste management's costs). It was decided then to remove the reactor unit in one piece, by constructing a material air lock adjacent to and enclosing the top of the reactor building (see figs. 1.6-7-8). The reactor vessel was filled in 11/2008 with 500 tons of light concrete in order to immobilize the radioactive dust and to stabilize the vessel (technique used also with Russian nuclear submarines). After removal, the reactor unit will be transported through air-cushion sled and several cranes to an interim storage facility under construction nearby. There the reactor will be kept for 30-60 years, allowing the achievement of a cost effective dismantling and waste management due to the decay of short-lived nuclides (like Co-60 and H-3) and, at the same time, the green field conditions establishment at the AVR site. Currently there exists no dismantling method for the AVR vessel, but it is planned to develop some procedure during the next decades: a major issue for the dismantling will be the management of the materials, considering the necessity to keep the radioactive waste fraction low by separating the lower contaminated (e.g. the bio-shield of 760 Mg) from the rest and the graphite from the carbon brick material, which is heavily activated (see table 4.3 for comparison).

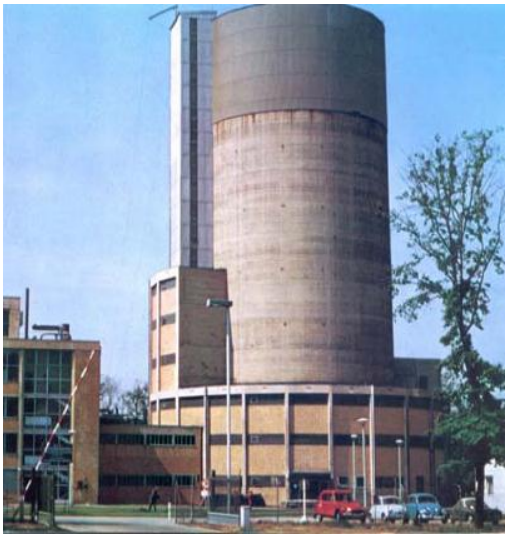

Figure 1.6: AVR in 1978

Figure 1.7: AVR today

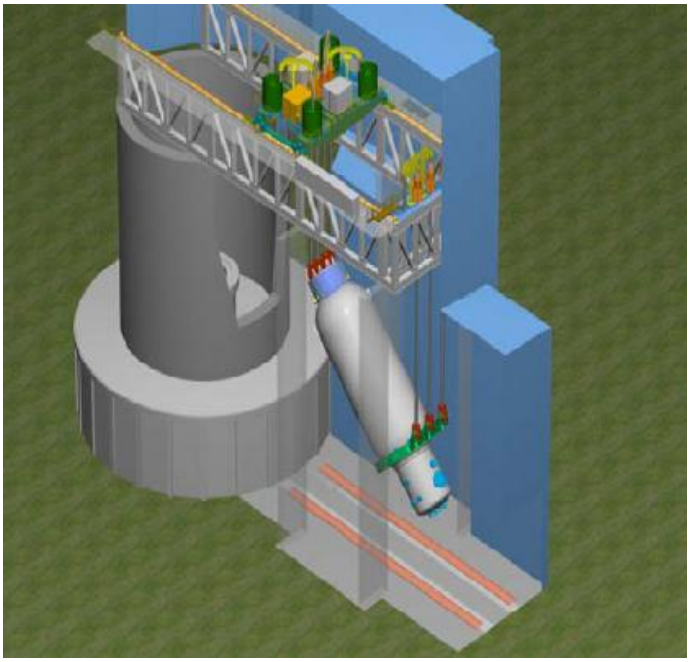

Figure 1.8: Reactor pressure vessel extraction within the new material lock

2. Graphite: Overview on Structure, Properties and Nuclear Applications

Graphite structure is fundamental from the point of view of chemical reactions[20] and response to neutron irradiation, in particular there is a significant difference between isotropic graphites and extruded ones. In this chapter a general overview of the main properties of graphite is presented, starting from the atomic point of view and discussing the most common characteristics distinguishing such material that make it suitable for many nuclear applications.

2.1 Graphite: Structure and General Properties

Graphite is a crystalline, low density and soft allotrope of carbon. The crystalline structure of graphite is due to a second type of combination of the atomic orbitals of carbon (or sp^2 hybridization), leading to hexagonal rings forming thin parallel planes (graphene). Each carbon atom is covalently bound (sp^2 σ bond) to three other atoms: the lowest energy state of this combination gives three equivalent bond orbitals directed in a plane at angles of 120° with an average C-C bond strength of 100 kcal/mole[21] and an in-plane C-C distance of 1.42 Å. The third unused p orbital forms a π bond perpendicular to the planar system of sp^2 bonds. The nature of the π bond is such that the electrons are quite mobile in any given layer plane, establishing so a delocalized electron system. Practically, after the formation of sp^2 planar hybrids connecting carbon atoms within each layer, p-electrons are left and they do not appertain singularly to the one or the other carbon atom; they are instead delocalized and relatively free to move, but only parallel to the layer: this explain the anisotropic electric and thermal conductivity of graphite.

The bonding electrons are all used in forming C-C bonds within the carbon layers, so the layers themselves are held together only by weak Van der Waals forces at a distance of 3.35 Å (on a perfect crystal).

The most important structural characteristics, giving to graphite many of its unique properties, are the system of strong chemical bonds forming large sheets of hexagonal rings where electrons are quite mobile and the great space between planar layers.

[20] Chemical reactions and gas adsorption will be discussed in chapter 6

[21] R.E. Nightingale, "*Nuclear Graphite*" ed. 1962. New York and London: Academic Press

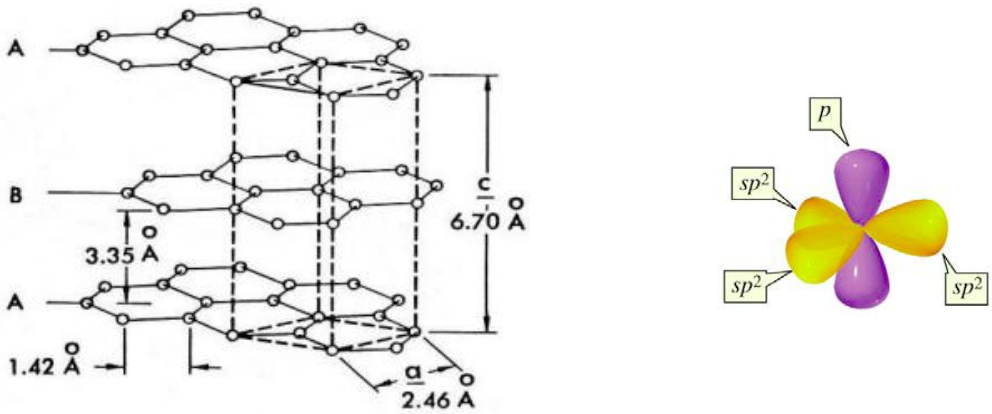

Figure 2.1: Ideal crystal structure of graphite (left) and Carbon hybridized orbital present in graphite (right)

There are two forms of graphite, differing in the way of layers overlapping: in the normal form -α-graphite- a sequence *ababab* is established (hexagonal) while in the β-graphite the sequence is *abcabc* (rhombohedral). The most common type is the hexagonal one and the theoretical density for both forms is 2.26 g/cm^3. It was proven through high temperature treatments that the fraction of rhombohedral graphite can be reduced, concluding that the hexagonal form is the most stable[22].

Most of solid carbons haven not an ideal crystalline structure: various degrees of ordering and value of interlayer space in addition with lattice defects and crystalline imperfections are present. The most disordered structure is called "turbostratic": the basal planes have slipped sideways relative to each other, causing the spacing between planes to be greater than ideal, so turbostratic carbons have disordered stacking through random rotation or displacement of ordered layers. The C-C bond distance remains constant.

[22] M. Nic, J. Jirat, B. Kosaba, "Rhombohedral graphite", IUPAC Compendium of Chemical Technology

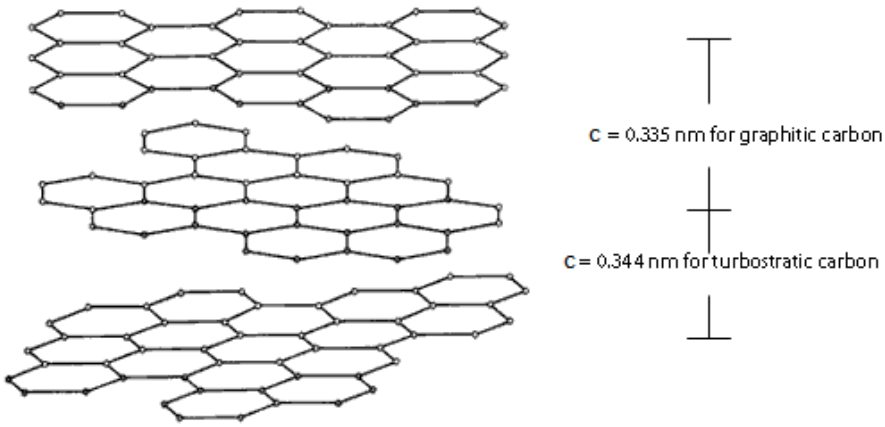

Figure 2.2: Turbostratic structure of graphite

In general, nuclear graphite presents a complex multi-scale organization. It can be more or less anisotropic and not completely graphitized. Triperiodical stacking of graphene layers forms crystallites: these can be more or less oriented, with a size of the order of few hundreds of nanometers. Several crystallites form grains, of typical size in the order of micrometers, which in turn produce a polycrystalline structure.

Isotropy of graphite is very important not because of the thermal conductivity but because of the dimensional changes by neutron damage. Blocks would creep in an uneven way if anisotropy is too large e.g. bowing of blocks. The porosity is also needed to accommodate the dimensional changes and to avoid cracking, but the porosity is also the location for impurities such as nitrogen.

Some general properties of synthetic graphite are listed below.

- High melting temperature (sublimation 3650 °C)[23];
- Low density (1.7-2.23 g/cm^3, about three times lighter than steel);
- Low hardness (1.5 that is about three times lower than the one for mild steel 4-4.5)[24];
- High electrical conductivity and thermal conductivity, based on free electrons. These property are determined by the size and the good degree of order of the crystallites;
- Low coefficient of thermal expansion;
- High thermal shock resistance;
- High strength (particularly compressive strength), which increases with the temperature rise;

[23] http://invsee.asu.edu/nmodules/carbonmod/point.html
[24] Mohs hardness from: http://en.wikipedia.org/wiki/Mohs_scale_of_mineral_hardness

- High stiffness (modulus of elasticity);
- High thermal resistance;
- High chemical and corrosion resistance, due to the great strength of the covalent bonds within the lattice, except for strong oxidizing agents;
- Good oxidation resistance. Graphite starts to be oxidized in oxidizing atmosphere at relative high temperatures;
- Good neutron moderation;
- Good machinability;
- Ability to absorb gases; [25]

in particular a nuclear grade graphite has to show also (see chapter 3 for more details):

- small neutron absorption cross section (high-ultra chemical purity)
- high dimensional stability under fast neutron irradiation

However, it has to be underlined that specific properties are varying with the graphite grade, the manufacture process and the presence of impurities.

Graphite grades can be characterized by six interrelated and mutually influencing parameters: purity, particle size, particle shape, surface and porosity. Selective influencing of these parameters results in the optimal combination of properties for the respective application. For example, crystallinity is of great importance because influences thermal conductivity, purity level for elements with high neutron-capture cross-sections, irradiation-induced modifications, dimension stability, machinability[26] and even chemical stability[27].

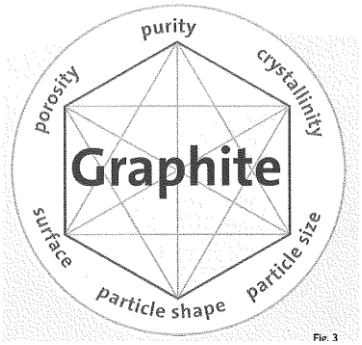

Figure 2.3: Influencing parameters characterizing graphite grades

[25] http://www.substech.com/dokuwiki/doku.php?id=graphite
[26] L. Wang, L.E. Jones, "X-Ray Diffraction of Nuclear Graphite"
[27] Indeed reactions take place preferentially at the defect sites and at the plane edges. More information in chapter 5

2.2 Nuclear Applications

The element carbon has the ability of slowing down fast neutrons without significant cross section of capture. Carbon is therefore a valuable material for the construction and operation of power reactors of various types, which were applying natural uranium, because of unavailability of enriched uranium for civil purposes in the past. These reactors are ranging from the CO_2 cooled reactor with a cooling gas temperature of 400 °C to the helium cooled high temperature reactor with operating temperatures beyond 800 °C. Only purified graphite can meet this special requirement, combining at the same time strength and good neutron irradiation behavior.[28] This means that its mechanical or physical properties, e.g. strength or lattice constants, are not allowed to be strongly influenced or affected by irradiation. This objective can be achieved only by using isotropic graphite showing homogeneous irradiation-induced dimensional changes. Unfortunately the AVR reflector graphite does not have such characteristic because of the manufacturing processes of more than 50 years ago which implied an extrusion stage: only little knowledge was available at that time about neutron irradiation effects on graphite (see chapter 3 for more details on the manufacture process).

The fields of application in the nuclear industry are widely varied and comprise the use of graphite as moderators, in fuel matrixes, as reflector, in thermal columns and in fuel-channel sleeves. The graphite qualities as moderator and reflector, combined almost uniquely with strength and high temperature stability, are the main reasons for the application of this material. In particular, concerning the AVR, graphite was chosen also due to its high-temperature strength and thermal conductivity to serve as structural material, reflector and fuel matrix, allowing in such way the integrity of the reactor at high temperatures under high neutron flux and permitting at the same time the heat removal to produce steam.

3. Manufacture of Nuclear Graphite

The manufacture process is a fundamental step for determining the final properties of graphite. The raw materials are one of the main sources of impurities that are found inside the graphite structure; however, a proper manufacture process is able to remove part of them, depending on the parameters and steps implied. After exposure to neutron irradiation, many of these impurities are likely to be activated, in relation with the neutron fluence and the neutron capture cross section, leading in some cases to consistent activities. High amounts of activation products result in a difficult dismantling strategy, since retrieval, handling,

[28] http://www.carbonandgraphite.org/

treatment and disposal of irradiated materials are strongly bound to their radiochemical characteristics. In particular some important radionuclides, showing particularly high activity in the AVR and high mobility in the environment, are tritium, radiocarbon, chlorine-36 and in addition calcium-41 and cobalt-60. The study of the nuclear reactions and relative cross sections can lead to identify the main precursors of such isotopes (see chapter 4), in particular some important ones are Lithium-6, Nitrogen-14, Chlorine-35, Sulphur-34, Calcium-40 and Cobalt-59. Many of these elements are already embedded in the raw materials used to produce graphite, with a strong dependence on their provenience but also on the manufacture process parameters and steps. Moreover, the location of such elements will be important to understand where the radionuclides could be concentrated, as in the case of radiocarbon that is believed to be enriched near all the available surfaces of graphite and carbon brick. This chapter is going to present all the steps of a typical manufacture process, highlighting the differences with the process used for the AVR carbonaceous materials and the different amounts of impurities found after the main steps. At last, the original recipes of AVR graphite and carbon brick are reported.

Graphite used in nuclear reactors is high purity synthetic graphite coming from the same, but modified, manufacture process of electro-graphite, having a polycrystalline structure. There are several general requirements for nuclear graphites, including density (≈1.8 g/cm3), crystallinity, coefficient of thermal expansion ($2.0\text{-}5.5 \cdot 10^{-6}$ K^{-1}) and strength (≈20 MPa). Additionally, high chemical purity, low reactivity in moisture (0.2 to 0.01 $mg/g \cdot h$) and low absorption cross section (about 4 mb) are desired.[29]

The most utilized raw materials in nuclear graphite manufacture are petroleum-coke, heavy residue of oil refining, used as filler and a coal-tar-pitch used as binder; natural graphite, carbon black and secondary graphite scrap can also be used. The conventional manufacture process of electro graphite was modified in the way to remove as much as possible the impurities with significant neutron-absorption properties (e.g. Boron, Cadmium). However, impurities ending up as problematic long-lived radioactive activation products such as ^{14}C, ^{36}Cl, ^{40}Ca etc. have not been in the focus in the early days of graphite manufacture.

[29] B. J. Marsden, "*Nuclear Graphite for High Temperature Reactor*", IAEA Technical Committee Meeting on "Gas Turbine Power Conversion Systems for Modular HTGRs", Palo Alto, California, November 2000

3.1 Raw Materials

3.1.1 Petroleum Coke

The most used filler materials are petroleum coke at first, metallurgical coke and anthracite. The first one is the best graphitizable, resulting in a high degree of crystallinity[30] in the final product. The petroleum coke is a by-product of oil refining, normally obtained through cracking of heavy refinery oil. The cracking process (≈500 °C, ≈35 bar) decomposes the larger hydrocarbons molecules in the crude oil into lighter fractions (e.g. gasoline), which are removed; the remaining reactive components form a heavy fuel oil. The most commercially used technique for cracking is the catalytic one.

The heavy by-products are then coked through the so-called delayed coking process: they pass through pipe furnaces with a temperature raised till 500 °C to establish further cracking of the stock; this is then transferred to an insulated drum where the coke forms and settles. Coke is removed from the drums by high pressure water jets.

The coking step is very important for the later graphitization: hydrocarbons polymerize into large polycyclic aromatic molecules that are aligning during the last stages of fluidity to form embryonic crystals. At this stage of development crystallites do not show three-dimensional order but rather a lamellar one, sufficient to cause alignment of adjacent crystals to varying degrees. The fixed carbon[31] in coke from a delayed coker ranges from 85 to 90 % and the volatile content ranges 7-16%; typical raw cokes impurities are listed in table 3.1, together with some measured values of a modern coke, obtained by PGNAA. In general, the impurity values depend strongly on the provenience of the raw materials.

Impurity	Range	Typicalvalue	Measured Value in a modern petroleum coke[32]
Total ash impurity [%]	0.05 - 0.3	0.1	n/a
Sulfur [%]	0.1 - 2.0	0.8	0.36 %
Vanadium [ppm]	3 - 500	15	n/a
Boron [ppm]	0.1 - 0.3	0.1	1.2
Nitrogen [%]	0.1 - 1.4	1.0	n/a
Hydrogen [%]	3 - 4.5	4.0	0.15
Chlorine [ppm]	n/a	n/a	70

Table 3.1: Typical impurities in raw petroleum coke

[30] High crystallinity means that the structure approaches the perfect crystal, showing then high thermal and electrical conductivity, a small c-spacing and a large crystallite size.
[31] Carbon that is remaining after heating to 1000 °C
[32] L. Szentmilklòsi, „*PGNAA Analysis for Forschungszentrum Juelich*“, 2011

In the AVR reflector graphite Shell petroleum coke has been used as raw material (today not available anymore). The petrol coke was produced mainly throw thermal cracking of residues from oil distillation after the process of delayed coking. Since the raw coke was still containing 10% of volatile species - mainly hydrogen - it had to undergo through a calcination process at 1300 °C. On this way a compound with less than 0.1 % of volatile species was obtained.

3.1.2 Coal-Tar Pitch

The ideal binder to be used with the petroleum-coke filler is the coal-tar pitch. It is a by-product of the coke production or coal gasification. The coal is heated up to 400-700 °C to obtain a solid fraction (coke) and a volatile one which, after being condensed, gives the coal-tar.

The tar composition varies widely depending on the used coal and the heating conditions in the coking oven. The coal-tar is typically distilled with a continuous method: it is heated up to 200 °C so water and light oils can be removed; then the remaining material is heated up to 400°C and dived into a fractionating column, where the distillate is separated into light oil, medium oil and heavy oil. What is remaining at the bottom of the fractionator is the coal-tar pitch. Its properties vary widely and they can be adjusted depending on the application of destination. The present compounds are thousands, mainly aromatics[33]: this is the main reason why this binder is the best one for electrographite production, since it is more graphitizable than any other material commercially feasible.

Approximately 70% of a typical binder is soluble in benzene, with an average molecular weight of 300. In the remaining 30% there is a fraction (9-16%) insoluble in quinoline, commonly referred to as "solid phase": it consists of carbon particles generally smaller than 10 μm in diameter, with a composition similar to the one of the whole pitch (table 3.2) except for the hydrogen content (2.6% instead of 4.2-4.5%).

Some fundamental properties owned by the binder are:

- Thermo-plasticity: the binder is solid at ambient temperature and fluid at higher temperatures (typical softening point is 100 °C);

- High carbon content, which can be easily deposited as bonding for the filler particles (carbon content in coal-tar pitch is 93% with 55%[34] of fixed carbon);

[33] A categorical statement of the composition of coal-tar pitch is impossible, but the C/H ration indicates the high content of aromatics.

[34] It is called also "coking value"

- High specific gravity, in the way to allow the deposition of the greatest number of carbon atoms in and around the filler coke particles (specific gravity is higher than any other binder: 1.3 g/cm^3)

Chemical constituents in coal-tar-pitch binders		
	Typical amounts found in literature	Recent Sample[35] measured by PGNAA
Total ash impurity [%]	0.03-0.3	n/a
Carbon [%]	92-93	95
Hydrogen [%]	4.2-4.5	4-4.5%
Sulfur [%]	0.6	0.56
Nitrogen [%]	1.1	n/a
Oxygen [%]	1.0-2.0	n/a
Chlorine [ppm]	n/a	130ppm

Table 3.2: Typical constituents of coal-tar pitch binders

As mentioned previously, the impurities content varies widely depending on the source of the coal and with the technique used in the pitch preparation. Typical values of impurities are 0.7 ppm boron and 7 ppm vanadium, but for nuclear graphite these levels drop to 0.2 ppm and 2 ppm respectively (due to the high capture cross section of such impurities).[36]

In the AVR reflector graphite, coal-tar pitch was used as binder, residual from the coal tar distillation. No more specific information are available. However, by comparing some impurity values found in literature with recent measurements of a modern-grade coal-tar pitch, it can be stated that no significant differences can be found in the composition (see table 3.2). Despite that, some further comparison with the carbon brick impurities showed that the coal-tar pitch used in the AVR formulation was much less pure (see section 3.3).

In conclusion, because of a strong variability of the impurities depending on their origin, it cannot be assumed that the one or the other is containing more impurities. In general, however, the coal-tar pitch binder is less pure than the petroleum coke (for example sulfur and chlorine are nearly the double in the pitch), so it can hypothesized that higher amount of impurities are present in the binder phase. However, the following treatments will remove part of these impurities.

[35] L. Szentmilklòsi, „PGNAA Analysis for Forschungszentrum Juelich“, 2011

[36] Many purification methods are available to remove many impurities: see chapter 6

3.2 The General Manufacture Process

3.2.1 CALCINATION

The first step to prepare the raw coke for the graphite manufacture is the calcination: the raw petroleum coke is heated up to 1300-1400 °C for few hours to remove the volatile hydrocarbons and to shrink the filler material before it is incorporated in the formed article. Normally a 25% weight loss occurs during the coke calcination, as a result of water loss (that was picked up when the coke was removed from the coker), volatile matter and dust losses. The calcination is a continuation of the cracking process: are present light tars and gases like H_2, CO_2, CO, CH_4. The removal of such gases from the edge of the larger aromatic arrays in the coke causes the disruption of carbon bonds. The crystalline order is then firstly reduced by the evolution of the volatiles and then thermal recrystallization occurs, leading to the increasing of the number of parallel layers. The hydrogen content of calcined coke is about 0.1%, but varies markedly with the calcining temperature.

It has to be underlined that differences in the particle shapes are due to the properties of the raw coke: a high degree of crystal alignment causes the material to fracture into flake or needle-shaped particles, whereas particle of less-ordered material are more cubical or spherical-shaped. The elongated particle shape causes the anisotropic properties of the crystal to be reflected in highly anisotropic properties of the graphite body. Some typical values of impurities embedded in calcined coke are listed in table 3.3. No data is available from a modern calcined coke.

Impurity	Range	Typicalvalue
Total ash impurity [%]	0.1-0.5	0.15
Silicon [ppm]	30-300	50
Iron [ppm]	30-1500	40
Vanadium [ppm]	3-500	15
Titanium [ppm]	1-20	10
Aluminium [ppm]	15-300	30
Manganese [ppm]	5-50	10
Nickel [ppm]	25-100	40
Calcium [ppm]	15-250	20
Magnesium [ppm]	5-50	10
Boron [ppm]	01-0.3	0.1

Table 3.3: Metallic impurities in calcined petroleum coke

3.2.2 CRUSHING AND SIZING

The calcined coke is screened and crushed to obtain particles with a diameter ranging from fractions of a millimiter to a centimeter. The material finer than 0.5 mm is milled and the so-called "flour" is obtained, with coke grains in the range of 2-300 μm. Coke particles and flour are stored in bins till the next mixing operation.

3.2.3 MIXING

A typical receipt for nuclear-grade graphite is a mixture of coke particles (0.4-0.8 mm) and coke flour (most of which is smaller than 200 μm in diameter) with a certain amount of binder. This depends strongly on the successive forming method: if the forming takes place by extrusion, the binder amount must be about 30 weight parts every 100 filler parts. When the binder is less than that, excessively high forming pressures are necessary, risking a material failure. When the binder is too much, the volatile evolution during the baking leads to a structurally weak material. If the forming process is the molding, the binder level can be varied in a wider range.

Normally some lubricant oil, pitch-insoluble, is added in about 3% in weight of the filler material, when the forming process is the extrusion. It is necessary to reduce the occurring frictions and it does not remain as carbon in the final product.

The mixing phase has the aim to produce a uniform distribution of filler and binder. Ideally, every filler particle should be covered with a binder film. The adopted technique is to mix at 170 °C in the way to fluidize the pitch, allowing it to flow between particles. After the mixing the article is cooled in rotating cylinders and sometimes water is used.

Concerning the AVR graphite, the detailed receipts are reported in section 3.3. However, the main size of the used particles was quite larger compared to the usual receipt. The filling dry material was mixed with the binder at 140 °C in a big mixing tool.

3.2.4 EXTRUSION

In the past, the extrusion process was the most commonly used to form the green article[37]. The reason of that is the semi-continuity of the process, economically convenient with the respect to the batch process of molding. Normally the extrusion press consists of a horizontal cylinder with a piston forcing the mixture through a die. At the end the so-called "green article" is produced, cooled with air or water and ready for the baking process. The problem

[37] The green article is the result of a mixture of filler coke and binder, ready for the first baking process to form baked carbon

resulting from such forming method stands on the particles orientation, i.e. the coke particles are oriented along the extrusion direction, leading to anisotropic graphite. It follows that many properties (e.g. the coefficient of thermal expansion, electrical and thermal conductivity, strength...) change significantly from the perpendicular to the parallel direction. The degree of anisotropy is influenced by the source of coke, which determines the main particle shape, and by the particle size. The anisotropy is lower when grains dimensions are higher. Graphite made from needle cokes have higher thermal and electrical conductivity and lower strength than similar graphite prepared from more isotropic cokes.

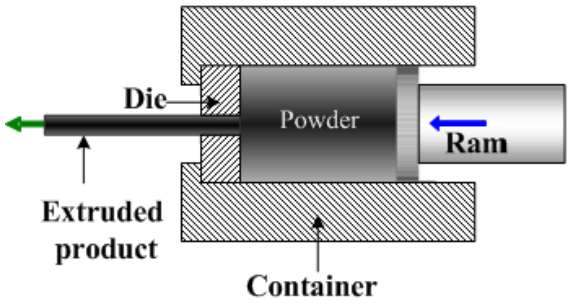

Figure 3.1: Scheme of the extrusion process

The AVR graphite was obtained through an extrusion process: the green body was molded at 100°C into an extrusion press. During the extrusion the green body was pressed through a heated shape with the dimensions of the successive graphite´s shape. The shape had been designed keeping into account the next shrinking during the graphitization process. The long shape was cut with the right dimension (350x350x1500 mm) and cooled with water.

3.2.5 MOLDING

The forming process of molding consists in compressing the filler-binder mixture in an enclosure of the desired shape. The resulting particle orientation is normal to the molding direction, giving an article with higher thermal and electrical conductivities and higher strength in the two directions normal to the molding force. This technique was abandoned in the past years since it is a batch process, more expensive and time consuming than the extrusion. A recent modification of such technique, called vibro-molding, showed the best results in the final product properties: the mechanically-produced vibration during the molding allows the random orientation of the particles, producing isotropic graphite at the end. Modern nuclear graphites are all produced via vibro-molding.

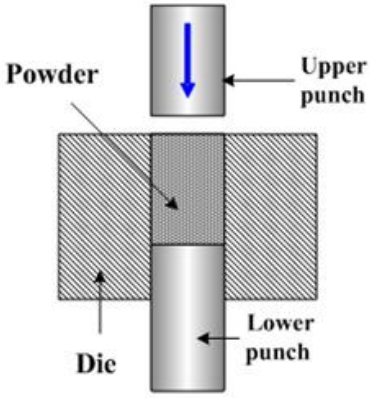

Figure 3.2: Scheme of a classical molding (not used anymore)

3.2.6 BAKING

The green article has to be baked to transform the binder in an infusible solid, maintaining the shape of the formed body. During the baking, in absence of air, pyrolysis of the binder occurs, generating a consistent amount of volatiles (10-12% of the article weight) which need to escape: the heating rate during volatilization must be low enough not to destroy the article. When the binder pyrolyses, large quantities of hydrogen are released, allowing polymerization and cross linking within the binder and between the binder and the filler materials. The temperature rises slowly while the flame is in contact with the baking chamber. To avoid green body cracking the temperature must follow a precise curve. The reached temperature is about 1000 °C (1150°C in the case of carbon brick desired as final product) and the articles experience normally a shrinkage of about 5% in volume: the volume of the binder is higher than the volume of the formed carbon, therefore carbonization results in the formation of pores, total relative volume of which (porosity) is determined by the binder quantity. Indeed the shrinking is proportional to the binder amount, so the usages of high binder fractions lead to a fragile structure with high internal stresses.

During the baking the green article is covered with packing material, a mixture of sand and calcined coke, which provides the necessary gas permeability and allows to prevent leaching of binder - becoming liquid during the baking – and its oxidation – due to the contact with air -. Typical time ranges for the baking process are in the order of some weeks (2-3), in addition to 2 more weeks for the cooling down (slow to avoid disruptions) and unpacking.

The baked carbon properties depend strongly on the final baking temperature, the crystallinity degree of the coke, the ratio particles/flour. At this stage, carbon is very brittle and difficult to machine. On the other hand, it shows low density (1.6 g/cm^3) and low thermal conductivity

(0.010 cal/sec cm °C), high coefficient of thermal expansion ($2 \cdot 10^{-6}$ 25-100 °C), high elastic modulus and high porosity (26%). Because of its properties, baked carbon is susceptible to thermal shock. Concerning chemical properties, large variations are observed so this intermediate product was not investigated in the past as the raw materials or the finished graphite.

In the case of AVR graphite the manufacture process was a standard one: the heating speed during the binder coking phase (between 350 and 500 °C) was 1-2 °C/h. Starting from 500 °C, temperature raised rapidly up to 1000 °C and stayed constant for 3 weeks. No information on the cooling step are available. In fig. 3.3 a virgin sample of carbon brick, used as insulator around the core, is shown. It can be noticed how much it is brittle and easily crushable.

Figure 3.3: Block of AVR Carbon Brick

In table 3.4 some values of important radionuclides´ precursors are reported. Concentration values have been obtained by PGNAA.[38]

Element	Mass Fraction Carbon Brick	Mass Fraction Modern Coal-tar Pitch
Li-6	n/a	n/a
B	7.7 ppm	0.79 ppm
N	0.6 %	n/a
S	0.65 %	0.56 %
Cl	50 ppm	130 ppm
Co	11 ppm	n/a

Table 3.4: Comparison among different impurities of AVR carbon brick and a modern coal-tar pitch

[38] Zsolt Révay, "*Prompt Gamma Neutron Activation Analysis*", December 2010, Nuclear Research Department, Institute of Isotopes, HAS, Budapest, Konkoly-Thege Miklosutca 29-33. 1121 Hungary

By performing a comparison among the values of a modern coal-tar pitch and some impurities found in the baked carbon it can be evinced that the original receipt involved less pure materials from the point of view of some impurities. A more detailed comparison is reported in section 3.4.

3.2.7 IMPREGNATIONS

The usage purposes of nuclear graphite request different (improved) properties than the one showed by the baked carbon. First of all, the porosity is far too high: the impregnation process has the aim to increase the density by reducing the porous volume. The basic idea is the same as the one used to produce baked carbon: using a binder that, after pyrolysis, deposits carbon in the voids. The coal-tar pitch is used here too, but its characteristics are different from the binder one: the heavier fractions normally present in a binder pitch are here missing. Typically the C/H ratio is 1.62 and 15% of the pitch is benzene soluble. The specific gravity is about 1.25 g/cm^3 with a softening point around 100°C.

The pitch is pre-heated to allow a deep penetration into the baked carbon´s structure. An autoclave is normally used with a temperature of about 200 °C: it is filled with baked carbon, then sealed and partially evacuated to remove some of the air from the pores. Then the pitch is injected with about 7 bar pressure for several hours: it is forced pneumatically to reach the whole available porosity and to fill it. At last the article is cooled with spray water.

In the case of AVR, after the first baking an impregnation process took place in 2 steps: firstly the impregnation chamber was evacuated and vacuum was established. Afterwards, coal tar pitch in pressure was inserted. After the impregnation, the impregnation pitch was baked with another baking.

Some density calculations performed with 10 massive samples extracted from a big block of AVR graphite and carbon brick, revealed a nearly homogeneous density, at least within the measurement uncertainties (±20 kg/m^3), with a mean value of 1.73 kg/m^3 for the graphite and 1.55 kg/m3 for the AVR carbon brick. From that, it can be affirmed that the original impregnation was well performed leading to a nearly homogeneous distribution of the pitch in the graphite blocks.

3.2.8 GRAPHITIZATION

Purpose of the graphitization process is to affect the crystal orientation and growth and to perfect the internal order: the amorphous precursor carbon transforms into crystalline graphite. The maximum temperature reached during this step is about 2800-3000 °C.

During the heating up step, which lasts in a couple of days with a heating rate of about 1°C/min, many different situations take place. Most of the hydrogen, for example, is released up to 1500 °C: the remaining material is carbon and metallic impurities. In the range 1500-2500 °C a crystal growth takes place, leading to a higher degree of crystallinity; a reduction of interlayer spacing is observed with a contemporary reduction of defects, improvement of stacking, suppression of vacations and dislocation. Above 2500 °C there is still a little crystal growth but the dominant effects are diffusion and annealing of crystallite imperfections. The high-temperature step lasts about 1-2 days, then long time is necessary to cool down the final product (up to 2 weeks to avoid excessive internal stresses and disruptions, see fig. 3.4). With this last step the final product shows a macroscopic density, electrical and thermal conductivity increase, while Young modulus, strength and expanding coefficient decrease.

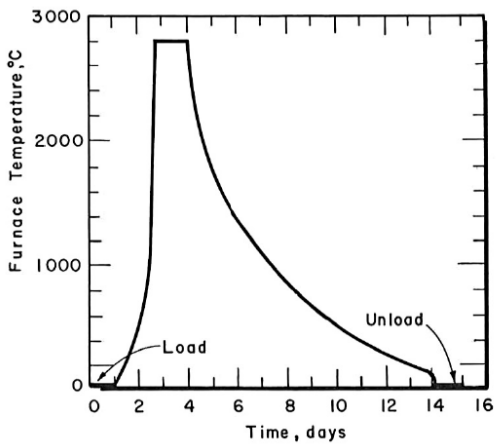

Figure 3.4: Typical time-temperature cycle for a large graphitizing furnace

The most used furnace is the Acheson one, invented in 1895 and originally used to produce silicon carbide. It is an electric furnace able to reach 3000°C. It consists of a horizontal bed of fire-brick tiles laid over concrete piers. At the extremes of the bed concrete head are placed, through which graphite electrodes carry the current inside the furnace. The baked bars (typically cylindrical) are stacked transversely in the furnace and the intervening spaces are filled with granular coke. The coke pack is sized in the way to afford the correct resistance for electrical heating (especially in the last stages). At last, the pack is surrounded by finely ground silicon carbide, coke and sand to provide thermal insulation. This type of furnace is preferable

to the Castner one since the heat is carried indirectly to the carbon bars through the granular coke.

For the point of view of this study, the graphitization process is of extreme importance, since there are many factors that are influencing the final product. In particular, the process first takes place under air. Because of the very high temperature all the reactions are very fast, so assuming that all the packing material is porous and doing a parallelism with the oxidation regimes typical of graphites, the boundary layer diffusion-controlled regime takes place. Indeed, the diffusion of oxygen through the packing material (SiC, sand, coke particles) is the limiting step. At sufficiently high temperatures even nitrogen starts to react, and the ambient that is establishing around the graphite is mainly composed by CO and H_2 coming from the pyrolysis of the hydrocarbons, both in the packing material and in the product itself. The most interesting step is the cooling one: it takes weeks, during which all the reaction are gradually shifting because of thermodynamic reasons. In particular, starting from high temperatures, the predominant gaseous species that are present during such step are CO and H_2 resulting from pyrolysis and N_2 from air, since oxygen is confined to the boundary up to a certain temperature. An important reaction that could take place during such step is the reversed Bouduard one:

$$2CO \Leftrightarrow CO_2 + C$$

According to Ellingham diagram, the overall free energy change of formation of CO_2 by oxidation of carbon is almost constant and indifferent of the temperature, while the free energy change of formation of CO is a decreasing line (with the temperature). These lines meet at 700 °C, so the Bouduard reaction implies that at higher temperatures the equilibrium is shifted to the endothermic formation of carbon monoxide, while at lower temperatures the equilibrium is shifted to the exothermic carbon dioxide side. In other words, at temperatures lower than 700 °C there is a massive formation of carbon particles, which could deposit on every available surface and/or forming bondings on the crystallite boundaries: since there are not sufficient conditions to let those particles aggregate or to be embedded in the graphite lattice, they can only deposit and/or chemically bond the porous structure of graphite (edge surfaces of crystallites, grains' surfaces, etc.), together with nitrogen and hydrogen. Considering that the porous structure is focused in the binder phase, generally less graphitized than the filler one, most of the available surface can be found here, so this is the first one which probably will react in a thermal treatment. In addition, the deposited carbon particles are expected to be quite small, obtaining in such way a considerable large surface area. It is

expected that those superficial carbon particles will react as first during a successive thermal treatment at a certain temperature, supposedly near or lower than 700 °C.

In the case of AVR graphite, the graphitization took place in electrical resistance furnaces of the Acheson type (see fig. 3.5). Many layers were created, surrounded with coke powder, and electricity go through them, raising the temperature up to 2800-3000°C. The furnace was insulated with silicon carbides (all around the graphite pieces) and the high temperature was maintained for 2 days.

An overview of the whole manufacture process is shown in fig. 3.6.

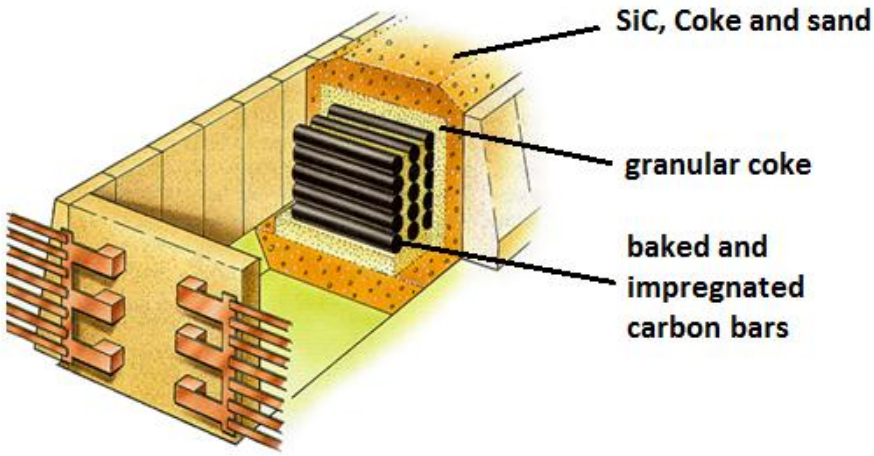

Figure 3.5: View of an Acheson furnace

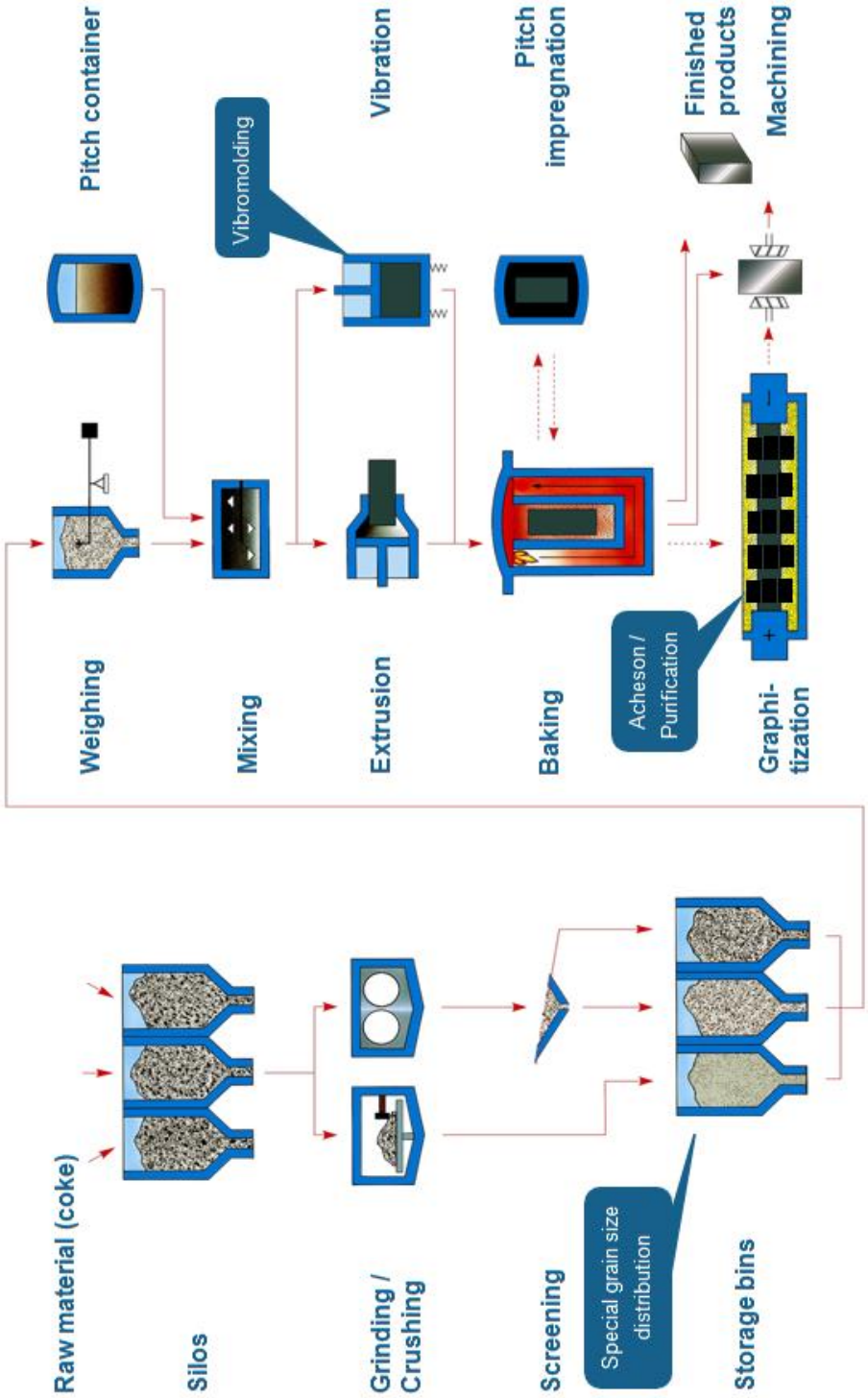

Figure 3.6: General scheme of the graphite manufacture process

3.2.9 THE FINAL PRODUCT

The raw materials influence to some extent the physical properties and impurities of graphite, together with the production process and the geometry of the finished piece. It is not possible to give a general set of properties for all nuclear graphites: they are produced with the objectives of obtaining high purity, high density, high isotropy and as much as possible resistance to radiation damage, but the specialized grades showing such properties may sacrifice other properties to attain these ends. For that, each application represents to some degree a unique problem.

For what concerns the AVR carbonaceous materials, the manufacture process was thought mainly to fulfill the requirements of operation, not reflecting the implications for waste management.

It is interesting to perform a comparison of some impurities among AVR reflector graphite and a modern coal-tar pitch. The atomic fractions for each element were obtained through PGNAA (Prompt Gamma Neutron Activation Analysis). The results are showed in a semi-logarithmic plot in fig. 3.7. It can be noticed that the AVR graphite is generally more pure than the modern coal-tar pitch, with the exception for Boron and Potassium. In particular, the sulfur fraction in the former is about 3 orders of magnitude lower than in the latter. Moreover, the hydrogen content in AVR graphite showed to be comparable with the one in the pitch.

Some typical pitch values, found in literature[39], showed about 4 times higher content of sulfur and hydrogen than a modern coal-tar pitch. Other impurity values were not available but, as a general observation, it can be stated that modern pitches are purer than the one used 60 years ago.

The interpretation of that result must take into consideration that AVR graphite was manufactured decades ago, with many uncertainties in the original receipt (see section 3.3) and without a well-developed process for nuclear graphite. Moreover, the impurities fractions in the original coal-tar pitch are unknown.

Considering the historical background, the high impurities levels in the AVR reflector graphite are not totally surprising. In particular Potassium and especially Boron resulted in higher mole fractions in the graphite than in the pitch. It is reasonable to expect then high impurities activation and higher neutron capture during the reactor operation than modern-grade graphites.

[39] R.E. Nightingale, "*Nuclear Graphite"* ed. 1962..New York and London: Academic Press

In recent times it was firstly thought to reproduce the virgin materials to perform some characterization studies but, because of the lacking of knowledge and because of the unavailability of the original raw materials, it resulted to be not feasible. Fortunately some unused graphite remained from the reactor building and allowed the performance of some studies (see chapters 7-8-9-10-11).

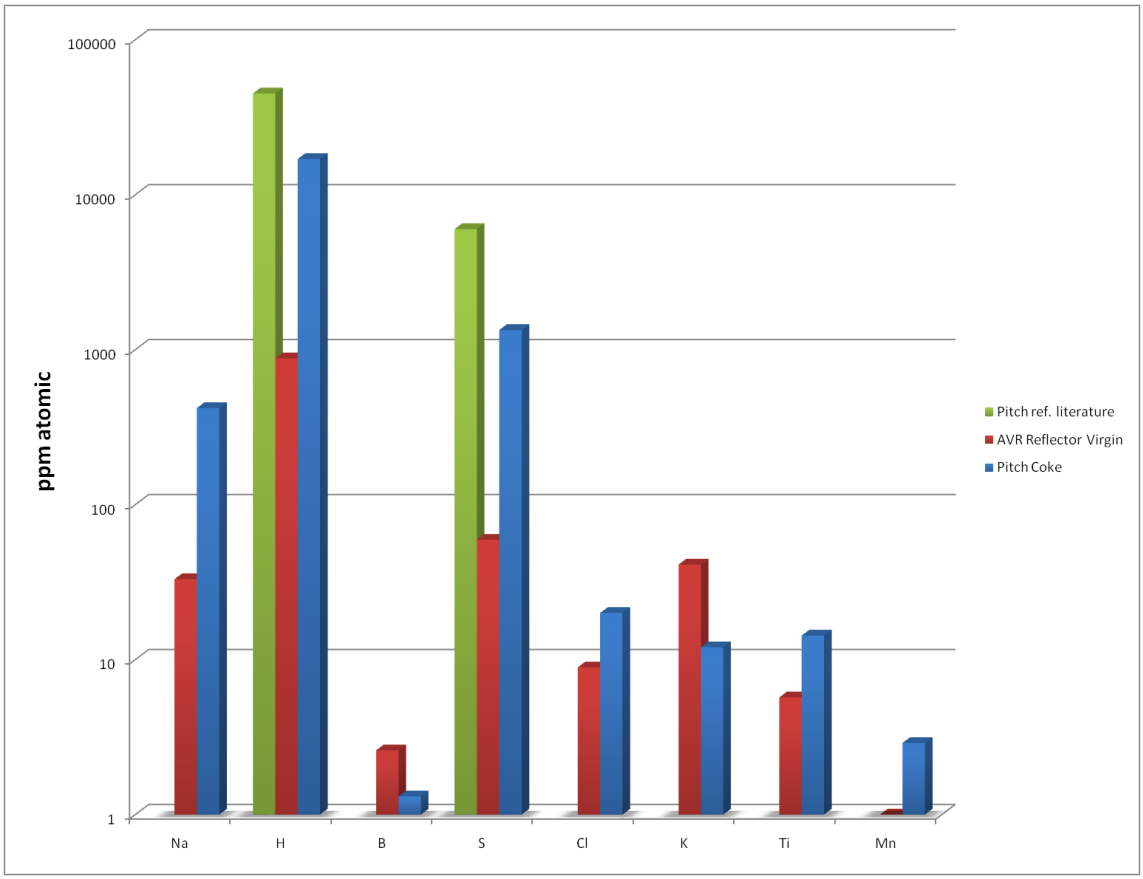

Figure 3.7: Comparison among some impurities of AVR reflector virgin graphite, a modern coal-tar pitch and values found in literature

3.3 AVR Graphite: Original Formulation

It was not easy to retrieve the original receipt for the AVR, built more than 50 years ago. Unfortunately many aspects are still unclear since the author himself was not able to provide more accurate information.

The inner graphite reflector consists of 315 graphite blocks. For the production, the inner reflector blocks were made in format 350x350x1500 mm. The production took place in a finely granular formulation with Shell coke grains (experiment 047/61 and 039/62):

Shell coke H110	0,75 - 1,0 mm	10 parts
Shell coke H110	0,4 - 0,75 mm	10 parts
Shell coke H110	1,0 - 4,0 mm	35 parts
Shell coke H110	dust	38 parts
Reactor graphite without iron	0-0,4 mm	7 parts

Additional 0,5 % HX (hexachlorobenzene) [40] used, based on 100 parts dried. Hexachlorobenzene was used as a porosity control agent in the manufacture of graphite.

Sometimes there was also a rough recipe (TE1) with up to 4 mm grain used (experiment 023/62):

Shell coke H110	1 - 4 mm	35 parts
Shell coke H110	0,75 - 1,0 mm	10 parts
Shell coke H110	0,4 - 0,75 mm	10 parts
Shell coke H110	dust	38 parts
Reactor graphite without iron	0-0,4 mm	7 parts

Additional 0,5 % HX (hexachlorobenzene) used, based on 100 dry parts.

Or (experiment 058/62):

Shell coke H110	1 - 4 mm	54 parts
Shell coke H110	0,75 - 1,0 mm	3 parts
Shell coke H110	0,4 - 0,75 mm	7 parts
Shell coke H110	dust	36 parts

Additional 0,5 % HX (hexachlorobenzene) used, based on 100 dry parts.

It is unclear in which proportions the various formulations were delivered.

[40] IARC Monographs Volume 79

The bottom layer was not made in the way it was thought firstly, i.e. with carbon bricks, but it was made in graphite.

Required blocks of this were in the format 500x500x2500mm. It was initially tried as material prepared by extrusion. The experiments were not successful (block cracked at the edges), since at that time there was too little experience in the extrusion of large sized rectangular block.

The blocks were then crushed in the formulation (experiment 065/62):

Graphite	4 - 10 mm	10 parts
Coke P4 mixture	1 - 4 mm	40 parts
Coke P4 mixture	0,75 - 1 mm	10 parts
Coke P4 mixture	powder	40 parts

Additives:	English rot[41]	0,7 parts*
	HX	0,5 parts*

* based on 100 dry parts.

It can be notices that all the different recipes implied relatively big particles (larger than 1 mm in diameter) than the normal sizes found in literature. Indeed, even a visual inspection of the AVR graphite, compared to a more recent one, can lead to this conclusion (see pictures 3.8 and 3.9).

Figure 3.8: View of a massive sample of AVR graphite

Figure 3.9:View of an unknown-grade graphite

[41] Unknown additive

3.4 AVR Carbon Brick: Original Formulation

The material was produced in November-December 1961 in Griesheim through molding with recipe B18/33:

Anthracite	4 - 10 mm	12 parts
Anthracite	1 - 4 mm	19 parts
Anthracite	0 - 1 mm	6 parts
Waste block from	1 - 4 mm	7 parts
the furnace	0 - 1 mm	6 parts
Zechen coke dust		50 parts

Additives:	Sulfur	3 parts*
	Tar	2,5 parts*

* based on 100 dry parts.

Due to production requirements the recipe of the carbon brick was changed starting from March 1963 (recipe B18/47):

Anthracite	4 - 10 mm	7 parts
Anthracite	1 - 4 mm	10 parts
Anthracite	0 - 1 mm	4 parts
Graphite	4 - 10 mm	5 parts
Graphite	1 - 4 mm	5 parts
Waste block from	1 - 4 mm	14 parts
the furnace	0 - 1 mm	6 parts
Zechen coke dust		49 parts
(from the annular oven)		

Additives:	Sulfur	3 parts*
	Tar	2,5-3 parts*

* based on 100 parts dried.

It is unclear in which proportions the various formulations were delivered. The first bottom layer was done in graphite instead of baked carbon.

Looking at the recipe, the presence of Sulfur has to be underlined, added in order to inhibit the graphitization of the green article. In fact, the aim of the baked carbon was to thermally-

insulate the reactor core, so it had to be as less as possible conductive: such requirements could be achieved with a low degree of crystallinity. On the other hand, the sulfur is an impurity that can be activated (see chapter 4).

PGNAA results allowed performing some comparisons among the two AVR carbon brick grades and the AVR reflector graphite (fig. 3.10). A view of a massive sample of AVR carbon brick is reported in fig. 3.11.
It can be stated that the AVR graphite is more pure than carbon brick of both formulations: this is due to the graphitization process which allowed a thermal purification.
By comparing the different impurities amounts of the four materials it can be evinced that the coal-tar pitch used in the formulation of the AVR carbonaceous materials, was much less pure that a modern-grade one.

In addition, considering the two Carbon Bricks recipes, the slightly higher purity of the second type can be explained with the usage of graphite among the raw materials: a high purity material was mixed with the other raw materials, resulting in a total higher mean purity. In general, it is expected a higher amount of activation products in the carbon brick than in the graphite, fact confirmed by many investigations and measurements (see chapter 4).

In conclusion, it has been proven that one of the most important sources of impurities is represented by the manufacture process together with the raw materials. In addition it can be expected the presence of CO and hydrogen bound with the structure, together with elemental carbon (chemisorbed on the crystallite surfaces) probably formed in the cooling down step of graphitization process. However, other sources of radionuclides´ precursors are for example nitrogen coming from air, which is likely to be chemisorbed on the graphite surfaces, in addition to the one probably already bound from the manufacture process. The variables on the impurities nature are several, so many uncertainties are still remaining. With the present study some of them will be particularly investigated, as the effective high surface concentration of nitrogen for example.

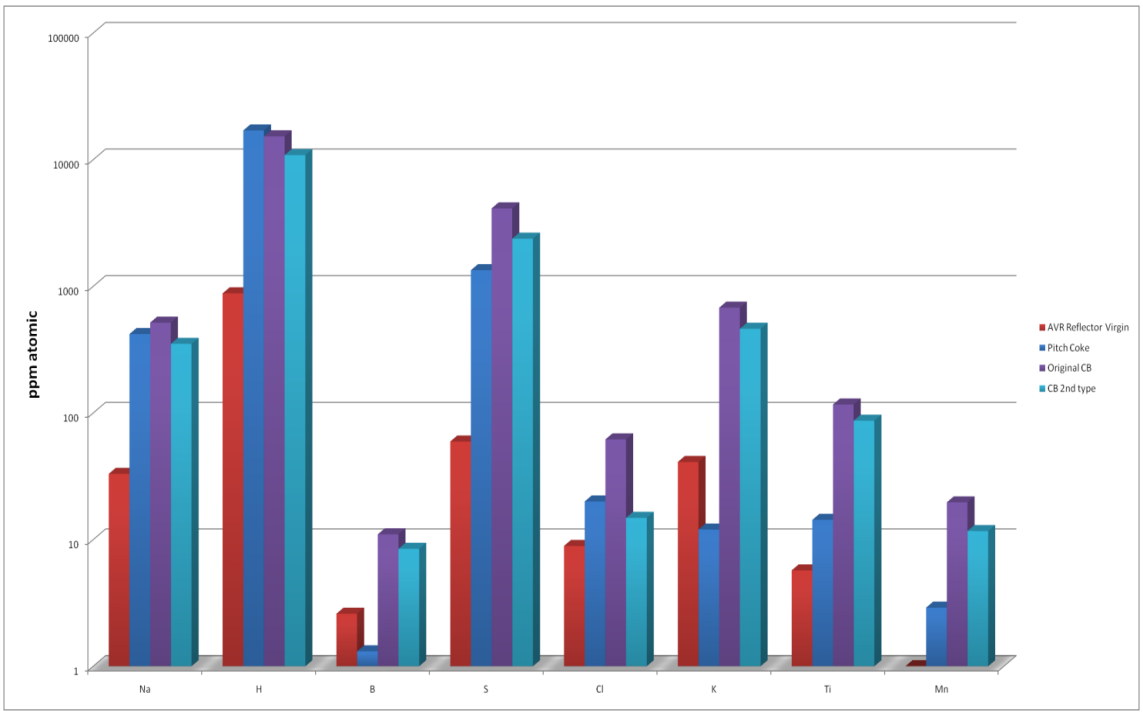

Figure 3.10: Impurities in AVR reflector graphite, Modern Pitch and Carbon bricks of two formulations

Figure 3.11: View of a massive sample of AVR carbon brick

4. Radionuclides in i-graphite: Inventory and Creation Mechanisms

In this chapter some of the most important radionuclides, from the point of view of their leaching behaviour and activity, are analysed. After an overview of the estimated inventory in the AVR some selected isotopes will be considered together with their creation mechanism: a fundamental approach to understand the position and distribution of radionuclides inside the graphite matrix is the study of nuclear reactions, which lead to the identification of the main precursors and of their possible locations. This knowledge can be of fundamental importance in order to establish a selective purification process.

4.1 Radionuclide Inventory and Distribution inside the AVR

It is difficult to measure/calculate precisely the activity inside the AVR for many reasons. The reactor is heavily contaminated (in some critical publications, it has been labelled as the most beta-contaminated reactor worldwide[42], except for those with severe accidents). Due to the pebble bed core direct measurements are extremely difficult as there are no access ways except the fuel loading tubes. After the end of operation a borehole was drilled through the side of the vessel and reflector structures to collect some small samples by introducing a probe inside the reactor core and making some visual inspections. After the measurement, the distribution of the different radionuclides was calculated taking into account the neutron flux distribution. Indeed, depending on the samples location, some uncertainties remain in subsequent inventory calculations. Due to the access restrictions it is not possible, for a more precise estimation, collecting many samples from different core regions and using them as references to verify an activation-diffusion model in the way to obtain a radionuclide mapping. The difficulties on this approach are several, considering that different fuel types were employed, temperature profiles inside the core were affected by high uncertainties, pebbles friction led to high amounts of dust production, the water-ingress accident of 1978 washed out much radioactivity and many other influencing factors. It can be stated, anyway, that the activity distribution shows some residual uncertainties.

[42] R. Moormann, "*A safety Re-Evaluation of the AVR*", Forschungszentrum Jülich, Jül-4275

More in detail, as an example, the graphite reflector can be considered:

- Top reflector: highest temperatures and considerable neutron fluence: high impurity activation and nuclide migration by diffusion are expected. (fluence= $1.5 \cdot 10^{21}$ cm^{-2} EDN, T= 1000 °C)[43]
- Upper side reflector: relatively high temperatures and highest neutron fluence: high impurity activation and nuclide migration by diffusion are expected. (fluence= $6.5 \cdot 10^{21}$ cm^{-2} EDN, T= 650 °C)
- Bottom: low temperatures, relatively low neutron fluence, high contamination (^{90}Sr and ^{137}Cs are mainly bound on dust[44]) due to pebble friction / wear and dust sedimentation.

Some calculations, referred to the year 2004[45], allowed to provide an estimation of the activity distribution in the reactor primary systems (see Table 4.1 and 4.2).

Nuclide	Activity (Bq)
H3	3.2 E15
Sr90	6.9 E13
C14	2.9 E14
Cs137	4.5E13
Co60	1.5 E14

Table 4.1: Estimation of main contaminants of primary systems (basis 2004)

Location	Activity (Bq)
Reactor Vessel	ca. 3.8 E15
Confinement Vessel	ca. 3.0 E12
Ring Building	ca. 1.0 E11
Warm workshop	ca. 5.0 E10

Table 4.2: Estimation of the activity distribution in the AVR plant (basis 2004)

[43] Association of GermanEngineers (VDI) - The society for energy technologies (PUBL.), "*AVR - Experimental High Temperature Reactor 21 years of successfull operation for a future energy technology*", VDI Verlag, Düsseldorf, 1990

[44] R. Moormann, "*A safety Re-Evaluation of the AVR*", Forschungszentrum Jülich, Jül-4275

[45] Proceedings of the 11th International Conference on environmental Remediation and Radioactive waste Management, ICEM2007, "*The AVR (HTGR) decommissioning project with new strategy*"

Considering the graphite reflector and the carbon brick insulator, at the end of 1988[46] the radionuclide inventory, reported in table 4.3, was calculated. What can be noticed is the higher amount of activity in the carbon brick insulator compared to the graphite one. The reason of that is the presence of high amount of impurities, leading to nuclear activation even with lower neutron fluence than the one in the reflector (some authors considered a medium neutron flux of $4 \cdot 10^{13}$ in the reflector and $1 \cdot 10^{13}$ in the insulator[47]). [48]Fission products are present due to diffusion through the fuel pebbles[49] and the reflector.

[46] Calculation performed at the end of 1988, Ref.: T. Podruzhina, "*Graphite as Radioactive waste: Corrosion behaviour under final repository conditions and thermal treatment*", Forschungszentrum Jülich, Institut für Sicherheitsforschung und Reaktortechnik Jül-4166

[47] P.G. Fischer, "*Verhalten von tritium in Reaktorgraphiten*", 1975

[48] Neutron fluence at the carbon bricks side is unknown

[49] Fission product were released by inferior-grade fuel pebbles at the beginning of the operation and possibly due to unexpected excessively high temperatures in the core

Radio nuclide	Half Life [y]	Total Activity [Bq]						Ratio Baked Carbon/Graphite[50]
		Reflector Graphite	Activity at the end of 2012	Specific Activity [51][Bq/g]	Baked Carbon	Activity at the end of 2012	Specific Activity [Bq/g]	
H-3	12.33	8.8 E14[52]	2.28 E14	3.4 E06	6.9 E15	1.79 E15	11.33 E06	3.33
C-14	5730	4.6 E12	4.587 E12	6.85 E04	2.9 E14	2.89 E14	1.83 E06	21
Cl-36	301000	1.5 E09	1.5 E09	2.24 E01	5.9 E10	5.9 E10	3.73 E02	16.65
Ca-41	102000	5.8 E10	5.8 E10	8.5 E02	4.5 E11	4.5 E11	2.8 E03	3.3
Fe-55	2.73	1.1 E15	2.48 E12	3.7 E04	4.0 E15	9 E12	56.9 E03	1.54
Co-60	5.271	4.2 E13	1.788 E12	2.67 E04	1.1 E15	4.68 E13	2.96 E05	11
Ni-63	100.1	4.1 E12	3.47 E12	5.18 E04	8.2 E12	6.94 E12	4.4 E04	0.85
Tc-99	211112	2.8 E07	2.8 E07	4.2 E-01	3.5 E07	3.5 E07	2.2 E-01	0.52
Cs-134	2.1	8.9 E11	3.23 E08	4.82	3.1 E13	1.12 E10	7.1 E01	14.7
Cs-137	30.2	6.5 E11[53]	5.53 E11	8.25 E03	7.9 E12[54]	6.73 E12	4.26 E04	5.16
Ba-133	10.54	3.5 E11	7.22 E10	1 E03	7.1 E11	1.465 E11	9.27 E02	0.93
Sm-151	90	4.5 E08	3.74 E08	5.58	1.8 E10	1.5 E10	9.5 E01	17
Eu-152	13.3	1.4 E07	4 E06	6 E-2	2.9 E07	8.3 E06	5.2 E-02	0.87
Eu-154	8.8	1.5 E11	2.265 E10	3.4 E02	3.0 E11	4.53 E10	2.87 E02	0.84
Eu-155	4.8	6.3 E10	1.97 E09	2.9 E-01	2.5 E12	7.8 E10	4.94 E02	1700
Ho-166m1	1200	2.2 E09	2.17 E09	3.3 E-01	4.3 E10	4.24 E10	2.68 E02	812
Sr-90	28.8	6.7 E11[55]	4.52 E11	6.75 E03	7.9 E12	5.33 E12	3.37 E04	12

Table 4.3: Radionuclide inventory estimation in AVR reflector graphite and Carbon Brick

Before stating any consideration it is important to underline that the macroscopic distribution of activity is absolutely not homogeneous, as confirmed by some measurements on small samples. In table 4.4 some values of specific activity of an exemplary sample are reported. The specimen was taken by drilling the AVR at different locations in the side reflector.

[50] The ratio is calculated considering the specific values in Bq/g

[51] The specific activity has to be intended as a rough mean one, but the value is not reliable since the radioactivity distribution is absolutely not homogeneous. It has been considered 67 tons graphite and 158 tons carbon brick

[52] Calculation performed at the end of 1988, Ref.: T. Podruzhina, "*Graphite as Radioactive waste: Corrosion behaviour under final repository conditions and thermal treatment*", Forschungszentrum Jülich, Institut für Sicherheitsforschung und Reaktortechnik Jül-4166

[53]Basis 2005 from M. Florjan, ""*Dekontamination von NukleargraphitdurchthermischeBehandlung*", Jul-4322, 2009

[54] Idem

[55] M. Florjan, "*Dekontamination von Nukleargraphitdurchthermische Behandlung*", FZJ-4322, 2009, valuere ported to year 2012

Nuclide	Graphite			Carbon Brick		
	Specific Activity 1999 [Bq/g]	Specific Activity 2012 [Bq/g]	Error [%]	Specific Activity 1999 [Bq/g]	Specific Activity 2012 [Bq/g]	Error [%]
H-3	1.2 E06	5.78 E06	30	3.8 E07	1.83 E07	30
C-14	63 E03	62.9 E03	20	3.7 E06	3.69 E06	20
Cl-36	24	24	50	800	800	50
Ca-41	<5000	<5000	50	DL		n/a
Fe-55	2.55 E03	94	20	1.22 E06	4.5 E04	20
Co-60	41 E05	7.4 E05	15	2.4 E06	4.34 E05	60
Sr-90	92 E05	6.73 E05	20	8.3 E03	6 E03	15
Cs-134	<210	<3		13 E03	178	60
Cs-137	4.4 E03	3.26 E03	15	4.4 E03	3.26 E03	60
Eu-152	<150	76.2		DL		
Eu-154	99.7 E03	35.8 E03	10	9 E04	3.2 E04	60
Eu-155	2.1 E03	321	15	3.75 E04	5.7 E03	60

Table 4.4: Exemplary results of a graphite sample and a carbon brick sample[56]

[56] B. Bisplinghoff, M. Lochny, J.Fachinger, H. Bruecher, "*Radiochemical characterisation of graphite from Juelich experimental reactor (AVR)",* InstitutfuerSicherheitforschung und Reaktortechnik, FZJ, 1999

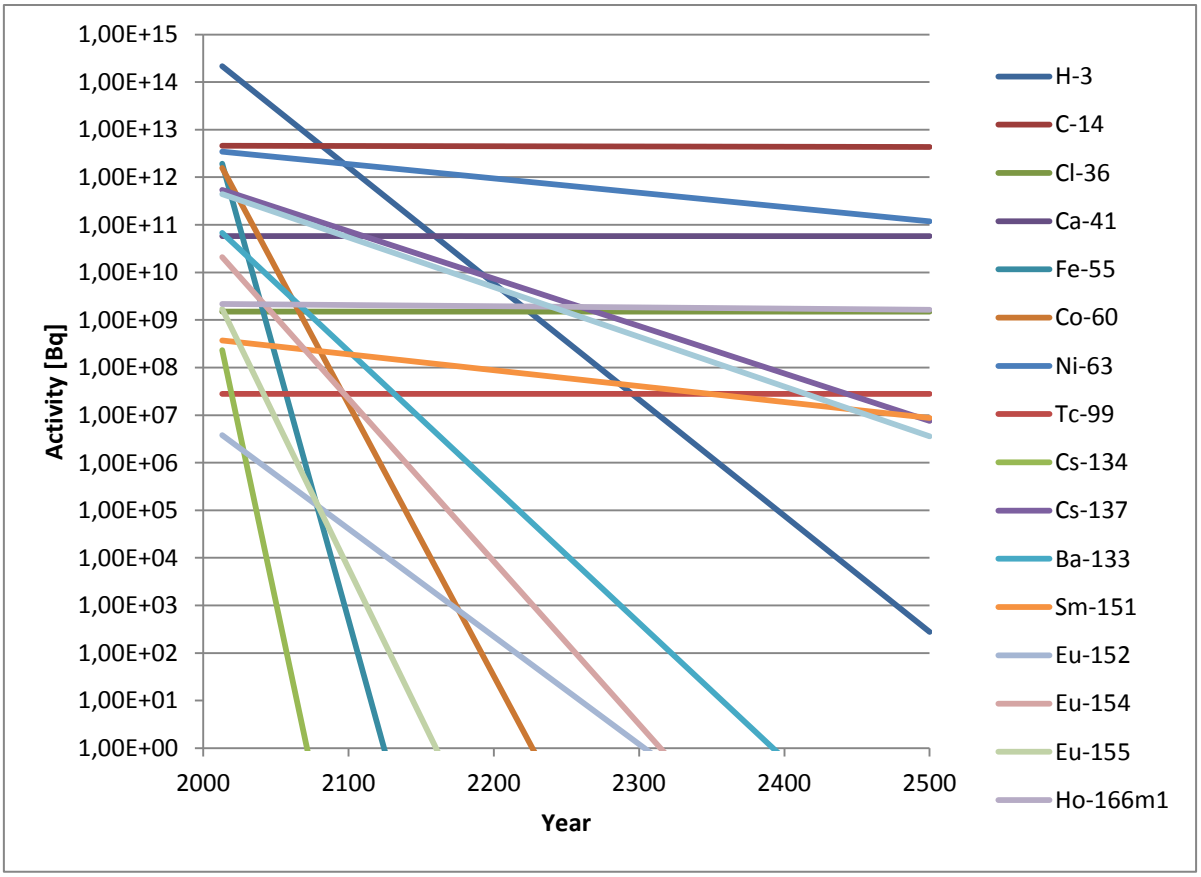

Figure 4.1: Radioactive decay of the AVR reflector inventory referred to table 4.3

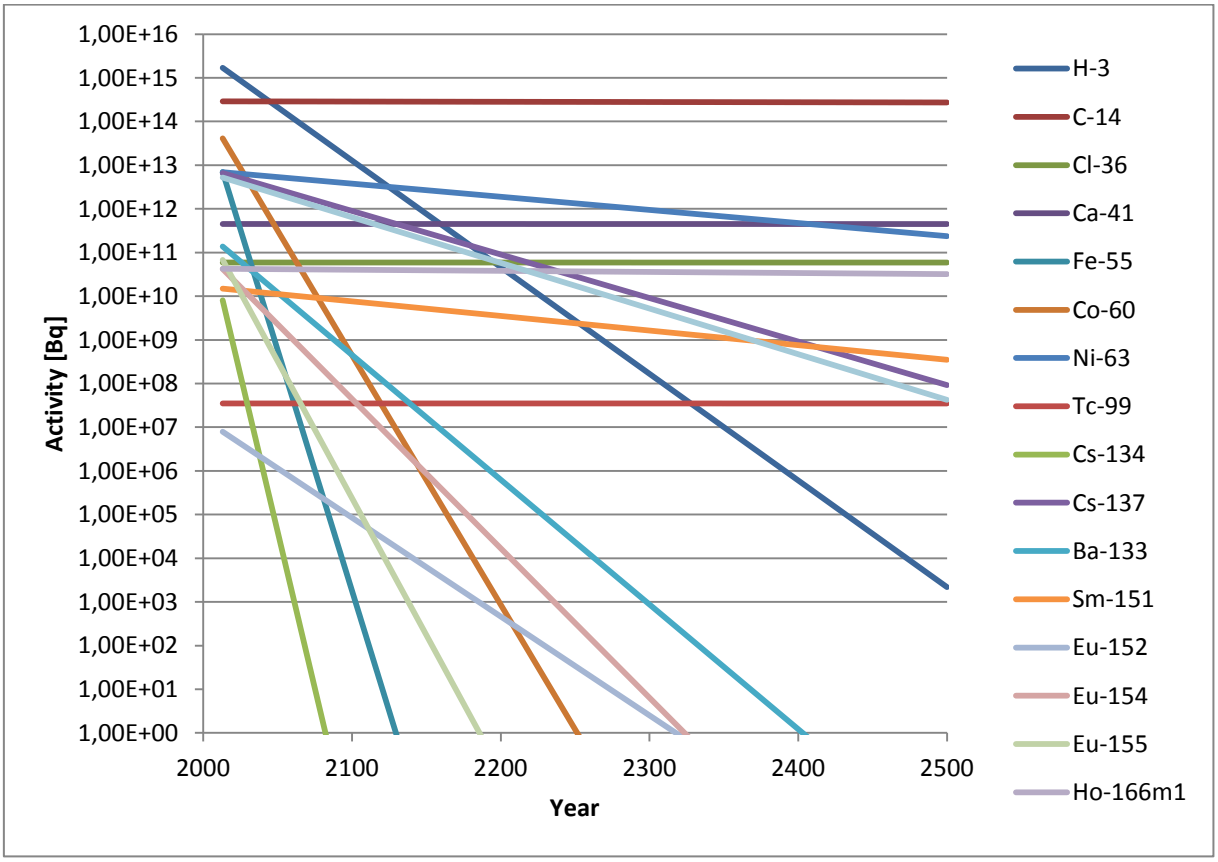

Figure 4.2: Radioactive decay of the AVR reflector inventory referred to table 4.3

By observing tables 4.3 and 4.4 and figs. 4.1 and 4.2 it can be stated that after a reasonable amount of time, in the order of decades, the short-lived isotopes will not represent a problem anymore. For example, in the year 2100 Cs-134 will be completely decayed, both in the reflector and the carbon brick insulator; Fe-55, Eu-152 and Eu-155 will have very low specific activities[57]. Similar considerations could be performed by observing figs. 4.1 and 4.2, but what has to be underlined is that many radionuclides, because of their long half-life, are not decaying in a significant way, representing so a problem for the future generations even after hundreds of years. From these statements, the "safe-enclosure" strategy is effective only for some crucial species, as tritium whose activity will be decayed of 3 orders of magnitude by year 2100 and Co-60 with 6 orders of magnitude of activity depletion.

Even though there are high uncertainties and discordances among different radionuclide inventories, estimated along the past years, it is evident that most of the activity is constituted by ^{3}H and ^{14}C. Other isotopes show important activities, as Fe-55 and Co-60, but their half-lives are quite short and, by waiting long enough time, their leaching behaviour will not be as critical as the one for ^{3}H and ^{14}C. In the present study Cl-36 is also considered, not because of its high overall activity but because it is highly soluble in water and mobile in the environment, depending on its chemical form.[58]

[57] Considering a homogeneous distribution over the entire reflector/insulator. It is an ideal consideration to give some information about the necessary time-scale to obtain reasonable activity depletions

[58] C. Vaudey, N. Toulhoat, N. Moncoffre, N. Bérerd, "*Chlorine speciation in nuclear graphite: consequences on temperature release and on leaching*", 2010

4.2 Radionuclides: Formation Mechanisms

In this section the main formation mechanisms of impurities by neutron activation will be analysed, in order to identify the main radionuclides´ precursors and to better understand the different sources.

4.2.1 Carbon 14

Carbon-14 is a long-lived radionuclide with a half-life of 5730 years. It represents one of the most active isotopes present in the AVR and, more in general, in many other reactor types. Many routes, resulting in the creation of radiocarbon, are possible; the most important are listed in table 4.5. The relative importance of the one or the other reaction depends on the reactor type and on many other factors. For example, reaction 1 will be important only in the HTGRs, while reactions 2 and 4 will occur in all reactors containing nitrogen as an impurity in the fuel, coolant, or structural materials. Reactions 3 and 5 occur in any reactor containing heavy-metal oxide fuels and/or water as coolant (or possibly as impurity present from the reactor construction of from a leakage in the steam-production line).

n	Reaction
1	$^{13}C(n,g)^{14}C$
2	$^{14}N(n,p)^{14}C$
3	$^{17}O(n,\alpha)^{14}C$
4	$^{15}N(fn,d)^{14}C$
5	$^{16}O(fn,^{3}He)^{14}C$

Table 4.5: Main neutron-activation reactions leading to C-14 production

Some nuclear databases have been consulted to do some considerations about the most important neutron reactions occurring in nuclear reactors. In particular the most recent available data has been considered: ENDF/B VII.0 (USA 2006), ENDF/B VII.1 (USA 2011), ROSFORD-2010 (Russia 2010) and CENDL-3.1(China 2009) database.

Considering the neutron energy spectrum of a nuclear fission reactor, in particular focusing on the thermal region, the cross sections for the reactions (1), (2) and (3) are plotted in figure 4.3-a. In particular, by considering exclusively the cross sections values, the reaction (2) has the highest one, followed by the reactions (3) and at last (1).

Some cross sections plots concerning fast neutrons reactions are shown in fig 4.3-b. In particular reaction (4) and (5) occur only at very high neutron energies, so even though the cross sections are considerable in many cases - up to 10^{-1} barns - the probability of a reaction (n,x) occurring at such energies is negligible compared to the ones in the thermal region.

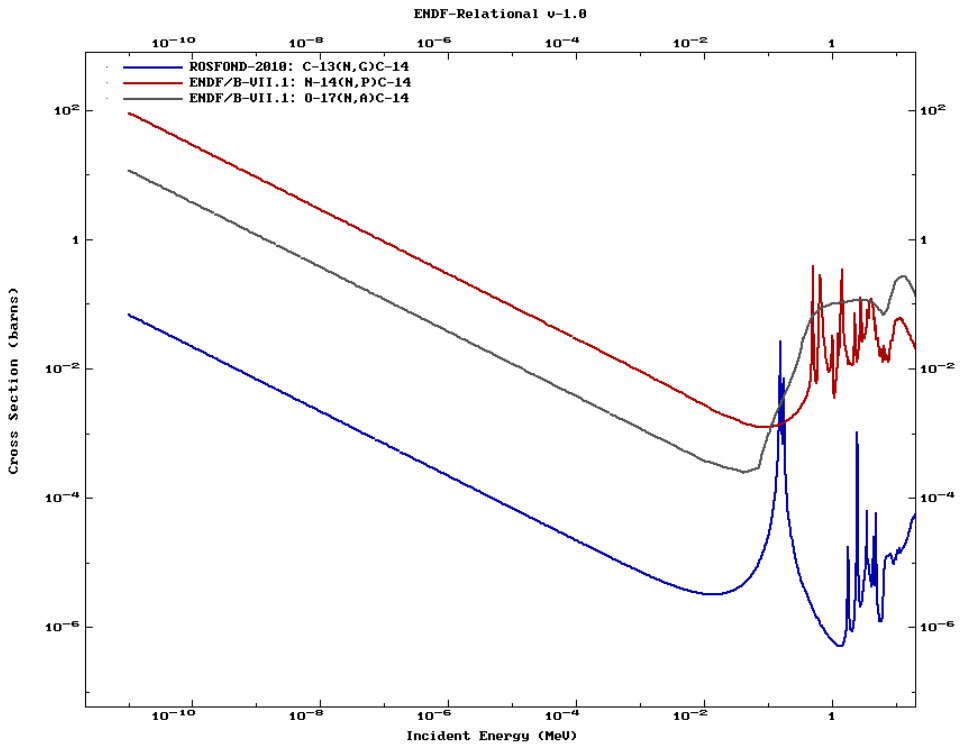

Figure 4.3-a: Cross sections of the above-listed reactions for C-14 production

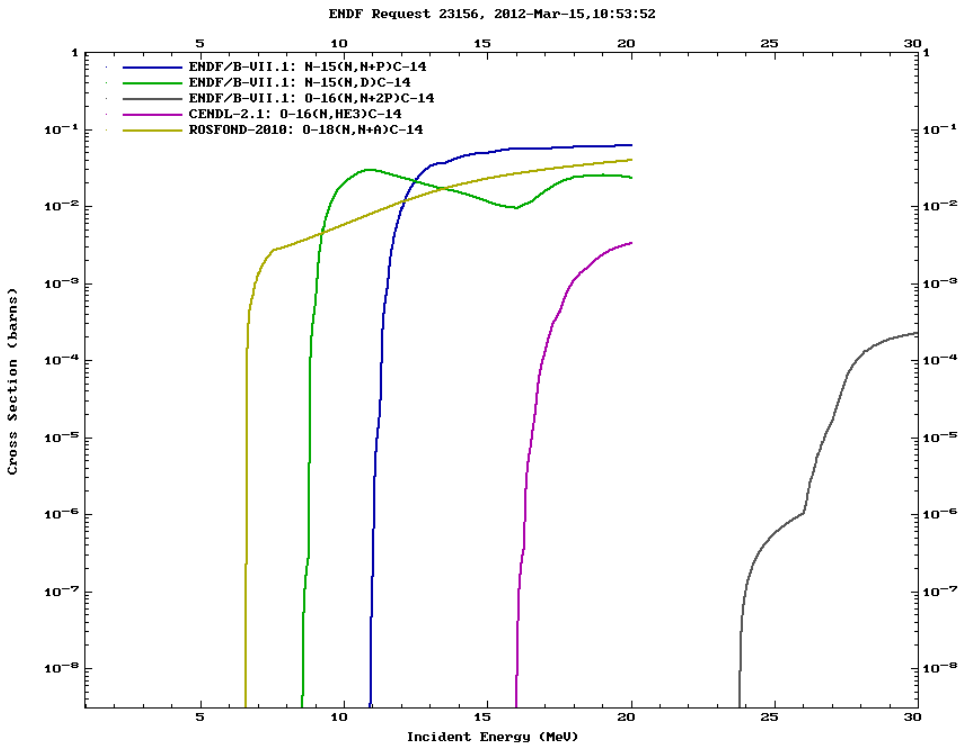

Figure 4.3-b: Cross sections of the above-listed reactions for C-14 production at high neutron energies

To have a clearer overview of the main ^{14}C precursors it is useful analysing the cross section plots divided by element of origin.

OXYGEN

The considered oxygen isotopes, in order to compare different reactions leading to the same final product, are ^{16}O,^{17}O and ^{18}O, involved in the following reactions:

$$^{16}O(n,n+2p)^{14}C$$
$$^{17}O(n,\alpha)^{14}C$$
$$^{18}O(n,n+\alpha)^{14}C$$

By comparison, exclusively based on the cross sections, it can be stated that the prominent reaction involving oxygen and generating ^{14}C is:

$$^{17}O(n,\alpha)^{14}C$$

The other oxygen isotopes´ reactions can be neglected because of their occurrence at very high neutron energies (and in any case due to their relatively low cross section). For a graphical comparison figures 4.6 and 4.7 can be observed.

NITROGEN

The considered nitrogen isotopes, to compare different reactions leading to ^{14}C, are ^{15}N and ^{14}N, involved in the following reactions:

$$^{14}N(n,p)^{14}C$$
$$^{15}N(n,n+p)^{14}C$$
$$^{15}N(n,d)^{14}C$$

The prominent ^{14}C-generating reaction, among nitrogen isotopes as precursors, is the $^{14}N(n,p)^{14}C$ (see picture 4.8 and 4.9 for a graphical comparison).

The other reactions can be neglected because of their occurrence at very high neutron energies.

CARBON

Considering a single-step reaction, the main reaction, among stable carbon isotopes as precursors, is the following (see picture 4.10 for a graphical comparison):

$$^{13}C(n,\gamma)^{14}C$$

However there is another creation route than could take place: starting from the most abundant stable isotope of carbon a 2-step reaction could be possible:

$$^{12}C(n,\gamma)^{13}C \qquad 1^{st} \text{ step}$$
$$^{13}C(n,\gamma)^{14}C \qquad 2^{nd} \text{ step}$$

The cross section[59] for the first reaction is about 0.00337 barns (see figure 4.11) and for the second reaction it is 0.00137 barns (see figure 4.11). By combination of the 2 reactions it results that such production route is much less probable than the single step one.

A more realistic approach to determine the relative contribution of the different isotopes would be to consider the above-mentioned reaction´s cross sections weighed with their respective natural precursor´s abundance and their concentrations in the AVR materials (in fact even though the cross section was relatively low for a certain reaction, the amount of the starting element could be so high that the reaction, previously not considered important, becomes predominant). This lead to obtain ^{14}N as the main responsible of radiocarbon production, ^{13}C is second in line and the less important is ^{17}O. The results, listed in table 4.6, are normalized with the respect of the most probable reaction to better understand the reactions contribution.

Radionuclide	Reaction	Cross Section (E_{th}) [b]	Natural Abundance of the Precursor	Precursor fraction in AVR reflector graphite (ppm)	Relative Reaction importance [adim]
Radiocarbon	$^{14}N(n,p)^{14}C$	1.8	99.636 %	270[60]	1
	$^{13}C(n,\gamma)^{14}C$	0.00137	1.07 %	100%	3 E-2
	$^{17}O(n,\alpha)^{14}C$	0.24	0.038 %	1380[61]	2.6 E-4

Table 4.6: Nuclear parameters for neutron activation production of ^{14}C from some precursors and their contribution

Wenzel et al. (1979)[62] investigated the production of ^{14}C in spent HTGR fuel elements and found that, as expected, ^{14}C production is a linear function of the neutron dose; in addition the fraction of ^{14}C derived from ^{13}C amounted to 26%, the one from ^{17}O was negligible and the one from ^{14}N amounted to 74%. However, it has to be underlined that fuel pebbles were made, in general, with a high-grade graphite, extremely pure compared to the reflector one: the original ^{14}N content amounted to about 40 ppm[63] instead of the 270 ppm measured in the AVR reflector graphite, so it is possible that the low relative amount of nitrogen contributed in a minor part to ^{14}C production. However, as a general statement, the predominance of ^{14}N for ^{14}C production is experimentally confirmed.

In fig. 4.4 a theoretical calculation of ^{14}C production in fuel elements is displayed as a function of the neutron fluence and the ^{14}N-impurity content, underlining once more the

[59] Cross sections are referred to neutron (thermal) energy of 0.025 eV

[60] Zsolt Révay, PGNAA, December 2010, Nuclear Research Department, Institute of Isotopes, HAS, Budapest, Konkoly-Thege Miklosutca 29-33. 1121 Hungary

[61] Idem

[62] U.Wenzel, D.Hertz, P.Schmidt, "*Determination of 14C in spent HTGR fuelelements*", Journal of Radioanal. Chem. 53, 1979

[63] Idem

predominance of Nitrogen in the radiocarbon production.[64] The assumed model did not consider the variation of ^{13}C during the reactor lifetime. A less simplified model should include such factor, which however is a minor one in the radiocarbon production.

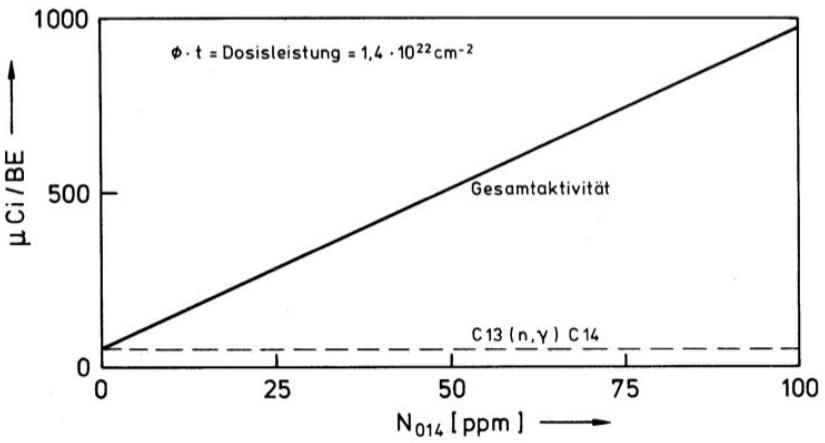

Figure 4.4: Theoretical C-14 production in an HTGR as a function of the fluence and the nitrogen content

4.2.2 Tritium

Tritium is a short-lived radionuclide, with a half-life of 12.33 years. It is one of the main reasons for which the "safe enclosure" strategy is generally adopted. The activity of such isotope in the AVR represents a consistent fraction of the whole inventory. In addition, Tritium is highly volatile and soluble in water, so it has to be considered with particular attention in every reactor dismantling step. Several routes, leading to tritium creation, are possible; the most important are listed in table 4.7. The relative importance of the one or the other reaction depends on the reactor type and on many other factors.

n°	Reaction
1	$^{3}He(n,p)^{3}H$
2	$^{6}Li(n,\alpha)^{3}H$
3	$^{2}H(n,\gamma)^{3}H$
4	$^{10}B(n,\alpha)^{7}Li$
5	$^{14}N(n,^{3}H)^{12}C$
6	$^{10}B(n,2\alpha)T$

Table 4.7: Some neutron activation reactions leading to H-3 production

[64] P.C. Schmidt, "*Alternativen zur Verminderung der C-14 emission bei der Wiederaufbereitung von HTR-Brennenelement*", Juel-1567, 1979

Tritium is produced in graphite, gas coolant and fuel source. Then it diffuses in graphite and fuel particles and it interacts with graphite surfaces (adsorption, desorption) over than being absorbed by the carbon matrix.

Considering the fuel inside the core, tritium production depends on the fissile material and the neutron spectrum. The fission yield for tritium is in the range of

$1.1 \cdot 10^{-4}$ tritons per fission of $^{233}U+n$ [65]

$193 \cdot 10^{-4}$ tritons per fission of $^{235}U+n$

Considering the reactor type, i.e. PMBR or HTGR, Deuterium can be neglected as primary source for tritium, but its creation cannot be completely excluded starting from ^{1}H through the following reaction:

$$^{1}H(n,\gamma)^{2}H \qquad 1^{st} \text{ reaction}$$

Then the deuterium can be activated in time in a second reaction:

$$^{2}H(n,\gamma)^{3}H \qquad 2^{nd} \text{ reaction}$$

Indeed, Hydrogen could be present as:

- Hydrocarbons and OH- functional groups: Hydrogen content in virgin AVR graphite was estimated around 74 ppm[66]
- Water gas reaction, when water is present for any reason and the temperature is sufficiently high;
- Water molecules, radiolitically broken: such content is difficult to estimate, but water presence in nuclear virgin graphite[67] is a signal of another possible activation route leading to tritium production; furthermore, the contribution of the AVR accident in 1978 has not to be forgotten, when 27 tons of water came out of the steam generator circuit into the core.

Considering that the cross section - at neutron thermal energies - of the first reaction is about 0.332 barns[68] and concerning the second reaction it is $0.5 \cdot 10^{-3}$ barns (see fig 4.12), it follows that such production route is much less probable than the others,[69] so a minor contribution is expected.

Furthermore, reaction (5) occurs at very high neutron energies (see fig. 4.14), so its contribution can be neglected. Reaction (6) takes place only at neutron energies higher than

---

[65] N.D. Dundey, "*Review of low mass-atom-production in Fast Reactors*", 1968,

[66] Zsolt Révay, PGNAA December 2010, Nuclear Research Department, Institute of Isotopes, HAS, Budapest, Konkoly-Thege Miklosutca 29-33. 1121 Hungary

[67] Drying experiments performed under air have shown water content in virgin AVR graphite around 300ppmw

[68] Cross sections are referred to neutron (thermal) energy of 0.025 eV, see fig. 4.13

[69] Compare the relative cross sections to have a clearer view

3 MeV, with a cross section of the order of tens of mbarns, so its contribution is expected to be a minor one. At last, the reaction (4) shows a very high cross section at thermal energies, 3837 barns, but it is occurring only at the shutdown rods side.

Lithium-6 is present in graphite as impurity: typical values for nuclear graphite are quite spread over orders of magnitude, depending on the manufacture process and the raw materials; some PGNAA showed in the AVR graphite a concentration of 220±44ppm$_w$[70] in virgin samples and 31± 2ppm$_w$[71] in irradiated samples coming from the reflector[72].

Helium-3 is present in the reactor because it is part of the utilized coolant (Helium) with an abundance of 0.137 ppm, ten times lower than the natural one[73].

Both reactions (1) and (2) have very large cross-sections (see fig. 4.12), but it would be interesting to understand which one is the predominant.

Assuming that the cooling gas in the AVR was never replaced (ideally closed-circuit), then the ^{3}He content is expected to decrease and the Tritium production, subsequently, to decline. However, since there was a continuous gas leakage from the primary circuit, a continuous "fresh-Helium" was used as refilling with the same ^{3}He abundance cited above[74]. It is expected so a higher initial production rate of tritium due to activated Li-6 impurities; once the Li-6 amount has sufficiently decreased, the main contribution to H-3 production comes from He-3: the saturation value is reached after many years due to the low Helium flow[75]. It follows that, after a certain time, the tritium production rate is constant.

Table 4.8 shows an overview of the relative contribution of the main reactions leading to tritium production. The final results are normalized with the respect of the most probable reaction to better understand the reaction prominence.

---

[70] Zsolt Révay, PGNAA December 2010, Nuclear Research Department, Institute of Isotopes, HAS, Budapest, Konkoly-Thege Miklosutca 29-33. 1121 Hungary

[71] Tamás Belgya, PGNAA December 2011, Sample P4 irradiated, 1.2355 g, , Nuclear Research Department, Institute of Isotopes, HAS, Budapest Konkoly-Thege Miklós street 29-33. 1121 Hungary

[72] Unknown position where the sample was taken inside the AVR reflector

[73] The He-3 fraction, at least at the beginning of the reactor life, is considered to be of 0.137 ppm, as stated in "*Verhalten von tritium in Reaktorgraphiten*", P.G. Fischer, 1975, p. 6. The Helium was extracted from natural gas deposits and not from air, in order to obtain 10 times lower activated products.

[74] Idem

[75] P.G. Fischer,"*Verhalten von tritium in Reaktorgraphiten*", 1975

Radionuclide	Reaction	Cross Section (E_{th}) [b]	Natural Abundance of the Precursor	Precursor fraction in AVR reflector graphite (ppm_w)	Amount of the overall precursor [kg]	Relative Reaction importance [adim]
Tritium	$^{3}He(n,p)^{3}H$	5330	0.137 ppm	coolant[76]	600	4.21 E-04
	$^{6}Li(n,\alpha)^{3}H$	940	6.577 %[77]	220	67E03[78]	1

Table 4.8: Nuclear parameters for neutron activation production of ^{3}H from some precursors and their contribution

The amount of Li-6 in the AVR carbon brick is not known precisely, but considering the generally higher concentration of impurities, compared to the AVR reflector graphite, it is reasonable to expect higher activation products. Some estimation, performed in the past, resulted in a confirmation of the Li-6 prominence in the first years of the reactor operation (see fig. 4.5).

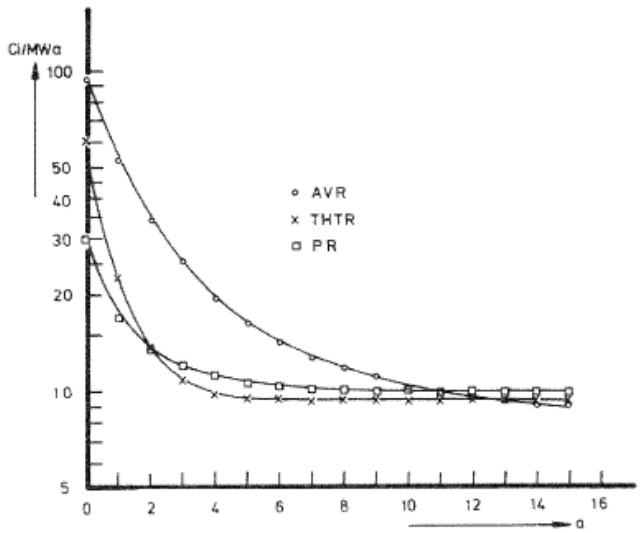

Figure 4.5: Theoretical H-3 production rate in some HTGR: in the AVR the H-3 is reaching the constant rate after longer time due to the higher amount of Li-6 impurity

[76] Virgin AVR graphite does not contain He isotopes at all, but Helium is used as coolant, so there is the possibility to have a neutron capture from ^{3}He generating ^{3}H. The total coolant amount in the reactor was about 600 kg.

[77] Mole fraction converted to mass fraction considering all the natural isotopes of the same element

[78] R.J. Printz, U. Quade, J. Wahl, "*Packaging requirements for graphite and carbon brick from the decommissioningof the AVR in consideration of the german final disposal regulations*"

4.2.3 Chlorine 36

Chlorine 36 is a long-lived radionuclide, with a half-life of about 301000 years. It is particularly relevant not because of its activity but because of the high mobility in the environment, especially in water.

Some important routes, leading to Chlorine-36 production, are listed in table 4.9.

n°	Reaction
1	$^{35}Cl(n,\gamma)^{36}Cl$
2	$^{39}K(n,\alpha)^{36}Cl$

Table 4.9: Some neutron activation reactions leading to Cl-36 production

Chlorine-36 is primarily generated as a result of neutron capture by ^{35}Cl, with a cross section of about 43.7 barns (see fig. 4.15). The neutron capture by ^{39}K has a cross section four orders of magnitude lower than the one for ^{35}Cl, so it can be assumed that the main contribution to ^{36}Cl creation is ^{35}Cl. Other isotopes could be activated and produce Cl-36 but the relative cross sections are considerable only at high neutron energies (see figs. 4.15-4.16). For example, Cl-37, Ar-36, Ar-37, K-40 are some of these precursors, but only Cl-37 is present in the AVR reflector in very small quantities; since its cross section is greater than 10^{-8} only for neutron energies greater than 10 MeV, Cl-37 can be neglected as a precursor.
Considering the natural precursors´ abundance and the precursors´ mole fraction in the reflector, the relative contributions of the different reactions are listed in table 4.10.

Radionuclide	Reaction	Cross Section (E_{th}) [b]	Natural Abundance of the Precursor[79]	Precursor fraction in AVR reflector graphite (ppm_w)	Relative Reaction importance [adim]
Chlorine	$^{35}Cl(n,\gamma)^{36}Cl$	43.7	74.72 %	30	1
	$^{39}K(n,\alpha)^{36}Cl$	0.0043	93.94 %	135	5.57 E-4
	$^{34}S(n,\gamma)^{35}S$	0.23	4.55%	160	1.71 E-3

Table 4.10: Nuclear parameters for neutron activation production of ^{36}Cl from some precursors and their relative contribution

Starting from ^{34}S, there is a possible multi-step route for ^{36}Cl production. The isotopic abundance of ^{34}S is 4.293 % and the reaction of interest is:

$$^{34}S(n,\gamma)^{35}S(\beta-)^{35}Cl(n,\gamma)^{36}Cl$$

with a cross section of 0.25 barns at 0.00253 eV(see fig. 4.17) for the first step ($^{34}S(n,\gamma)^{35}S$). ^{35}S is characterized by a half-life of 87.5 days, leading to a decay product ^{35}Cl. Preliminary

[79] Mole fraction converted to mass fraction considering all the natural isotopes of the same element

calculations have revealed a relative contribution in the order of 0.1%. Moreover, considering the very low cross section of S-34, two orders of magnitude lower than the one involving ^{35}Cl, and the relative abundance, S-34 can be considered a secondary contributor.

4.2.3 Calcium 41

Calcium 41 is a long-lived radionuclide, with a half-life of about 102000. Its activity was estimated to be about 2 orders of magnitude lower than the one of C-14. Its removal would contribute to lower the activity of the contaminated carbonaceous materials with the final purpose of a possible waste-declassification.

The main reactions leading to the production of Ca-41 are listed in table 4.11.

n°	Reaction
1	$^{40}Ca(n,\gamma)^{41}Ca$
2	$^{42}Ca(n,2n)^{41}Ca$
3	$^{43}Ca(n,2n)^{41}Ca$

Table 4.11: Some neutron activation reactions leading to Cl-36 production

By considering the neutron capture cross section, the main reaction is the (1) with 0.4 barns at thermal energies (see fig. 4.18). The other reactions take place only at very high neutron energies (>10 MeV), so their contribution to the Ca-41 generation is negligible.

In the end, it results that the most important reactions and the relative precursors are listed in table 4.12.

Reaction	Main Precursor
$^{6}Li(n,\alpha)^{3}H$	Lithium-6
$^{14}N(n,p)^{14}C$	Nitrogen-14
$^{35}Cl(n,\gamma)^{36}Cl$	Chlorine-35
$^{40}Ca(n,\gamma)^{41}Ca$	Calcium-40

Table 4.12: Main neutron reactions and relative precursors

Considering fast neutrons in general, even if they are participating in many activation reactions, their contribution in many cases is orders of magnitude lower than the ones in the thermal region. Moreover some of those reactions are taking place only with highly energetic neutrons, so even considering the average fission neutron energy of 2 MeV the very low probability of occurrence of most of those highly endothermic reactions can be stated (see prompt neutron energy spectrum example for ^{235}U in fig. 4.19).

In conclusion, it is necessary to point out an observation about cross sections: in this chapter it has been considered a neutron thermal energy of 0.0253 eV, corresponding to a temperature of about 273 K. However, a more accurate approach should distinguish every transversal section of the reactor, starting from the bottom (at about 550 K, or 0.0474 eV) to the top (at about 1190 K, or 0.1025 eV). Despite that, the performed calculations intended to provide an idea of the relative contribution of different precursors and, considering that many cross-section´s spectra are simply shifted (or parallel), the obtained considerations would lead to similar results. In addition, the best approach should consider the entire cross section´s spectra, building either a mean weighed value or a multi-group model, but it is out of the scope of this study.

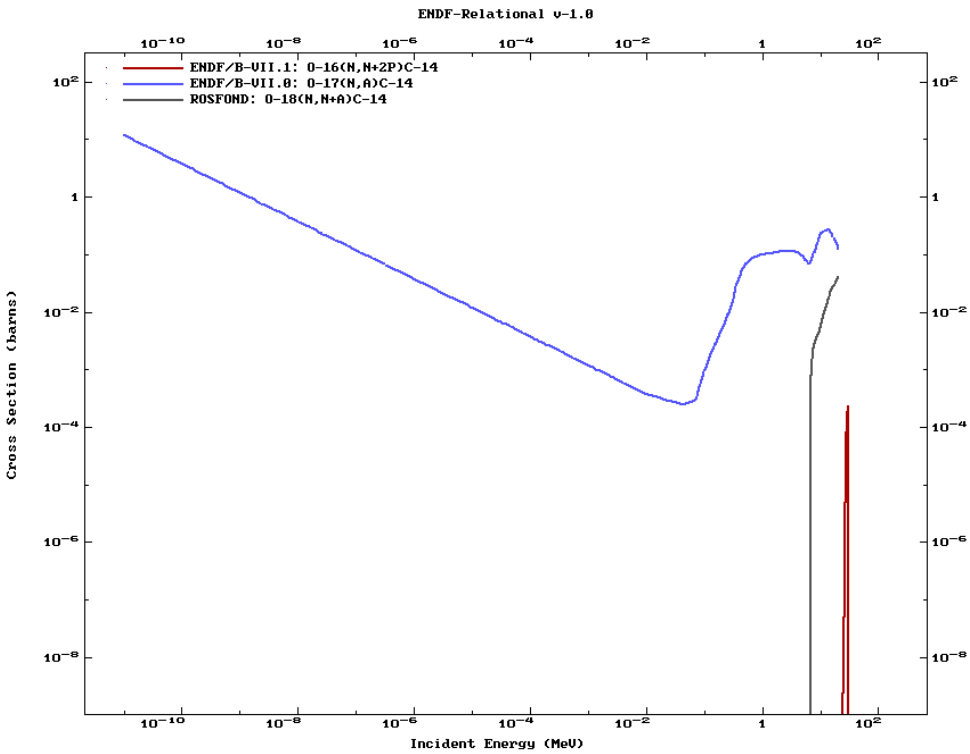

Figure 4.6: Cross section versus incident neutron energy of three reactions of oxygen isotopes leading to C-14 production

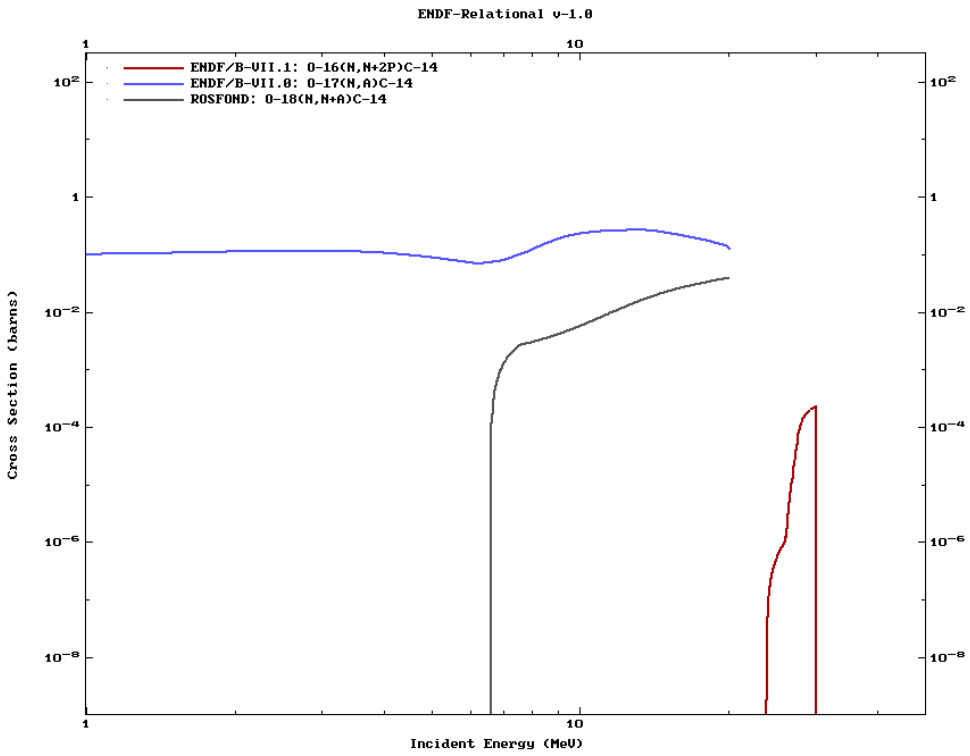

Figure 4.7: Cross section versus incident neutron energy of three oxygen isotopes reactions leading to C-14 production, zoomed at high neutron energies

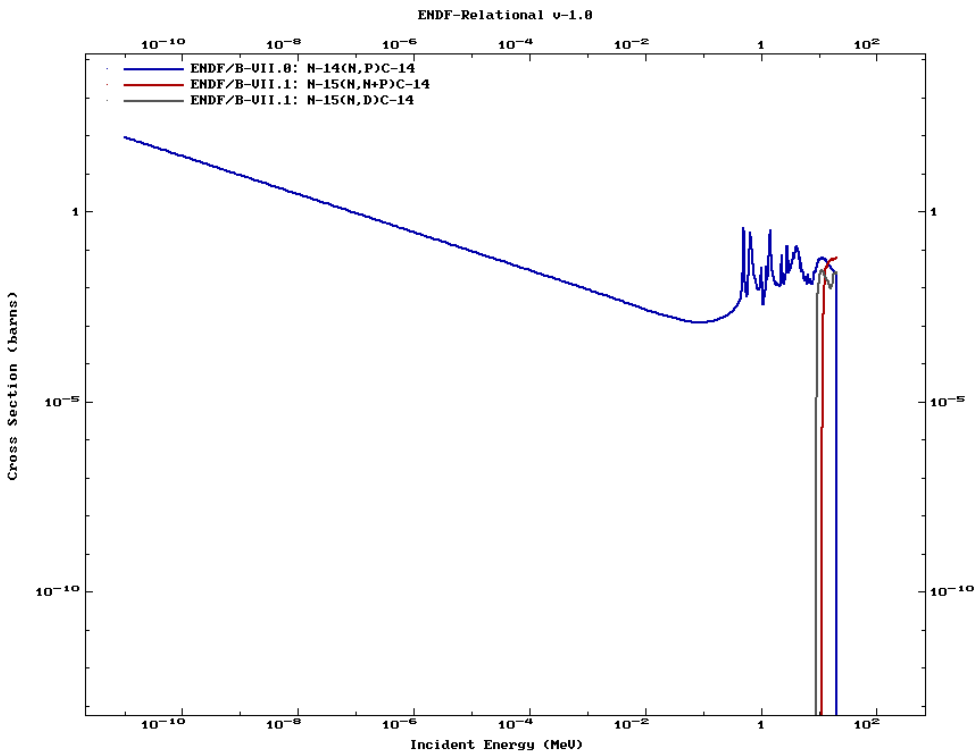

Figure 4.8: Cross section versus incident neutron energy of three reactions of nitrogen isotopes leading to C-14 production

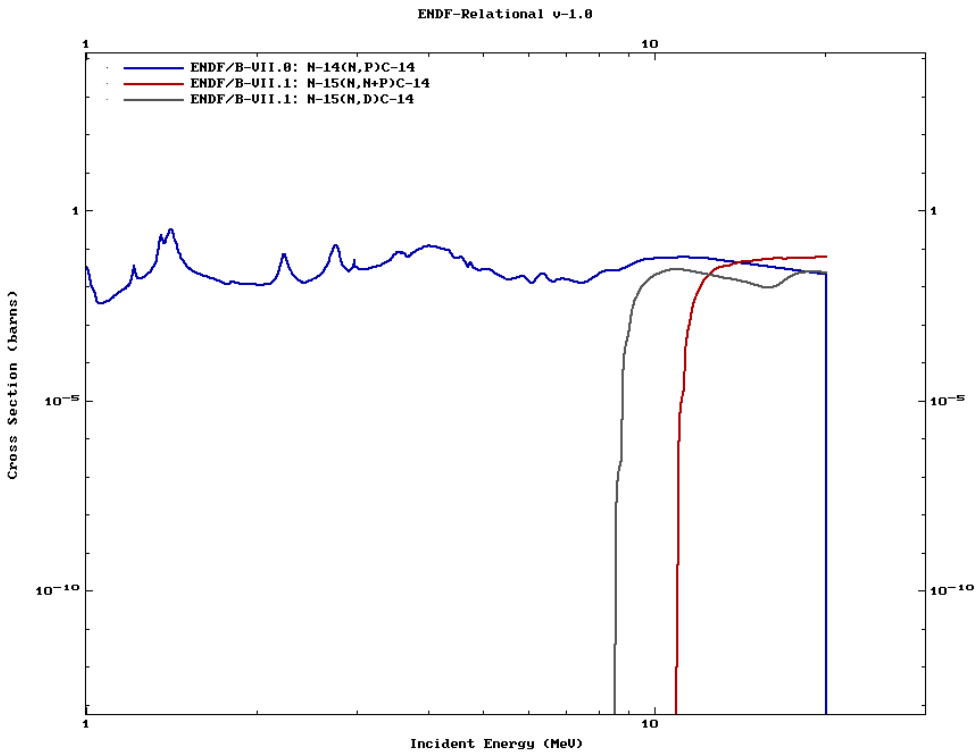

Figure 4.9: Cross section versus incident neutron energy of three nitrogen isotopes reactions leading to C-14 production, zoomed at high neutron energies

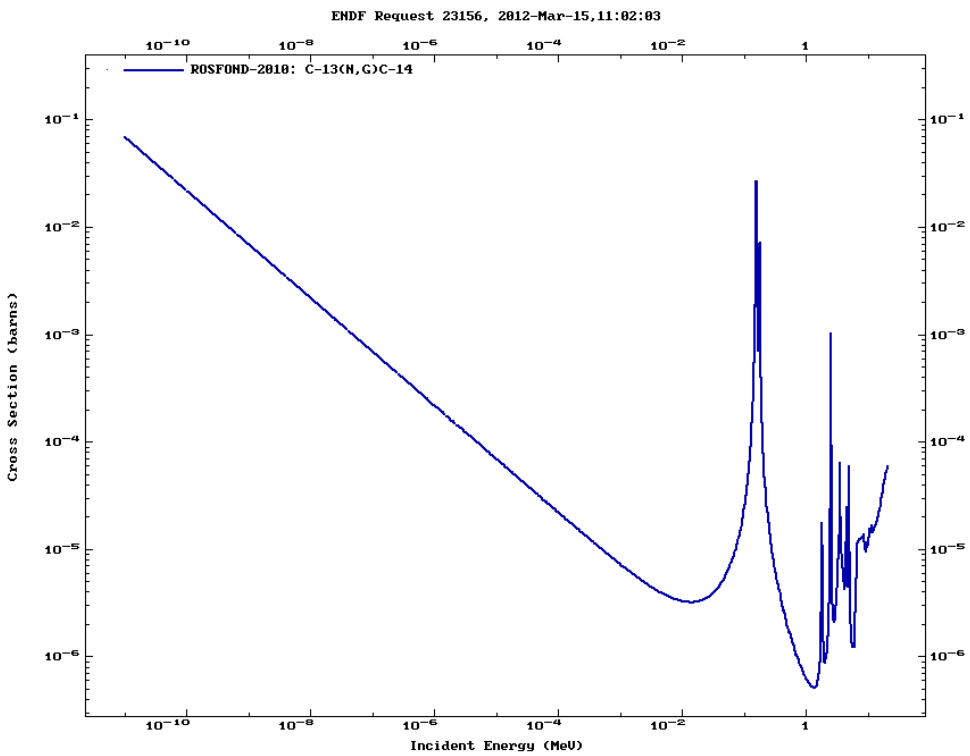

Figure 4.10: Cross section versus incident neutron energy of the neutron reaction of C-13 leading to C-14 production

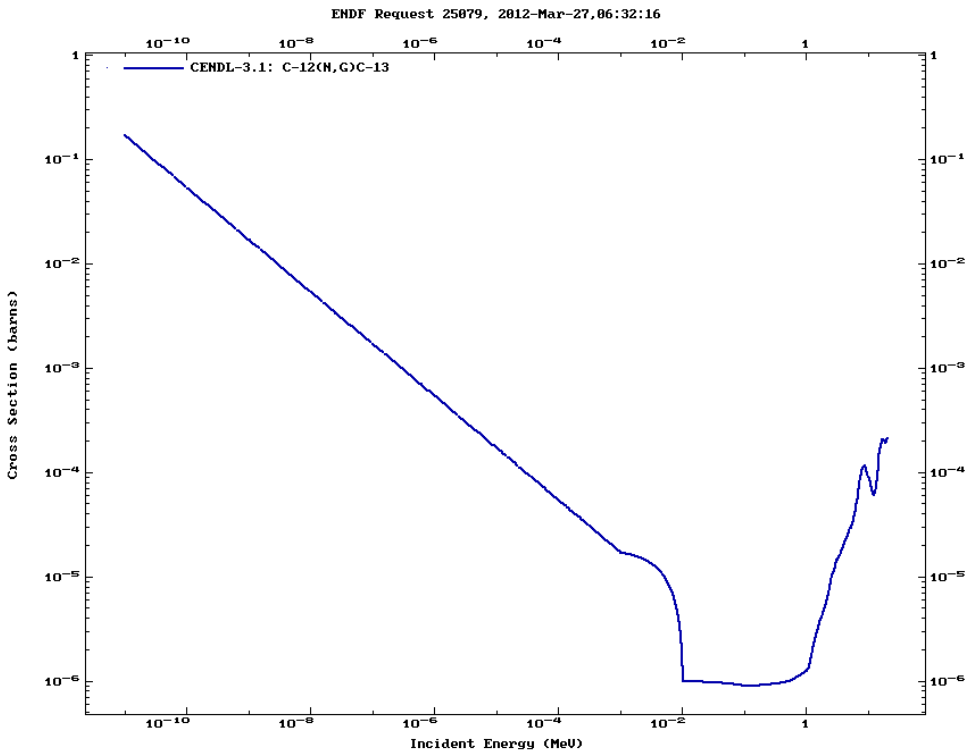

Figure 4.11: Cross section versus incident neutron energy of the neutron reaction of C-12 leading to C-13 production

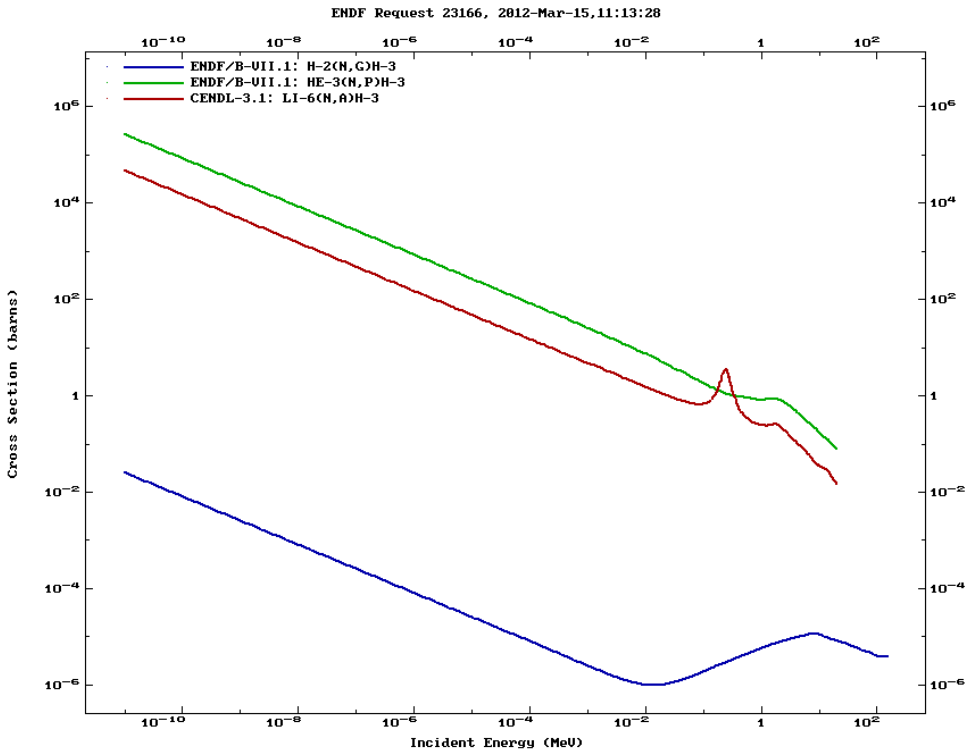

Figure 4.12: Cross section versus incident neutron energy of the main reactions leading to H-3 production

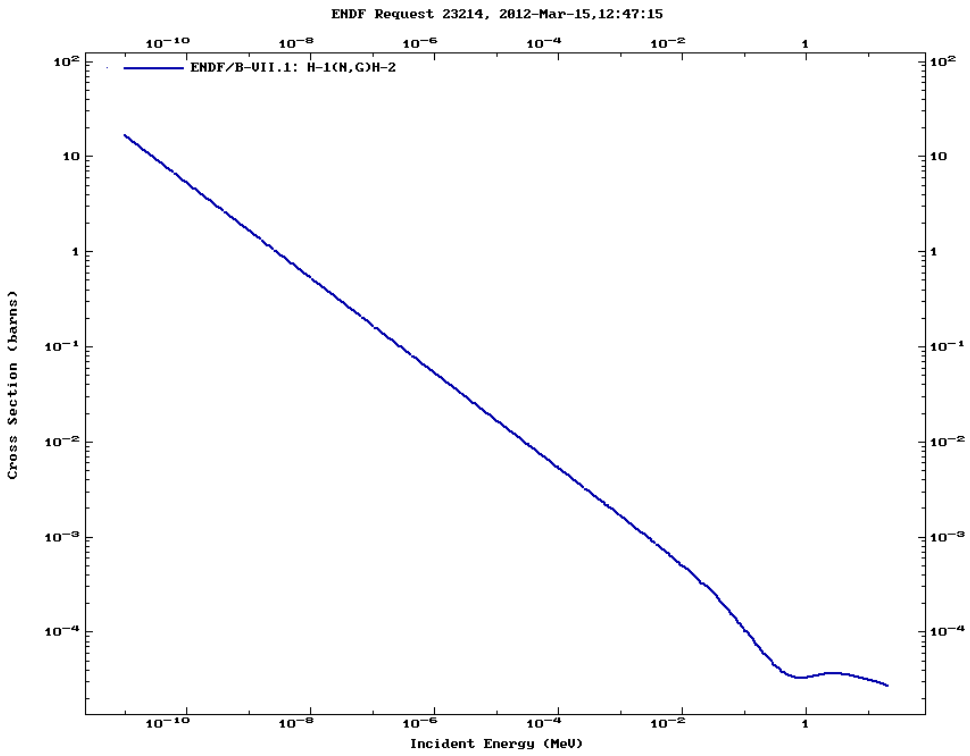

Figure 4.13: Cross section versus incident neutron energy of the reaction of H-1 leading to deuterium production

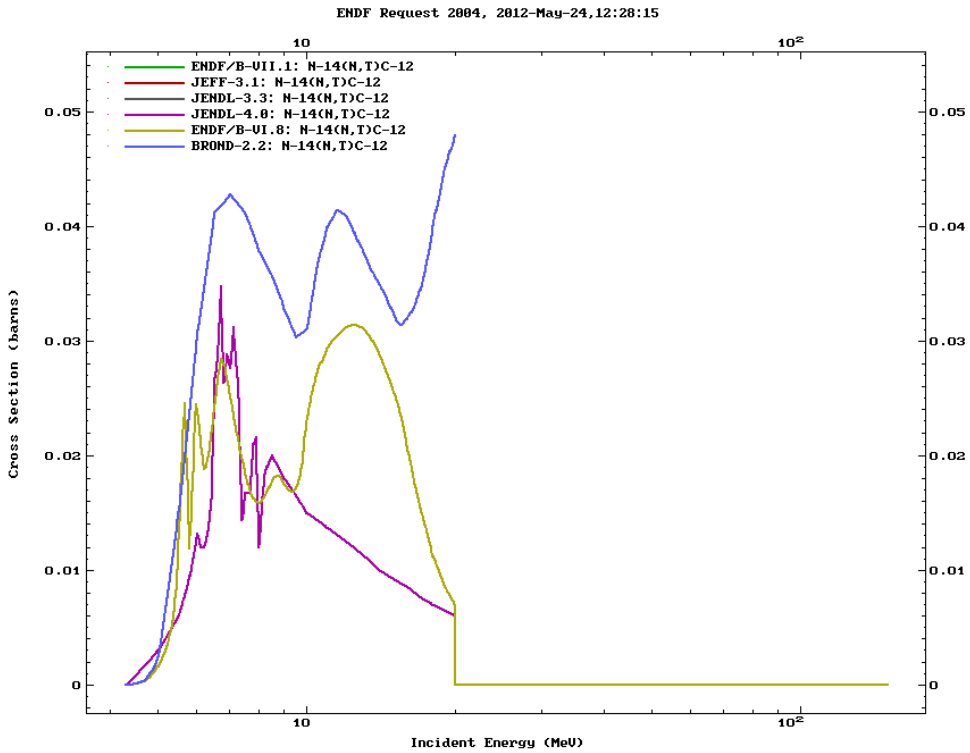

Figure 4.14: Cross section versus incident neutron energy of some reactions of N-14 leading to H-3 production

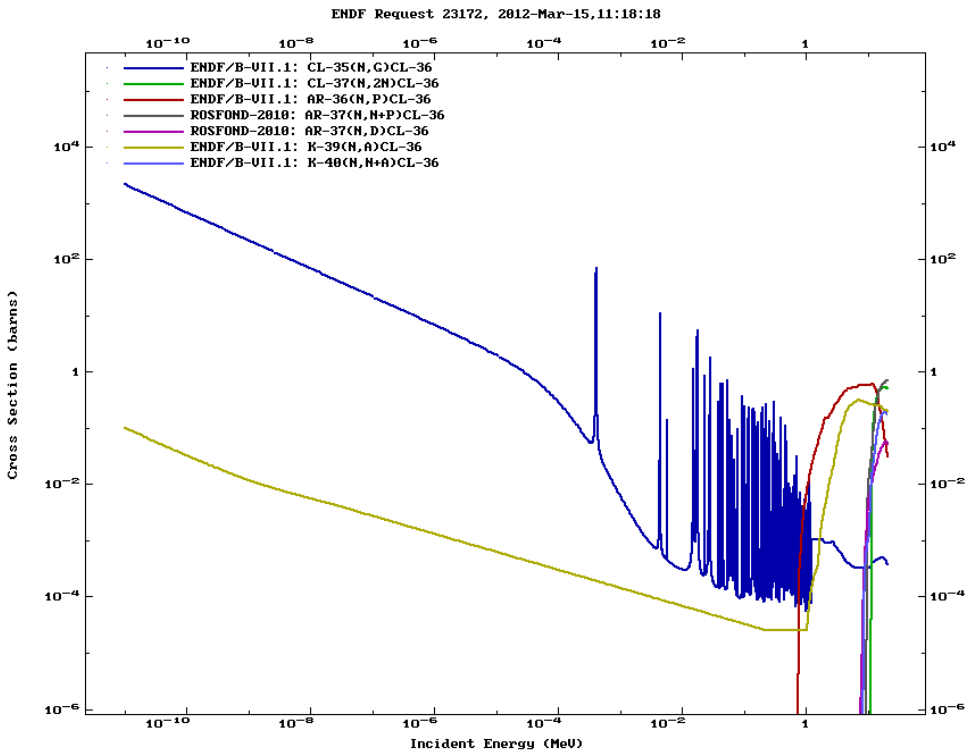

Figure 4.15: Cross section versus incident neutron energy of some reactions leading to Cl-36 production

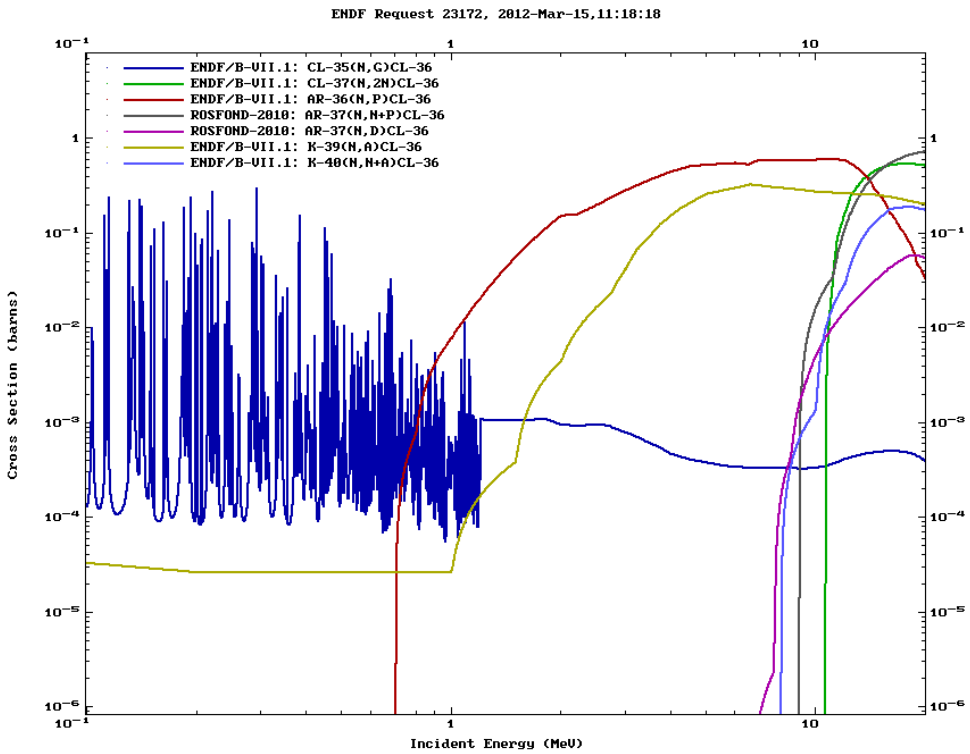

Figure 4.16: Cross section versus incident neutron energy of some reactions leading to Cl-36 production, zoomed at high neutron energies

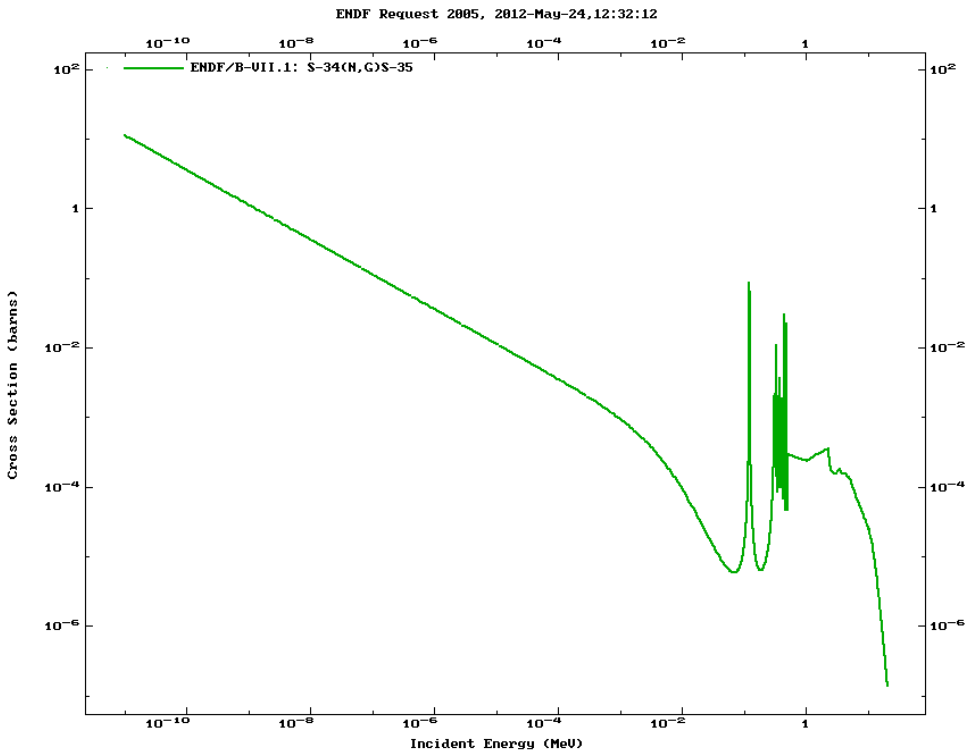

Figure 4.17: Cross section versus incident neutron energy of the S-34 reaction leading to S-35 production

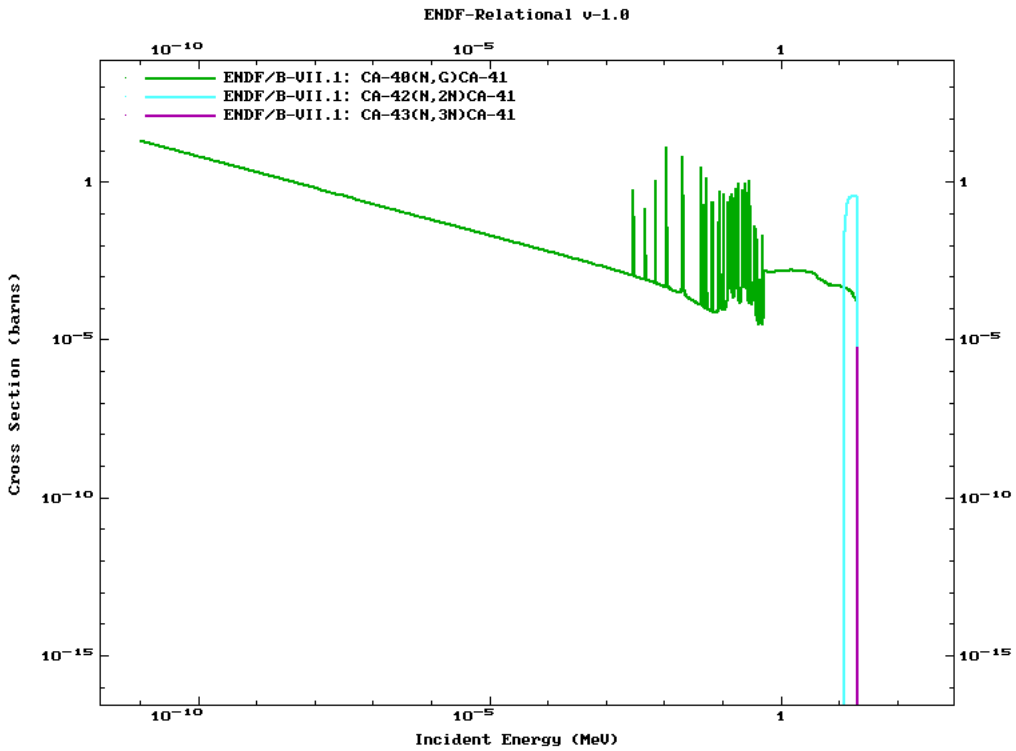

Figure 4.18: Cross section versus incident neutron energy of the Ca-40, Ca-42, Ca-43 reactions leading to Ca-41 production

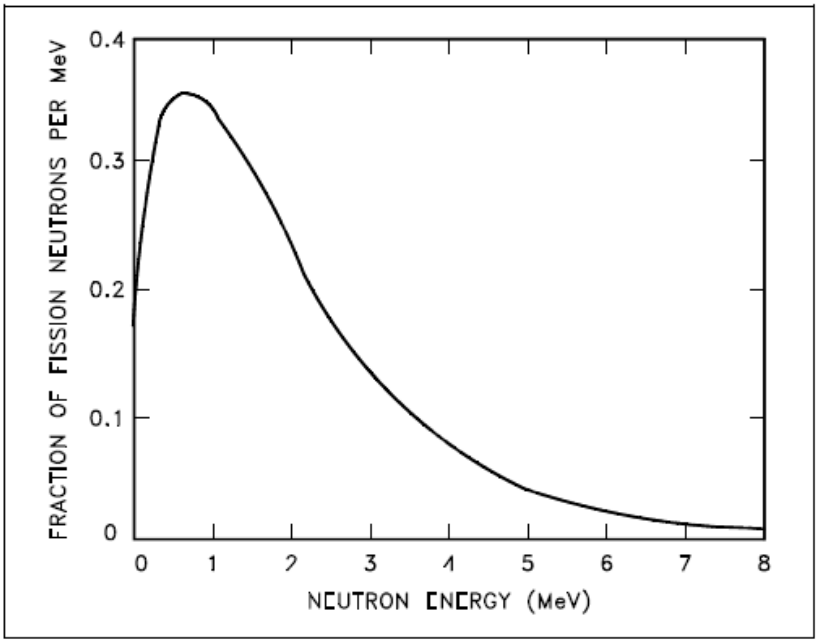

Figure 4.19: Prompt fission neutron energy spectrum from thermal fission of ^{235}U

5. Graphite: Chemical Reactions, Gas Desorption and Radionuclide Release Mechanisms

This chapter is firstly focused on the main chemical reactions and regimes that can be established with graphite. The development of a thermal purification process has to take it into account, in order to reach the radionuclides in the graphite matrix through an optimization of the treatment parameters. In the particular case of this study, the species of interest are believed to be originally embedded in the graphite structure, both coming from the manufacture process and from chemisorption during contact with humid air. From this point of view, the temperature influence on adsorption and desorption of many gases can lead to identify the released species from the surfaces: the reduction of the impurities due to thermal treatment can be exploited on virgin graphite to reduce the activation products or, assuming a similar release mechanism for the relative radionuclides, to obtain at least a partial decontamination and/or a proper conditioning. At last, the release mechanisms of three important and particularly leachable species (tritium, radiocarbon and chlorine-36) will be analysed, considering what has been discovered in literature and taking into account measurements in former experiments.

5.1 Reactions Occurring with Graphite

The oxidizing environments of interest are air (oxygen), carbon dioxide and water (steam). Reaction mechanisms are varied depending on the oxidation regime at which they are taking place and, moreover, many parameters are impacting them. In fact, many factors are influencing reactions as, for example, temperature, surface area, structure changes due to neutron damage, partial pressure of the oxidant, presence of catalysts, oxidant flow rate, etc. A first approach to well separate different reaction mechanisms consists in distinguishing different regimes occurring at different temperatures.

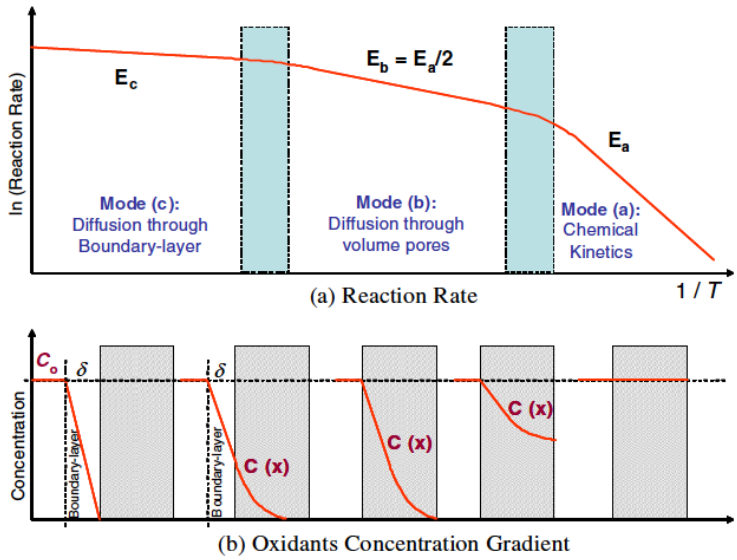

Figure 5.1: Scheme of the three typical regimes occurring in reactions with graphite

- Chemical regime

  It occurs at relatively low temperatures and the reaction between graphite and oxidizing gases takes place very slowly. The oxidizing gases can penetrate deep into the graphite: their concentration and the resulting oxidation are nearly uniform through the whole depth of penetration. Oxidation rate is controlled by chemical reactivity.

- In-pore diffusion controlled regime

  In this regime the oxidation rate is controlled by a combination of in-pore diffusion and chemical reaction. The concentration of the reactant and, therefore, the burn-off, vary exponentially with the depth: it is possible to distinguish an oxidation profile.

- Boundary Layer controlled regime

  At high temperatures the reactivity is so high that all gases are reacting at the surface of the graphite sample. The concentration of oxidising gases varies sharply at the graphite surface. The exterior surface is severely attached by the oxidizers, while the

interior material is not damaged. The superficial surface area and the oxidant partial pressure are the dominating factors

There are no distinct temperature boundaries between the three regions, but rather a progressive transition as the temperature increases.

One of the studies on the temperature effects on graphite oxidation behaviour, performed with graphite IG-11 used in the HTR-10, showed some typical results[80]. The above-listed three regimes were quite well distinguishable and, in particular for dry air, the three regions showed to be:

- 400-600 °C: oxidation controlled by chemical reaction, with activation energy of 158.56 kJ/mol (170 kJ/mol in literature)
- 600-800 °C: oxidation kinetics controlled by in-pore diffusion, with activation energy of 72 kJ/mol
- 800-1200 °C: oxidation controlled by the boundary layer with very low activation energy

Concerning the reaction of graphite with water, the three regimes can be observed too with different temperatures ranges. In particular the upper temperature limit for the graphite-water steam reaction is about 850 °C for the chemically controlled regime[81]. The in-pore diffusion controlled regime is established at temperatures between 850 °C and 1250 °C, with water concentration decreasing with the increasing distance from the surface: it results in a strong decrease in the reaction rate. The boundary layer controlled regime takes place, for the water steam-graphite reaction, at temperatures between 1250°C to 1400 °C, resulting in the water consumption focused only on the surface: there are ideally no reactions inside the solid.[82]

Reactions involving graphite are very complex and many studies are looking for a deeper understanding of them. What can be observed at the outlet of a thermal reactor can be the result of many different chemical reactions, even going through single and multi-step reactions, which lead to producing common species as CO, CO_2, H_2 and CH_4.

---

[80] Luo Xiaowei, R. jean-Charles, YuSuyuan, "*Effect of Temperature on graphite oxidation behavior*", INET Tsinghua University, Beijing, China; CEA Cadarache, France; 2003

[81] T. Podruhzina, "*Graphite as radioactive waste: corrosion behaviour under final repository conditions and thermal treatment*", Juel 4166, 2004

[82] W. Delle; K. Koizlik; H. Nickel, "*Graphitische Werkstoffefürden Einsatz in Kernreaktoren*", München, Karl Thiemig AG 1983

- Reactions with Oxygen

(5.1) $$C + \frac{1}{2}O_{2(g)} = CO_{(g)} \qquad \Delta H^{83} = -110.5\ kJ/mol$$

(5.2) $$CO_{(g)} + \frac{1}{2}O_{2(g)} = CO_{2(g)} \qquad \Delta H = -283.0\ kJ/mol$$

(5.3) $$C + O_{2(g)} = CO_{2(g)} \qquad \Delta H = -393.5\ kJ/mol$$

All these reactions are exothermic and thermodynamically favoured, but graphite does not react readily with air. Indeed, reaction between air and nuclear graphite are typically not measurable below 350 °C and becomes significant above 400 °C. A typical oxidation rate is 3-8·10^{-10} kg·kg^{-1}·s at 400 °C[84]. As temperature gets higher, the reaction (5.1) becomes dominant, among the three above-listed. Indeed, at high temperatures, the CO formation is favoured compared to the CO_2, considering the free energy change.[85]

- Reactions with Carbon Dioxide

(5.4) $$C + CO_{2(g)} \rightarrow 2CO_{(g)} \qquad \Delta H = +172\ kJ/mol$$

Normally the reaction of graphite with CO_2 is negligible up to 625 °C.[86] Moreover, the reaction is endothermic, so it does not have the same safety implications as the reaction with air.

From another point of view, this reaction is one of the most important for the purposes of this study. In particular the reversed one could lead to the formation of small carbon particles on the graphite surfaces (mostly in the porous structure) during the cooling step of the manufacture process.

- Reactions with Water

(5.5) $$C_{(g)} + H_2O_{(g)} \rightarrow CO_{(g)} + H_{2(g)} \qquad \Delta H = +131\ kJ/mol$$

This reaction is called "water-gas reaction".

Secondary homogeneous reactions:

(5.6) $$CO_{(g)} + H_2O_{(g)} \rightarrow CO_{2(g)} + H_{2(g)} \qquad \Delta H = -41.1\ kJ/mol$$

Called "water gas shift reaction".

In the case of water ingress inside the reactor core, the water-gas reaction could lead to producing explosive gases, such as CO and H_2. Generally the reaction with water is insignificant below 800 °C.[87]

- Reactions with Hydrogen

[83] Standard enthalpy of formationat 298 K
[84] A. Blacard, "*The Thermal Oxidation of graphite*", 2000
[85] Compare the Gibbs free energy change in a typical Ellingham diagram
[86] A. Thurlbeck, "*Summarised Compatibility Review of Reactor materials for CO2-cooled Graphite moderated Reactors*", TRG Report 267 (1962)
[87] A. Blacard, "*The Thermal Oxidation of graphite*", 2000

(5.7) $$C_{(s)} + 2H_{2\,(g)} \rightarrow CH_{4(g)} \qquad \Delta H = -71.81\ kJ/mol$$

Secondary homogeneous reactions:

(5.8) $$CO_{(g)} + 3H_{2(g)} \rightarrow CH_{4(g)} + H_2O_{(g)} \qquad \Delta H = -205\ kJ/mol$$

The reaction of graphite with hydrogen occurs only at high temperatures (T>1000 °C) to form methane.[88]

The general reaction mechanism is the following: oxidant species are transported to the graphite surface, they are adsorbed (physisorbed) and then a chemical bonding occur (chemisorption). Then reactions are taking place, forming for example C-H bonds in reaction (5.7). At last CO and other products desorb and are transferred from the graphite surface to the gas phase: the general scheme can be described by a Langmuir-Hinshelwood one[89]. It can stated so that the kinetics of graphite oxidation reactions are quite complex[90] and depend on many parameters: temperature, partial pressure of oxygen or other oxidizing gas, activation energies for the adsorption of oxygen and desorption of CO and CO_2, gasification products, surface active free sites and complexes, impurities which could act as catalysts and graphite microstructure. In addition the neutron damage, the rate of product removal and the porosity could affect significantly the kinetics too.[91]

Catalysis could complicate the reactions occurring with graphite. Impurities, acting as catalysts, offer and alternative reaction pathway to the oxidizing reaction. On the other hand, some elements act as oxidation inhibitors, as Boron for example.[92,93]

Some authors[94] reported that a catalytic activity of some metals on the oxidation of graphite is shown primarily by Calcium, followed by Iron and Vanadium for water vapour-graphite reactions. Successive experiments[95] proved that Aluminium and Silicon are not catalytically affecting the oxidation of graphite with water vapour. Moreover Calcium catalytic activity was not evidenced, probably due to its different chemical form among the different graphites observed, resulting to be likely in form of a catalytically inactive salt together with other impurities. In conclusion, it was found that gasification rates were proportional (linear) with the volume concentration of the total impurities: in other words,

---

[88] W. Keim, A. Behr, G. Schmitt, "*Grundlagender Industriellen Chemie*", 1986
[89] J.W: Stainmard, "*Graphite oxidation - A literature Survey*", 1990
[90] M.S.El-Genk, J.-M. Tournier, "*Proceedings of the 2010 International Congress on Advances in NuclearPowerPlants (ICAPP '10)*", Paper No. 10159, 2010
[91] A. Blacard, "*The Thermal oxidation of graphite*", 2000
[92] Idem
[93] M. Okada, T.Sogabe, "*Behaviour of gas desorption and gas permeability of carbon materials*"
[94] P.A: Thrower, G.K. Mathew, N.J. McGinnis, "*Carbon 20*", 1982
[95] S. Nomura, H.Imai, K. Fujii, M. Shindo, "*Relation between gasification rates and gas desorption behaviour with metallic impurities of carbon and graphite materials for the HTTR*"

the corrosion of graphite under water vapour seems to be governed by the catalytic action of the metal impurities present in the graphite.

Oxygen (and other) atoms could be embedded in the crystal basal planes in various forms, but typically they are bonded at the edges of basal planes and with the "dangling" carbon atoms. Indeed, because of the strong covalent bonding within the basal planes, the favourite sites for sorption and, consequently, chemical reactions are the edge and prismatic surfaces: these are called active surfaces (ASA). In particular, the zig-zag faces, the arm-chair faces and the defects, as dislocation or vacancies in the structure, are the preferred locations of chemical reactions.[96,97]

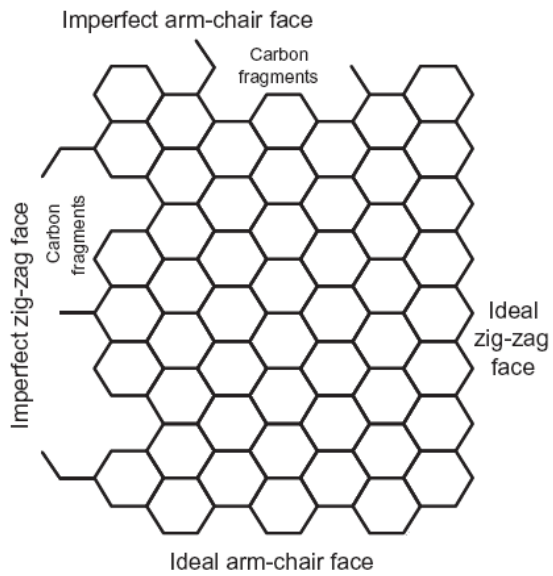

Figure 5.2: Edge configurations of a graphite basal plane

As previously mentioned in this section, the oxidation of graphite involves a rapid chemisorption of oxygen onto the surface followed by the formation of stable complexes. The rates of CO and CO_2 production and of graphite gasification depend on the surface fractions of free active sites and complexes, which change with temperature and oxygen pressure.[98] In general, oxidation rates for baked carbon are usually greater than those for graphite owing to poorer crystallinity (majority of defects and available sites for chemical reactions) and to the catalytic effects of the ash.[99]

[96] W. Jiang, G. Nadeau, K.Zaghib, K. Kinoshita, "*Thermal analysis of the oxidation of natural graphite - effect of particlesize*", Thermochimica Acta 351, 2000

[97] J.M. Thomas, "*Chemistry and Physics of Carbon, vol. 1*", 1965

[98] S. El-Genk Mohammed, J.M.P. Tournier, "*Development and validation of a model for the chemical kinetics of graphite oxidation*", J.Nucl. Mat. 411 (2011)

[99] R.E. Nightingale, *"Nuclear Graphite"* ed. 1962.New York and London: Academic Press

A particular reaction that typically occurs during reactor operation is the radiolytical corrosion. In particular, it was observed in all gas-cooled reactors implying carbon dioxide as coolant (AGR, Magnox, UNGG): the dissociation of such molecule by nuclear radiation leads to produce oxygen ions able to react with graphite and to results in consistent mass loss (up to 30% at the end of reactor life). Such corrosion mechanism strongly affects graphites coming from CO_2-cooled reactors, which consequently will show different behavior under repository conditions and during thermal treatments.[100] Radiolysis of water is also important in case of ingress in a graphitic core or under repository conditions, resulting in enhanced corrosion of the materials, probable isotope exchange reactions and consequently higher risks for safety and nuclide release.

For what concerns the species which are supposed to be originally embedded in the structure, coming from the manufacture process, the release mechanism is slightly different: in the above-mentioned regimes the oxidants have to enter through the macroscopic surface, then they are adsorbed and react. In this case the reactants are already chemisorbed on the microscopic surfaces (see model of Fromherz[101]), so diffusion might only affect the transport of the reaction products or of the released gases, which might react again while they are transported to the macroscopic surface. At last CO and other products are released and transported to the gas phase, so the general scheme for the embedded species can be seen as a modified Langmuir-Hinshelwood scheme, where the reactants are already chemisorbed in the microscopic surfaces.

5.2 Gas Adsorption and Desorption in Graphite: Effects of Temperature on Release

Polycrystalline carbon materials show typical filler particles with an average size from μm to deca-μm. During the baking process, in the binder phase, a network of pores is established; pore volume ranges from 9 to 23 % and most of the pores are open. This results in a surface area, depending on pore size i.e. on the filler particle size, of about 1 m^2/g. From this it is reasonable to expect a tendency to adsorb and desorb gases, available in the atmosphere where carbon materials are placed/stored. Typical adsorbed gases are H_2O, hydrocarbons, CO, N_2, H_2. [102]

[100] See chapter 6 for more details

[101] T.Fromherz, C. Mendoza, F. Ruette, "*Chemisorption of atomic H,C, N and O on a cluster-model graphitesurface*", 1993

[102] M. Okada, T.Sogabe, "*Behaviour of gas desorption and gas permeability of carbon materials*", Toyo Tanso Company, IAEA-TECDOC-690, 2003

Generally speaking, adsorption is the adhesion (both for physical adherence or bonding) of ions and molecules on the surface of a solid (e.g. graphite in this case). It can be distinguished in two branches, categorized through the binding energy of the adsorbate on the substrate: physi-sorption, characterized by Van der Waals forces (bonding energy 10-100 meV), and chemi-sorption (bonding energy >0.5 eV), characterized by covalent bonding of chemical species at the exposed surface. On the other hand, absorption in a process in which atoms and molecules enter the bulk phase, of graphite in this specific case.

It is believed that graphite samples, left for long time under atmospheric conditions, i.e. exposed to O_2, N_2, H_2O and other minor gases, will experience chemisorption of such gases (indeed physic-sorption can be observed only at low temperatures, since the mean thermal energy at room temperature is about 26 meV).

A model from Fromherz,[103] related to the chemisorption of many elements (H,C,N,O) on a cluster-model graphite surface showed that Hydrogen is chemisorbed on the graphite basal plane in a specific location, with a higher adsorption energy compared to the other elements. This implies that Hydrogen is able to diffuse on the graphene surface only when its chemical bond is broken, as for the other elements, but in its case higher temperatures are necessary.

In the past years few analysis have been performed with virgin carbonaceous materials.

An interesting observation, performed by Atsumi[104] during some hydrogen absorption experiments, revealed that long exposure of graphite samples to ambient air let the trapping sites to combine with oxygen atoms, resulting in a much lower affinity for the hydrogen atoms.[105] Outgassing at 1550 °C were necessary to desorb the occluding gases, since previous trials at 1200 °C were not successful to free the trapping sites (edge surfaced of crystallites). During such treatments, CO and CO_2 were released under vacuum conditions. O_2 cannot be released from chemically bonded sites since the bonding energy of C-O is larger than that of C-C. If oxygen is not removed from the trapping sites, it results in a higher diffusion coefficient for hydrogen, due to the lack of trapping sites.[106]

Former experiments[107] of SL2 graphite in inert atmosphere, in particular nitrogen, have shown the removal of many compounds, mostly oxygenated ones: CO, CO_2, water, NO_2 and HCl, respectively ordered from the higher to the lower measured one. It suggests that many oxygen compounds are sorbed within the graphite structure.

---

[103] T.Fromherz, C. Mendoza, F. Ruette, "*Chemisorption of atomic H,C, N and O on a cluster-model graphite surface*", 1993

[104] H.Atsumi, J. Nucl. Mat., 307-311 (2002)

[105] Idem

[106] Idem

[107] C.E. Vaudey, N. Toulhoat, N. Moncoffre, "*Thermal Behaviour of chlorine in nuclear graphite at a microscopic scale*", J. Nucl. mat. 395 (2009)

An interesting experiment, performed with isotropic virgin graphites,[108] used TDS (Thermal Desorption Spectroscopy). More in detail, vacuum was achieved in the thermal chamber, followed by thermal treatment with a simultaneous measurement of the desorbed gases through a QMS (quadrupole mass spectrometer). Investigated temperatures were 200, 400, 500 and 700 °C with a heating rate of 1 K/s for 3 hours. After the 1st experiment each sample was cooled down and kept for one day in the chamber, then reheated up to 1000 °C at the same heating rate. It was clearly found that the amount of desorbed gases became significantly smaller after thermal purification. Total pressure of gases from purified graphite was found to be smaller than the unpurified one. After 5-6 months of exposure in the atmosphere the gas desorption was investigated in the same way, and no significant difference with the reheating experiment was observed.

Summarizing the observed pre-baking effect, after 3 hours at 200 °C outgases were reduced of about 10 % with respect to the not pre-treated sample. After 3 hours at 400 °C, a 20% less outgassing was observed. At last, desorption curves after pre-baking at 700 °C for 3 hours showed to be nearly back at ground level. Although different graphite-grades were investigated, the pre-treatment showed similar effects. These results are in accordance with what reported[109]Polovina, i.e. that oxygen begins desorbing at around 200 °C.

What can be understood from those experiments is the reduction of the impurities due to thermal treatment, with a large amount of desorbed gases during the first treatment and a smaller amount in further ones, depending on the graphite ash content and the pre-treatment temperature. It was found that main outgases were hydrocarbons (including CH_4), H_2O, H_2 and CO. One of the aims of the present work is to investigate which gases are being released during thermal treatment under inert atmosphere, in order to prove what was observed in the past and to help to better understand the release mechanisms.

[108] M. Okada, T.Sogabe, "*Behavior of gas desorption and gas permeability of carbon materials*" , Toyo Tanso Company, IAEA-TECDOC-690, 2003

[109] M. Polovina, B. Babic, "*Carbon*" 35, 1997

5.3 Overview on the release mechanisms of radionuclides

This section will analyse the release mechanisms of three leachable radionuclides: radiocarbon, tritium and chlorine. After some initial consideration and some calculations about the recoil energy, information found in literature together with developed models and some results obtained in former experiments are reported. The investigations on the release mechanisms have been developed in different ways along the years, focusing in particular on tritium, which is one of the most modelled nuclides, not deepening the behaviour of other important isotopes, such as ^{14}C and ^{36}Cl. In particular, no models have been established for them and very less data are available for ^{36}Cl, so many investigations are planned for a deeper understanding of such leachable species. From the point of view of virgin graphite it could be interesting to optimize as first the parameters of a thermal treatment and then compare the results with i-graphite, eventually produced artificially by implanting some radionuclides and using them as tracers to study the release behaviour.

5.3.1 Carbon-14

Carbon-14 is a pure beta emitter with a maximum energy of 158.1 keV, with a half-life of 5730 years. It is present in graphite most likely as covalently-bound elemental carbon. Referring to the considerations performed in chapter 4, the precursors of C-14 are mainly N-14 and C-13. The C-13, natural isotope of carbon, is assumed to be homogeneously distributed over the bulk of graphite.[110] Starting from that, the C-14 resulting from C-13 is supposed to be distributed in the same homogeneous way.

It would be interesting to calculate the recoil energy of C-14 from the reaction $^{13}C(n,\gamma)^{14}C$. The recoil due to the impact of the neutron is negligible considering the thermal energies zone, where the reaction cross-section is the highest (compare chapter 4 for more details).

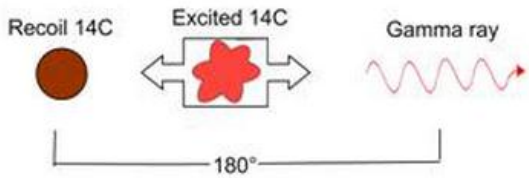

Figure 5.3: Scheme of the gamma-ray emission from an excited C-14 atom

From the momentum conservation of the ^{14}C-γ system it results that:

$$MV_d = \frac{E_\gamma}{c}$$

with M= mass of the daughter nuclide
V_d= speed of the daughter nuclide

[110] It will be proven in chapter 8 through some SIMS experiments

E_γ= energy of the emitted gamma-ray in MeV
c = speed of light

by squaring and multiplying by 1/2 both sides it results:

$$E_R = \frac{1}{2}\frac{{E_\gamma}^2[MeV^2]}{M[amu]\cdot c^2} = \frac{1}{2}\frac{{E_\gamma}^2[MeV^2]}{M[amu]}\frac{1}{931.46}\left[\frac{amu}{MeV}\right]\cdot 10^6\left[\frac{eV}{MeV}\right] = 536.79\cdot\frac{{E_\gamma}^2}{M}\ [eV]$$ [111]

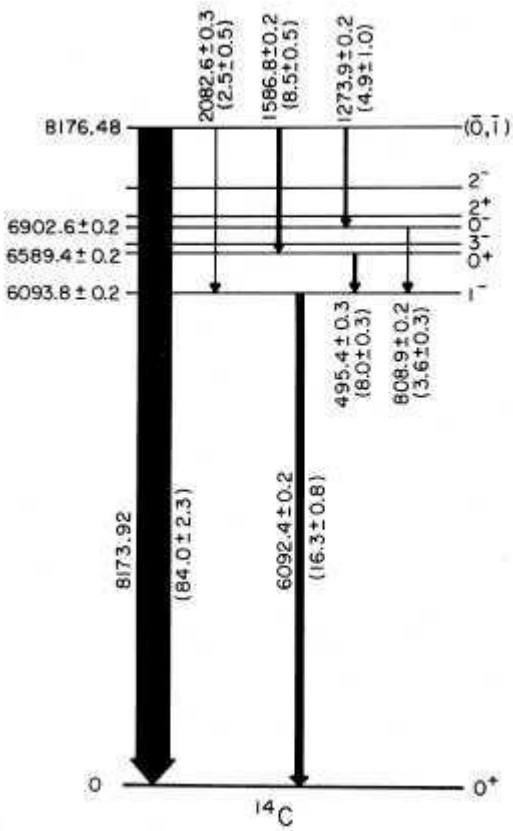

Figure 5.4: Decay scheme of C-14 from thermal neutron capture of C-13.
Energies are in keV and the intensities (in brackets) are referred to 100 neutron captures

Eγ	[keV]	8173.92	6092.4	2082.6	1586.8	1273.9	808.9	495.4
Iγ	[%]	84	16.3	2.5	8.5	4.9	3.6	8
E_R	[eV]	2561.2	1422.8	166.3	96.5	62.2	25.1	9.4

Table 5.1: Recoil energies of the C-14 nucleus after gamma emission

By observing the calculated recoil energies in table 5.1 and considering all the possible bonding energies of carbon (respectively 3.61 eV, 6.36 eV and 8.70 eV for C-C, C=C and C≡C), it can be stated that the C-14 atom will not remain in the bound form, at least immediately

[111] Some authors reported 536 as a numeric value (E.W. Haas, R. Hofmann, F. Richter, "*Errors in activation analysis by nuclear recoil*", Journal of Radioanalytical Chemistry, Vol. 69, 1982). Some others 533 (R.R. Coltman, C.E. Klabunde, D.L. McDonald, J.K. Redman, "*Reactor Damage in pure materials*", J. of Appl. Physics 33, 3509, 1962) .

after it is born. Considering a mean energy threshold to displace an atom of 25 eV[112], in most of the cases the recoil nucleus is displaced from the lattice, with a residual energy value equal to the difference (E_{Recoil}-$E_{displacement}$). More recent E_d values range from 12 up to 60 eV.[113] However, the displacement energy is expected to vary with direction in crystals, higher for in-plane displacements than for out-plane ones, and with the displaced atom, since there are two distinct atomic sites in hexagonal graphite. Banhart advised a value of 15-20 eV along the c-axis and about 30 eV for the in-plane direction[114].

Takahashi et al. [115] hypothesized that any C-14 included in the bulk graphite is hardly released to the outside. Such hypothesis is assumed in this study too: considering that most of the C-13 will be in the bulk of the graphite, it is believed that the resulting C-14 will not be easily released, showing so an improved leaching behaviour. It must not be forgotten, anyway, that C-13 is only a minor contributor to radiocarbon production.

Takahashi et al.[116] reported a value of the carbon recoil energy in $^{14}N(n,p)^{14}C$ of about 4.9 eV, claiming the not-breaking of the C=C bonds. In the following, some calculations are performed to check this value.
Similarly to what has been done in this section, it is considered the reaction $^{14}N(n,p)^{14}C$, and the conservation of momentum of the p-^{14}C system results in:

$$E_R = \frac{E_p}{M}$$

with E_p= proton energy

M= mass of the daughter nuclide

The proton energy amounts to 0.58 MeV[117], leading to 41.4 keV of recoil energy for C-14. The calculation of Takahashi has been discredited: the recoil energy is so high that the atom will break any type of bonding and will be displaced from its position (even though embedded in the graphite lattice), being most probably ionized due to the high velocity and favouring so the chemical bonding with first either species it encounters.

---

[112] S.Blow, J. Phys. D., Appll. Phys. 4 (1971)
[113] R.H.Telling, M.I. Heggie, "*Radiation defects in graphite*", Philosophical Magazine, Vol. 87, 2007
[114] Idem
[115] R. Takahashi, M. Toyahara, S. Maruki, H.Hueda, T. Yamamoto, "*Investigation of morphology and impurity of nuclear grade graphite, and leaching mechanism of carbon-14*", p.7
[116] Ibidem, p.8
[117] A. BETHE, 1950, Rev. Mod. Phys., 22, 213.

Depending on the energy of the recoiled nucleus and on the nature of the materials, the recoil ranges may result up to several 10^{-6}m.[118] Other displacements occur for nuclear radiation, with an estimated range of a primary-knocked carbon atom around 500 nm, considering neutron energy of 1 MeV.[119] Considering the mentioned ranges it is unlikely that any C-14 is released out of the graphite crystalline matrices. This assumption is supported in this study, so several measurements will investigate the nitrogen distribution in the AVR graphite (see chapter 8).

There are many discussions about the possible location of N-14: it originates from raw materials, manufacture process and chemisorption due to long exposure of graphite to ambient air. Typical nitrogen amounts of raw petroleum coke, found in literature, range between 0.1% and 1.4%, with a typical value of 1%.[120] Concerning coal-tar pitches, it was not found any typical value in literature and it was not possible to measure it by PGNAA.[121] During the manufacture process, part of the nitrogen is released, since the carbon brick samples, simply baked at 1150 °C, showed nitrogen contents around 0.5-0.6%. Moreover, after graphitization, the final product, in the case of AVR graphite, showed nitrogen fractions around 230 ppm. Similar values were found in SLA2 graphite.[122]
Takahashi et al.[123] measured, through SIMS analyses, that nitrogen (CN^-) is concentrated mostly near the graphite surface, in the first tens of nm (about 30 nm). Moreover, after a thermal treatment at 400°C, no differences were observed: it was stated that nitrogen is sorbed on the graphite surface in a stable way. The variation of nitrogen concentration in the depth direction suggested that nitrogen molecules cannot penetrate interior of nuclear-grade graphite, protected by scale-like graphite planes, so the nitrogen stays mainly on the surface. C-14 release was estimated to occur from the first superficial nanometer of the graphite surface. It has to be underlined, however, that the investigated samples had very low radioactivity and the experiments were performed at relatively low temperatures. It is expected that a highly radioactive graphite, as the AVR one, will show considerable amounts of mobile carbon due both to the old-grade manufacture and to radiation damage. Moreover,

---

[118] E.W. Haas, R. Hofmann, F. Richter, "*Errors in activation analysis by nuclear recoil*", Journal of Radioanalytical Chemistry, Vol. 69, 1982
[119] R.H.Telling, M.I. Heggie, "*Radiation defects in graphite*", Philosophical Magazine, Vol. 87, 2007
[120] R.E. Nightingale, "*Nuclear Graphite"* ed. 1962..New York and London: Academic Press
[121] The samples were prepared under air, so a consistent amount of air was inside the specimens' container, resulting in a too high nitrogen background.
[122] Zsolt Révay, PGNAA December 2010 , Nuclear Research Department, Institute of Isotopes, HAS, Budapest, Konkoly-Thege Miklosutca 29-33. 1121 Hungary
[123] R. Takahashi, M. Toyahara, S. Maruki, H.Hueda, T. Yamamoto, "*Investigation of morphology and impurity of nuclear grade graphite, and leaching mechanism of carbon-14*",

higher temperature treatments could results in nitrogen removal, leading to lower the C-14 inventory after neutron irradiation. At last, as a general statement, many experiences in the past have studied the different behaviour of different grades of graphite, so every grade has to be treated in the appropriate way, even though some similar phenomena could be observed.[124]

Some experiments have shown that most of the ^{14}C is located on the outer and inner surface of the porous graphite, so the statements of Takahashi et al. have been partially discredited, at least referring to AVR and Merlin graphite.[125,126]

Thermal treatments[127] of T. Podruzina showed results related to the temperature, the used sample and the utilized gases. C-14 started to be released at about 800 °C. The most promising results, concerning AVR reflector graphite, were obtained at 1060 °C in inert atmosphere (argon), with a fractional release $\%^{14}C/\%^{12}C=20$ and mass loss in the order of 1%.

Connecting to the past experiences and the present knowledge, this work will be focused also on the removal of some important radionuclide´s precursors: among those, nitrogen is one of the most important.

5.3.2 Hydrogen-3

Tritium is a pure beta emitter with a maximum energy of 18.61 keV, with a short half-life: 12.33 years. It is one of the most important radionuclides present in the AVR due to the very high activity (see chapter 4 for more details). It would be interesting to calculate the recoil energy of tritium in the reaction (5.3.2.0) to understand whether tritium will stay in a bound state or not:

(5.3.2.0) $$^{6}Li(n,\alpha)^{3}H$$

The energy conservation and the momentum conservation implies that respectively:

(5.3.2.1) $$\begin{cases} \frac{1}{2}M_d V^2 + \frac{1}{2}M_\alpha v^2 = Q \\ M_d V = M_\alpha v \end{cases}$$

[124] The reference is connected with the past experiences on Merlin and AVR graphite, that showed sometimes completely different behaviour under the same treatment conditions. See T. Podruhzina's experiments.

[125] J. Fachinger, W. von Lensa, T. Prodruhzina, "*Decontamination of nuclear graphite*", Nuclear Engineering and Design 238 (2008)

[126] In chapter 8 it will be proven that N-14 is concentrated the more in the graphite surface through SIMS analysis, similarly to what Takahashi et al. have done in the past

[127] T. Podruzhina, "*Graphite as radioactive waste: corrosion behaviour under final repository conditions and thermal treatment*", Juel 4166, 2004

the kinetic energy of the alpha particle is:

(5.3.2.2) $$E_\alpha = \frac{1}{2} M_\alpha v^2$$

by solving system (5.3.2.1) and substituting in the equation (5.3.2.2), it results

(5.3.2.3) $$E_\alpha = \frac{Q}{1+\frac{M_\alpha}{M_d}}$$

With a Q-value of +4.79 MeV it results in an alpha energy of 2.053 MeV and subsequently a recoil energy of 2.737 MeV of the ^3H (in literature it was found 2.729 MeV[128]). Such recoil energy is sufficient to break any bond, dislocate and ionize the nuclide, which will react with the first species it will encounter. It was found in literature that the recoil range of H-3 in graphite is about 32 μm[129].

The form of tritium in i-graphite could be HTO (adsorbed tritiated water), C-OT (oxygen functional groups) or Hydrocarbons (C-T). The main release mechanisms of tritium are likely to be desorption of HTO, isotopic exchange, pyrolysis of functional groups and hydrocarbons, and following diffusion of HT and HTO.

Concerning tritium release, many experiments and have been established.
A theoretical models of Katayama[130] showed that tritium trapped on the graphite surface of a small particle (with diameter in the order of μm) can be removed rapidly even at room temperature, through isotopic exchange reaction with water steam. Even a partial pressure of 10 Pa could be sufficient to obtain the same removal factors as in the case of a thermal treatment at 900 °C with 100 Pa hydrogen stream. However, tritium trapped inside of graphite can be released only at temperatures higher than 1000 K.
The high mobility of trapped tritium, occurring only at high temperatures, has been discussed previously in another theoretical model.[131]

Atsumi et al.[132] developed and validated a model to describe the behaviour of hydrogen in graphite, before and after neutron irradiation.

---

[128] E.W. Haas, R. Hofmann, F. Richter, "*Errors in activation analysis by nuclear recoil*", Journal of Radioanalytical Chemistry, Vol. 69, 1982
[129] H.Atsumi, K. Tauchi, "*Hydrogen absorption and transport in graphite materials*", Journal of alloys and compounds", 356, 2003
[130] K.Katayama, M. Nishikawa, "Release behaviour of tritium from graphite material", 2001
[131] T.Fromherz, C. Mendoza, F. Ruette, "*Chemisorption of atomic H,C, N and O on a cluster-model graphite surface*", 1993

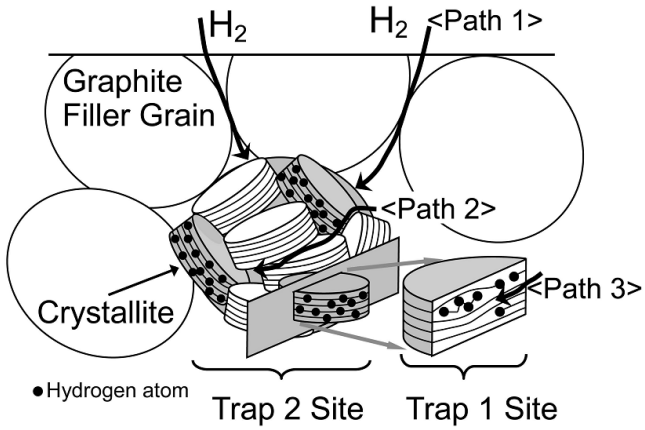

Figure 5.5: Hydrogen trapping sites and transport in a graphite material

The model identifies two trapping sites for hydrogen in graphite: interstitial cluster loop edge sites (trap 1) with an enthalpy of 4.6 eV and carbon dangling bonds at edge surfaces of crystallites (trap 2) with an adsorption enthalpy of 2.6 eV. The trap 2 is predominant in unirradiated graphite and it represents normally 80% of the total. In addition, neutron irradiation showed to increase hydrogen retention up to 100 times more than that in unirradiated graphite, with a prominence of trap 1 sites.[133]

Concerning the hydrogen absorption mechanism, at the initial stage hydrogen can reach a graphite filler grain through open pores (path 1 in fig. 5.5); then the molecules dissociate into atoms and migrate into a filler grain along graphite crystallites in a sequence of trapping and detrapping (path 2 in fig. 5.5); this stage can be reproduced as a diffusion-controlled process. The last stage of hydrogen migration should be an intercalate diffusion between graphite lamella (path 3): this stage is controlled by the detrapping reactions at trap 2. Trap 1 sites revealed experimentally to be more stable than trap 2, during high temperatures thermal treatments (1550 °C). On the other hand, the desorption process should be controlled by detrapping from Traps 1 and 2, due to a higher energy of trapping (2.6 and 4.6eV respectively) than the activation energy of diffusion (about 1.3 eV)[134]. More in detail, some Thermal Desorption Spectra of hydrogen from graphite showed two peaks, respectively at 735 K and 1220 K: such results could be interpreted with a diffusion-controlled process. However, the fundamental process of desorption for both peaks would be recombination but, due to the long path to the surface, hydrogen will be successively trapped and detrapped,

[132] H.Atsumi, T. Tanabe, T. Shikama, "*Hydrogen behaviour in carbon and graphite before and after neutron irradiation - Trapping, diffusion and the simulation of bulk retention*", J. Nucl. Mat. 417, 2011
[133] Idem
[134] H.Atsumi, J. Nucl. Mat. 313-316 (2003)

resulting in an apparent diffusion as the dominant process of desorption.[135] Even though TDS spectra showed two peaks, it is believed they are actually three: the desorption of hydrogen with an activation energy of 1.3 eV is assumed to be a recombination-controlled process. [136] In conclusion, three kinds of desorption processes are representative of hydrogen desorption in graphite.

Experimental desorption spectra of nuclear graphite from Fischer[137] confirmed three peaks of hydrogen emissions at about 400 °C, 700-750°C and 1000 °C. The release seems to fit well with what was stated by Atsumi, with a desorption characterized by three processes at different activation energies. It has to be underlined, however, that a peak was observed around 150 °C, leading to believe that the simple water release could results in tritium release. Some experiments of Dr. Vulpius resulted in apparent activation energies for HT release of 3.15 eV and 2.33 eV for HTO, with an average of 2.74 eV in accordance to the value found by Fischer and Atsumi.

Another model of Chiu and Haasz[138] found that there exist two different diffusion channels in the crystallites. It was shown that the inner surface area of porous graphite available for transport of hydrogen plays a major role on hydrogen release. However, M. Warrier[139] proved the release dependence on void fraction and void size.

Considering the policrystalline structure of graphite, three diffusion channels can be established[140]: along the a- and c-axis and along the grain boundaries. The c-axis diffusion does not appear to be plausible because of the high activation energy. Considering these assumptions, differences on the tritium release are expected between isotropic graphites and anisotropic ones: in the latter the hydrogen atoms hardly penetrate the layer plane. This was proven by Saeki[141], who obtained significant differences on the relative activation energies, with a factor of 2.5 higher for the anisotropic graphites.

Many experiments on different graphite grades[142,143] showed that tritium release is, in general, increasing with the temperature.

---

[135] H.Atsumi, S. Tokura, M. Miyake, J. Nucl. Mater. 155-157 (1988)

[136] H.Atsumi, K. Tauchi, "*Hydrogen absorption and transport in graphite materials*", J. of Alloys and Compounds 356-357, 2003

[137] P.G. Fischer, "Zum Verhalten von tritium in Reaktorgraphiten", J.Nucl. Mat. 1977

[138] A.A. Haasz, P. Franzen, J.W. Davis, S.Chiu, C.S. Pitcher, Journal of Applied Physics, 77, 1995

[139] M. Warrier, "*Multi-scale modelling of hydrogen isotope transport in porous graphite*", PhDDissertation, University of Greisfswald, Germany, 2004

[140] K.Ashida, K. Watanabe, "*Diffusion costants of tritium in graphites and compensation effect*", J. Nucl. Mat. 183, 1991

[141] M. Saeki, "*Effects of pyrolitic carbon structure on diffusivity of tritium*", J. Nucl. Mat. 131, 1985

[142] J.Woerner, W. Botzem, S.D. Preston, "*Heat treatment of graphite and resulting tritium emissions*"

In particular, Fachinger et al.[144] observed a fast initial release of tritium under thermal treatment in argon atmosphere, connected with the desorption from the active superficial sites: tritium desorption was not limited by diffusion in pores; however it was supposed that higher temperatures would have resulted in higher fractional releases. Tritium release from graphite started from 800 °C, increasing with temperature. The most promising treatment for tritium removal is likely to imply high temperatures and argon atmosphere, to obtain at the same time high fractional releases of tritium and low graphite burn-off.

5.3.3 Chlorine-36

Chlorine is normally present in nuclear graphite, resulting from impurities in the raw materials that have not been removed or from purification processes (see chapter 5). Normal values of Chlorine content in nuclear graphite range from some ppm to about 50 ppm. In the case of AVR graphite it amounts to about 30 ppm, much higher than in SL2 graphite, around 8 ppm[145]: the reason of that stands on the different raw materials, the manufacture process and also the purification process. Indeed, the purification treatment with halogens is able to remove sulphur and many metallic impurities (see chapter 6), but in the case of AVR graphite no purification process was used.

Chlorine-36 is a pure beta emitter with a maximal energy of 708.7 keV. It is a long-lived radionuclide with a half-life of about 301000 years and it is easily mobile in the environment. In particular it could represent a consistent problem in case of water ingress into the storage site.[146] Moreover, the impact on the environment would be significant due to its high soil-to-plants transfer factor[147].

To understand whether the formation of Cl-36 could displace the nuclide from its position the resulting recoil energy has to be calculated. The recoil energy of ^{36}Cl from the reaction $^{35}Cl(n,\gamma)^{36}Cl$ was calculated with eq. (5.3.3.1)

(5.3.3.1) $$E_R = 536.79 \cdot \frac{{E_\gamma}^2}{M}\ [eV]$$

with M= mass of the daughter nuclide
E_γ= energy of the emitted gamma-ray in MeV
E_R recoil energy in eV

---

[143] T. Podruzhina, "*Graphite as radioactive waste: corrosion behaviour under final repository conditions and thermal treatment*", Juel 4166, 2004
[144] J. Fachinger, W. von Lensa, T. Prodruhzina, "*Decontamination of nucelar graphite*", Nuclear Engineering and Design 238 (2008)
[145] Zsolt, Revay, "*PGNAA measurements*" for Forschungszentrum Jülich, 2010
[146] Toulhoat P., "*Scientific bases for nuclear waste management*", Mat. Res. Soc. Symp.Proc., 2007
[147] S.C. Sheppard, L.H. Johnson, B.W. Goodwin, J.C. Tait, D.M. Wuschkle, C.C. Davidson, "*Waste Manage*",16 (1997)

Gamma rays range from 517 to 8579 keV. The recoil energy resulted in 4 eV for a 0.5 MeV gamma-ray to 1.1 keV for a 8.6 MeV gamma-ray. Since the mean energy to displace an atom from its lattice site is about 25 eV,[148] in most cases the ^{36}Cl will be displaced. The displaced Cl-36 will be a free uncharged atom or an electrically charged species, extremely reactive in both cases with the first either species it encounters.[149]

The release of Chlorine-36 depends on different processes, such as water saturation or water access into the graphite pore spaces. In addition, its chemical form is fundamental to determine the solubility in water, diffusion and retention behaviour.

Previous experiments on virgin UNGG SL-2 graphite[150] were performed through implantation of ^{37}Cl to simulate the behaviour of ^{36}Cl displaced from its original site through recoil. It was shown that Chlorine started to be released even at low temperatures (200 °C). At higher temperatures, around 20% of chlorine was released after 4 h treatment at 500 °C, through open pores as a preferential way, with an activation energy E_a<0.1 eV: the low value of the activation energy showed that chlorine loss was athermal. The release for higher temperatures (up to 800 °C) reached a plateau of 30 %.

Experiments on irradiated graphite[151] showed similar results, with a rapid release of Chlorine in the order of 50% in Magnox graphite and 30% in AGR graphite. These results point toward the existence of two chemical forms of chlorine, with different thermal stabilities. Following this hypothesis, during the reactor lifetime, the most "mobile" fraction will be released.

Further experiments on SL2,[152] performed in inert atmosphere at 10°C/min up to 1000 °C, confirmed what previously stated showing that HCl desorbs between 200 and 600 °C, with a peak around 350 °C followed by a shoulder around 450 °C, observed also for the oxygenated gases. Such desorption dynamic could reflect the presence of two location with different accessibilities, putting in evidence, for the chlorine, the existence of two chemical forms: some XPS (X-Ray Photoelectron Spectroscopy) analysis confirmed the existence of chlorine as inorganic (around 30% fraction, probably ClO_2^- or ClO_3^-) and organic (around 70% fraction, in the form of sp^2 bonded C-Cl) in virgin SL2 graphite. The most mobile fraction, removed by thermal treatments, resulted in the inorganic one, with a release increasing with

[148] S.Blow, J. Phys. D., Appll. Phys. 4 (1971)

[149] A.M. Clayton, A. Harper, C.J.Wheatley, AEA Technology, "*Behaviour of chlorine in nuclear graphites*", UK NIREX report, 1996

[150] C.E. Vaudey, N. Toulhoat, N. Moncoffre, "*Thermal Behaviour of chlorine in nuclear graphite at a microscopic scale*", J. Nucl.mat. 395 (2009)

[151] A.M. Clayton, A. Harper, C.J. Wheatley: "*Behaviour of chlorine in nuclear graphites*",1996

[152] C.E. Vaudey, N. Toulhoat, N. Moncoffre, "*Chlorine speciation in nuclear graphite: consequences on temperature release and on leaching*", Radiochim. Acta 98, 2010

temperature[153]: a thermal treatment of 4 h in vacuum (10^{-4} Pa) at 1000 °C showed the complete removal of the inorganic fraction. Moreover, successive investigation excluded the presence of metallic-chloro species in the SLA2 virgin graphite and confirmed the presence of Chlorine (up to 50 μm depth) prevalently in the organic form.[154] Since the organic fraction showed to be the more resistant to thermal treatments it is believed that the same one is the less leachable during dismantling and disposal of graphite.

It has to be underlined, however, that the SL2 reactor was a CO_2-cooled gas reactor and, in addition, the graphite grade is unique for every reactor: the observed results could reflect the AVR graphite behaviour too but, as observed in many cases[155], the release efficiencies are different for similar experiments, due to the high number of influencing variables affecting the graphite behaviour/characteristics. In addition, considering the i-graphite, the operating conditions in the reactor could affect significantly the Chlorine speciation. Some SIMS mapping of SLA II graphite showed a heterogeneous distribution of chlorine at a scale of 100 μm^2; in particular chlorine was observed as aggregates into spots smaller than 5 μm. Moreover, the heterogeneous ^{35}Cl distribution found to be not related to the presence of pores (appearing as black holes in the SIMS analysis).[156] After the thermal treatment it was observed a decrease of the signal/noise ratio of the spectra with increasing annealing temperature: this confirms the release of Chlorine during the treatment.

The pre-treatment to remove chlorine would reduce the radionuclide inventory at the end of the reactor life. From this point of view, the new industrial purification methods of virgin graphite have been slightly changed, replacing the chlorine with fluorine (see chapter 5). On the other hand, thermal treatments of i-graphite seem to be effective in general, but considering the special grade of the AVR graphite some investigations are needed to comprehend the effective removal of such radionuclides and the behaviour of the irradiated graphite in a geological repository.

---

[153] Idem

[154] C.E. Vaudrey, C. Gaillard, N. Toulhoat, N. Moncoffre, M.L.Schlegel, L. Raimbault, "*Chlorine speciation in nuclear graphite studied by X-Ray Absorption Near Edge Structure*", J. Nucl. Mat. 418 (2011)

[155] Results from similar thermal treatments on Merlin and AVR graphite were different

[156] C.E. Vaudrey, C. Gaillard, N. Toulhoat, N. Moncoffre, M.L. Schlegel, L. Raimbault, "*Chlorine speciation in nuclear graphite studied by X-Ray Absorption Near Edge Structure*", J. Nucl. Mat. 418 (2011)

6. Decontamination Methods for i-Graphite

Radioactive waste with negligible heat generation makes up approximately 90 per cent of the total radioactive waste in Germany but is only responsible for 0.1 percent of the total radioactivity of radioactive waste requiring final storage. Approximately 94000 cubic meters of such waste with negligible heat generation is currently stored in intermediate storage facilities above ground; experts expect a further 186000 cubic meters by the year 2040.
After introducing a standardized radioactive waste classification system, a particular repository for the disposal of German carbonaceous waste will be introduced, focusing the attention of the fact that, generally, the waste acceptance criteria govern the requirements for conditioning and treatment. At last, a comparison among different purification method will be performed, focusing the advantages and disadvantages of every treatment.

6.1 Waste Classification

There are many ways to classify radioactive waste. IAEA proposed firstly a three classes-qualitative[157] classification system that has been updated along the years up to the latest definition of six different classes.

- *Exempt waste* (EW): Activity levels at or below clearance levels given in Ref. [[158]], which are based on an annual dose to members of the public of less than 0.01 mSv
- *Very Short- Lived Waste* (VLSW): Waste that can be stored for decay over a limited period of up to a few years and subsequently cleared from regulatory control according to arrangements approved by the regulatory body, for uncontrolled disposal, use or discharge.
- *Very Low Level Waste* (VLLW): Waste that does not necessarily meet the criteria of EW, but that does not need a higher level of containment and isolation and, therefore, is suitable for disposal in near surface landfill type facilities with limited regulatory control.
- *Low Level Waste* (LLW): Waste that is above clearance levels, but with limited amounts of long-lived radionuclides. Such waste requires robust isolation and containment for periods of up to a few hundred years and is suitable for disposal in engineered near surface facilities. This class covers a very broad range of waste. LLW

[157] IAEA proposed the first waste classification in 1970, revised in 1981 and at last in 1994.
[158] IAEA, "*Application of the Concepts of Exclusion, Exemption and Clearance*", IAEA Safety Standards Series No.RS-G-1.7, IAEA, Vienna (2004).

may include short-lived[159] radionuclides at higher levels of activity concentration, and also long-lived radionuclides, but only at relatively low levels of activity concentration.

- *Intermediate Level Waste* (ILW): Waste that, because of its content, particularly of long lived radionuclides, requires a greater degree of containment and isolation than that provided by near surface disposal. However, ILW needs no provision, or only limited provision, for heat dissipation during its storage and disposal. ILW may contain long-lived radionuclides, in particular alpha emitting radionuclides that will not decay to a level of activity concentration acceptable for near surface disposal, during the time for which institutional controls can be relied upon. Therefore, waste in this class requires disposal at greater depths, of the order of tens of meters to a few hundred meters.
- *High Level Waste* (HLW): Waste with levels of activity concentration high enough to generate significant quantities of heat[160] by the radioactive decay process or waste with large amounts of long lived radionuclides. Disposal in deep, stable geological formations usually several hundred meters or more below the surface is the generally recognized option for disposal of HLW.[161]

Quantitative values of allowable activity content for each significant radionuclide are specified on the basis of safety assessments for every individual disposal site.

The developed classification scheme provides a framework for defining waste classes within national waste management strategies and to serve as tool to facilitate the communication on radioactive waste safety. The boundaries between the classes are not intended to be seen as hard lines but rather as transition zones whose precise determination will depend on the particular situation in each State. The classification scheme covers all types of radioactive waste.

The aim of such classification is to give a clear and simple method to separate radioactive wastes and to decide which management strategy can be adopted. It would be necessary that different countries could adopt the same limits. In spite of the above-described

[159] In terms of radioactive waste safety, a radionuclide with a half-life of less than about 30 years is considered to be short-lived

[160] The previous classification system quoted a corresponding thermal power of 2-20 kW/m^3 but it has been removed since the thermal power is a matter of safety considerations of a geological disposal facility. However, HLW has a typical specific activity in the range of 10^4-10^6 TBq/m^3

[161] IAEA, "Classification of Radioactive Waste", General Safety Guide no. GSG-1, Vienna, 2009

classification, some countries classify radioactive waste according to the facilities in which this waste is generated or by the processes that generate such waste. In particular some states classify i-graphite as Intermediate Level Waste (ILW) whilst others regard it as Low-Level Waste (LLW). I-graphite that has been removed from reactors is presently stored in interim storages (silos, vaults and other buildings) awaiting a final management solution.

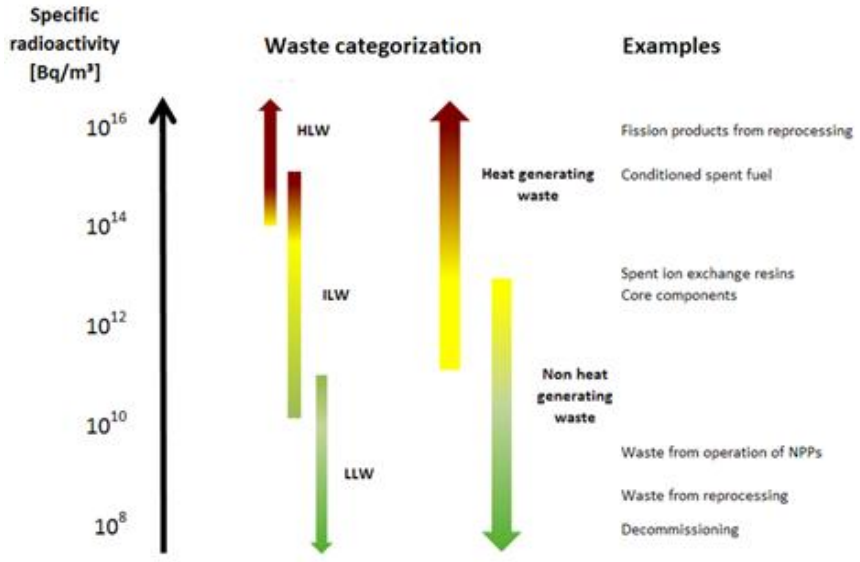

Figure 6.1.1: Scheme of the three-classes waste classification system compared to the heat-generating classification

6.2 Options for the Disposal of Irradiated Graphite in Germany

6.2.1 Repository Konrad

The pit Konrad (Schacht Konrad) is an abandoned iron ore mine proposed as a deep geological repository for medium and low level radioactive waste in the city Salzgitter in southeast Lower Saxony, Germany. It has two shafts of which Schacht Konrad I is approximately 1232 meters deep and Schacht Konrad II is around 1000 meters deep.

It is the first repository that has been licensed according to nuclear law. Morsleben was erected in the former DDR without a corresponding participation of the public; the Asse mine was established as research mine and operated according to Mining Law and Radiation Protection Ordinance[162].

The pit operated only for 15 years, starting from 1961. Thus, it does not feature the high degree of utilization of old salt mines which, like Morsleben and Asse, were used for radioactive waste disposal. For example, Asse's rock conformation and its former intensive

[162] http://www.endlager-konrad.de/cln_153/nn_1272768/EN/Subjects/Preface

usage caused water infiltrations resulting in sealing failures of some waste-containers: Cesium leakage was observed after a short time period.[163] In addition, waste will not be stored in old mining cavities in the Konrad repository but all emplacement galleries will be newly driven.

The ore deposits are situated 800 to 1300 meters below the Earth surface and are exceptionally dry. An up-to-400m thick roof of clayey layers seals the mine from groundwater and also from the Salzgitter channel located above the mine. This means that the storage area of the Konrad repository has no hydraulically effective connections to near-surface groundwater.

The establishment of the technical installations for the disposal and storage chambers started. The conversion is taking several years and storage is scheduled to start in 2013.

6.2.2 Konrad Acceptance Requirements and CarboDISP Project

The Konrad repository is approved for a maximum of 303000 cubic meters of waste,[164] even though the available volume is much higher.

Waste acceptance requirements for Konrad repository have been established on the basis of a site-specific safety-assessment. Different requirements have to be fulfilled to choose a proper package:

- package geometry
- total activity inventory of repository: for example the maximum disposal activity at the end of the Konrad operation is $6 \cdot 10^{17}$Bq for Tritium and $4 \cdot 10^{14}$Bq for radiocarbon
- activity limits per package
- dose rate limits
- weight limits
- mass limits

The disposal of i-graphite in the German KONRAD repository is investigated within the German CarboDISP project, which is complementary to the European CARBOWASTE project. The total ^{14}C activity being allowed for KONRAD is only $4 \cdot 10^{14}$ Bq.[165] With an overall storage capacity of 303000 m^3 this results in $1.32 \cdot 10^9$ Bq/m^3, as an average. For the disposal of ^{14}C-

[163] http://www.bfs.de/en/endlager/asse/grundlagen/geschichte.html

[164] http://www.endlager-konrad.de/cln_153/nn_1996290/EN/Subjects/Origins

[165] P. Brenneke, *"Anforderungen an endzulagernde radioaktive Abfälle"* (Vorläufige Endlagerbedingungen, Stand: April 1990 in der Fassung vom Oktober 1993) - Schachtanlage Konrad -. 1993. BfS-ET-3/90-REV-2.

waste in KONRAD different limits result from three safety analyses that have to be considered. Most restrictive ^{14}C limits arise from safety analysis for internal operation (T ~ 50°C), classified by ^{14}C release from the waste container:

1. If a maximum release of <1% of the total ^{14}C inventory can be guaranteed, the limit is $1.8 \cdot 10^{10}$Bq per container either individual or in average within a batch of containers. This means that about 22000 waste containers will be needed to accommodate the allowed total ^{14}C activity of $4 \cdot 10^{14}$Bq. Taking as a basis a typical container volume of 10 m^3 (Type V KONRAD-Container) the number of containers corresponds to about 70% of the total repository volume.
2. If the 1% limit cannot be kept but ^{14}C releases may range up to 10%, then the maximum ^{14}C activity of a waste container must not exceed $1.8 \cdot 10^{9}$Bq resulting in a ten times higher repository volume which exceeds the KONRAD capabilities.
3. At last, if ^{14}C release cannot be specified the limit is even more restrictive being $1.8 \cdot 10^{8}$Bq per container.

Under this background, the CarboDISP project will focus on the ^{14}C release mechanisms under KONRAD operating and disposal conditions for German i-graphite waste including irradiated carbon brick, which contains a much higher ^{14}C contamination because of the rather high nitrogen concentrations already present in the virgin material.[166]

Following the above-mentioned restrictions, a direct disposal of the AVR contaminated materials (graphite and carbon brick) in the repository Konrad is out of question, resulting in the 0.5 % of the licensed activity for tritium and in the 72.5 % of the licensed activity of radiocarbon (option 1): the absolute necessity of a conditioning/decontamination process led the scientific community, in particular the Forschungszentrum of Juelich, to investigate on the release behaviour of AVR graphite (together with other ones) and to look for the efficient treatment& conditioning methods to meet the Konrad acceptance requirements.

[166] In general carbon bricks contain higher amounts of impurities than graphite, leading to higher activation products after neutron irradiation

6.3 Purification Methods

6.3.1 Purification Methods Developed in the Carbon Industry

In the carbon industry three methods have been developed to purify graphite:

1. Usage of extremely pure raw material or purify it a priori: this method is very restrictive as to choice of raw material. Generally the purification a priori is not adopted since it is preferred to perform all the interventions in the last stages of the manufacture.
2. Thermal purification of formed graphite: the graphitization step is conducted at sufficiently high temperatures to cause impurities to diffuse out of the graphite. This method is relatively inexpensive but does not remove completely all the impurities.

The reached temperatures are normally higher than the one used for normal graphite, i.e. 2800-3000 °C in the Acheson process. In general, all low-boiling impurities are removed by graphitization; the remaining ones form carbides. These impurities are extremely stable, often far beyond their vaporization temperatures, since they can be often found at imperfections within the graphite crystals: for example Boron Carbide has a melting point of 2350 °C and Vanadium Carbide melts at 2800 °C. The fact that during thermal purification impurity atoms must diffuse out of the graphite results in a lower degree of purification compared to the thermo-chemical process (3). In general, the thermal purification is facilitated by using petroleum coke as packing material instead of metallurgical coke because of the lower amounts of impurities embedded in it.

3. Chemical purification by using halogens in form of both halide-gases or halide-salts. This method produces the purest graphite, but it is expensive.

Halides are able to penetrate bulk graphite and graphite lattice, react with impurities and remove them as volatile halide species. The most used techniques imply Freon-12 (CFC) or Chlorine (Cl_2). The typical sequence consists on introducing chlorine gas when the furnace reaches 1000 °C and shifting to Freon when a temperature of 2000 °C is reached. During the cooling step the furnace is flushed with nitrogen or inert gas to remove the residual chlorine gas from the porous graphite. It has to be underlined that it is impossible to remove completely the above-mentioned gases, which will represent an additional impurity leading to neutron activation. However it is a matter of benefits/costs: normally the advantages gained through graphite purification are much more important that the disadvantages resulted from residual halides from the thermo-chemical purification process. Fluorine can be used instead of chlorine, with the advantage of removing boron in addition to the other

impurities. The obtained purity depends on the cross sectional area of the graphite and on its permeability: the gases must diffuse into the material and the impurities must diffuse out.

It is possible to use also halide salts, usually sodium fluoride (NaF). Normally the purification with salts is performed during the graphitization stage, in the way to take advantage of the thermal power spent anyway to produce graphite, saving so time and energy. The positioning in the furnace of such purification compounds must allow the salt volatilization at high temperatures (T>2000 °C) so they are not in direct contact with the graphite but they are all around it. The purification yield is similar for both procedures implying halide gases or salts.

In table 6.3.1 some representative impurity levels are reported to give an idea of the effective purification efficiency of the above-mentioned processes.

Early graphites, including the AVR one, were developed by using a simple thermal purification method in conjunction with the graphitization process. This led to considerable impurity amounts resulting, after nuclear activation, in high activities and in turn in considerable problems during retrieval, handling, treating and storage of such materials.

Nowadays most nuclear graphites, used as moderator or reflector, are thermo-chemically purified using fluorinated compound, in order to avoid the contamination by chlorine and to reduce the presence of the successively-activated Cl-36.

	Impurity level [ppm]		
Impurity	**Unpurified**	**Thermally purified**	**Chemically purified**
Total ash	1600	540	5
Silicon	94	46	<1
Iron	310	10	<2
Vanadium	30	25	<0.2
Titanium	34	11	1
Aluminum	40	2.5	0.1
Calcium	320	147	1.4
Boron	0.5	0.4	0.06
Sulfur	175	19	10

Table 6.3.1: Representative impurity levels of three classes of graphite[167]

[167] Nightingale, R.E. ed. 1962. *Nuclear Graphite*. New York and London: Academic Press

6.3.2 Comparison among some Purification Methods

As described in section 6.2.2, the necessity of an intervention on the irradiated graphite arises from the waste acceptance criteria of the designed repository. In fact, a mere cementation of i-graphite would not result in a proper conditioning since the organic carbon would not be fixed, as eventual carbon monoxide.[168] In the specific case of Konrad waste acceptance criteria a conditioning treatment could correspond to a purification one. In fact, if the chosen method were able to improve graphite behaviour with regards to radionuclide leaching, at the same time it could be possible to remove significant amounts of radioactivity. In the best case a declassification of the waste could occur, but it would request a very complex method since many nuclides are removable in different ways.[169] The final target, however, is to close the life-cycle of graphite, in order to reduce the considerable amount of radioactive wastes arising from decommissioned NPP: after being used in a reactor it will be purified and be re-used in the nuclear field.

The first, easiest method that could be thought is the simple burning of graphite. Unfortunately it will not solve the graphite problem and, on the contrary, the risk of releasing ^{14}CO and $^{14}CO_2$ in the environment will arise. An option could be to segregate the off gases, connecting to the similar solution of CO_2 sequestration, but the risk of leakage in the environment would be too high. Another option consists on precipitating the CO_2 in a solid form. Even though this option were safer, a mere burning of the entire amount of i-graphite followed by precipitation would increase the total volume of waste.[170]

A second option to decontaminate/condition i-graphite is represented by electrolysis. It is performed in two steps: the graphite is disintegrated by formation of graphite oxide and, afterwards, an anodic oxidation takes place. The $^{14}CO_2$ is accumulated in the anodic off-gas while other radionuclides are released through isotopic exchange or electro-migration. The great disadvantage of such method is represented by the mass gain due to graphite oxidation, ranging up to 23%, so further treatments are necessary to reduce again the graphite. On the other hand, the ^{14}C and ^{3}H released can be very high (up to 79% and 86% respectively).[171] However, this can strongly depend on the operational history of the graphite (temperature, atmosphere, neutron dose, radiolytical mass loss etc.), because this has an

[168] Cementation is able to fix CO_2 as a carbonate, but all the other forms of carbon are not retained properly
[169] Not all of them are known
[170] See next section
[171] Experiments of Dr. Vulpius, Forschungszentrum Jülich

impact on the location and concentration of radionuclides. Despite the disadvantages, such treatment seems to be a promising one, supposing to use it as part of a multi-step process to avoid a dilution of tritium in the electrolyte.

A further option is represented by a chemical treatment: in this case the graphite becomes in contact with an acidic solution, able to penetrate deeply into the pore system. In that way, the removal of radionuclides as ^{14}C and ^{3}H would be ensured even at room temperatures. Some experiments with a solution of H_2SO_4 and HNO_3 resulted in a high release of tritium (90%) and low release of ^{14}C (14%).[172] The tritium is released for isotopic exchange with the solution. However, long time is necessary for the treatment, up to 3 months for a single sample. Moreover, the used solution must be decontaminated in turn: the treatment seems not to be convenient, without pre-extraction of tritium.

Moreover, thermal treatments are considered. Their aim is to separate selectively the nuclides from the graphite matrix, producing at the same time as low as possible graphite oxide. For this scope, different temperatures and different gases are used. Former experiments have obtained great result concerning tritium release (up to 90%), but ^{14}C release was very limited, except for the cases with high graphite burn-off. A stand-alone thermal treatment, at the present state, could only contribute to the conditioning of the carbonaceous waste. Indeed high values of ^{14}C removal cannot be achieved, considering its probable not homogeneous distribution: only the most superficial contamination is likely to be depleted but, from point of view of the leaching behaviour, it represents an important improvement. Many researches are in progress to optimize the treatment parameters and to better understand the nuclides release mechanisms. Once the radionuclides are released in gaseous form (^{14}C and ^{3}H), it is necessary to segregate them or to precipitate them. In the case of tritium, it can be done by isotopic exchange reaction with and HNO_3 solution. The ^{14}CO can be oxidized to $^{14}CO_2$ and be precipitated as carbonate or solid carbon. (see next section for further details)

A particular treatment could be represented by in-situ radiolytical process. This implicit process was observed in CO_2-cooled reactors, in particular in the UNGG and Magnox ones. Since the used coolant is CO_2, radiolytical oxidation could occur. In that way, the graphite is "treated" during the reactor operation, but careful must be taken for the released gases. In addition, consistent high mass loss could take place (10-40%), leading to structural damage of graphite. However, past experiences showed ^{14}C and tritium amounts much lower than in

[172] Data from Dr.Vulpius, Forschungszentrum Juelich

other reactors, leading to declare that the major contributor to ^{14}C production was the ^{13}C, as it is assumed that this part of the ^{14}C is preferably kept in the bulk of the graphite crystals.[173] It has been proposed to apply in-situ purification methods at the end-of life of reactors, before permanent shutdown.

Among the chemical methods, the intercalation seems to be a promising one. Graphite is immersed in a solution of H_2SO_4 and H_2O_2 and partially oxidizes at room temperature. In short time the graphite structure is destroyed, allowing the release of many radionuclides. Further treatments are necessary for the solution and the produced exfoliated graphite. Once it has been treated by removing most of the radionuclides, it can be compacted again in a stable way.

Referring to the previous section 6.3.1, supposing that radioactive species show identical chemical properties than the non-radioactive ones (e.g. Cl-36 and Cl-35), the chemical purification process with halogens seems to be one of the best suitable for the removal of many impurities. Considering an efficient treatment, i.e. the thermo-chemical one, it would be necessary for and industrial process implying big blocks in an Acheson furnace with exhaust gas cleaning facility to condense the vapours leaving the material. The contamination problem, however, seems to be only partially solved in this way, since the ^{14}C content could not be totally reduced, except the part which is generated via nitrogen activation and thus exposed at the outer and inner surfaces.
Another promising solution could be represented by a first thermal treatment, able to remove most of the tritium, followed by graphite chemical exfoliation. In this particular case, during the exfoliation process, all the volatile nuclides are free to escape because of their destroyed traps/bonds: for example tritium, if not removed previously, could be released to the air or could isotopically be exchanged with the acidic solution, resulting in a larger amount of waste.

In conclusion, looking forward to the development of an industrial purification process, the best option seems to be the multi-step one, including for example a first thermal treatment followed by a chemical one. A radionuclide removal with the lowest release of normal carbon has to be achieved, otherwise in the end higher volumes will result and the treatment itself will become disadvantageous for disposal. In addition, successive treatments must produce materials (containing the radioactive isotopes) with improved leaching behaviour in comparison with the irradiated graphite.

[173] This fact has been discredited in chapter 4: the major contribution to C-14 comes from Nitrogen-14

In table 6.3.2 the above-described treatments with the respective advantages/disadvantages are summarized.

Treatment	Advantages	Disadvantages
Burning	• Easiest way	• Risk of CO, CO_2 release in the environment • Higher volume for disposal if gases precipitated as carbonates
Electrolysis	• High Release of C-14	• Mass gain up to 23% • Further treatment necessary for graphite oxide
Chemical by acidic solutions	• Deep penetration into pore system	• Leaching solution has to be treated • Low releases in long time
Heat treatments	• Highest release of H-3 • Low oxidation • Possible reuse of materials	• Present low release of C-14
Radiolitical in-situ 'treatment'	• Possibly best option • Oxidation and heat together	• Possible high mass loss 10-40% • Possible structure failures • Applicable only at End-of-Life
Graphite exfoliation	• Access to all radionuclides for successive separation • Graphite powder compacted afterwards	• Leaching solution has to be treated

Table 6.3.2: Comparison among different purification treatments of carbonaceous materials

6.3.3 Off-gas Processing: some Options to Precipitate Radiocarbon

A generic process of thermal type for graphite purification leads to obtain off gases where many radionuclides are present, e.g. $^{14}CO_2$, ^{14}CO, HTO, HT.

Even though the specific problem is related to the nuclear field, a similar one in the energy generation industry is the CO_2 segregation. In this case, however, the radiocarbon-dioxide is considered, so standard segregation techniques are not advisable: the ephemeral amount of radioactive matter requires more efficient retention methods.

Many strategies are under study and even though some of them are applicable, nowadays an industrial-scale process of $^{14}CO_2$ conversion/retention does not exist.

6.3.3.1 Obtaining Carbon in Solid Form

A first process could adopt the following reaction:

$$CO_2 \Rightarrow C + O2 \qquad (\Delta H=393{,}5\ kJ/mol)$$

which, being extremely endothermic, requires consistent amounts of energy.

An alternative to that is represented by the Bouduard reaction to obtain solid carbon as soot:

$$2CO \Rightarrow C + CO_2 \qquad (\Delta H=-\ 171.5\ kJ/mol)$$

unfortunately, this way allows to recover only half of the carbon atoms.

Another option is represented by the graphite gasification with hydrogen:

$$C + 2H_2 \Rightarrow CH4 \qquad \text{(formation of methane)}$$

$$CH_4 \Rightarrow C + 2H_2 \qquad \text{(pyrolysis of methane)}$$

These methods lead to obtain carbon in form of soot, difficult to handle, treat and store in a safe way.

Nowadays, the most used method for the final storage of nuclear graphite is the incorporation in concrete.

More efficient methods consist of transform CO/CO_2 in a solid form as a carbonate.

6.3.3.2 A more Complex Solid: Conversion of CO_2 in Alkaline Earth Carbonate

This process allows precipitating, directly on through a double alkali process, the carbon dioxide.

In the following, some calculations are performed to allow some evaluations from the point of view of the final storage.

The so-called carbonation reaction is:

$$X(OH)_2+CO_2 \Rightarrow XCO_3+H2O$$

with X=Ca, Sr, Ba

It is considered here the molar volume for each species, in order to evaluate the final occupied volume starting with the same amount of carbon.

$$V_{mol}=M_{mol}/\rho$$

In table 6.4.2 are showed some calculated values for different carbonates.

ElementUsed	M [g/mol]	Density [g/cm^3]	Vmol [m^3/mol]	Relative volume [-]
C	12	2.09-2.23	5.38-5.74 · 10^{-6}	1
$MgCO_3$	84.31	2.96	28.50 · 10^{-6}	5-5.3
$CaCO_3$	100.09	2.93	34.44 · 10^{-6}	6-6.4
$SrCO_3$	147.63	3.74	39.47 · 10^{-6}	6.9-7.3
$BaCO_3$	197.34	4.43	44.55 · 10^{-6}	7.8-8.3

Table 6.3.3: Comparison among different carbonates properties

Considering the calculated values it seems that the conversion of carbonaceous materials, through thermal treatments, in CO_2 is not convenient from the storage point of view: generated volumes range from 5 to 8 times higher than the original one. Indeed, this statement would be right if the logic behind were the simple burning of graphite.

If it were possible to selectively separate ^{14}C in form of ^{14}CO, $^{14}CO_2$ or ^{14}C, the disadvantage of obtaining higher final volumes would be apparent: the volume fraction of $^{14}C/C_{tot}$ is extremely low, in the order of ppm or tens of ppm depending on the neutron fluence, so a volume increasing would lead anyway to acceptable values for the final storage.

Then extracting most of the ^{14}C from the graphite, being the volume of the radioactive materials very small compared with the containing matrix, would lead to reconsider the conversion method as an advantageous one, at least from the point of view of the occupied space.

In conclusion, it has to be considered that carbonates typically show a bad leaching behaviour for an hypothetical water ingress scenario in the repository: the mean dissolution speed in acidic water (pH=4) is $1.65 \cdot 10^{-10}$mol/cm^{2}s for the calcite,[174] about 10^{-13}-10^{-14}mol/cm^{2}s for the magnesite in a pH range 4-8 and 10^{-11} - 10^{-12}mol/cm^{2}s in a pH range 0-4,[175] against the 10^{-16}mol/cm^{2}s for the graphite[176].

From that is can be stated that further studies are necessary to find a more stable matrix containing the ILW from ^{14}C.

[174] J.G. Brown, P.D. Glynn, "*Kinetic dissolution of carbonates and Mn oxides in acidic water: measurement of in situ field rates and reactive transport modeling*", Applied Geochemistry, Vol.18 n.8, 1225, 2003

[175] O.S.Pokrovsky, J. Schott, "Processes at the magnesium-bearing carbonates solution interface. II. Kinetics and mechanism of magnesite dissolution", Geochimica et Cosmochimica Acta, Vol.63 n.6, 881, 1999.

[176] W.J. Gray, "*A study of the oxidation of graphite in liquid water for radioactive waste storage application*", Radioactive Waste Management , Vol.3 n.2, 137, 1982.

6.3.3.3 Conversion in Silicon Carbide

There are two variations of this method: using the whole graphite or using the ^{14}C-enriched fraction, previously removed by other treatments. In general, measured activities of C-14 leached from irradiated graphite showed to be much higher compared to the ones leached from the SiC made from this graphite, up to a factor of 100. Then the SiC represents a valid option for i-graphite conditioning. The preferred option, however, is to imply the ^{14}C enriched part of graphite, since the volume gain with the present method is in the order of 300 % of the original graphite´s one. In fig. 6.3.3 a SiC synthesis process is shown.

TiC and ZrC have also been proposed as waste matrix. The latter would allow using another radioactive waste form (e.g. LWR fuel cladding) together with irradiated graphite, in a way that no additional uncontaminated material would be used.

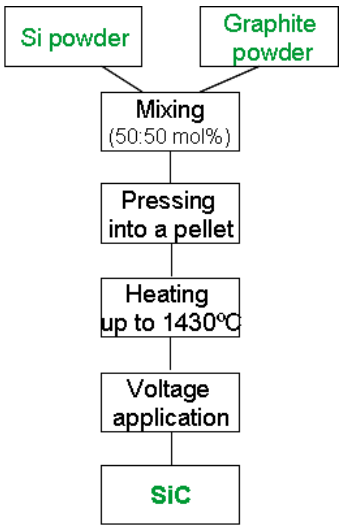

Figure 6.3.3: Flowchart of the SiC formation method

6.3.3.4 Isotopic Separation

It is a method based on the differences of weight among different isotopes, but generally it is rather expensive and complex.

7. Experimental Choices

In the previous chapters the different stages of the life-cycle of irradiated graphite have been discussed for identifying the main contributors of radioactive contamination and their potential release or removal characteristics. Under this background, the experimental choices have to be selected.

7.1 Virgin Materials: Separation of Different Histories

In this work virgin materials, in particular AVR graphite, have been selected to perform some investigations on the effects of thermal treatments and to prove the existence of many embedded chemical species. The reasons behind this choice have been various. In particular, referring to chapter 3, even at the beginning of its life nuclear-grade graphite is unique under many aspects, because of the particular receipt used for its production, the raw materials and the manufacture process. After a temporary storage, the materials are used in the designated reactor: such time period could affect significantly the radionuclide production during the reactor operation. Normally, after the final product is ready, the manufacturer seals it in proper packages in order to avoid the contact with pollutants: as previously mentioned, the prolonged contact with air could lead to adsorption of many gases and humidity on the graphite surfaces and porous structure (see chapter 5). A possible problem could arise during the building of the reactor, when the graphite positioning takes place under atmospheric conditions (air with moisture). It is likely that most of the materials used in the past were positioned without any precaution in that way.
Moreover, the study of virgin materials could help to understand the sources of different precursors, in order to avoid in future application such pre-contaminations and resulting, at the end of the reactor life, in a lower activity of the involved materials. Indeed, many factors are influencing the radionuclide production and migration: even by using the same material in different reactors or in different reactor zones different amounts of contamination are expected. Neutron fluence, temperature and temperature excursions, gases present in the environment of operation are some of the determinant factors which will affect the inventory, contamination and the leaching behaviour under different conditions. From these considerations it follows that a full understanding of the entire contamination route results to be difficult by investigating only the final radioactive product.

Another advantage of using virgin materials stands on the lack of activity, so their handling and treating will not be dangerous and will not request the safeguards measures necessary in

radioactive laboratories. Of course, the development of a purification treatment cannot be focused only on virgin materials, but its development could go through that and, probably, it could be even accelerated. From this point of view, on the basis of the small samples (~ 1-3g) measured in the past, the activity of a larger sample (200 g) of irradiated AVR graphite was estimated in the order of GBq. In addition, there are no massive samples available, due to the fact that only a borehole has been drilled through the irradiated reflector regions. The access to larger samples of i-graphite is a general problem, as most graphite components reside in the cores, awaiting their future retrieval.

It is true that irradiated and virgin graphites show much different behaviour under some aspects, but it is believed that the driving physic-chemical mechanisms are the same: this is the main hypothesis of this work.

Experiments performed in the past,[177,178,179] revealed some uncertainties and not fully understood results. In particular the high initial high release of radionuclides, during thermal treatment and under argon atmosphere, was not well explainable: it was hypothesized that many oxidants could be already embedded in the graphite matrix, resulting in the creation of oxide products that are affecting the release of some radionuclides (e.g. tritium and radiocarbon).

In fig. 7.1.1 a schematic view of the different histories of nuclear-grade graphite is shown. By investigating virgin materials, the first two, i.e. manufacture history and storage during construction, can be better understood, together with their influence on the successive employment in the designated reactor.

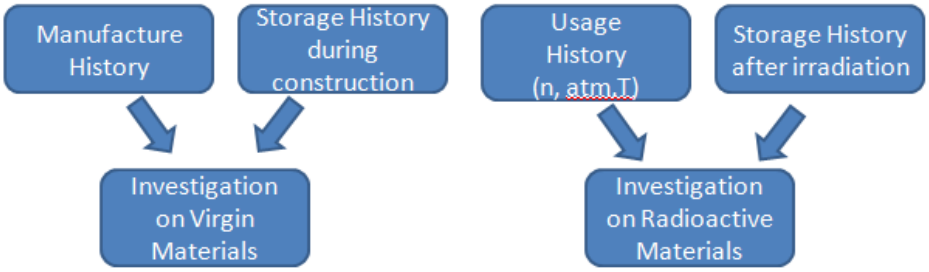

Figure 7.1.1: Scheme of different histories of a nuclear-grade graphite

[177] J. Fachinger et al, "*Decontamination of nuclear graphite*", Nuclear Engineering and Design 238 (2008)
[178] M. Florjan, "*Dekontamination von Nucleargraphit durch thermische Behandlung*", Juel-4322, 2009
[179] T. Podruzhina, "*Graphite as radioactive waste: corrosion behaviour under final repository conditions and thermal treatment*", Juel 4166, 2004

7.2 Treatment Parameters and Sample Selection on the Basis of Former Experiences

A short analysis of the most significant previous experiences[180,181] is reported in this section, in order to choose the best conditions for an efficient removal of volatile/mobile radionuclides.

Sample influence: massive samples experienced higher fractional releases of C-14 than powder samples.[182] The milling was supposed to increase the surface area of ^{14}C-not-enriched graphite, leading to considerable mass losses and low radiocarbon release in relation to C-12 release. The tritium release as well showed to be lower: it is likely that the isotope exchange with humidity released part of the tritium in the ambient air. Following these considerations, the selected sample resulted in a massive one with much higher weight. This also provides a much better chance to characterize the chemical compounds, which are released from the sample during thermal treatment.

Temperature: Tritium showed to be removed more effectively at high temperatures, with a fractional release increasing at higher temperatures.[183,184,185] Radiocarbon, on the other hand, showed to be not dependent on the temperature but rather on a slight oxidation of the surfaces, since it is believed to be concentrated the more in the outer and inner surface of the porous graphite samples.[186] Therefore, the chosen treatment temperature resulted in 1300 °C, following the results obtained in former experiments.

Atmosphere: concerning Tritium, the most effective removal was obtained by using inert gases. Radiocarbon showed to be removed in higher fraction with argon and water steam (65 kPa). However, addition of reactive gases showed an increase on the release together with a higher oxidation of the graphite matrix. A selective oxidation could be the best option to remove as much radiocarbon as possible without important mass losses. For that reason the argon represents a good choice, also for radiocarbon release.

---

[180] T. Podruzhina, "*Graphite as radioactive waste: corrosion behaviour under final repository conditions and thermal treatment*", Juel 4166, 2004
[181] J. Fachinger, W. von Lensa, T. Prodruhzina, "*Decontamination of nuclear graphite*", Nuclear Engineering and Design 238 (2008)
[182] Idem
[183] T. Podruzhina, "*Graphite as radioactive waste: corrosion behaviour under final repository conditions and thermal treatment*", Juel 4166, 2004
[184] M. Florjan, "*Dekontamination von Nuclear graphit durch thermische Behandlung*", Juel-4322, 2009
[185] J. Fachinger, W. von Lensa, T. Prodruhzina, "*Decontamination of nuclear graphite*", Nuclear Engineering and Design 238 (2008)
[186] Idem

In conclusion, the process parameters have been identified as following: 1300°C under inert gas (argon).

Concerning the inert gas choice, hypothetically speaking, there would not be any difference in choosing argon or nitrogen. Considering that nitrogen is one of the precursors of interest and taking into account that nitrogen could react with the graphite surface, the only alternative resulted in the argon.

In figs. 7.2.1-5 some former experimental results[187] are reported to give a clearer view of the discussion reported above. Different graphite grades were investigated and showed typically different total fractional releases. However, similar parameters during thermal treatment resulted in similar radionuclides release behaviour, even with different removal efficiencies.
To clarify the concept it is considered an example: looking at ^{14}C release in fig. 7.2.2, massive samples of Merlin and AVR graphite under argon at 1060 °C show a similar steep release; in the case of AVR the release is limited,[188] but it is believed that the reason of that is the lacking of oxides, already consumed in the first treatment step, which would allow more radiocarbon to be extracted. On the other hand, since the treatment was performed under inert gas, assuming a non-homogeneous distribution of ^{14}C and hypothesizing a higher concentration on the grain boundaries, it follows that the oxidising species were probably already embedded in the material itself. Some results pointing in that direction can be observed in fig. 7.2.3: a high release of ^{14}C occurs in the first minutes of the treatment, then the release ceases. Following this line of thoughts, Florjan[189] performed repeatedly a similar experiment (fig. 7.2.1), exposing the sample to the ambient air between four successive treatments on the same sample: it was observed a lower but proportional release of ^{14}C as in the first experiment, leading to the conclusion that a slight oxidation of the graphite surfaces was probably the best treatment.[190] Proving the existence of oxidizing species inside the graphite is one of the aims of the present work. In addition, the form of released radiocarbon is also important: the possible options are CO_2, CO and small particles of carbon. During the treatment it is likely to observe all these emissions, but their temperature of occurrence and the timing are probably different, as it will be proven in section 8.3.

---

[187] T. Podruzhina, "*Graphite as radioactive waste: corrosion behaviour under final repository conditions and thermal treatment*", Juel 4166, 2004
[188] Up to 20% with mass loss in the order of 1%
[189] M. Florjan, "*Dekontamination von Nucleargraphit durch thermische Behandlung*", Juel-4322, 2009
[190] The atmosphere was not completely inert in that case since the oven was opened in order to insert the sample. However a slight oxidation is still supported as the probable responsible for a good yield of C-14 removal

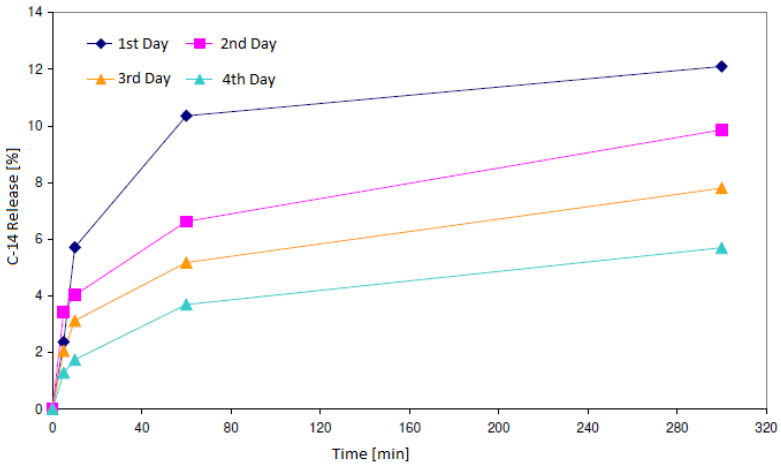

Figure 7.2.1: ^{14}C release vs time during former thermal treatments

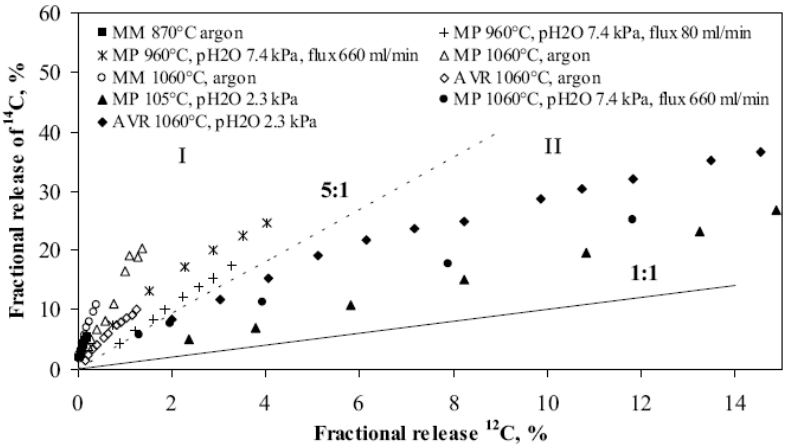

Figure 7.2.2: ^{14}C release vs 12C% release during former thermal treatments[191]

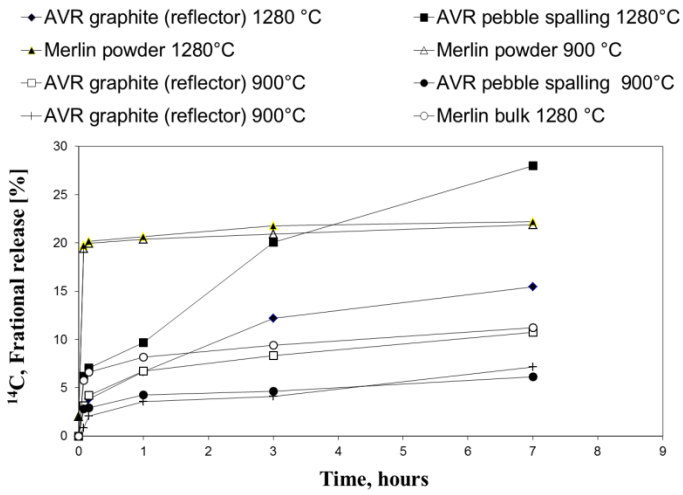

Figure 7.2.3: ^{14}C% fractional release vs time during former thermal treatments under nitrogen[192]

[191] T. Podruzhina, "*Graphite as radioactive waste: corrosion behaviour under final repository conditions and thermal treatment*", Juel 4166, 2004

Considering tritium release, similar observation can be done, even though the release mechanism is totally different compared to ^{14}C. The best results obtained point to a total fractional release of tritium up to more than 90% at 1280°C, much higher than the one at 1060 °C (43%). Furthermore, in fig. 7.2.5 it can be seen a similar steep increase on the tritium release during the first treatment step, leading to hypothesize desorption of tritium and hydrogen from the surface sites. The expected chemical forms of tritium being released are HT and HTO. Linking it to the virgin graphite experiments and assuming the hypothesis that tritium behaves in the same way as the non-radioactive H_2 and H_2O, a similar release should be experienced, probably with higher amounts of water.[193]

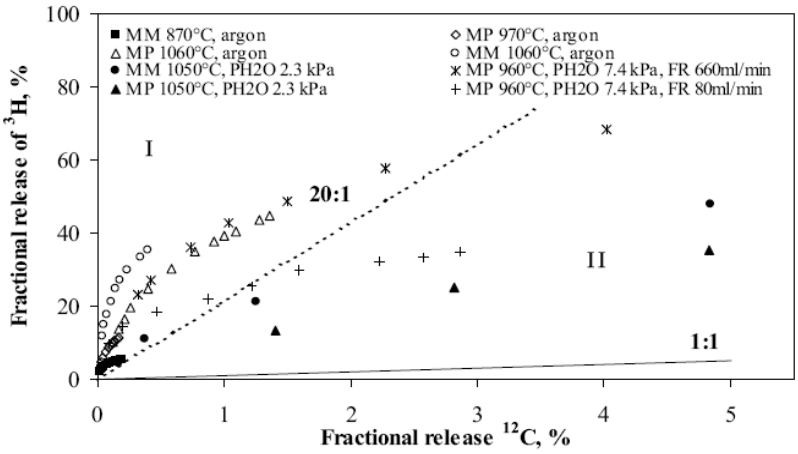

Figure 7.2.4: ^{3}H% release vs ^{12}C% release during former thermal treatments under different conditions[194]

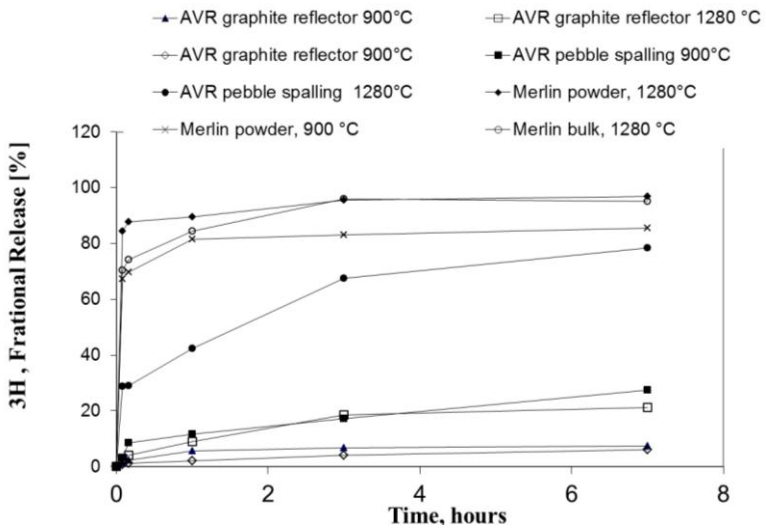

Figure 7.2.5: ^{3}H% release time during former thermal treatments under nitrogen atmosphere[195]

[192] M. Florjan, "*Dekontamination von Nucleargraphit durch thermische Behandlung*", Juel-4322, 2009
[193] See section 8.3 for more details
[194] T. Podruzhina, "*Graphite as radioactive waste: corrosion behaviour under final repository conditions and thermal treatment*", Juel 4166, 2004
[195] M. Florjan, "*Dekontamination von Nucleargraphit durch thermische Behandlung*", Juel-4322, 2009

8. High Temperature Thermal Treatment Experiments

The first part of this chapter will present the equipment used, accompanied with a short description. In a second instance the sample preparation procedure will be described. At last there will be a presentation of every successful experiment, distinguished according to the used equipment.

8.1 Equipment Used

To check repeatability and to rely on the obtained results different equipment have been used to perform similar experiments. Indeed it will be discovered, afterwards, that every equipment present its own problems, but the overall view of the results can lead to understanding the real emissions coming from the investigated sample.

8.1.1 Induction Oven Facility

The Induction oven facility is formed by the following main components:

- Middle frequency generator
- Power supply and Control Unit
- Cooling Unit
- Induction Oven
- Pyrometer

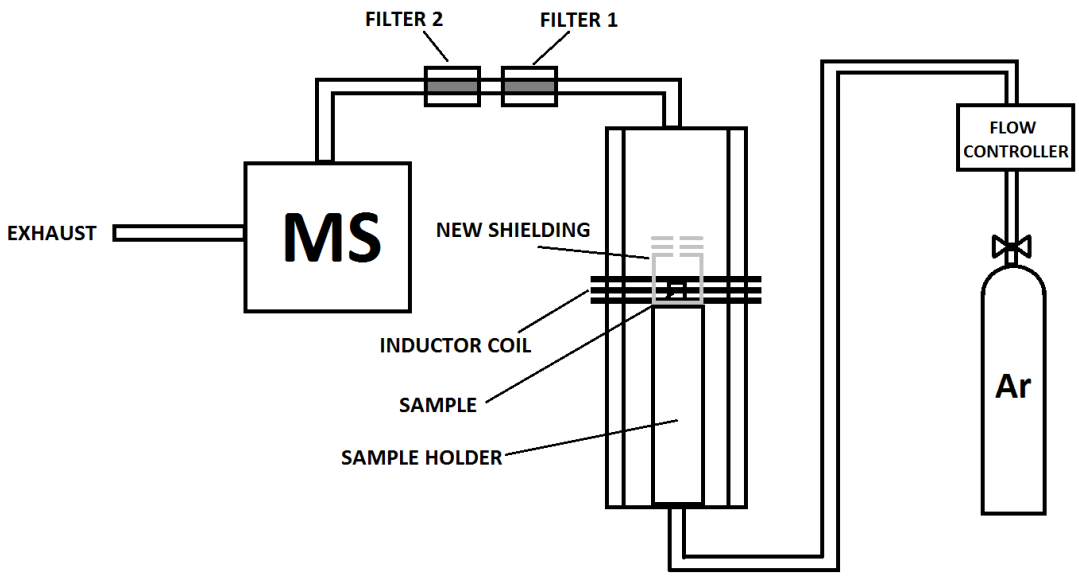

Figure 8.1.1: Overview of the experimental set up with the induction oven

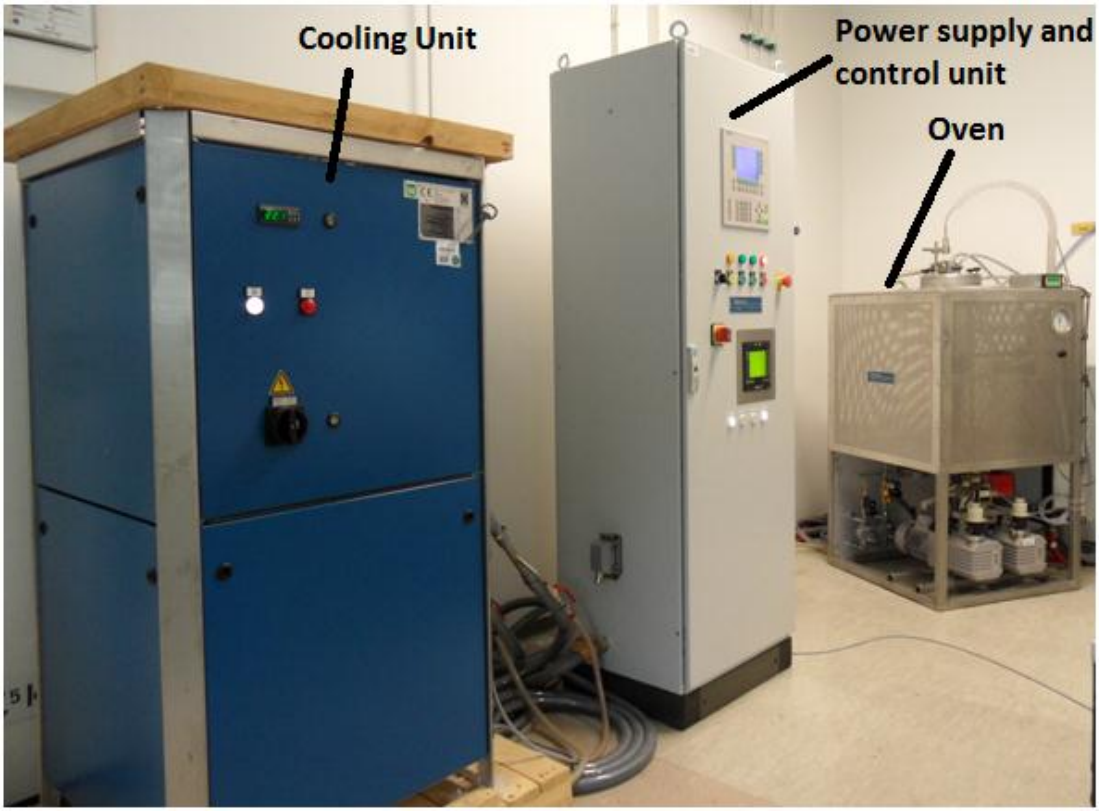

Figure 8.1.2: Overview of the Induction Oven Facility

Working principle

The working principle is based on induction heating: an electrically conducting sample is heated by electromagnetic induction because of the generation of eddy currents (or Foucault currents) within the material; due to the electrical resistance, Joule heating takes place. In the induction heater an electromagnet is placed, through which a middle-frequency current (AC) is passed. The working method is aswith an electrical transformer: the sample behaves like a short-circuited secondary (leading to high currents), whereas a coil connected to the AC power supply forms the primary circuit. Generally speaking, the AC frequency used depends on the object size, material type, coupling (i.e. energy transfer between the work coil and the object to be heated) and the penetration depth.

Middle frequency generator

The 3-phase main supply goes first through a 3-phase rectifier inside the "Power supply and control unit", and it is transformed to DC voltage of about 580V. Then capacitors are used to filter the current. The converter transistors transform DC into middle frequency AC. The current is led over connecting capacitors to the primary side of the output transformer, placed at the oven side. The secondary transformer is connected in series with 2 capacitors (the tank capacitors amount to 17 uF total) and the induction coil.

The oscillator exciting is realized through the control electronics. The control pulses for the converter are frequency modulated and because of this the output power is regulated through changing the oscillating frequency.

Rectifier, capacitors, transformer, transistors, inductor coil are water cooled and protected with water flow switch and thermo switch.

The inductor coil, connected at the converter, can work with the tank capacitance in the frequency range from 10 to 30 kHz.

Control unit

A Siemens control system is installed on the "Power supply and control unit". Because of the complexes operations it was preferred to install a secondary control unit, directly connected to the Siemens' one, for the normal operations concerning heat treatments.

In the same cabinet is placed the power supply and all the safety tools to prevent overloads and overheating.

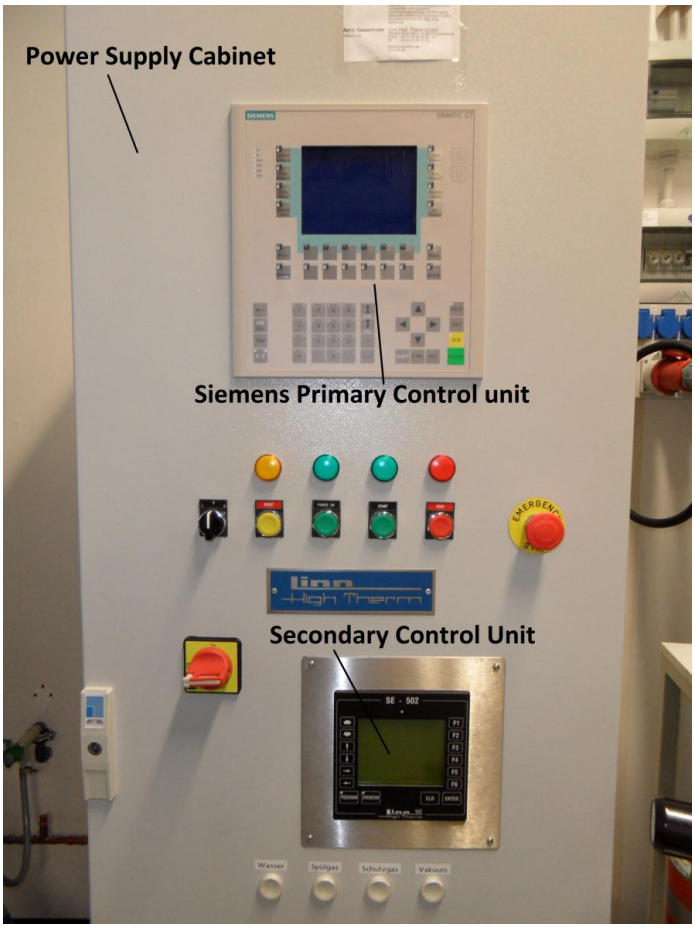

Figure 8.1.3: Front view of the control and power supply unit

Cooling unit

To obtain stationary conditions or in any case proper conditions to safeguard all the heat generating and heat sensitive equipment, a cooling unit is used. In particular have to be cooled the oven, the power supply unit and the middle frequency generator.

A water tank, an air-cooled chiller and a control unit for the water temperature form the unit.

The chiller uses R407C gas with a cooling power of 10.7 kW at the limit temperature of 37°C.

The evaporator consists of a heat exchanger gas-water immersed into the water tank. The condenser is formed by a gas-air heat exchanger provided with a fan.

The water is mixed with a special compound to prevent evaporator corrosion. The water tank is connected to two separated circuits, one for the power supply cooling and the other for the induction oven cooling. A water pump guarantees a continuous water flow of 1.4 m^3/h with a pressure of 4 bar. The control unit measures the water tank temperature: as the temperature rises over the set value, a switch is automatically closed to activate the chiller. When water temperature reaches one grade below the set temperature, the switch is opened again.

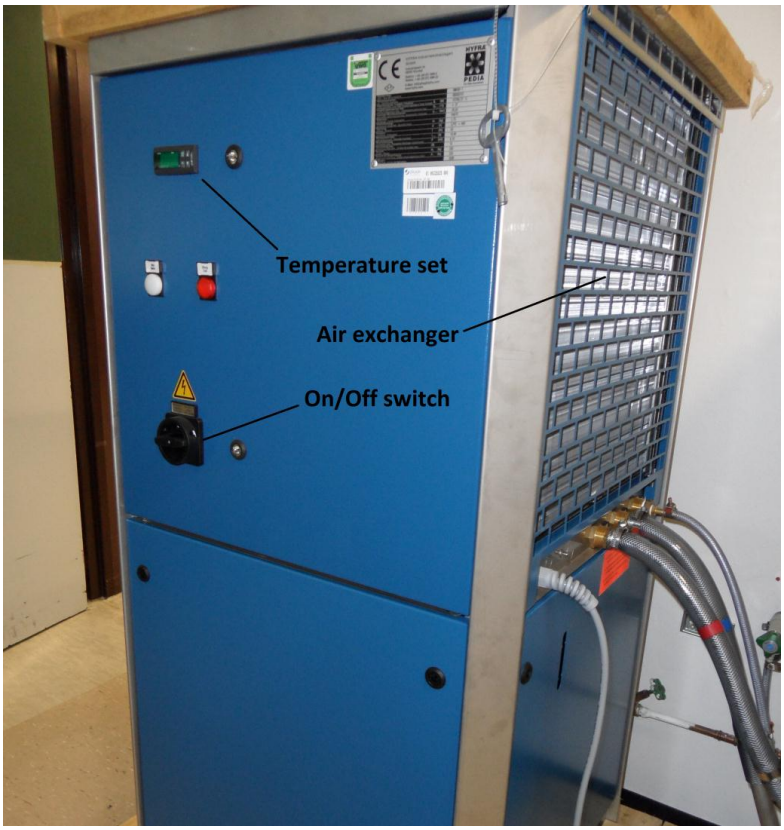

Figure 8.1.4: Overview of the cooling unit

Induction Oven

The induction oven from Linn High Therm GmbH is the most important part of the equipment. It has been designed specifically for treating massive samples of graphite.

The central part is formed by the sample to be treated upon a holder. Two concentric quartz tubes are surrounding it, with a coolant flowing in the middle. The induction coil is placed outside these tubes and it is connected to the middle frequency generator, at the oven side.

On the top a pyrometer probe is placed, necessary to point the sample and to measure the high temperatures reached in the oven. At the bottom 2 vacuum pumps working in parallel are placed, together with two flushing gas valves. In the back side there are input connectors for the process gases. The gas outlet is placed at the oven top, the inlet at the bottom. The gases are provided via 50 liters bottles and a centralized gas-distribution line.

For safety reasons a grid is surrounding the oven to prevent further damage in case of quartz glass breaking.

At the oven outlet, two filters in series are installed. Their purpose is to avoid the contamination of the Mass Spectrometer with carbon particles. The mean pore size is $140\ \mu m$ for the first one and $5\ \mu m$ for the second.

By using an induction oven it is possible to have a clean and well-controllable heating process compared to most other means of heating.

Figure 8.1.5: Overview of the Induction Oven

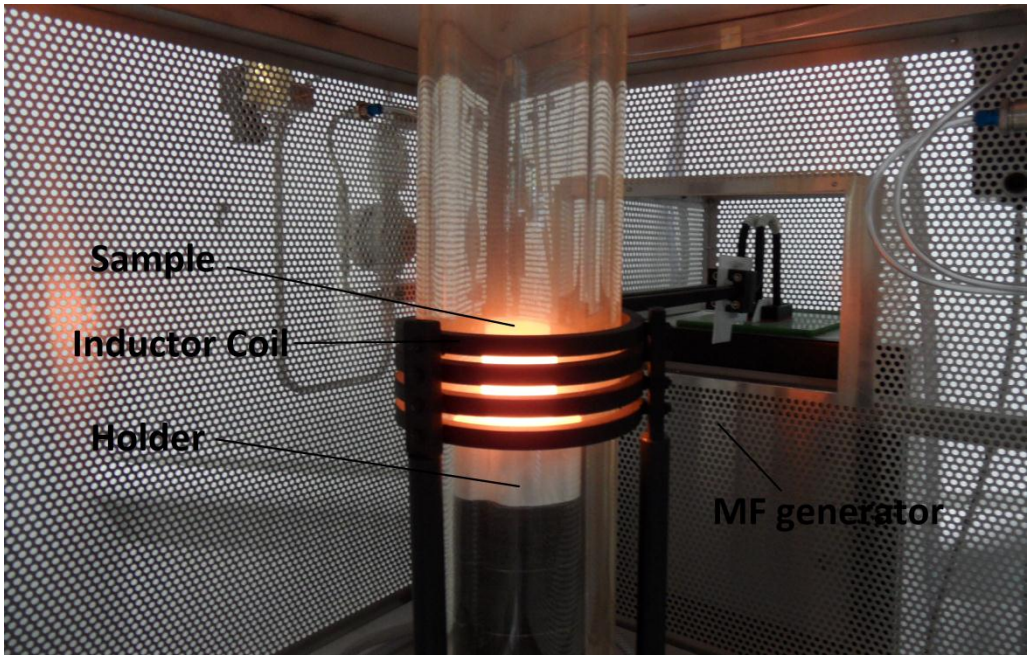

Figure 8.1.6: Inside view of the Induction Oven

Pyrometer

A Pyrometer is a measurement device whose working principle is based on electromagnetic radiation emitted in the infrared range (wavelength approx 0.74-300 μm). The IR radiation is measured immediately outside the oven through a receiver, connected in turn with an optic fibre to the device. The receiver is furnished with a laser pointer, in order to precisely point the surface to measure. The optimal distance has been calibrated by the manufacturer by adjusting the pointer focus: the fixed distance is the one between the receiver and the top surface of the sample.

The pyrometer is used as a feedback-control device (fig. 8.1.7) with respect to the Middle Frequency generator, allowing in such way the power regulation and subsequently the temperature of the sample.

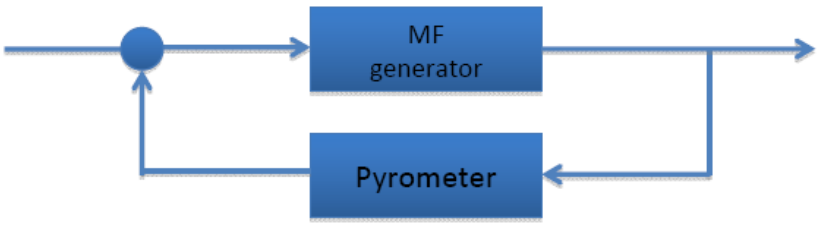

Figure 8.1.7: Schematic representation of the pyrometer feedback action

8.1.2 Mass Spectrometer

The system consists of a quadrupole Mass Spectrometer QMS 200 (PRISMA™), the vacuum recipient, the pumping station, a control unit (PCU201) and the Computer (PC). The Mass Spectrometer (MS) is equipped with a crossbeam ion source (double wire) to obtain a good linearity over a wide range of concentrations and a Channeltron (Secondary Electron Multiplier) detector. Furthermore, a Faraday detector is built in, less precise that SEM and used to measure high gases concentrations and to check the calibrations reliability. One detector or the other can be chosen via software interface: the MS is controlled via the PC by the IPI QuadStar™ Software.

Vacuum is generated by a rotary vane vacuum pump in combination with a turbo molecular pump. The first is able to work up to 10^{-5} bar, then the second one is able to reach 10^{-9} bar. Because of the high revolution speed of the turbomolecular pump (up to 120000 rpm) it is necessary a purge gas (Argon) to prevent materials deposition. A pressure gauge PKR 261 is installed in the recipient for service purposes. By means of this gauge the rest gas and the operating pressure can be measured.

A set of calibration gases of well-known concentrations are needed to calibrate the MS; the calibration step is the most important for this equipment and it is fundamental to obtain good results.

The system is naturally air-cooled. Figs. 8.1.8 and 8.1.9 show respectively the vacuum scheme of the MS and the outside view of the machine.

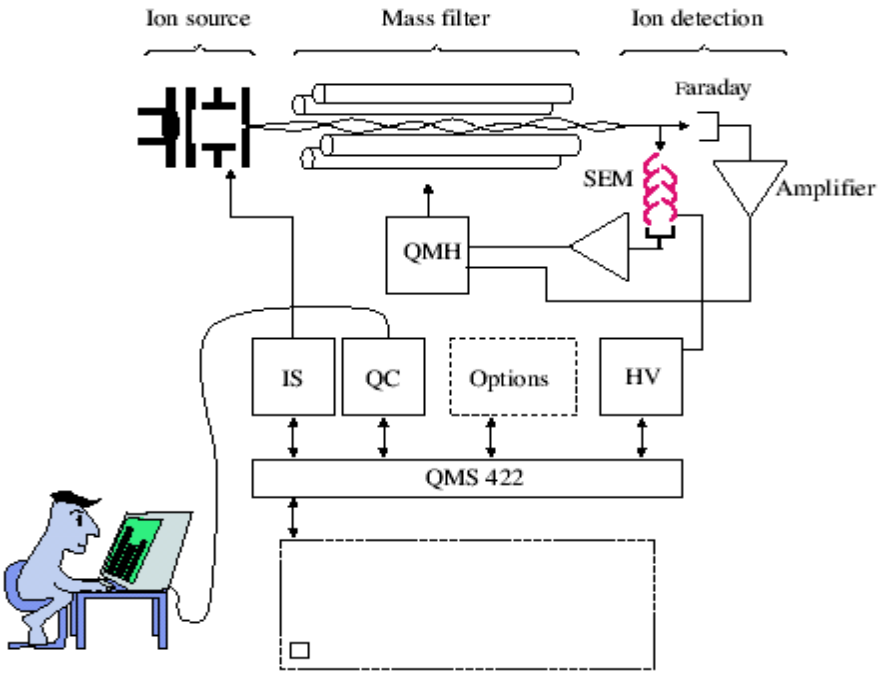

Figure 8.1.8: Scheme of the Mass Spectrometer System

Figure 8.1.9: View of the Mass Spectrometer (left) next to the Induction Oven (right)

8.1.3 Thermogravimetric Oven

The Thermo-Gravimetric Analyser (TGA) is used to measure mass losses at high temperatures over time. For the experiments the TGA Setsys Evolution by Setaram was used. The exterior view of the TGA of Setaram is shown in pictures (8.1.10-12).

The sample is suspended in the oven (in most cases with a crucible) and it is exposed to a regulated atmosphere with up to two gases (main gas and mixed gas) or vacuum. The Setsys Evolution can reach temperatures till 1600 °C. In fact of the high temperatures in the TGA, the crucible has to be produced from a temperature resistant material like platinum or ceramics (like Al_2O_3). In addition, the crucible material has to be not reactive with the sample or the used gases inside the oven.

The crucible is connected to the microbalance through a platinum wire. The sample is focused in the middle of the heating chamber and its position changes over time because of the weight change. The measured values, however, are raw ones: as the temperature changes, the properties of the flowing gas are modified, resulting in an apparent mass gain. Then, a baseline is obtained by repeating the same treatment with a non-reactive sample: once it will be subtracted from the raw data, clear results will be achieved.

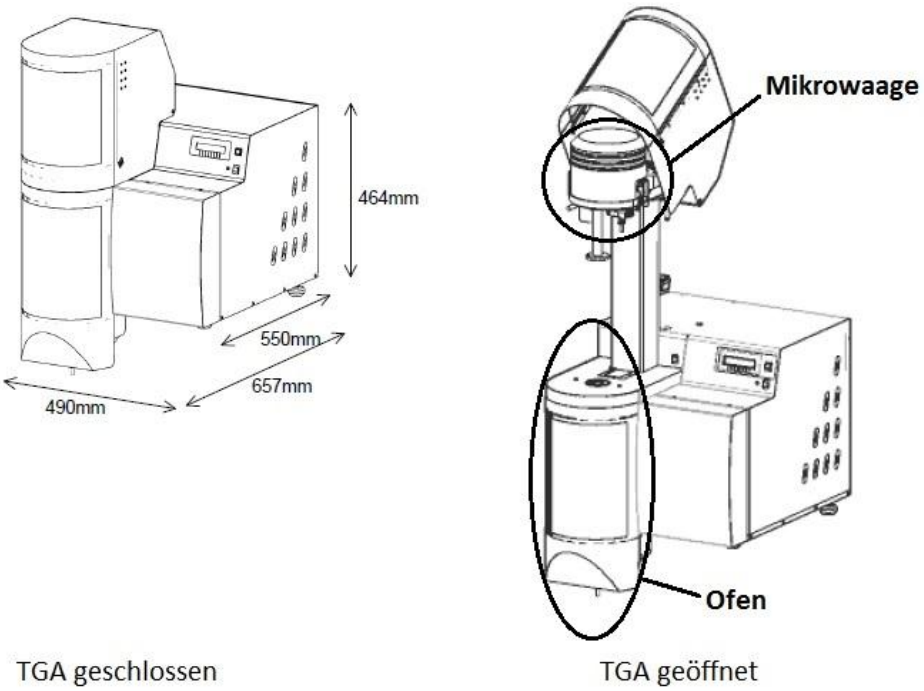

Figure 8.1.10: SETSYS Evolution from SETARAM (exterior view)

The temperature is controlled by a thermocouple [5] that is fixed under the sample and can be changed for different temperature areas (see fig. 8.1.12). The heating is realized by a graphite-heating element [1] flushed by Argon gas to prevent an oxidation of the element. Graphite felt is providing thermal isolation [3]. The oven surface [2] is made of Al_2O_3 ceramic. Atmosphere gases are coming from the inlet [4] and are leaving the TGA over the outlet [7] and pass a backpressure valve [6].

Figure 8.1.11: TGA Oven (left) together with the Mass Spectrometer (right)

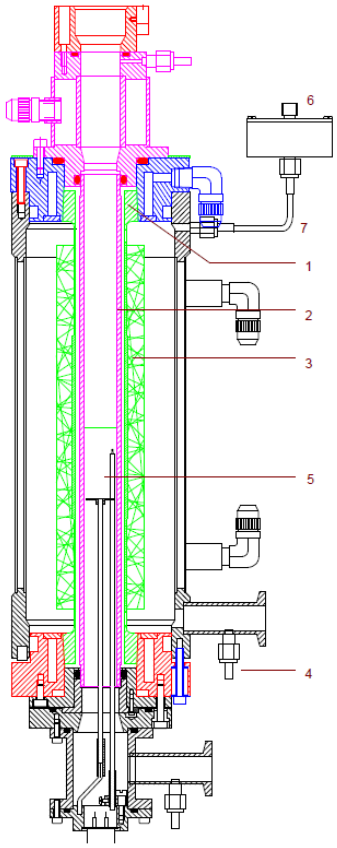

Figure 8.1.12: SETSYS Evolution from SETARAM (oven)

8.2 Sample Preparation

Virgin samples were found in a container next to the AVR building. For the present study only the AVR graphite (ARS-AMT grade[196]) has been considered, whereas the unknown grade graphite has been used to check the proper running of the induction oven.

The cutting technique to produce the samples consisted of using CNC machines performing a dry cut, in the way to contaminate as less as possible the samples surfaces (e.g. with water). On the other side it is impossible to have a perfect cut without changing the superficial structure: the cutting itself consisted on a pre-treatment, developing high local temperature and generating consistent amounts of carbon powder. The only way to completely avoid this artefact would be to cut the big block (see Fig. 8.2.1) keeping untouched one external surface. Unfortunately this was not done but, since the block is still available, it could be a future task to prove to which extent the sample preparation is affecting the results. However, the bulk material is believed to be pristine. From this point of view, massive samples would be less affected by the preparation than the small ones: for this reason, and many others,[197] different samples of different size were prepared (figs. 8.2.2-3).

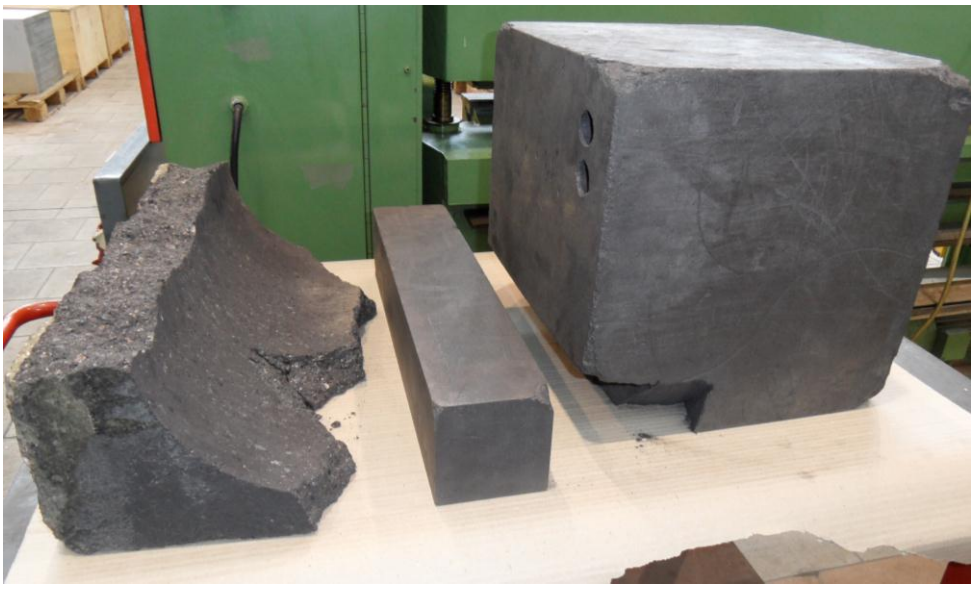

Figure 8.2.1: Coarse material before being cut in smaller samples.
Left: Carbon Brick, middle: Unknown grade graphite, right: AVR grade graphite

[196] ARS/AMT grade graphite from Sigri Elektrographit, used in the AVR as a reflector and structural material

[197] Different samples sizes were chosen according to previous experiences (see chapter 7) and also to fit with the different equipment used (Induction Oven, TGA, small electric oven)

Figure 8.2.2: Massive samples of AVR graphite, H50Ø50 mm

Figure 8.2.3: Small sample used both in the TGA and the small electric oven, H20Ø8 mm

8.3 Performance of Experiments

This section will introduce all the experiments performed through thermal treatments with different equipment. Purpose of these experiments was to measure the on-line gaseous emissions occurring during a treatment under argon, in the way to understand whether oxidant species are already embedded in nuclear graphite. The intention is to give a contribution to the understanding of the reactions that take place and to the removal mechanisms of some species.

8.3.1 Experiments with the Induction Oven

Before starting the experiments with AVR virgin graphite in the oven, many tests have been performed with another graphite grade to check the response of the equipment during different regimes and temperatures. The oven behaviour was found to be not optimal and the temperature revealed strong uncertainties, due to the non-linear response of the system on the one hand and due to the wrong measurements of the pyrometer on the other hand. In addition it was found that the treatment chamber was not perfectly sealed: many interventions were necessary to find the leakages. As a result of that, with the exception for the first experiment, several improvements have been achieved resulting in a cleared on-line measurement, less affected by secondary gaseous sources overlapping the real emissions. The interventions were, in particular, the following:

- Substitution of all the original sealing with high-vacuum ones made of aluminium instead of rubber;
- Helium leakage tests, through a Helium bottle and the mass spectrometer, to check the tightness of every single connection;
- Substitution and improvement of the vacuum line, in particular it was also inserted a manual valve to exclude the vacuum line when not necessary;
- Design of a new sample holder,[198] in order to have a less porous media;
- Cycles of vacuum and flushing with Argon, before starting an experiment, revealed to remove part of the water present in all the inner surfaces of the treatment chamber. Such water was probably originated by the exposure to ambient air (with moisture). A pre-treatment would have been the best, with the oven emptied, in order to thermally remove all the adsorbed water; unfortunately, since the oven is an induction one, a conductive specimen would have been necessary to have a temperature raise. It was performed a trial

[198] See Appendix 1.6

with a vanadium specimen, but the oven revealed strong instabilities, leading to the failure of the cooling unit and to the necessity of shutting down the facility.

The first experiment ("AVR 1") was performed before the above-mentioned interventions, so it was repeated ("AVR 2") in order to check the reliability of the on-line emissions.

In the following the experiments performed with the induction oven facility are presented, together with the obtained results. The discussion is divided in relation to the equipment and to the type of experiment. The choice of some operational parameters has been discussed in chapter 7, resulting from consideration based on former experiences.

8.3.1.1 Experiment "Massive AVR 1" in Argon Atmosphere

Sample

Dimensions	Ø50H50 mm
Initial Weight	172.0615 g ± 0.1 mg
Final Weight	171.8554 g ± 0.1 mg
Mass Loss	206.1 mg (0.12 %)
Parameters:	
Argon flow	7 l/h
Relative Pressure	1 bar
Heating/cooling rate	about 5° C/min
Max Temp.	1300 °C
Holding time at High Temp.	20 hours

Notes about the experiment

The results reported in figs. 8.3.1 and 8.3.2 are referred to the first successful experiment performed with the induction oven facility.

The sample was inserted inside the oven as received, after the cutting process. No visible amounts of dust were observable. The sample holder was a new-made Al_2O_3, used to substitute the previous one in order to have a less porous and reactive structure during the treatment.[199]The experiment was performed with the thermocouple inserted in the oven, sealed through a Teflon seal.

After having sealed the treatment chamber, vacuum was established, followed by flushing with argon for some hours in order to get rid of most of the gases/water present in the chamber.

[199] See Appendix 1.6 for more details

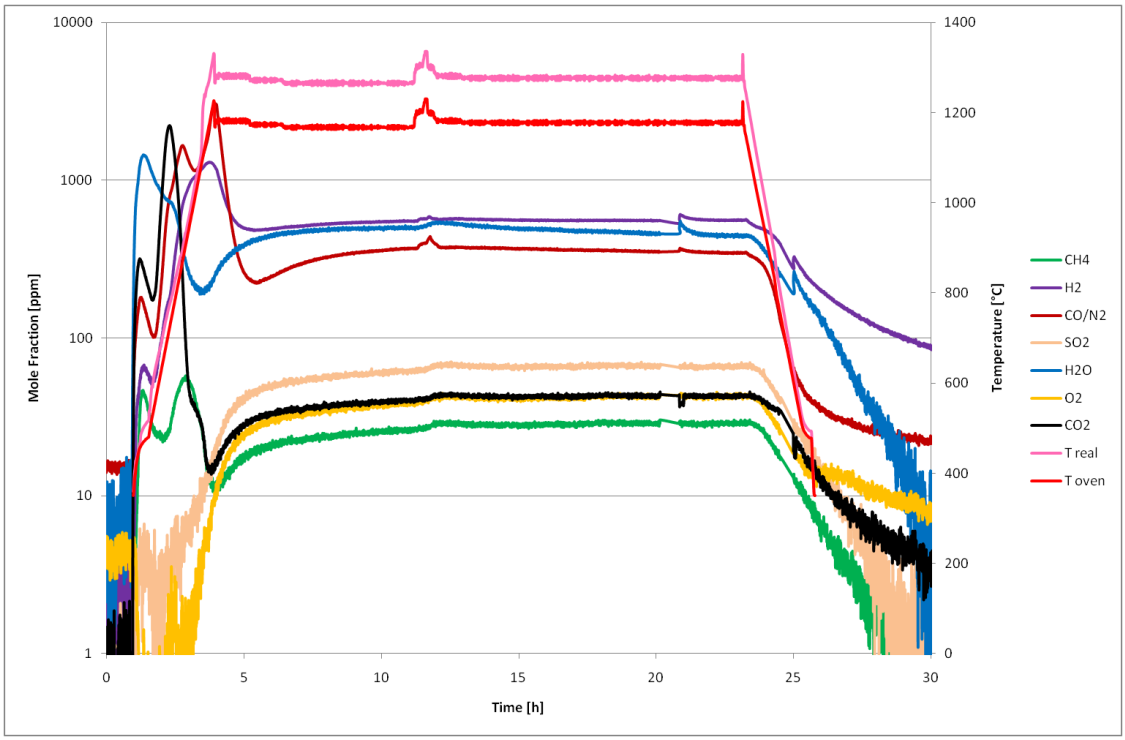

Figure 8.3.1: On-line gaseous emissions from AVR graphite, massive sample "AVR 1", semi-log plot

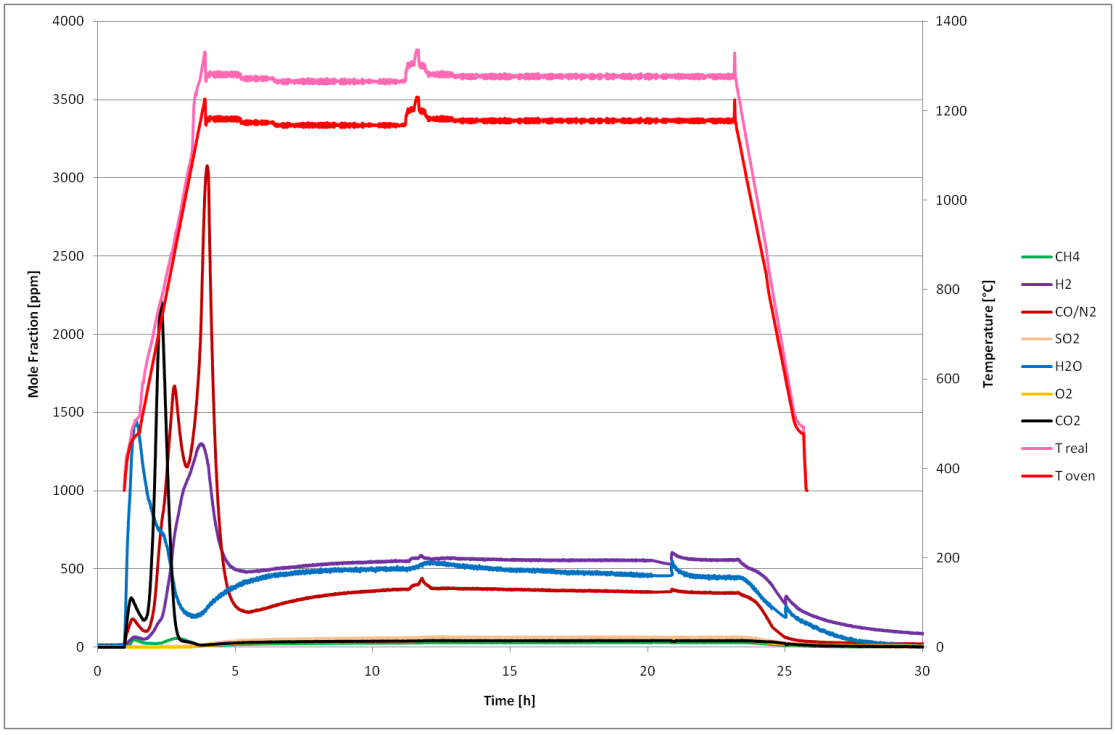

Figure 8.3.2: On-line gaseous emissions from AVR graphite, massive sample "AVR 1", linear plot

8.3.1.2 Experiment "Massive AVR 2" in Argon Atmosphere

Sample

Dimensions	Ø50H50 mm
Initial Weight	169.5858 g ± 0.1 mg
Final Weight	169.3782 g ± 0.1 mg
Mass Loss	207.5 mg± 0.1 mg (0.122 %)

Parameters:

Argon flow	6 l/h
Relative Pressure	1 bar
Heating/cooling rate	about 5° C/min
Max Temp	1300 °C
Holding time at High Temp.	6 hours

Notes about the experiment

This experiment is identical to the "AVR 1" one. It was performed to check repeatability of the results, since many influencing factors on the emissions have been gradually discovered and partially solved along the experimental work.

The experiment was performed without thermocouple, to avoid as much as possible any air income, so the temperature showed in magenta (figs. 8.3.3 and 8.3.4) is an extrapolated one.

The Al_2O_3 sample holder was pre-treated in order to remove all the unwanted impurities.[200]

The supply gas line was completely by-passed since its precision in the flow measurement and its air tightness were not as expected. The vacuum line has been completely re-built with many gas valves in order to improve the oven tightness.

Before starting the experiment, many vacuum/flushing cycles have been performed along the 24 hours preceding the treatment.

[200] See Appendix A1.3

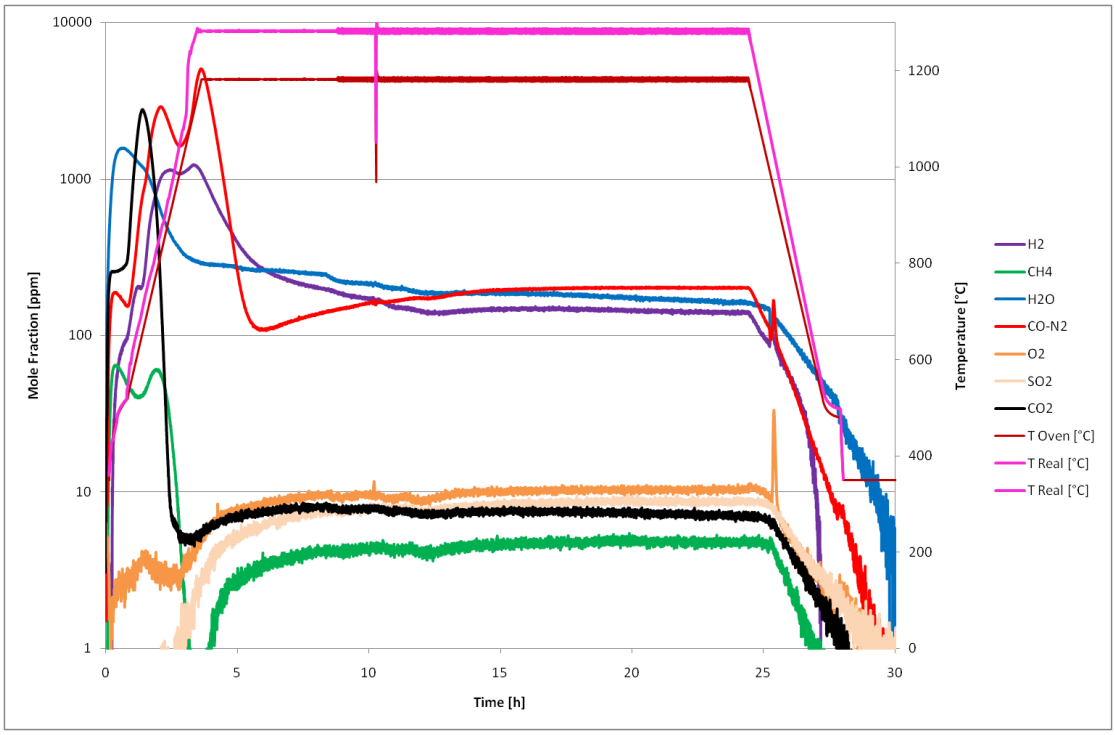

Figure 8.3.3: On-line gaseous emissions from AVR graphite, massive sample "AVR 2", semi-log plot

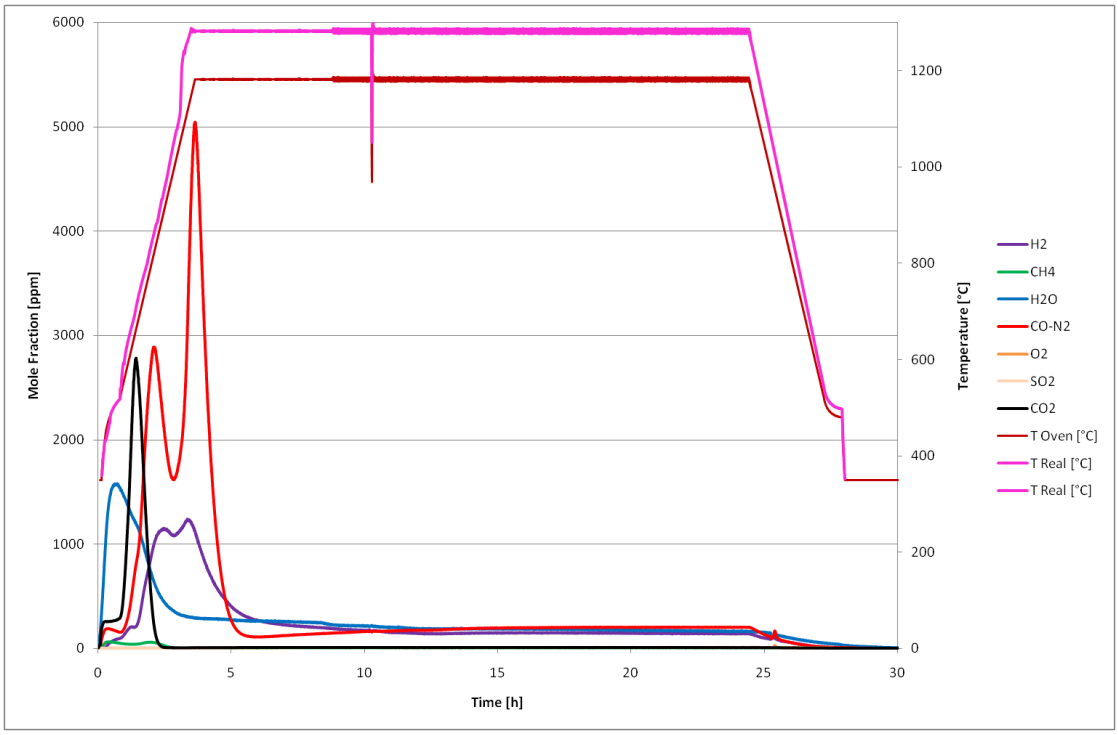

Figure 8.3.4: On-line gaseous emissions from AVR graphite, massive sample "AVR 2", linear plot

8.3.1.3 Experiment "Massive AVR 3" in Argon Atmosphere

Sample

Dimensions	Ø50H50 mm
Initial Weight	169.9510 g ± 0.1 mg
Final Weight	169.7645 g ± 0.1 mg
Mass Loss	186.5 mg± 0.1 mg (0.11 %)

Parameters:

Argon flow	6 l/h
Relative Pressure	1 bar
Max Temp.	1300 °C
Heating/cooling rate	about 5° C/min
Holding time at High Temp.	6 hours

Notes about the experiment

The results of the experiment "AVR 3" are reported in figs. 8.3.5 and 8.3.6.

The sample was inserted inside the oven as received, after the cutting process. No visible amounts of dust were observable.

The Al_2O_3 sample holder used in this experiment has been previously used in other ones. Since high amounts of carbon dust (and not only)[201] were found on the surfaces surrounding the specimen, the holder has been purified by thermal annealing under oxygen at 1300 °C[202], in order to have no overlapping with the gases coming from the sample.

The thermocouple, used in the experiment "AVR 1" has been removed to avoid as much as possible air ingress in the treatment chamber. The temperature measured by the pyrometer is shown as red line in figs. 8.3.3 and 8.3.4, while the extrapolated temperature, on the basis of the temperature calibration,[203] is shown as magenta line.

After having placed the sample and sealed the oven, vacuum and successive flushing have been used to remove as good as possible the gases and the water present inside the treatment chamber. This step took many hours and the experiment started only after the gaseous signals, measured with the mass spectrometer, were showing stable values.

---

[201] The elements found in the Al_2O_3 holder/thermal shield are discussed in chapter 11.3

[202] More information about this "purification/regeneration" treatment are found in appendix A1.3

[203] Refer to appendix A.1.1

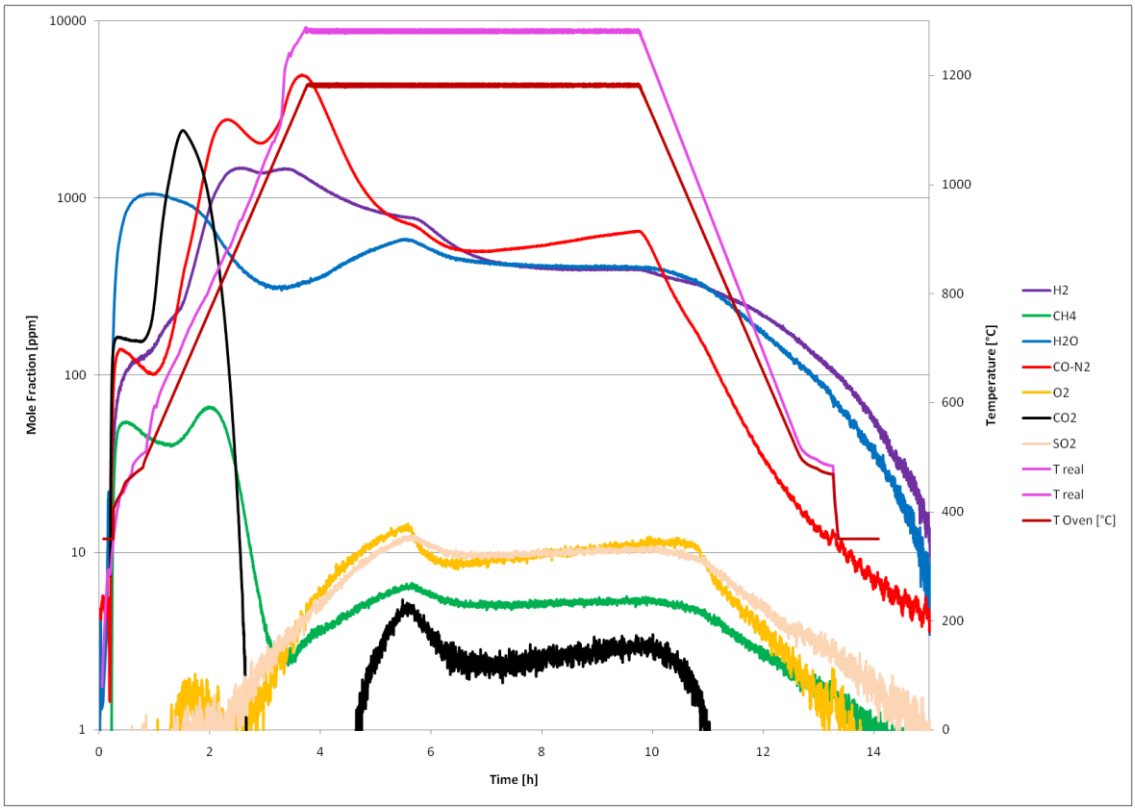

Figure 8.3.5: On-line gaseous emissions from AVR graphite, massive sample "AVR 3", semi-log plot

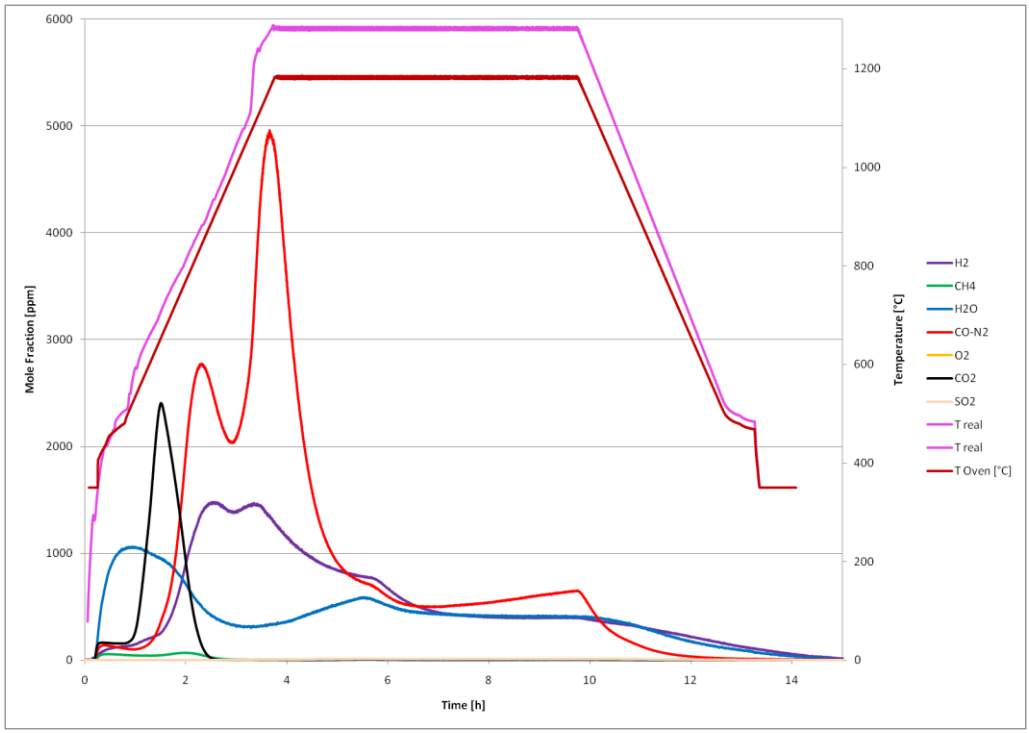

Figure 8.3.6: On-line gaseous emissions from AVR graphite, massive sample "AVR 3", linear plot

8.3.1.4 Experiment "Massive AVR 3T" in Argon Atmosphere

Sample

Dimensions	Ø50H50 mm
Initial Weight	169.7626 g ± 0.1 mg
Final Weight	169.6984 g ± 0.1 mg
Mass Loss	64.2 mg± 0.1 mg (0.038 %)

Parameters:

Argon flow	6 l/h
Relative Pressure	1 bar
Heating/cooling rate	about 5° C/min
Max Temp.	1300 °C
Holding time at High Temp.	6 hours

Notes about the experiment

This experiment was performed in order to better understand the influence of the gases embedded in the graphite. After the first treatment, the sample was exposed to ambient air for 24 hours, then the sample holder was changed and the treatment chamber was cleaned, in order to restore the same conditions as the first treatment.

No thermocouple was used. The displayed temperature is the one measured by the pyrometer (dark red line in figs. 8.3.7 and 8.3.8).

The Al_2O_3 sample holder has been previously baked under oxygen in order to clean it as good as possible.[204]

As for the other experiments, vacuum and flushing with argon were established until the measured signals in the MS were stable (about 1 day).

[204] See appendix A1.3

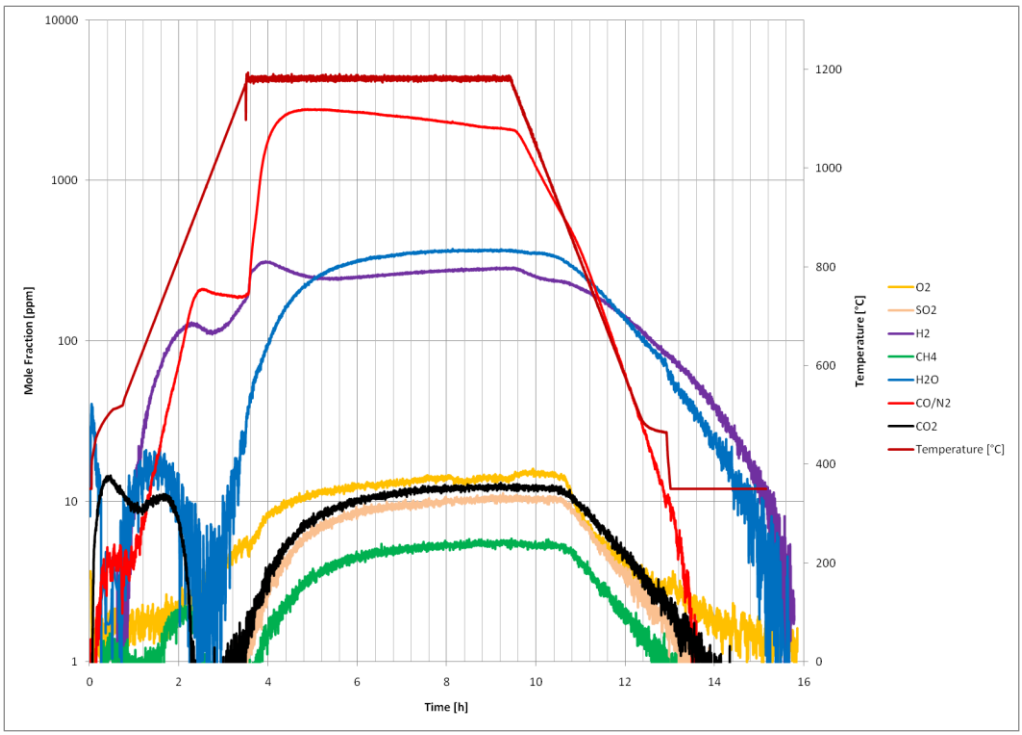

Figure 8.3.7: On-line gaseous emissions from AVR graphite, massive sample "AVR 3T", semi-log plot

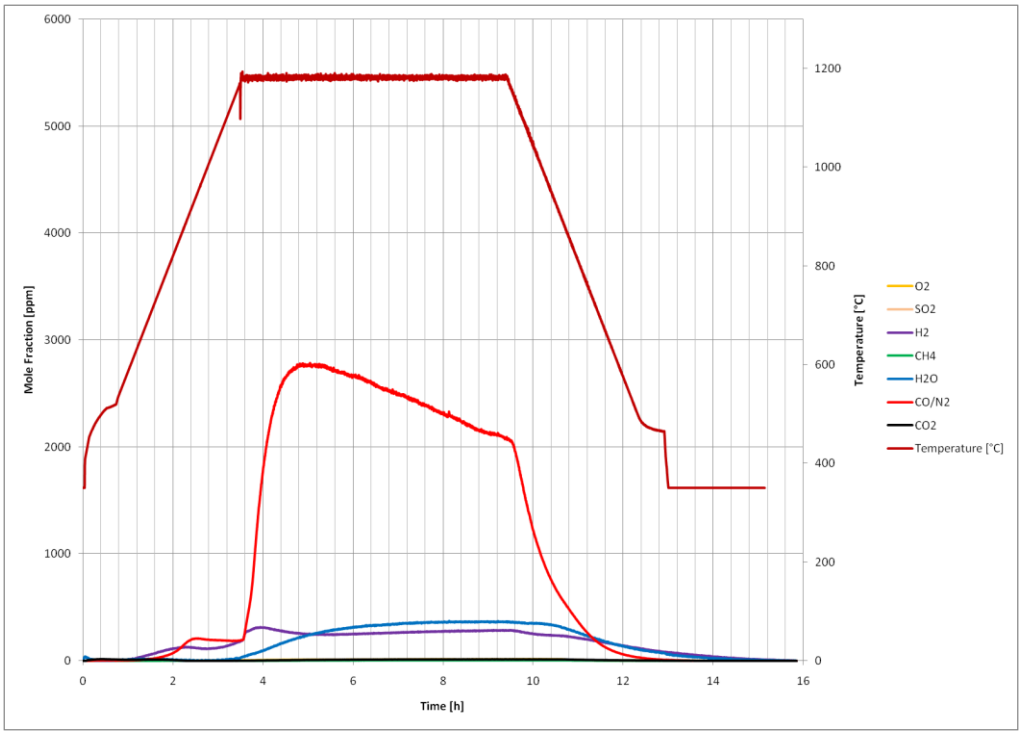

Figure 8.3.8: On-line gaseous emissions from AVR graphite, massive sample "AVR 3T", linear plot

8.3.1.5 Experiment "Massive AVR FT" in Argon Atmosphere

Sample

Dimensions	Ø50H50 mm
Initial Weight	169.5867 g ± 0.1 mg
Final Weight	169.5171 g ± 0.1 mg
Mass Loss	69.6 mg ± 0.1 mg (0.041 %)

Parameters:

Argon flow	6 l/h
Relative Pressure	1 bar
Heating/cooling rate	about 1000° C/min
Max Temp.	about 1300 °C
Holding time at High Temp.	few minutes

Notes about the experiment

The emissions showed in fig. 8.3.9 are the result of an involuntary experiment: it was supposed to be a normal experiment like the others presented previously, but a communication problem occurred between the control unit and the pyrometer. As a consequence of that, the control unit was not measuring any signal, showing to be at temperatures lower than 350 °C: the middle frequency generator was set to the maximum power, resulting in a very steep increase of the real temperature. The communication problem was discovered after few minutes and the fault connection was restored. The resulting temperature signal is showed in fig. 8.3.9 in light red color.

After short time, it was decided to stop the experiment since all the inner quartz tube of the treatment chamber showed to be completely covered by carbon particles. After opening the oven´s chamber it was surprisingly found that the sample was intact.

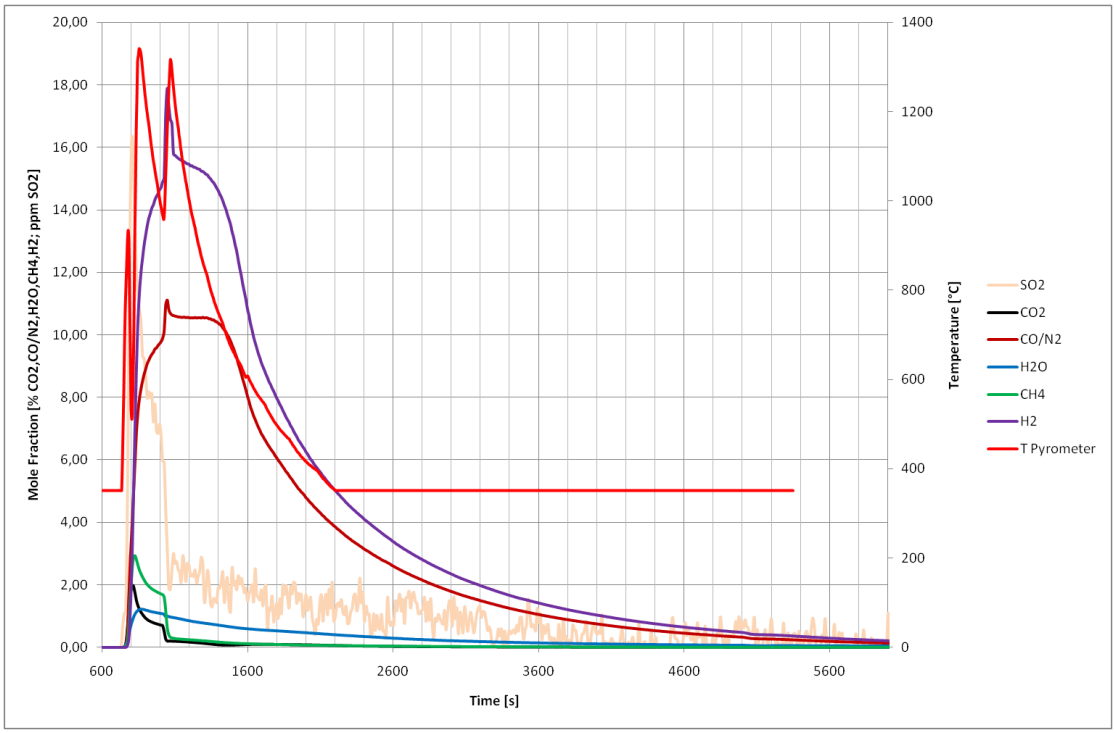

Figure 8.3.9: On-line gaseous emissions from AVR graphite, massive sample "AVR FT", linear plot

Interpretation of the experiment "Massive AVR FT"

A steep increase of the temperature has led to strong internal stresses in the graphite sample, due to the very high heating rate. As a result of that, together with the presence of species embedded in the graphite matrix, part of the structure was likely to be oxidized/damaged, releasing consequentially a high amount of carbon particles and other gases. As reported by Hinssen et al.,[205] the dust formation is induced by the oxidation of the micro pore system (surface oxidation) but, in this case, it has been probably enhanced by the very high heating rate. Looking at fig. 8.3.9 it has to be highlighted that the y-axis is showing mole fraction percentages values for all gases, except for the sulfur dioxide. The highest amount of such gases is respectively 18% for the hydrogen, 11% for the carbon monoxide, 3% for the methane, 2% for the carbon dioxide, about 1 % for the water and at last a peak of 16 ppm of sulfur dioxide is observable. The mass loss, obtained by weighing the sample before and after the treatment, resulted in 0.041%. The surprising fact is that such mass loss was obtained in few minutes, while former treatments showed comparable mass losses in a time-scale of 6 hours[206]. Further investigations will be necessary to better

[205] H.K. Hinssen, K. Kuehn, R. Moormann, B. Schloegl, M. Fechter, M. Mitchell, "*Oxidation experiments and theoretical examinations on graphite materials relevant for the PBMR*", J. Nucl. Engineering and Design 238, 2008

[206] The mass loss in other experiments occurred mainly during the initial step, but the presence of small amounts of water coming from an external source led to a continuous, but slow, oxidation. More details in section 8.3.2

understand the effect of the heating rate with the release of gases and carbon particles from graphite. However, as a general statement, referring to what has been observed in the other experiments here discussed, it can be affirmed that the amounts of released gases and especially carbon particles are increasing with the increasing heating rate.

8.3.2 Discussion of the Experimental Results Obtained with the Induction Oven

One of the purposes of the experiments here discussed was to investigate which elements are already embedded into the AVR graphite by measuring the on-line off-gases during a well-defined thermal treatment under inert atmosphere. Moreover, by comparison with experiments performed on i-graphite in the past, a parallelism will be studied in order to better understand the release mechanisms of some radionuclides. The parameters of the treatments are reported in sections (8.3.1.1-5).

Before analyzing the gaseous emissions, it is interesting to do a general comparison among the total mass losses of the different experiments (see tab. 8.3.1).

Experiment	Treatment time at high Temperature [h]	Mass Loss
AVR 01	19.4	0.12
AVR 02	6	0.11
AVR 03	20.8	0.122

Table 8.3.1: Comparison among measured mass losses from the experiments in the induction oven

The mass losses have been obtained by weighing the sample before and after the thermal treatment.

As previously mentioned, the first experiment "AVR 1" has been repeated ("AVR 2") in order to have a confirmation of the measured emissions: from the point of view of the mass loss no significant differences were found. In fig. 8.3.10 all the observed weight losses are plotted: the blue dots correspond to the experiments in the induction oven, the red one to a 6-hours-experiment in the TGA (see section 8.3.4). A rough interpolation is done to give a first idea of the possible correlation of weight loss with treatment time. According also to older tests, it is not sufficient to evince any definitive conclusion since treatments shorter than 6 hours have not been established yet.

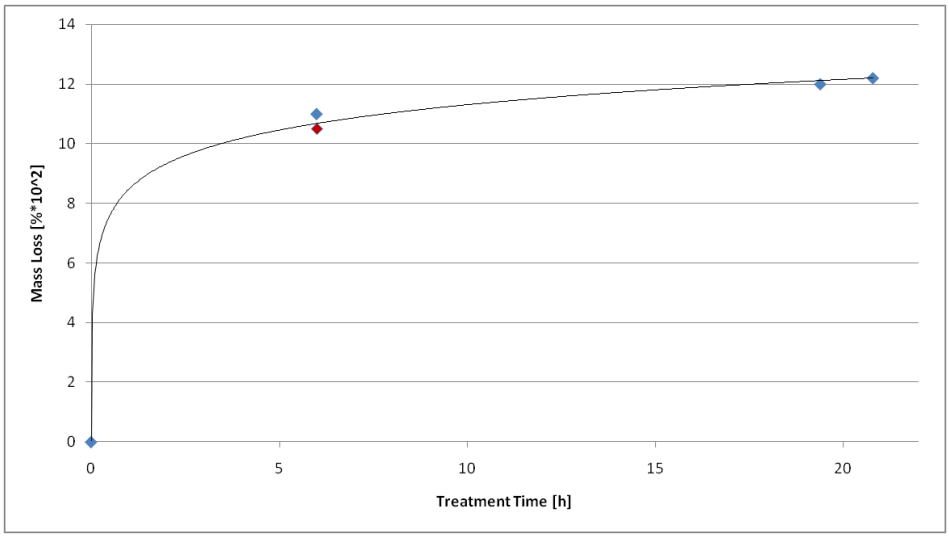

Figure 8.3.10: Rough interpretation of the mass loss dependence with treatment time

It is going to be analyzed, then, the off-gases measurement of the experiments "AVR 1", "AVR 2", which are related to the same treatment time, and "AVR3"; refer to figs. 8.3.1 and 8.3.2 for the first, to figs. 8.3.5 and 8.3.6 for the second and to figs. 8.3.3 and 8.3.4 for the last.

The air income in the oven during the first experiment was estimated around 40 ppm of nitrogen from air, at 6 l/h of argon flow with a pressure of 2 bar absolute at ambient temperature. For what concerns the second and third experiments, with the same conditions, the estimated value of nitrogen income was about 10 ppm. It was observed, however, that the oven was not completely air tight during the high temperature step (up to few tens of ppm of oxygen income were measured). It has to be underlined that, because of the overlapping of different ion fragments in the MS, the carbon monoxide and the nitrogen were measured together, so the displayed values were equal to the sum of the two gases.[207]

For a clearer description and interpretation of the results, every observed gaseous emission will be singularly analyzed in a first step. The considered temperature is the extrapolated one after a temperature calibration with a thermocouple.[208]

WATER

The very first chemical released species is water, with an initial peak of about 1400 ppm in AVR1, 1500 ppm in AVR2 and 1100 ppm in AVR3 (at about 500 °C in all cases). Taking into account that the oven is an induction one, the heat is generated directly in the sample and then transferred to the surrounding materials through thermal radiation, convection and conduction. For this reason, it can be assumed that the initial amount of released water is coming directly from the sample. As the temperature gets higher, more surfaces will

[207] See appendix A1.5 for more information
[208] See appendix A1.1 for more information

participate to the water emission: the initial peak of water flattens slightly and then decreases to 200 ppm (AVR2) or about 300ppm (AVR1 and AVR3) at 1100 °C. During the high temperature step the water signal becomes more or less stable around 500 ppm (AVR1), 200 ppm (AVR2) and 400ppm (AVR3): it is not thinkable to have a real water emission from the sample at such high temperatures (1300 °C at the sample side), so the only reasonable explanations could be:

- The water is released from all the inner surfaces of the oven, as the temperature gets high enough;
- The water is released from the Al_2O_3 sample holder: in this case it is expected a lower release after its pre-baking treatment[209];
- Since the oven is water cooled, at high temperatures there could be small water ingress inside the treatment chamber.

In fact, the AVR2 experiment showed 2.5 times lower emissions than AVR1 during the high temperature step, as a consequence of the pre-baking of the sample holder and the longer flushing of the chamber before starting the experiment.

It was intended to perform some experiments under argon atmosphere, but the presence of water has led to an equivalent treatment with a mixture of gases: argon and water-steam. To give and order of magnitude of the amount of water, it is estimated a water partial pressure in the range from 80 Pa to about 160 Pa, respectively for AVR2 and AVR1[210], during the high temperature step.

Looking at the reaction 5.5 (here reported from chapter 6.1) , for each mole of water there should be one mole of H_2 and one of CO: it means that the mole fraction of hydrogen and carbon monoxide should be about the same, otherwise there are other important sources for these compounds.

$$H_2O + C \rightarrow H_2 + CO \ (\Delta H = +131 \text{ kJ/mol}) \tag{5.5}$$

By investigating the working principle of the mass spectrometer, the higher H_2 signal could result from the presence of water, so in these experiments we can consider the reaction [5.5] as the main reaction occurring at 1300°C.

A confirmation of the improved water source removal can be found by observing tables 8.3.2 and 8.3.3: the CO/H_2O value is quite low for AVR1, considering that a water gas reaction is taking place, and it is more realistic in AVR2 (around 1). In the case of AVR3 some

[209] See appendix A1.3 for more information
[210] The value for AVR3 is in the middle

abnormal emissions of CO were observed (see CO section), resulting in higher CO/H_2O ratios. Moreover, by observing the cumulative water calculated in figs. 8.3.11 and 8.3.12, it can be clearly seen the lower amount of the AVR2 compared to the AVR1 experiment, thanks to the precautions and the pre-treatment steps adopted.[211]

Distinguishing all the above-mentioned sources by analyzing the gaseous emissions is not possible, even after having improved the pre-treatment steps. For that reason, some drying experiments have been performed to have an idea of the water content of graphite: three samples, previously weighed, have been heated under air at 150 °C for 24h and then weighed again. It has been found a mean value of lost water around 250 ppm_w (corresponding to about 40-50 mg/sample). However, the water released in such way could not be representative of the entire effective amount released during high temperature treatments, since there could be water released at temperatures higher than 150 °C.[212]
Some calculations on the overall water content, starting from the on-line emissions, resulted in about 121 mgH_2O (AVR1), 66 mgH_2O (AVR2) and 51 mgH_2O (AVR3) for the entire process and about 19 mgH_2O (AVR1), 26 mgH_2O (AVR2) and 20 mgH_2O (AVR3) for the heating step.[213] Even following the adopted precautions, it was not possible to eliminate secondary sources of water. It is likely that the water release occurring after short time from the beginning of the experiment is a combination of water from the sample, from the sample holder and from the inner surfaces of the oven. Considering the overall treatments, it can be observed in figs. 8.3.11-12 that a steeper release of water occurs in particular in the first hours during the heating step.

From the i-graphite point of view, some considerations can be evinced from the analyzed experiments. In particular, for what concerns the release of tritium, the presence of water inside the graphite matrix could act as a carrier for the radionuclide, considering also a possible isotopic exchange reaction or a radiolytic corrosion process taking place, even at relatively low temperatures. From the point of view of the i-graphite storage, this could represent a not-negligible problem since an exposure even at relatively low temperatures could result in a partial tritium removal, leached to the surrounding environment.

---

[211] Longer flushing and vacuum cycles, pre-baking of the holder, etc., see section 8.3.1
[212] Refer to the experiments with the TGA for a better comprehension
[213] Values are indicative since all of them had to be manually calculated due to the unavailability of a proper software. Moreover, many emissions revealed to come from different sources and not only from the sample. However, what is important is the step on which the gases are released, that for the graphite under argon it corresponds mainly to the heating up step

A confirmation of this theory could be achieved by performing some experiments on massive samples of radioactive graphite at different temperatures. Linking this phenomena to other experiments, referring in particular to Fischer,[214] desorption experiments showed that most of the tritium was released at high temperatures but it was observed also a low-temperature release, in particular with a peak at about 200 °C and also around 400 °C, depending on the specimen. Connecting the present work with former ones, some common features can be observed. In particular, referring to the work of Podruhzina[215], it was observed a high initial release rate of tritium, followed by much slower releases. The reason of that higher release could be connected with the presence of water, initially released from the sample, as here observed. However, the investigated samples were mostly powder ones, so it is possible that part of the tritium had already been removed; in addition, powder samples could have carried different amounts of water compared to massive samples.

Some experiments of Florjan[216] showed an initial steep release of tritium during a HTTT[217] both under inert gas and water/inert mixture, too.

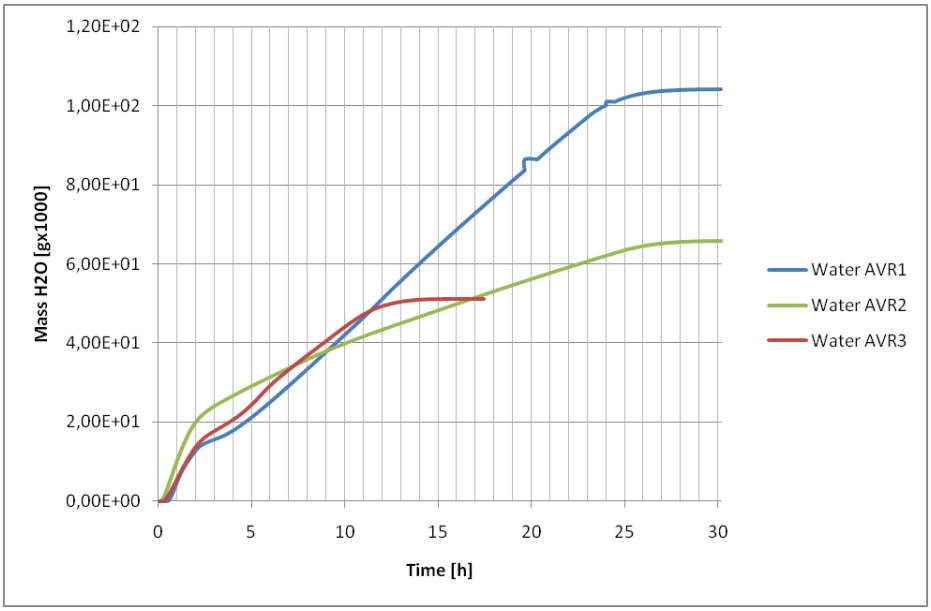

Figure 8.3.11: Cumulative release of water from different massive samples during thermal treatments in the Induction Oven, linear plot (indicative values)

[214] G. Fischer, "*Zum Verhalten von Tritium in Reaktorgraphiten*", Jul-1238, 1977

[215] T. Podruzhina, "*Graphite as radioactive waste: corrosion behaviour under final repository conditions and thermal treatment*", Juel 4166, 2004

[216] M. Florjan, "*Dekontamination von Nucleargraphit durch thermische Behandlung*", Juel-4322, 2009

[217] High Temperature Thermal Treatment

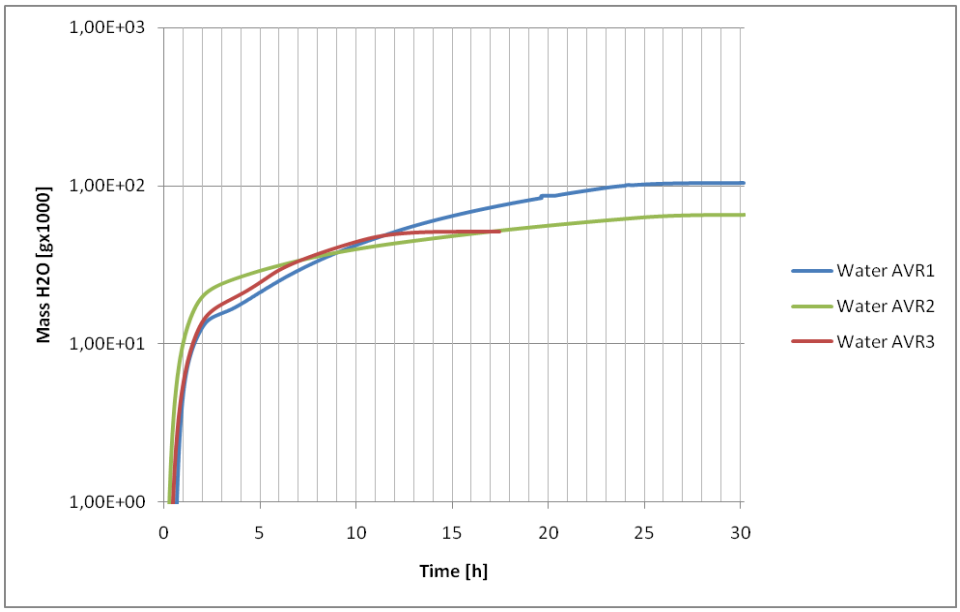

Figure 8.3.12: Cumulative release of water from different massive samples during thermal treatments in the Induction Oven, semilog plot (indicative values)

In conclusion, the water emitted from the graphite sample could represent a consistent amount of the total mass loss during exposure at high temperatures under inert gas, ranging from 25% to even higher values, if the release at temperatures higher than 150 °C is considered. The removal of tritium as HTO could be promoted by the initial high amount of water released during the heating up step. Experiments to check the release of water with temperature have been performed with the TGA (see section 8.4).

CARBON MONOXIDE

As previously mentioned, CO and N_2 were measured together due to the overlapping of many ion fragments (m/e).[218] However, some considerations could lead to individuate the possible (temperature-) zones where the one or the other could be released.

The CO signal appears at relatively low temperatures, starting from about 180 °C and reaching a plateau of 170 ppm (AVR1), 190 ppm (AVR2), 120 ppm (AVR3) at about 450 °C. As the temperature gets higher, a peak of 1640 ppm (AVR1), 2800 ppm (AVR 2,3) is observed at about 850 °C, followed by a second peak of 3000 ppm (AVR1), 5000 ppm (AVR2,3) at the maximum temperature of the treatment (ca. 1300 °C). As the high temperature step is reached, the CO signal generally falls down and stabilizes more or less at the same value as H_2: 400 ppm (AVR1), 200 ppm (AVR2), 500 ppm (AVR3).

The interpretation of these results is not immediate, since many influencing variables are likely to affect the measured values.

[218] More details in the Appendix A1.5

Referring to the values reported above and looking at tables 8.3.2-3-4 it can be stated that the high temperature step in the AVR1 experiment shows a higher amount of water, compared to the others, since the CO/H_2O ratio is very low; the AVR2 better shows the water-gas reaction, while AVR3 reveals a slightly higher CO emission. By comparing the peaks height, it is noticed that at high temperatures the production of CO is higher in the AVR2 and AVR3. In addition, the presence of two peaks of CO does not find a reasonable explanation, except for the case in which the Al_2O_3 holder is reacting. In fact, after the treatment was done, the Al_2O_3 thermal shielding and holder showed to have reacted with the sample since consistent amounts of carbon particles were found on them. This lead to the conclusion that the aluminum oxide is not inert, as it was expected looking at the parameters furnished by the manufacturer. The occurring reaction is the following:

$$Al_2O_3 + 3C \Rightarrow 2Al+3CO \ (+1337 \text{ kJ/mol})$$

Such reaction can explain the excessively high CO production, especially during the high temperature step. In conclusion, one of the two peaks, probably the one at higher temperature, could be the product of the reaction of carbon with the alumina holder. The contact between the two can occur in two ways: the first one is linked with the sample support, the second one is the thermal shielding, which can become in touch with the sample when it is not well fixed; moreover, a consistent amount of carbon particles is expelled from the sample during the treatment, leading to secondary products.[219]

The other peak could be partially explained with the water-gas reaction, since water depletion is observed. In this case, however, a simultaneous production of H_2 should occur, but the amount of hydrogen is about half of the overall CO production, so there is another reaction at the same time. It is likely that the reaction in question is the Bouduard one:

$$C+CO_2 \Rightarrow 2CO \ (+171.5 \text{ kJ/mol})$$

in fact, as the temperature gets higher, the peak of CO_2 decreases and a contemporary raising of the CO is observed.

The uncertainties on the interpretation of these results has led to the decision to perform similar experiments with other equipment and, then, to compare the results afterwards.

However, considering figs. 8.3.13 and 8.3.14, a very steep cumulative release of carbon monoxide is observable, as it could have been expected from the on-line emissions (see fig

[219] The emission of carbon dust has been observed in all the experiments, in particular in the "AVR FT"

8.3.6 for example).[220] As the temperature stabilizes, the release becomes much lower. In addition, what has been previously discussed about the reactivity of the alumina holder can find another confirmation on figs. 8.3.13-14: in the experiment AVR1 the alumina was used without any pre-treatment, resulting in a lower reactivity and then lower CO emissions; after the thermal pre-treatment,[221] the reaction with carbon showed to be strongly enhanced, in particular in the experiment AVR3 where the sample became in touch with the thermal shielding but also in the experiment AVR2 where the only contact sample-Alumina was related to the holder.[222] In any case, even not taking into account such contribution, the release rate of CO is higher in the heating up step than in the high temperature one.
At last, concerning nitrogen, it is believed that it is released during the heating up step, at relatively low temperatures, in concomitance with the CO_2 peak or even before, but a proof of that requires other experiments in the next future.

Considering former experiments, Podruhzina[223] performed a multi-step experiment in argon and water vapour: the release of ^{14}C started to occur significantly from 800°C, temperature at which the water-gas reaction is in the chemical-controlled regime. However, high mass losses were observed, probably due to the excessive amount of water which caused a first steep release of radiocarbon followed by a deep corrosion of the graphite[224]. From the experiments in argon, an initial higher percentage release was observed with lower mass losses: it was hypothesized that the reason of that were the oxidants already embedded in the graphite, causing a slight oxidation of the ^{14}C-enriched surfaces. This work seems to confirm that hypothesis, since many oxidants are embedded in graphite in various forms and they are released during treatments in argon atmosphere. Linking to the work of Florjan, similar considerations can be performed.

In conclusion, for what concerns the release of CO,[225] it can be stated that the higher initial release could explain the similar high initial release rates of radiocarbon, coming from a slight oxidation of the graphite surfaces. From this point of view, the role of the functional groups (such as O-, OH-) present in the graphite structure is fundamental to guarantee an

[220] The values are indicative: what is important for this work is the release rate which shows to be higher during the first step of the experiment.
[221] See appendix A1.3
[222] See figs. A.1.6.6-7 in Appendix A1.6
[223] T. Podruzhina, "*Graphite as radioactive waste: corrosion behaviour under final repository conditions and thermal treatment*", Juel 4166, 2004
[224] The sample was pulverized, so it is possible that the fraction of C-14 was not concentrated anymore near the surfaces due to the destruction of the pore-structure
[225] Together with the peak of CO_2 emitted

efficient removal. It has to be underlined that the fraction of radiocarbon which is wanted to remove is the one concentrated on the sample surfaces, internal and external ones, since it is considered to be the most mobile one.

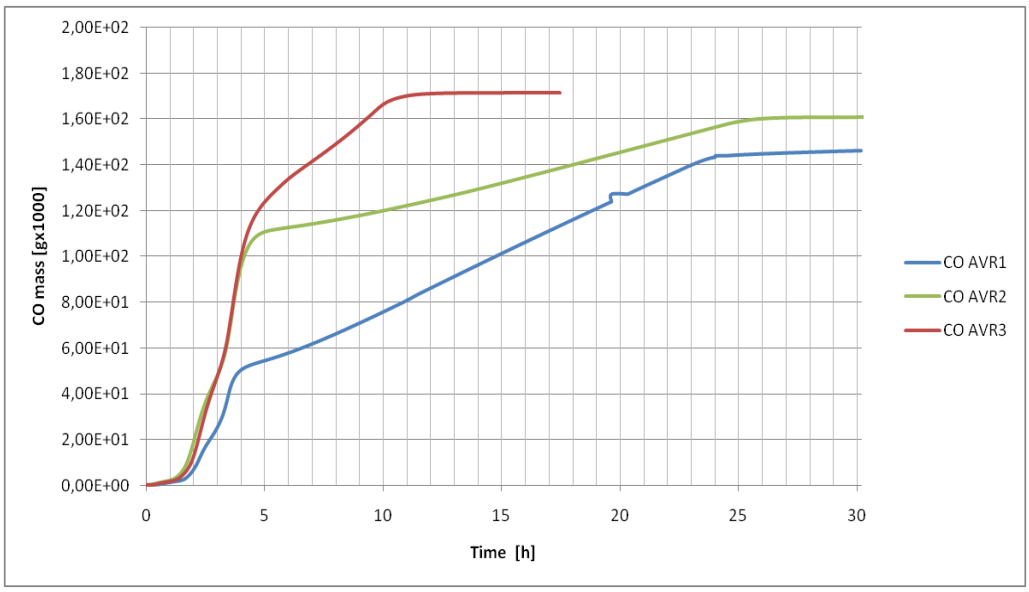

Figure 8.3.13: Cumulative release of CO from different massive samples during thermal treatments in the Induction Oven, linear plot (indicative values)

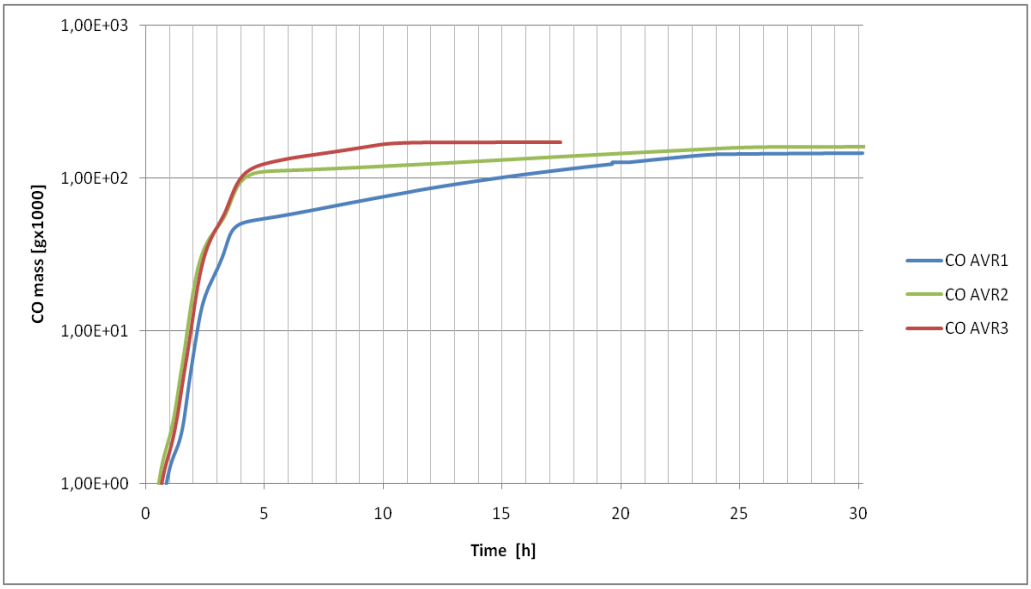

Figure 8.3.14: Cumulative release of CO from different massive samples during thermal treatments in the Induction Oven, semilog plot (indicative values)

CARBON DIOXIDE

The CO_2 signal starts to be released at low temperatures (<400 °C) and then it follows two well-distinguished steps. The first one is a sharp peak, centered around 2000 ppm (AVR1), 2400 ppm (AVR3) and 2700 ppm (AVR3) at about 650-700 °C (see figs. 8.3.1-3-5). The second step is characterized by very low values of CO_2 during the high temperature stage. The latter, more evident in AVR1 (50 ppm) than in the over experiments (<10ppm for AVR2 and AVR3), can be interpreted as a result of air ingress: indeed, oxygen was observed at the same time, showing that such emission was caused by air income inside the oven. What is interesting the most for this study is the very well defined peak observed in the heating up step. It could be interpreted as the removal of the "most mobile" part of the carbon by a pyrolysis /oxidation process.

In fig. 8.3.15 the calculated cumulative CO_2 releases, related to the three experiments in discussion, are reported. The repeatability of the emissions is confirmed by AVR2 and AVR3, showing nearly identical values; the different values of AVR1 could be caused by different boundary conditions of the experiment, since it was performed as the first one, before the interventions on the oven facility.[226]

Referring to former experiments,[227,228] the considerations are similar than those for CO, i.e. the steep initial release of ^{14}C during former treatments with i-graphite can be linked here with the removal of CO_2 as the first one and, at higher temperatures, as CO: it can be observed in fig. 8.3.16, where the CO and CO_2 cumulative emissions for the three experiments are reported.[229] After the initial release, a plateau was observed in the work of Florjan and Podruhzina under argon treatment, since no more oxidants were available: it can be linked to this case, even though a well-defined plateau was not identifiable due to the presence of a small water income (together with minor amounts air).

It is believed that part of the carbon initially removed, both in organic form or as CO_2 and later CO, was originated during the cooling step of graphitization, forming bonding on the top of the crystallites (chemisorbed) or in part precipitating as small particles. The chemisorption of carbon is supported by a study of Fromherz.[230]

---

[226] Described in section 8.3.1

[227] T. Podruzhina, "*Graphite as radioactive waste: corrosion behaviour under final repository conditions and thermal treatment*", Juel 4166, 2004

[228] M. Florjan, "Dekontamination von Nucleargraphit durch thermische Behandlung", Juel-4322, 2009

[229] All the emissions of AVR1 are slightly shifted towards, since the time steps were slightly different; however the steep initial increase of CO_2 is observable.

[230] T.Fromherz, C. Mendoza, F. Ruette, "*Chemisorption of atomic H,C, N and O on a cluster-model graphite surface*", 1993

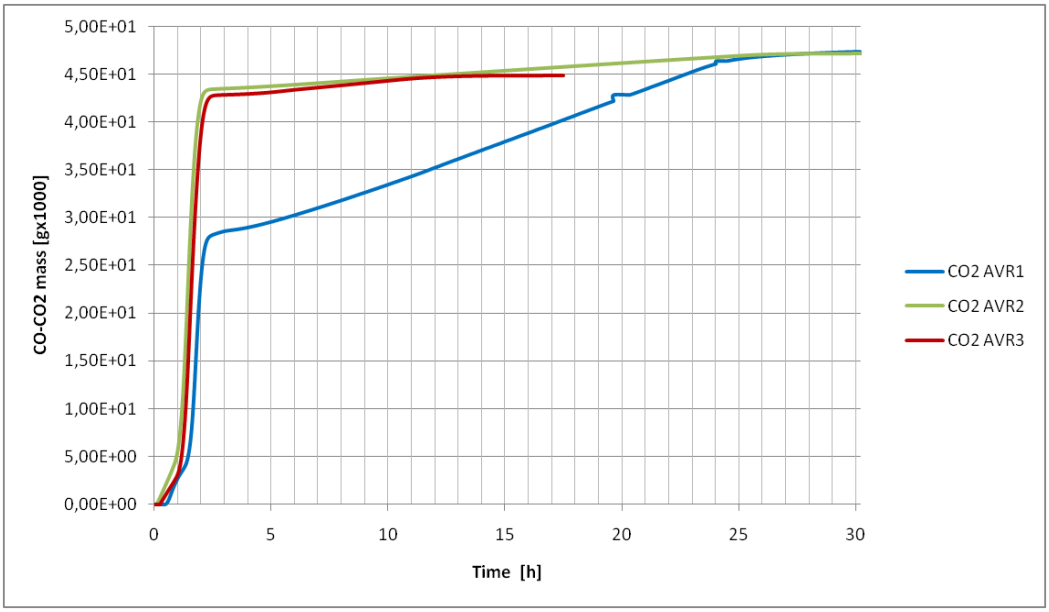

Figure 8.3.15: Cumulative release of CO_2 from different massive samples during thermal treatments in the Induction Oven, linear plot (indicative values)

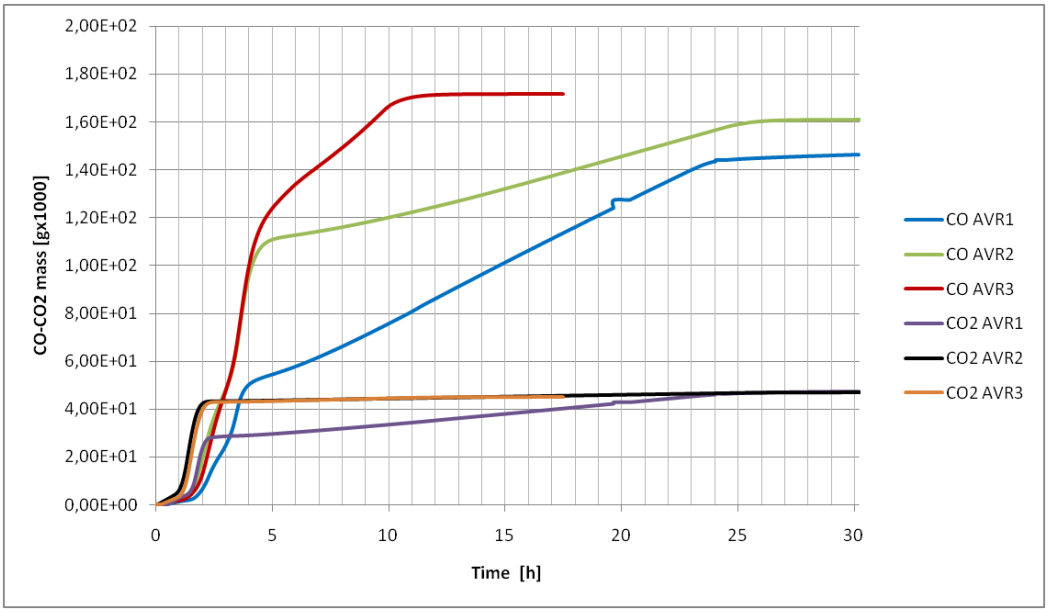

Figure 8.3.16: Cumulative release of CO and $CO_2$from different massive samples during thermal treatments in the Induction Oven, linear plot (indicative values)

METHANE

Methane was measured in higher amounts during the heating up step. It appears at relatively low temperatures, in the order of 300 °C, showing a first peak of about 46 ppm (AVR1), 60 ppm (AVR2) and 50 ppm (AVR3) at 400-450 °C and a second one of 56 ppm (AVR1), 60 ppm (AVR2) and 65 ppm (AVR3) and at 800-850 °C. It was measured also during the high temperature with a constant value of 25 ppm (AVR1) and <10 ppm (AVR2-3). The interpretation of the high-temperature presence of methane involves the coexistence of carbon and hydrogen, since it is unlikely that it results from a pyrolysis process occurring in the sample after many hours of treatment under argon. The reaction of interest could be equation 5.7:

(5.7) $$C_{(s)} + 2H_{2\,(g)} \rightarrow CH_{4(g)} \qquad \Delta H = -71.81\ kJ/mol$$

It is believed that this reaction is not taking place at the sample side, but in the much colder walls of the shielding, plenty of carbon particles released from the heating up step.[231] The presence of hydrogen is guaranteed at high temperatures by the water-gas reaction, already discussed previously. A confirmation of this hypothesis could be that the emissions were retarded in comparison with the sample temperature, since the time constant of the holder is different and its temperature changes are shifted and smoothed compared to the sample's one. Looking at the cumulative profiles in figs. 8.3.17-18 it can be noticed that the methane emissions are similar in AVR2 and AVR3, while the releases were much higher in the experiment AVR1: this fact can be explained with the reaction 5.7 together with a higher amount of water, representing in such case the limiting reactant. This hypothesis founds confirmation on the hydrogen emissions, higher in the AVR1 experiment than in the others.

Concerning the methane released in the first step (see figs. 8.3.1-3-5), the presence of two peaks suggests the existence of different types of hydrocarbons embedded in the graphite, pyrolysing at different temperatures. It has to be reminded that hydrocarbons are present in form many of different compounds both in the filler coke and in the binder pitch[232]: a better understanding could derive from a wider and more precise m/e spectra measured at constant temperatures. The total measured methane release in the heating up step amounted to 0.7 mg (AVR1), 0.9mg (AVR2) and 1 mg (AVR3).

[231] See appendix A1.3

[232] F. Karaca, T.J. Morgan, A. George, I.D. Bull, A.A. Herod, M. Millan, R. Kandiyoti, "*Molecular mass ranges of coal tar pitch fractions by mass spectrometry and size-exclusion chromatography*", Rapid Commun. Mass Spectrom. 2003; 23: 2087-2098

The discovery of methane, excluding the one from secondary reactions, is of great importance from the point of view of the AVR dismantling. When it will be found inside the vessel, depending on the accumulated quantities there could be a further safety concern.[233] However, it is believed that it is present in minor quantities, but it has to be considered a priori in order to establish a proper treatment including also the radioactive gases in addition to the carbonaceous materials. For example, the technique of cementing graphite in order to condition it for the disposal is not capable to retain gases different from CO_2, leading to the probability of radioactivity escape.

An interesting discussion is related to the form of methane: it could be $^{14}CH_4$, CTH_3, CH_2T_2 and other combinations. It is important to know whether the carbon or the hydrogen is radioactive, in order to separate them in a proper way. This task, however, seems to be not easily prosecutable and it should be the object of further studies. Anyway, it is probable that methane will be found in all the possible combinations, but the relative fraction of the one or the other could be different.

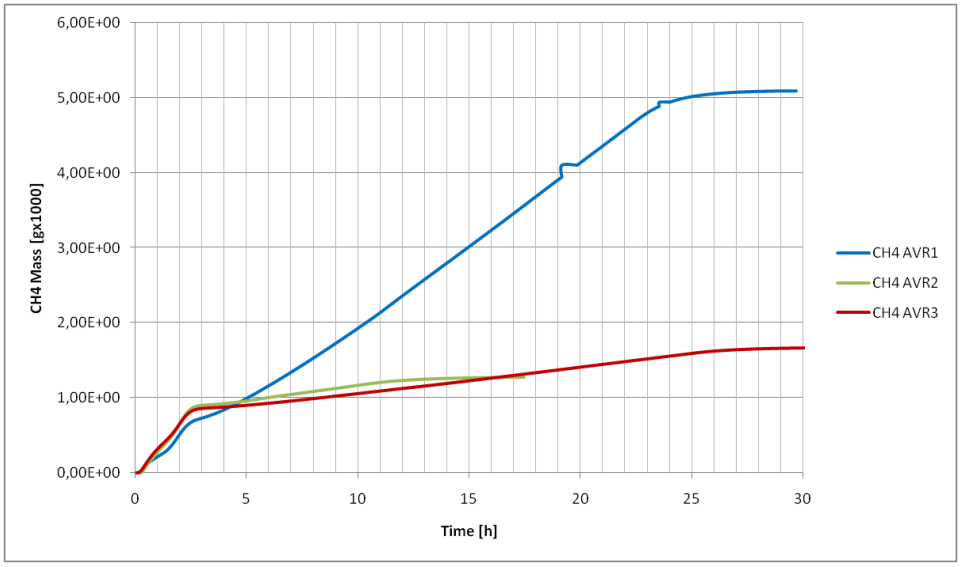

Figure 8.3.17: Cumulative release of CH_4 from different massive samples during thermal treatments in the Induction Oven, linear plot (indicative values)

[233] It is not retained by cement

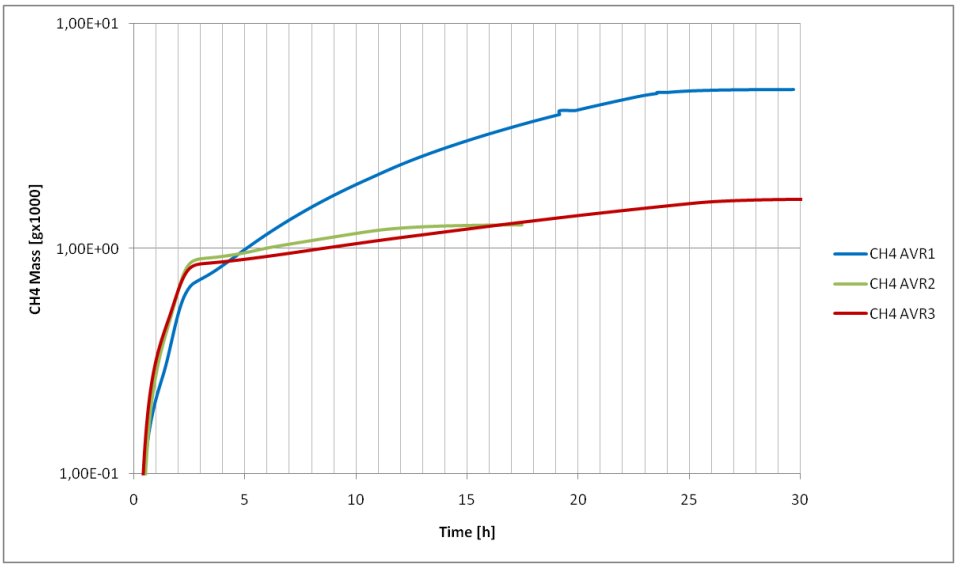

Figure 8.3.18: Cumulative release of CH_4 from different massive samples during thermal treatments in the Induction Oven, semilog plot (indicative values)

HYDROGEN

Hydrogen started to be measured at low temperatures, from 350-400 °C with few ppm, increasing with the temperature. However part of the signal could derive from water.[234] Starting from 700 °C is it observed an increase in the signal, together with a CO increase. The maximum emission of H_2 is reached at the maximum temperature with 1300 ppm (AVR1), 1230 ppm (AVR2) and 1450 ppm (AVR3) at 1300 °C. It follows a decrease and a more or less stabilization in correspondence with the CO signal.

As considered previously, the water gas reaction seems to be the dominant one at high temperatures.

Looking at figs. 8.3.19 and 8.3.20 it can be noticed a slightly higher release rate in the first step, followed by a constant release rate during the high temperature phase. In the case of AVR1 the H_2 production was the highest due to the larger amount of water, present inside the oven and, practically, it follows the evolution of the water signal.

Referring to previous experiments of Podruhzina and Florjan, it is possible that the initial release of hydrogen here observed is connected with the higher initial tritium release. However, it is believed also that the release of water will play a significant, if not more important, role on the tritium removal. Indeed, previous experiments of Dr. Vulpius[235] showed the predominance of tritium in the form of HTO.

[234] Normally the ratio H_2/H_2O is about 1/200, following the calibration of the Mass Spectrometer
[235] Dr. Vulpius, Forschungzentrum of Juelich

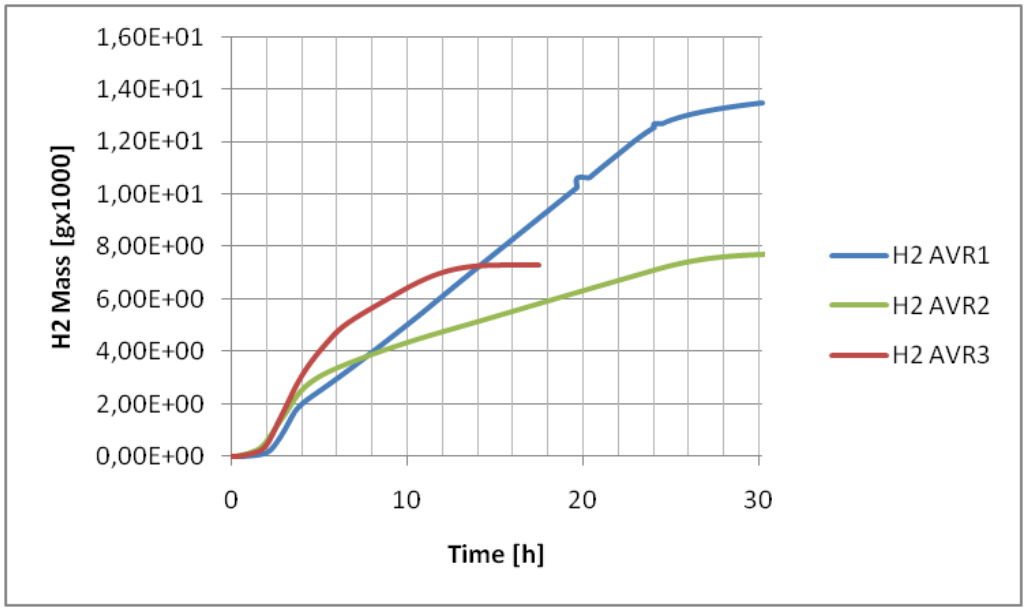

Figure 8.3.19: Release of H_2 from different massive samples during thermal treatments in the Induction Oven, linear plot (indicative values)

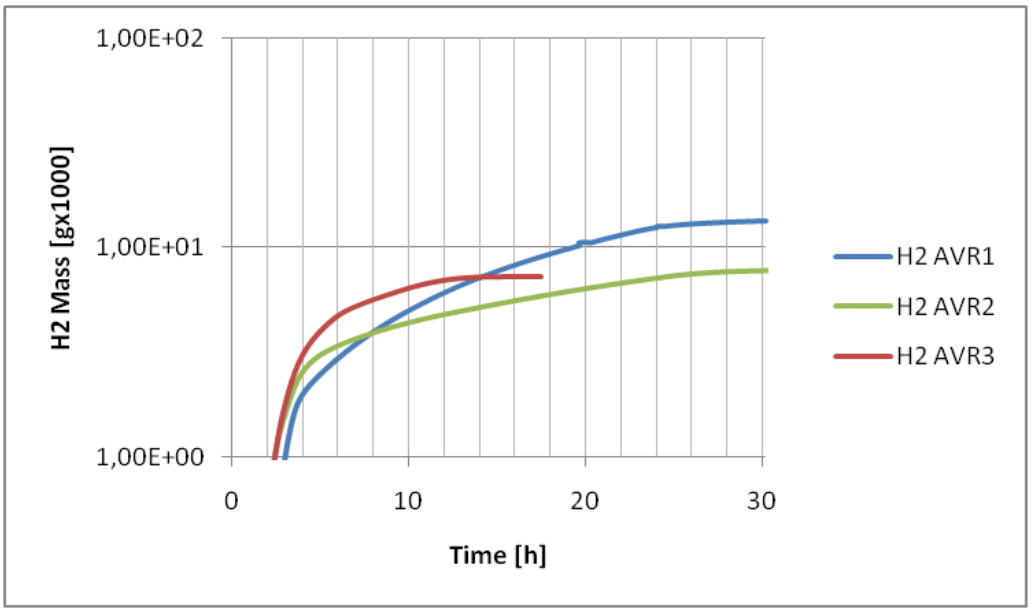

Figure 8.3.20: Release of H_2 from different massive samples during thermal treatments in the Induction Oven, semilog plot (indicative values)

SULFUR DIOXIDE

The release of SO_2 was never measured in the past. A small signal is recorded starting from about 400 °C with few ppm. As the temperature increases the signal raises till it stabilizes around 60 ppm (AVR1), 10 ppm (AVR2,3). The differences in the measured values between the two experiments are focused on the improved air tightness, among the other interventions on the oven. In particular, it can be noticed that in the high temperature step (see figs. 8.3.1-3-5) the SO_2 signal is directly correlated with the O_2 signal. Considering that the air income was reduced after the experiment AVR1, consequently sulfur dioxide emissions were reduced. From this consideration, the probable removal mechanism of sulfur could be the presence of small quantities of oxygen: it can be evinced by figs. 8.3.21-22, where the higher amount of sulfur dioxide removed in the AVR1 experiment compared to the others can be highlighted. However, it is likely that part of the sulfur remained on the sample surface, as successively confirmed by several SIMS and SEM analyses (see chapters 9 and 11).

Moreover, considering former experiments,[236,237] performed under inert gases and taking into account the generally higher mass loss (up to 10 times higher), sulfur was never detected for several reasons, some certain and some others hypothetical:

- The used instruments were not designed to detect sulfur;
- The investigated samples were in a pulverized form or in small samples, with weights in the order of one gram. Considering that even for a 170 grams sample low amounts of SO_2 have been here detected, it is necessary an extremely precise equipment to measure SO_2 in the off-gases coming from small samples: such equipment was not available in the past. In the TGA experiments (next section) it was proven that SO_2 was detectable only after long time and in a fraction comparable with the detection limit of the mass spectrometer.
- Another reason for which sulfur was never noticed before stands on the dimensions of the analyzed samples. It can be presumed that sulfur was removed by oxidation, after having migrated to the sample surface, hypothesizing that a possible removal mechanism is the oxidation; considering that the mass losses found in the past were ranging up to 100 times the ones observed in the present work, the hypothesis of sulfur removal by oxidation is plausible. Following these considerations, previous SEM (Scanning Electron Microscope) analyses were not able to identify sulfur on the graphite surface, both because of its removal

[236] M. Florjan, "*Dekontamination von Nucleargraphit durch thermische Behandlung*", Juel-4322, 2009
[237] T. Podruzhina, "*Graphite as radioactive waste: corrosion behaviour under final repository conditions and thermal treatment*", Juel 4166, 2004

through oxidation and partially because of the detection limit of the XRF (X-Ray Fluorescence Analysis) equipment included in the SEM facility.

Linking the finding of sulfur to i-graphite, an isotope of such element (S-34) is a probable secondary precursor of Cl-36, as demonstrated in chapter 4: its removal before the graphite usage in a reactor could result in a partial reduction of the final activated product. On the other hand, assuming that the driving removal mechanism could be similar to the one for chlorine, a thermal treatment under inert atmosphere could remove effectively the radionuclide. This hypothesis, however, should be demonstrated by other experiments: further investigations (SIMS in chapter 9) partially supported such hypothesis, but the last step that will validate the theory is the study of an irradiated graphite sample under thermal treatment.

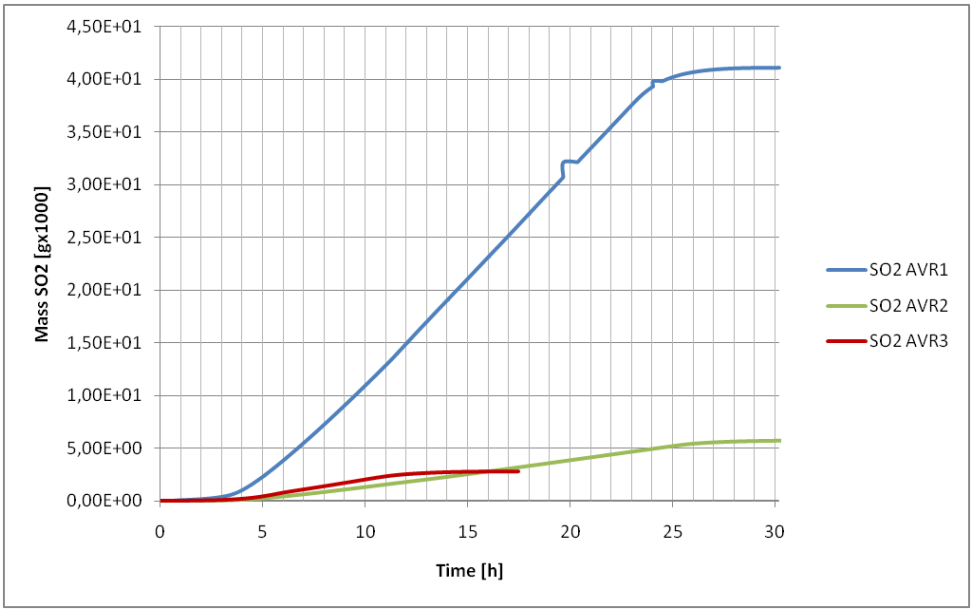

Figure 8.3.21: Release of SO_2 from different massive samples during thermal treatments in the Induction Oven, semilog plot (indicative values)

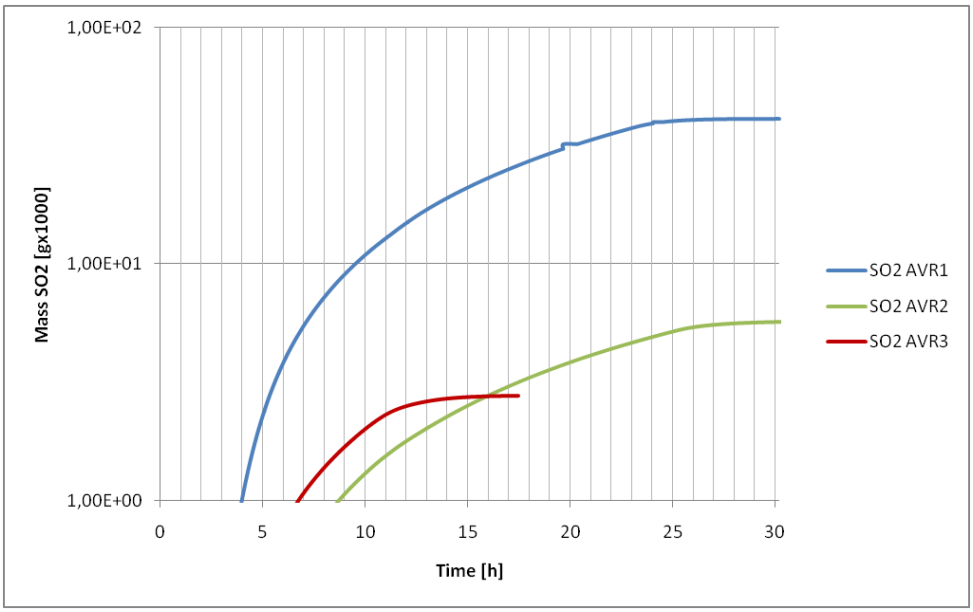

Figure 8.3.22: Release of SO_2 from different massive samples during thermal treatments in the Induction Oven, semilog plot (indicative values)

OXYGEN

Oxygen was measured only because of air income in the oven, especially during the high temperature steps. After the experiment AVR1, the oven tightness was improved and, as a result of that, the detected oxygen revealed to be lower in the other experiments.

In conclusion, following the results here obtained it has been proven a high initial release of many chemical species, mainly formed during the initial step of the experiment: the presence of oxidants inside the graphite has been proven. In particular the expected embedded species are likely to be water and functional groups like O-, OH- but also hydrocarbons. Taking into account previous experiences with radioactive graphite, it can be stated that the initial stages of the thermal treatments, both under argon or slightly oxidizing gases, are fundamental for the release of both ^{14}C and ^{3}H. The former is likely to be released through a slight oxidation of the outer and inner graphite surfaces (pores), releasing organic carbon and a well-defined peak of CO_2 followed by a fast increase of CO at higher temperatures. Considering the higher concentration of ^{14}C on the surfaces,[238] the inefficiency on its removal at higher temperatures is proven, since the CO_2 peak occurs between 600°C and 700 °C: under slightly oxidant atmosphere the simple oxidation of graphite occurs after a while, removing so mostly ^{12}C; in addition, high temperatures

[238] Verified in chapter 9

(1300°C) and presence of water are likely to be inefficient due to the instauration of the boundary layer controlled regime, resulting in a mere oxidation of the outer sample surface. Concerning tritium, it is likely to be initially released due to the water emissions, probably in the form of desorbed HTO due to isotopic exchange reaction and, after, by recombined HTO, other than HT.[239] Methane was measured, revealing the necessity of a proper method to oxidize it and to separate the relative radionuclides. Sulfur dioxide was also detected, leading to open new theories and considerations linked to the possible removal of Cl-36 and its precursors through thermal treatment.

[239] In particular, previous experiments of Dr. Vulpius, FZJ Juelich, revealed that most of the tritium is released in form of HTO (up to 90%)

8.3.3 Discussion of the Results from the Experiment "Massive AVR 3T"

The experiment "Massive AVR 3T" is going to be discussed separately with the respect of the other experiment: it was conceived in order to investigate the effect of a first thermal treatment on the gaseous emissions evolving during a second identical treatment after air exposure, to prove that most of the outgases measured in the first treatment were the result of chemical reactions involving embedded species as reactants. In particular, the sample in question was treated through the experiment "Massive AVR 3", resulting in a mass loss of 0.11%. Then the sample was exposed to ambient air for 24 hours in order to allow the contact with moisture, oxygen and nitrogen and to favor their partial adsorbtion. The boundary conditions of the experiment were the same, since the sample holder was replaced with a clean one after the first treatment and the chamber was cleaned carefully.

The results of the second treatment revealed many important aspects. (see figs. 8.3.7 and 8.3.8).

For example, the water released in the heating up step showed a maximum of about 20 ppm, compared to the previous 1100 ppm, measured from the very same sample, and the total measured water emission decreased of a factor of about 2.5 (see figs. 8.3.20-21). However, not all the water is retained to originate from the sample: the lower amount of water released at high temperatures could be linked to the first treatment, since the oven was opened in order to clean it and change the sample holder, exposing the inner surfaces to moisture for relatively short time; on the other hand, in the heating up step it was observed a strong reduction of measured water, in comparison with the first treatment, and it can be linked mainly to the sample, with an integral reduction factor of about 60. It would be interesting to perform another experiment on the same sample, after several months of exposure to the air, in order to better understand the source of the water. Previous works on gas desorption spectra[240] revealed no significant changes in the gaseous emissions during a repeated thermal treatment of the same sample after many months, leading to the conclusion that many oxidizing species were already embedded in the graphite structure, removed in the first treatment. However, the graphite grade was different than the one here considered but it is believed that a prolonged exposure to air will result in a mass gain mainly due to water adsorption and lower amounts of nitrogen and oxygen, since the relative fractions originally embedded in the graphite were removed in the first treatment.

[240] M. Okada, T. Sogabe, "*Behavior of gas desorption and gas permeability of carbon materials*", Toyo Tanso Company, IAEA-TECDOC-690, 2003

Concerning the carbon dioxide, which showed a typical peak of about 2500 ppm in the first treatment, it revealed to be significantly reduced to a maximum of 15 ppm peak, with a reduction factor of the peak of 170 times and an integral reduction of about 90 during the heating step (about 20 for the whole treatment, see figs. 8.3.27-28).

For what regards hydrogen, the main difference was found in the heating up step, with an integral reduction of a factor 10 and a total reduction for the entire process of about 3 times (see figs. 8.3.29-30). Also for this element it can be stated that a fraction of the hydrogen observed during the first treatment was coming from the pyrolysis of hydrocarbons (C-H) and functional groups, originally embedded inside the graphite: such fraction has been removed during the first hours of the first treatment. Linking this fact to the i-graphite, this observation supports the initial high removal of tritium, emitted also as HT: some experiments showed that its relative contribution to the total removal ranges up to 10%.[241]

At last, carbon monoxide showed to have a steep increase as the high temperatures were reached, resulting from a probable enhanced reaction of the sample with its Al_2O_3 support: it can be clearly seen on fig 8.3.8. The sample heavily reacted with the alumina holder probably due to the lacking of carbon particles being emitted and deposited/reacted with the holder surface. For that reason, the overall amount of CO at the end of the experiment was comparable with the first results (see figs. 8.3.25-26) but in the heating up step it can be estimated an integral reduction factor of about 17.

All the other emissions are similar to what has been described previously.

In fig. 8.3.32 the sample's base made of aluminum oxide, which was in contact with its support, is shown. The different reaction of the two treatments can be observed, resulting in the lighter circle (first) and in the darker circles (second), confirming the stronger reaction in the second treatment.

In conclusion, the measured mass loss for the reheating treatment showed to be 0.038%, i.e. about three times lower than the one in the first treatment, in accordance with the contemporary reduction of many emissions here discussed. From the point of view of the emitted species, the thermal treatment of virgin graphite has shown an improved behaviour at high temperatures, which can be connected with a similar improved one under repository conditions. Moreover, the high relative removal of carbon dioxide, water, carbon monoxide and hydrogen in descending order, during the heating up step of the first treatment can be directly linked to the high initial removal of ^{14}C and ^{3}H observed in former similar

[241] D. Vulpius, experiments performed at the Forschungzentrum of Juelich

experiments. In particular some experiments performed by Florjan[242] showed high initial release rates of C-14 not only during the first treatment but after every thermal treatment in descending orders, with intermediate air exposure. Considering the present work, it can be stated that the initial high release of C-14 is probably caused by the oxidation of the sample surfaces, higher in the first treatment step due to the presence of oxidants. The origin of these oxidants is double: in the first treatment most of them is embedded in the graphite structure, leading to CO and a very well defined CO_2 peak emission; in the successive treatments, the oxidants´ origin has to be assigned to the boundary conditions of the experiments and to the adsorption of many gases, occurred during the exposure to ambient air. Following these considerations, the first treatment on i-graphite should show C-14 released in the initial treatment step firstly as $^{14}CO_2$, followed by ^{14}CO at higher temperatures (see fig. 8.3.31). An evaluation of the relative total fraction CO/CO_2 cannot be performed in a reliable way starting from the present results, since the presence of Al_2O_3 has heavily influenced them. Similar experiments should be performed with different equipment or with a different holder in order to avoid multiple sources of CO.

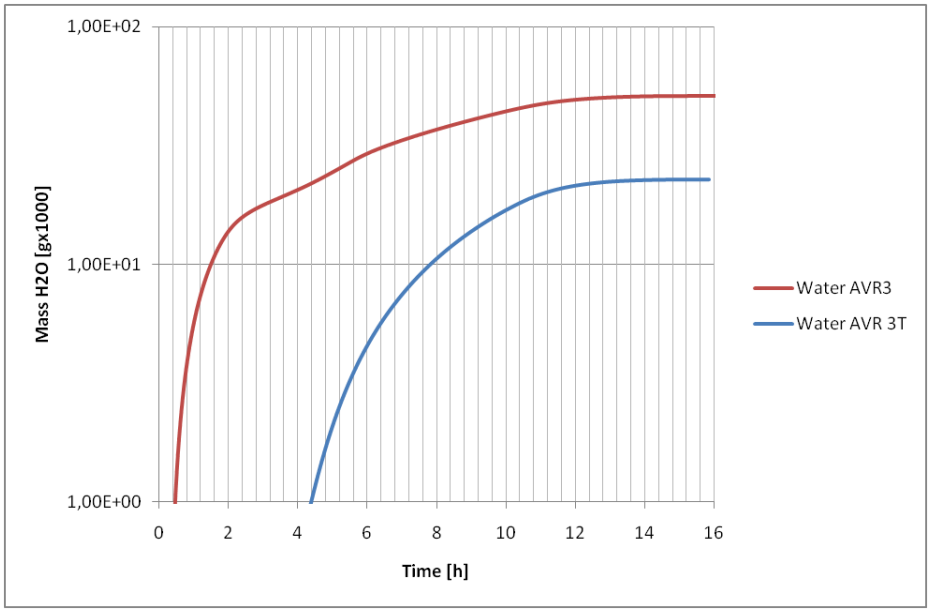

Figure 8.3.23: Comparison among the cumulative water emissions during successive treatments AVR3 and AVR3T of the same sample, semilogplot (indicative values)

[242] M. Florjan, "*Dekontamination von Nucleargraphit durch thermische Behandlung*", Juel-4322, 2009

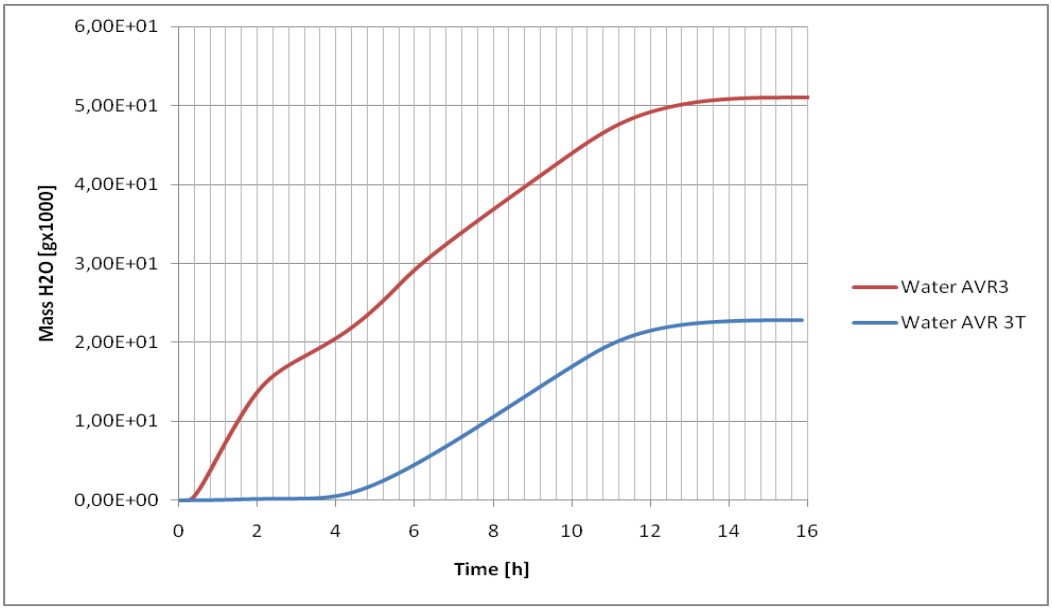

Figure 8.3.24: Comparison among the cumulative water emissions during successive treatments AVR3 and AVR3T of the same sample, linear plot (indicative values)

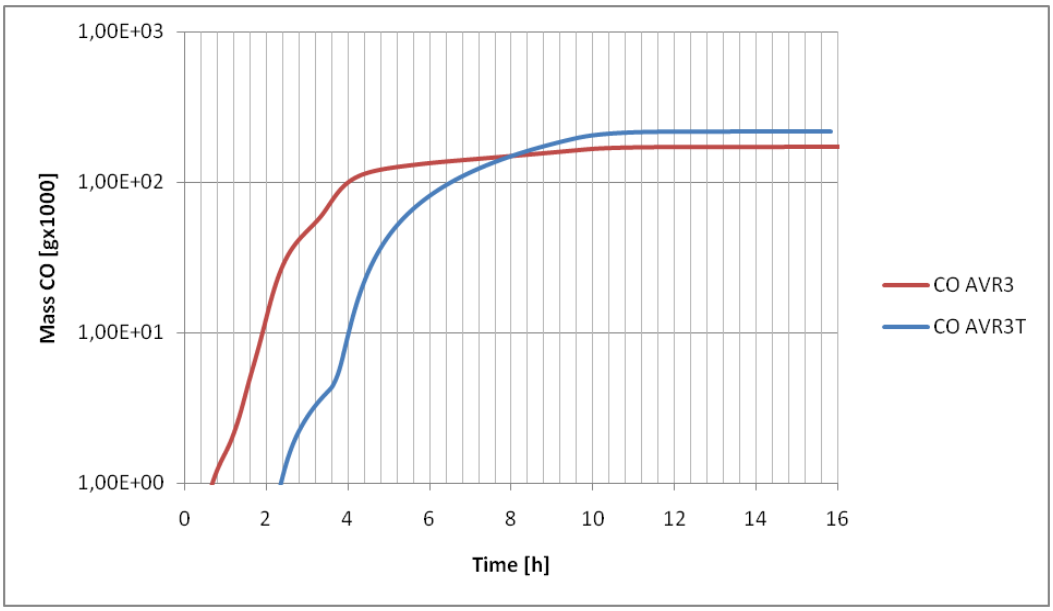

Figure 8.3.25: Comparison among the cumulative CO emissions during successive treatments AVR3 and AVR3T of the same sample, semilog plot (indicative values)

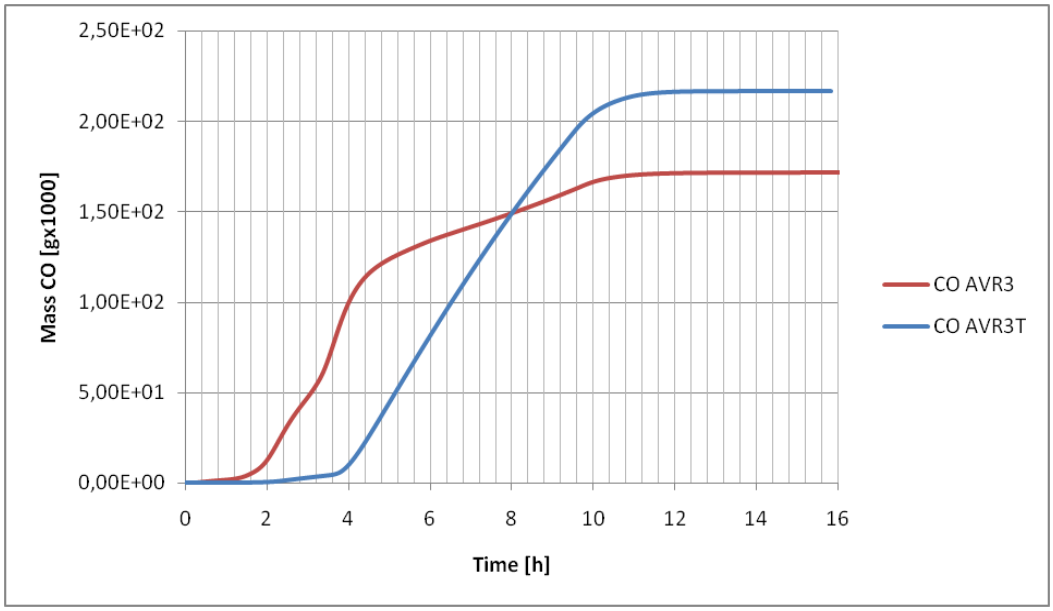

Figure 8.3.26: Comparison among the cumulative CO emissions during successive treatments AVR3 and AVR3T of the same sample, linear plot (indicative values)

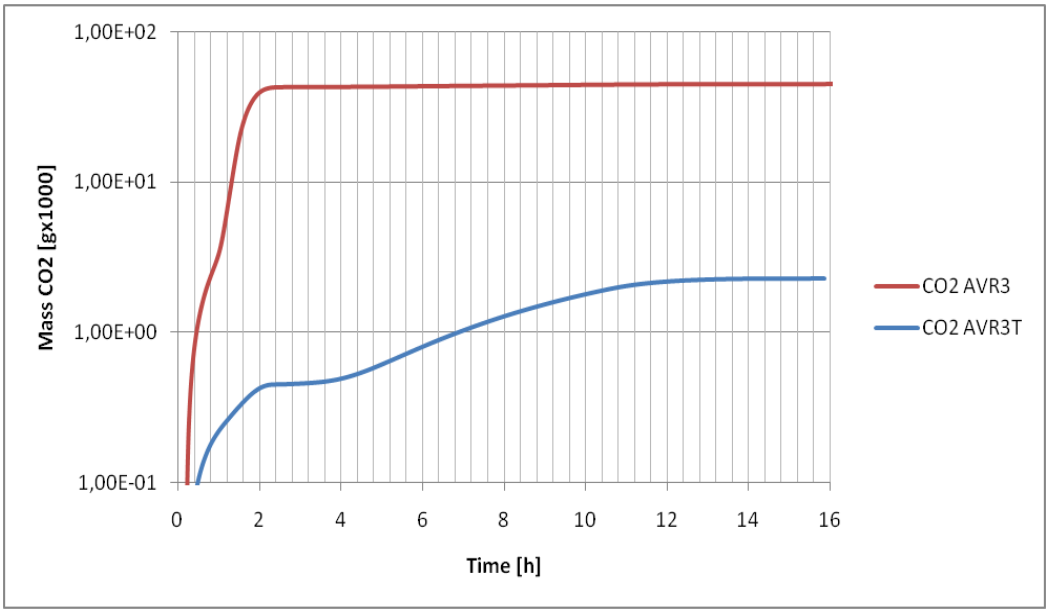

Figure 8.3.27: Comparison among the cumulative CO_2 emissions during successive treatments AVR3 and AVR3T of the same sample, semilog plot (indicative values)

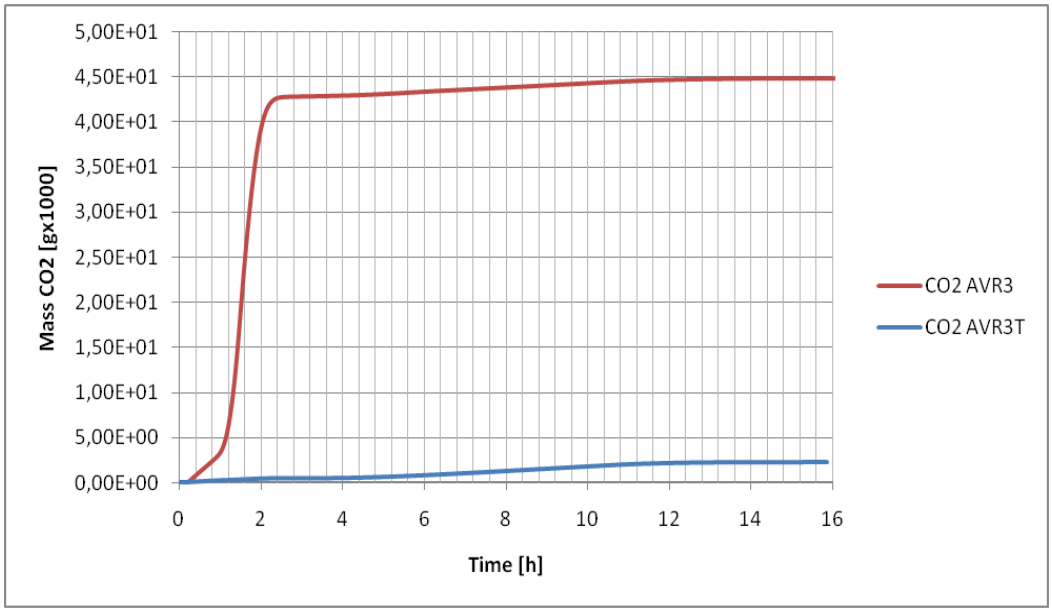

Figure 8.3.28: Comparison among the cumulative CO_2 emissions during successive treatments AVR3 and AVR3T of the same sample, linear plot (indicative values)

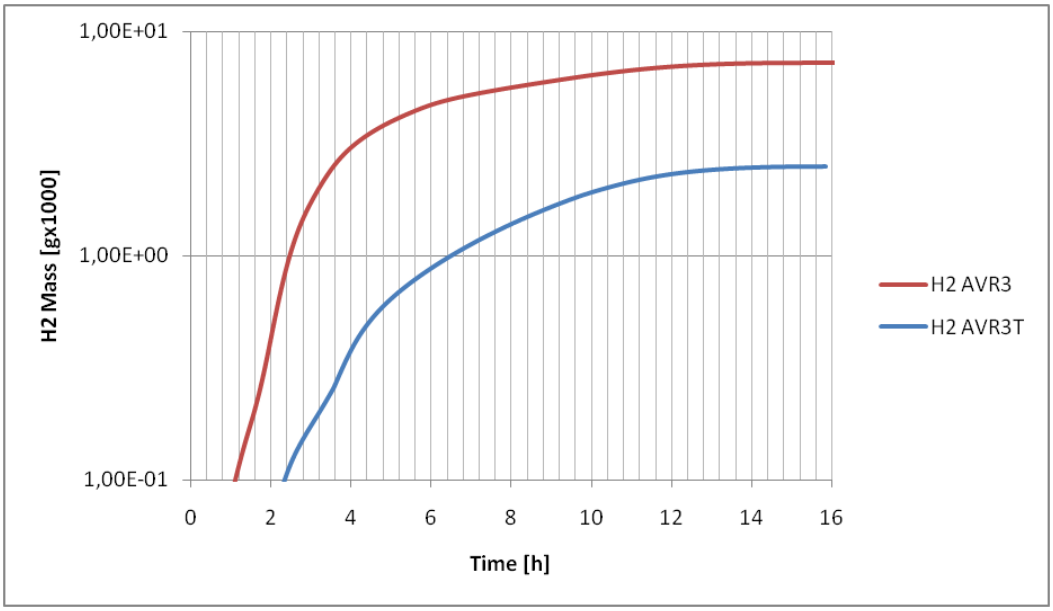

Figure 8.3.29: Comparison among the cumulative H_2 emissions during successive treatments AVR3 and AVR3T of the same sample, linear plot (indicative values)

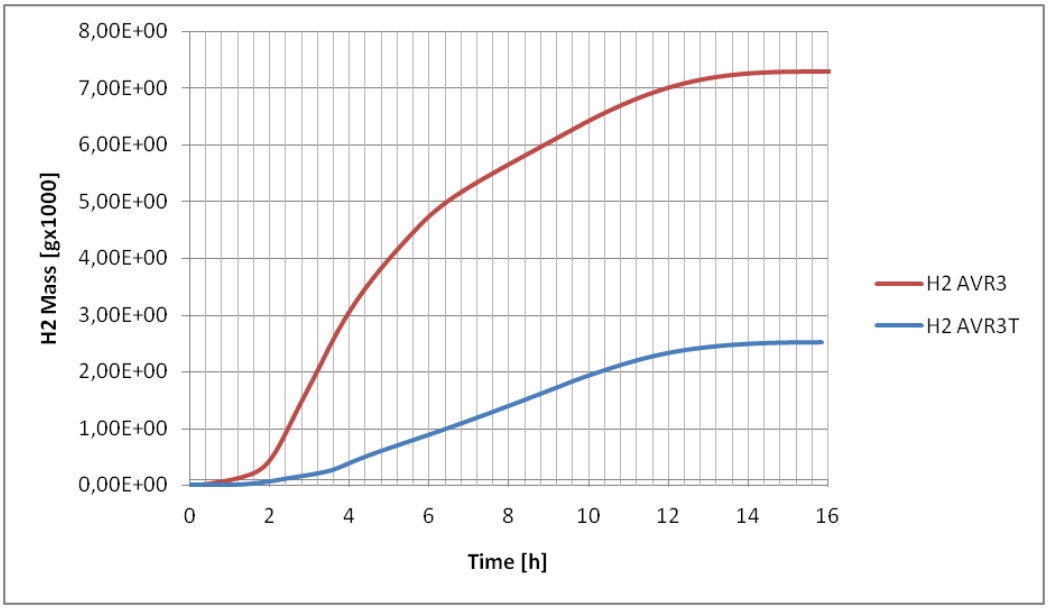

Figure 8.3.30: Comparison among the cumulative H_2 emissions during successive treatments AVR3 and AVR3T of the same sample, linear plot (indicative values)

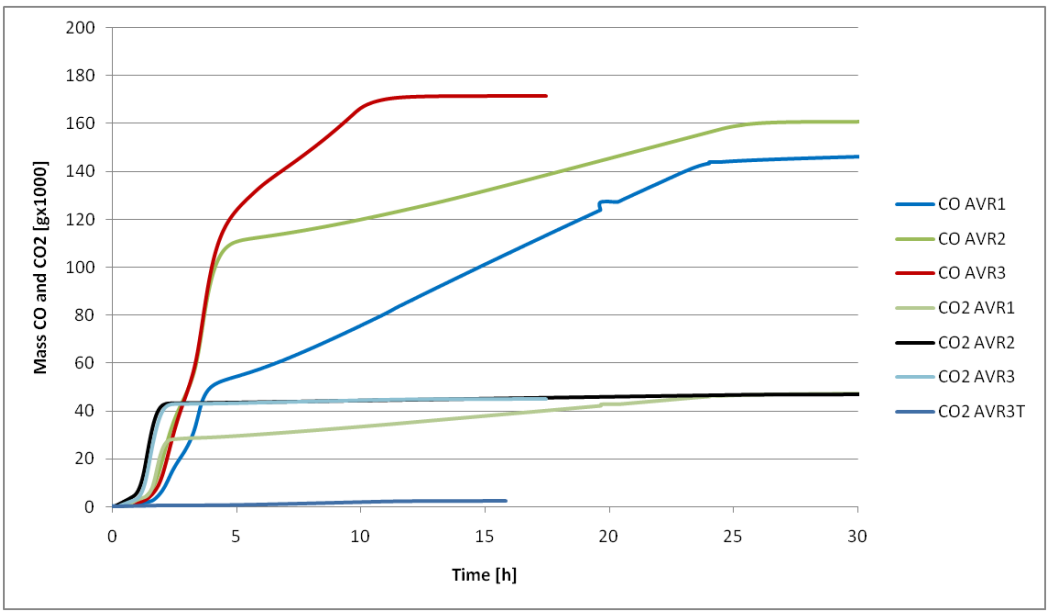

Figure 8.3.31: Comparison among the cumulative CO and CO_2 emissions during several treatments, linear plot (indicative values)

Figure 8.3.32: View of the sample bottom: the reacted areas are the dark cycles, corresponding to the Al_2O_3 supports

In table 8.3.1 are reported some values calculated starting from the MS measurements, relative to the experiment "AVR 01".

Treatment Time	CO/CO_2	CO/H_2	CO/H_2O	H_2/H_2O	T mean [°C]
Heating					
1	58.44	1.32	3.82	2.38	1281
2	7.77	0.49	0.57	1.17	1274
3	7.77	0.53	0.58	1.09	1269
4	8.54	0.59	0.64	1.08	1266
5	8.92	0.63	0.68	1.09	1265
6	9.11	0.65	0.71	1.09	1265
7	9.19	0.67	0.73	1.10	1265
8	9.59	0.70	0.77	1.11	1292
9	8.73	0.67	0.71	1.07	1284
10	8.75	0.66	0.73	1.10	1277
11	8.76	0.66	0.74	1.12	1277
12	8.67	0.66	0.75	1.14	1277
13	8.57	0.65	0.75	1.15	1277
14	8.47	0.65	0.76	1.17	1277
15	8.32	0.65	0.76	1.18	1277
16	8.27	0.64	0.77	1.20	1277
17	8.63	0.63	0.75	1.19	1277
18	8.37	0.62	0.76	1.22	1277
19	8.15	0.62	0.78	1.25	1277
19.4	8.09	0.62	0.78	1.26	1278
Cooling Down					

Table 8.3.2: Ratio among different gases released during thermal treatment of sample "AVR 1"

In table 8.3.3 are reported some values calculated starting from the MS measurements, relative to the experiment "AVR 02".

Treatment Time	CO/CO_2	CO/H_2	CO/H_2O	H_2/H_2O	T mean [°C]
Heat up					
1	424.98	3.30	8.79	2.48	1281
2	37.49	0.63	0.95	1.45	1281
3	14.86	0.38	0.43	1.13	1281
4	15.77	0.47	0.49	1.03	1281
5	17.20	0.56	0.56	1.01	1281
6	19.32	0.64	0.68	1.05	1281
7	20.61	0.73	0.76	1.04	1277
8	22.25	0.80	0.84	1.04	1281
9	23.95	0.86	0.92	1.07	1281
10	24.70	0.91	0.97	1.07	1281
11	25.50	0.94	1.02	1.08	1281
12	25.93	0.96	1.05	1.09	1281
13	26.33	0.97	1.06	1.10	1281
14	26.56	0.98	1.09	1.11	1281
15	26.99	0.98	1.11	1.13	1281
16	27.16	0.99	1.13	1.14	1281
17	27.35	1.00	1.16	1.16	1281
18	27.76	1.00	1.18	1.17	1281
19	27.98	1.01	1.20	1.19	1281
20	28.36	1.01	1.22	1.20	1281
20.8	28.73	1.02	1.24	1.22	1281
Cool Down					

Table 8.3.3: Ratio among different gases released during thermal treatment of sample "AVR 2"

In table 8.3.4 are reported some values calculated starting from the MS measurements, relative to the experiment "AVR 03".

Treatment Time	CO/CO_2	CO/H_2	CO/H_2O	H_2/H_2O	T mean [°C]
Heat up					
1	419.34	2.42	7.04	2.71	1281
2	73.63	1.02	1.55	1.50	1281
3	52.40	1.01	1.24	1.23	1281
4	51.25	1.28	1.30	1.02	1281
5	54.43	1.50	1.45	0.97	1281
6	59.43	1.69	1.64	0.97	1281
Cool Down					

Table 8.3.4: Ratio among different gases released during thermal treatment of sample "AVR 3"

8.4 Experiments with the TGA equipment

The Thermo Gravimetric Analyser has been chosen to check the repeatability of the previously observed results, also in a different scale, to confirm the probable emission of water at relatively high temperatures (>150°C) and to investigate the important temperature steps with the regards of the gaseous emissions. The first purpose has been achieved by repeating the same treatment as in "AVR3" and by comparing the results. The water emissions and the connection of emissions-to-temperature have been obtained by a multi-step temperature treatment. Following the presentation of each experiment, there will be a discussion of the results, in order to highlight the similarities and to make relative observations.

8.4.1 Experiment "AVR Square 1" under Argon atmosphere

Sample

Dimensions	14x14x4 mm
Weight Initial	1.3376 g ± 0.1 mg
Weight Final	1.3362 g ± 0.1 mg
Mass Loss	1.4 mg (0.105%)
Parameters:	
Argon flow	3.6 l/h
Relative Pressure	1 bar
Heating rate	5 °C/min
Maximum Temp.	1300 °C
Holding time at High Temp.	6 hours

Notes about the experiment

This experiment was established to have a confirmation of some emissions previously observed in treatments with the induction oven. The sample was chosen to fit with the small treatment chamber of the TGA but the weighing was not considered: indeed the sample was characterized by an improper shape to be used in the TGA, since the fluid dynamics requires cylindrical specimens to avoid fluctuation in the weighing.[243] More than that, the TGA was equipped with a quite precise thermocouple and a better temperature control system than the induction oven.

[243] The sample's shape is not supposed to change during the treatment: a cubical sample is more likely to change its shape compared to a cylindrical one, modifying consequently the fluid dynamics

Before starting the experiment the treatment chamber was flushed with Argon for few hours, but this precaution did not allow to get rid of some water inside the system (see the discussion for more details).

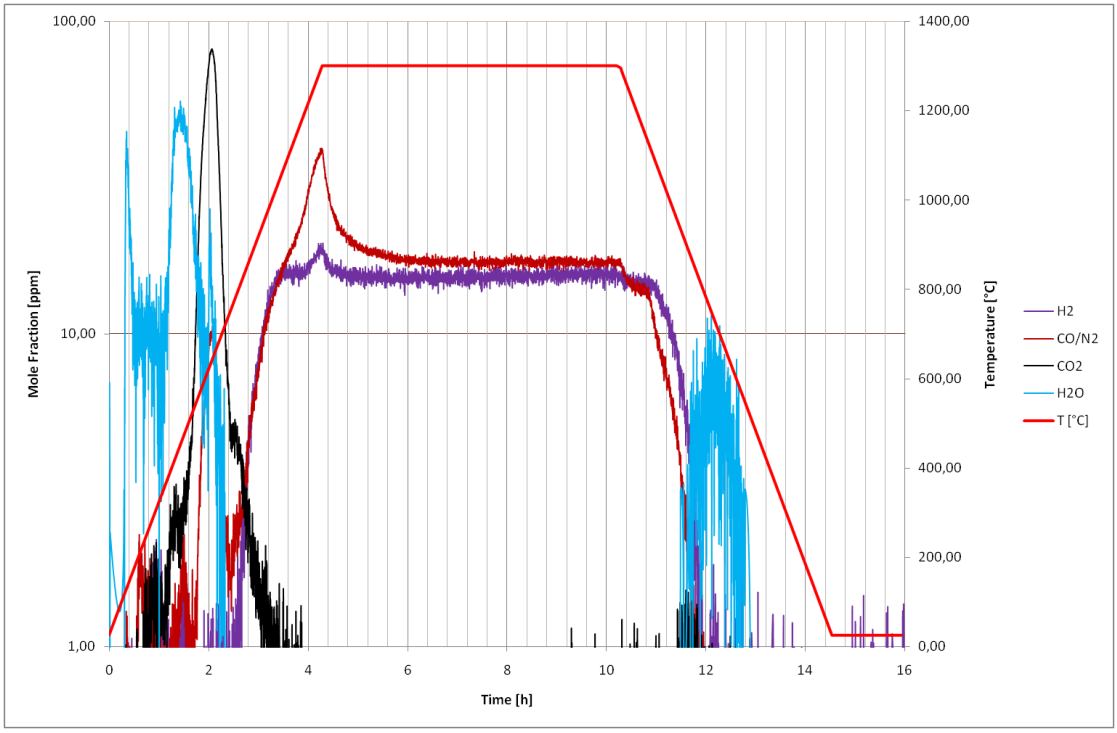

Figure 8.4.1: On-line gaseous emissions from AVR graphite, sample "AVR Square 1", semilog plot, water signal is indicative

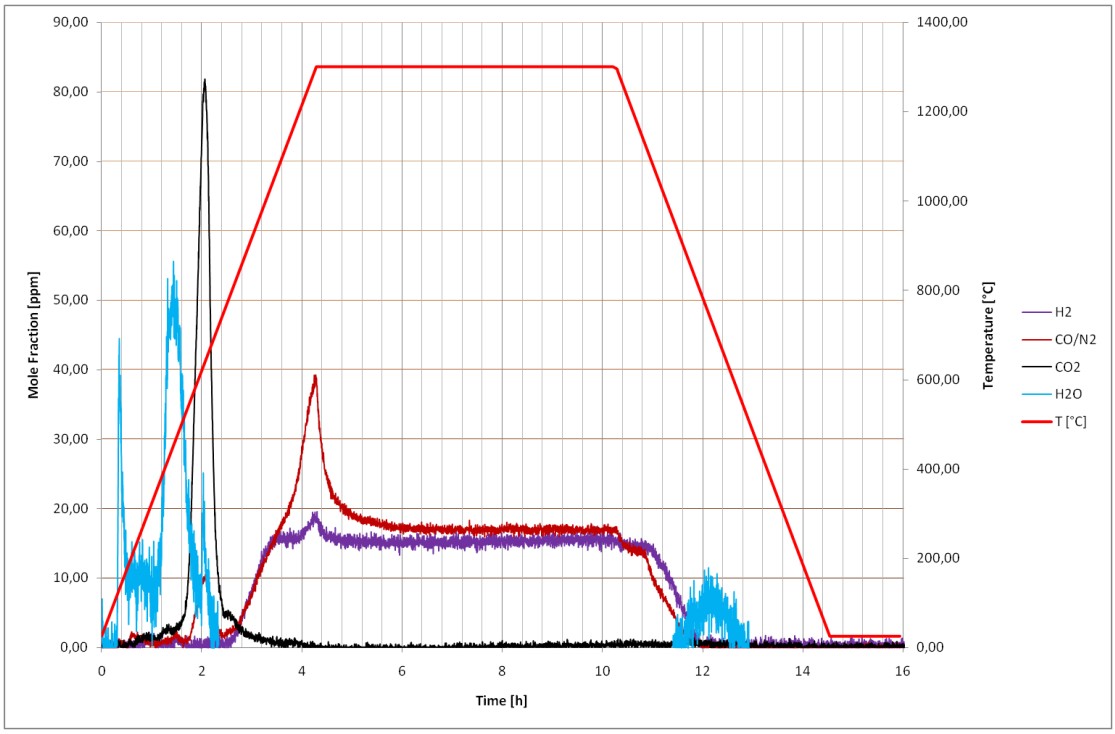

Figure 8.4.2: On-line gaseous emissions from AVR graphite, sample "Square 1", linear plot,water signal is indicative

8.4.1.1 Interpretation of the results

The sample used in the TGA was a small one, with a weight in the order of 1 g, so it was expected that the relatively low emissions previously measured (as SO_2, CH_4) would not have been detected by the mass spectrometer. However, the purpose of the experiment was to check some emissions, in particular the CO one. In previous experiments (section 8.3.1) some uncertainties were underlined by the presence of two different peaks of carbon monoxide, one of which was probably linked to the presence of the Al_2O_3 holder. Regarding figs. 8.4.1-2 it can be noticed the complete missing of one of the two CO peaks, confirming the reactivity of the alumina holder. In addition, the transitory peak of CO and H_2, observable as the maximum temperature is reached, is probably caused by the relative fast temperature change, which lead to a disequilibrium between diffusion of water and chemical reaction; in particular, there is a transient among the in-pore diffusion controlled regime and the mass transfer (or boundary-layer diffusion controlled) regime, considering that the upper level for the former is about 1250°C. At high temperature, the equilibrium is reached and the water-gas reaction is the dominant one, as observed in the other experiments. Another possible explanation could regard some embedded species, reacting at relatively high temperature. In addition, it is possible that many impurities play the role of catalysts for many reactions, so more investigations are necessary for a better understanding.

It has to be noticed that the pre-cleaning of the treatment chamber was established for short time compared to the other equipment, resulting into excessive amounts of water still present during the experiment. In figs. 8.4.1-2 the reported water values are indicative, since they were obtained by subtraction of a not-stable background. For this reason, the relative emissions of CO and H_2 are much higher than the ones observed during other experiences previously described (sec. 8.3). Because of that, it was not possible in this experiment to demonstrate that the graphite mass loss is occurring only during the first steps of an argon thermal treatment since the weight-loss, induced by the oxidants already present in graphite, was overlapped by the oxidation caused by external water. An exception to that is represented by the typical peak of CO_2, observed here, too, with a maximum of 80 ppm at about 650 °C. Considering the uncertainties in the temperature measurements of the induction oven, the peak is considered to occur at the same temperature. In addition, it is believed that a certain amount of dust is likely to be released, probably during the same step, due to an oxidation-induced effect in the porous structure (near-surface oxidation). The carbon dust was not visible in the TGA due to the usage of a small sample. The relative

cumulative CO and CO_2 emissions of this experiment and the one related to the induction oven are plotted in fig. 8.4.3: it can be noticed the enhanced CO production in the induction oven because of the presence of the alumina holder; on the other hand, the CO_2 emission is comparable and it shows only during the heating up step. In conclusion, the measured mass loss revealed in 0.105 % which, compared to the 0.11% obtained with massive samples, lead to the conclusion that the experiments were repeatable, in spite of the secondary emissions and uncertainties in the boundary conditions.

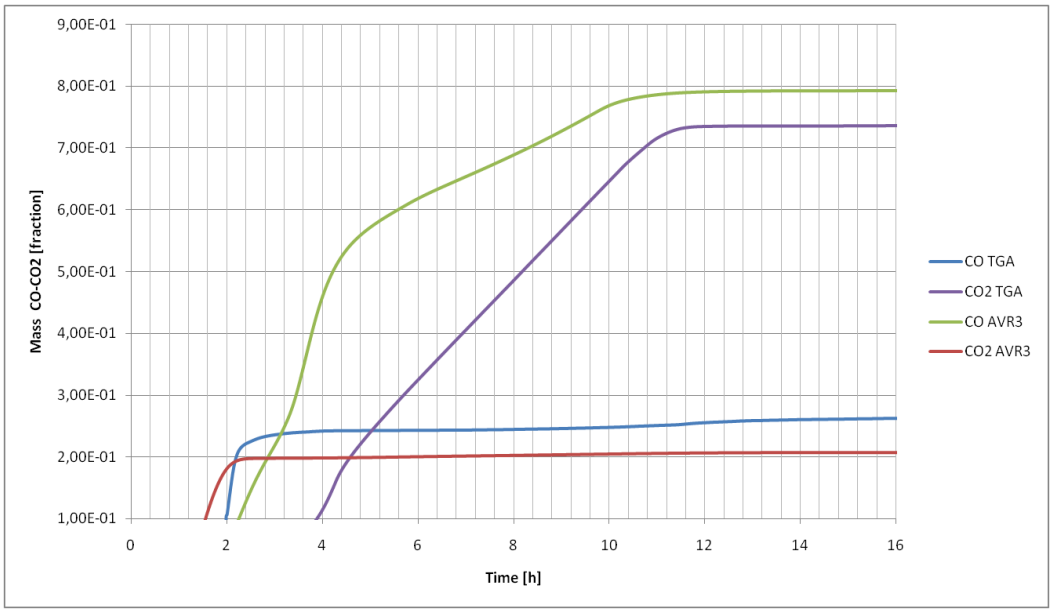

Figure 8.4.3: Comparison among the relative cumulative emissions of CO and CO_2 from the TGA and the Induction oven (indicative values)

8.4.2 Experiment "AVR Heat Step 01" under Argon atmosphere

Sample

Dimensions	H20Ø8 mm
Weight Initial	1.7769 g ± 0.1 mg
Weight Final	1.7742 g ± 0.1 mg
Mass Loss	2.7 mg (0.152%)

Parameters:

Argon flow	3.6 l/h
Relative Pressure	1 bar
Heating rate	5 °C/min
Maximum Temp.	1300 °C
Holding time at High Temp.	steps of 100 °C holding for 3 hours each step

Notes about the experiment

This multi-step treatment was thought to investigate the temperature dependence of many gaseous emissions. The heating rate and the maximum temperature are the same as in the other experiments, while the holding time is fixed in 3 hours for each step, in order to allow all the reactions to occur with a sufficient constant-temperature time.

As made in the other cases, the treatment chamber was flushed for some hours with argon, in order to obtain a clean environment before starting the treatment.

Figs. 8.4.4 and 8.4.5 show the gaseous emissions, measured by the Mass Spectrometer, during the thermal treatment.

Fig. 8.4.6 shows the weight signals obtained from the TGA: the temperature is showed with the red line and the green line represents the gross weight signal. A TGA requires a calibration to produce clean results (see section 8.1.3), two sample dummies were used to produce the "baseline" to be subtracted: the first one, made of Al_2O_3, revealed to be inappropriate, leading to results similar to the raw ones; the second one, made of fused quartz, allowed to produce very realistic values up to 1000 °C, since it is the maximum operative temperature of fused quartz.

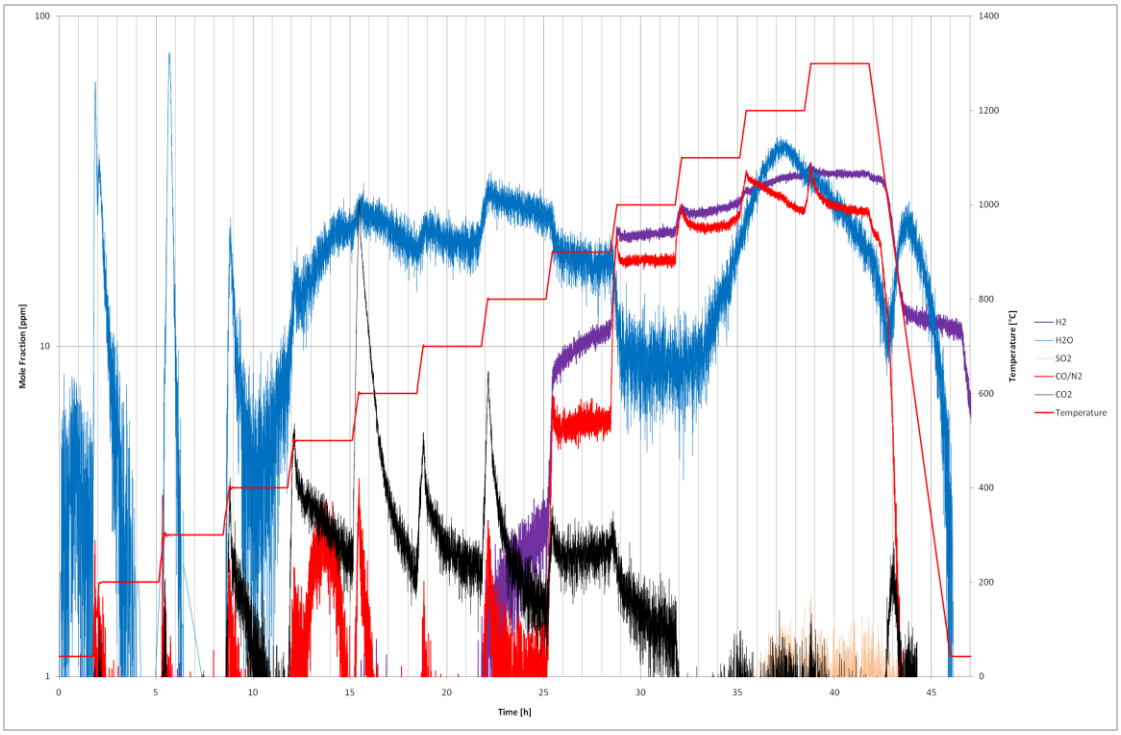

Figure 8.4.4: On-line gaseous emissions from AVR graphite, sample "CR 01", semilog plot

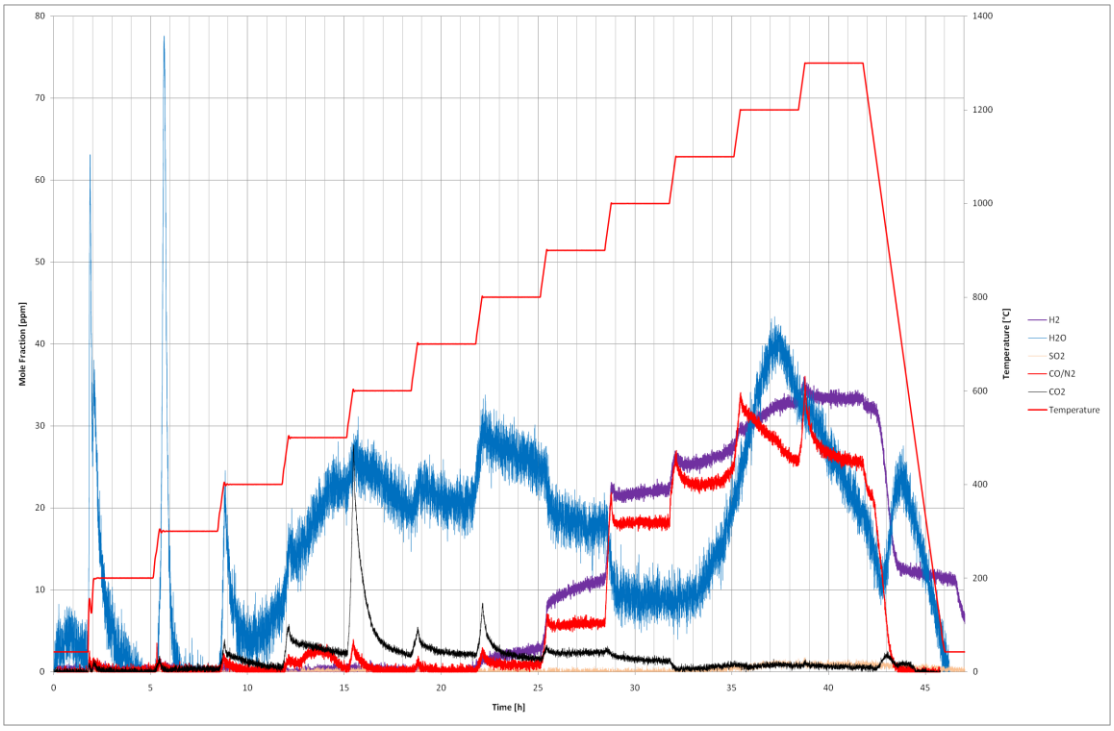

Figure 8.4.5: On-line gaseous emissions from AVR graphite, sample "CR 01", linear plot

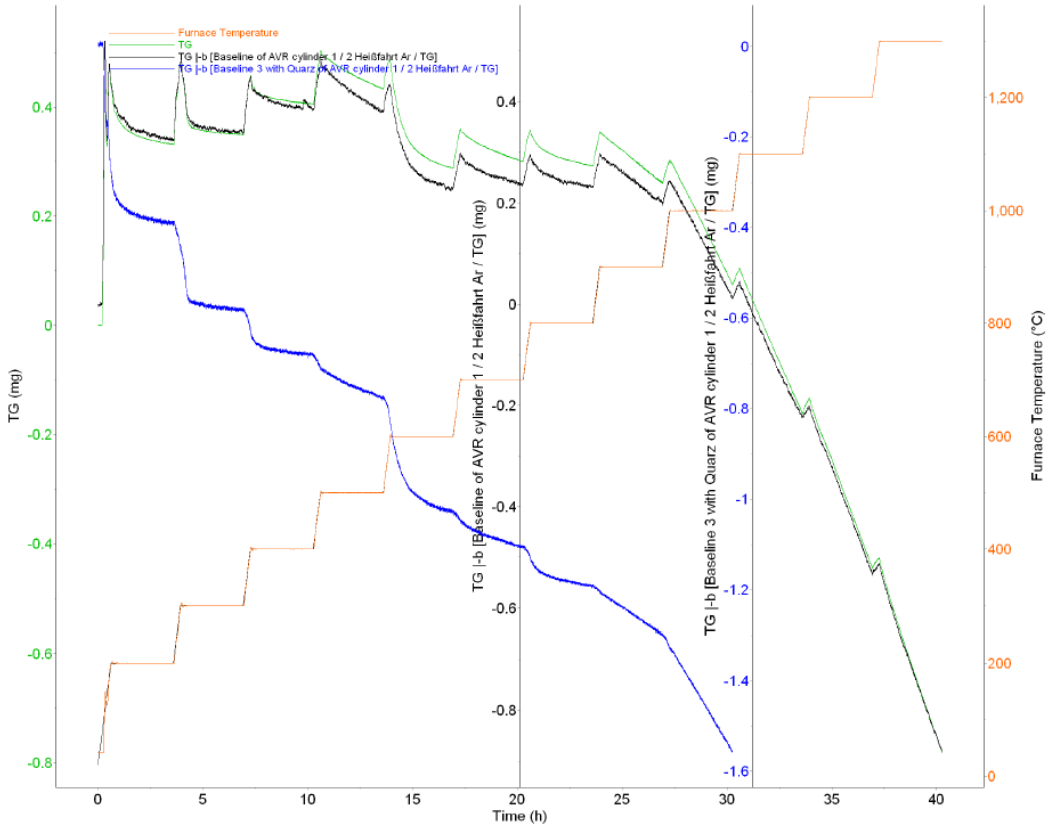

Figure 8.4.6: On-line weight measurement of AVR graphite, sample "CR 01", TGA

8.4.2.1 Interpretation of the results

The experiment was carried out to show the on-line emissions during a treatment in inert atmosphere. It is clear that a consistent amount of water was released from an external source so, de facto, the treatment atmosphere was similar to a mixture of water-steam and argon. It is hard to give an evaluation of the partial pressure of water since the source was not stable during the entire experiment. However, to give an order of magnitude, by considering the maximum value of water and the total pressure in the treatment chamber, it results an order of 10^2 Pa of partial pressure. In particular, referring to previous works,[244,245] the used water vapour partial pressure was 2.3 kPa and 7.4 kPa: the relative high amount of water used during similar treatments, even though at temperatures of about 1000 °C, led to a relatively high mass loss compared to the one measured here: mass losses more than 100 times higher than here were observed. On the other hand, considering previous treatments in argon atmosphere,[246] the mass loss ranged between 10 times to values compatible with

[244] J. Fachinger et al, "*Decontamination of nuclear graphite*", Nuclear Engineering and Design 238 (2008)
[245] T. Podruzhina, "*Graphite as radioactive waste: corrosion behaviour under final repository conditions and thermal treatment*", Juel 4166, 2004
[246] Idem

the present work. Of course, a direct comparison is not possible since the treatment and the temperature steps are different, but generally lower mass losses have been measured in all the experiments of this work.

As the temperature starts rising to reach the first plateau at 200 °C, it is observed a consistent mass loss: linking to the contemporary measured gaseous species, such mass loss (about 0.4 mg from the TGA signal, fig. 8.4.6) is explainable with the water removal from the sample. Similarly, the second step, at 300°C, shows a second consistent weight reduction (of about 0.2 mg) in concomitance with water being removed most probably from the sample (compare figs. 8.4.5 with 8.4.6). In general, for each temperature step the sample experiences a mass reduction, since more energy is provided and more sites become accessible, but one of the most important ones occurs at 600 °C: the mass loss is about 0.25 mg, considering the entire step, with a steep variation in the first part. Such value corresponds most probably to the release of carbon dioxide, a typical peak that was observed during every experiment here presented; however, more experiments are necessary to correlate such steep mass loss with the typical CO_2 peak. Starting from 900 °C the loss of mass for each step increases, being 0.1 mg at 900 °C and about 0.25 mg at 1000 °C. Higher temperatures could not be investigated due to the lacking of a proper baseline, necessary to produce reliable data.[247] The effects of water on the TGA measurements are still not clear, so future experiments should clarify this point.

Moreover, the comparison of the TGA and MS signal allows the interpretation of further results. Except for the water peak at 200°C, first step in which it is reasonable to measure water emissions, the marked peaks at 300°C and partially at 400°C demonstrated the release of water at relatively high temperatures; further experiments should verify the effective origin of such water, hypothesized to come from the sample. In addition, the high amount of water, measured starting from the late 400 °C step or, more markedly, from 500 °C on, is not supposed to be released from the sample: the TGA should have measured otherwise a steep mass loss as in the first three steps. At last, the high increase in the mass loss-per-step, starting from 900 °C, can be explained with the water gas reaction. Regarding the MS signal, it is observable that H_2 and CO appear and increase with the temperature, together with a reduction of the water signal. Such reaction is in accordance to literature (see chapter 6.1), i.e. it is endothermic and it becomes significant at temperatures above 800-850 °C.

(5.5) $$C_{(g)} + H_2O_{(g)} \rightarrow CO_{(g)} + H_{2(g)} \qquad \Delta H = +131\ kJ/mol$$

[247] More info in section 8.1.3

As it can be observed from the reaction 5.5 (here reported from section 6.1), at each mole of water corresponds a mole of CO and one of H_2. Looking at figs. 8.4.4 and 8.4.5, considering that part of the H_2 signal is derived from the water signal[248] and taking into account some uncertainties in the measurements, it can be stated that the mole fractions of H_2 and CO are present in the same amount, leading to confirm the establishment of the water gas reaction.
At high temperatures (>1000 °C), where the TGA signal cannot help anymore in the emissions interpretation, the water gas reaction is the dominant one, but the observed water peak does not find explanations linkable to the sample emissions, so it is supposed to come from an external source. The initial higher peak experienced both by CO and H_2 in each step can be related with a transient disequilibrium between diffusion and chemical reactions, leading to higher initial reaction rates followed by an equilibrium profile.[249] Concerning reaction rates of graphite with water there is a clear temperature dependence,[250] as reported in literature, [251] together with a shape dependence up to about 830 °C.
In conclusion, the initial release of water, up to temperature steps of 300°C and partially 400 °C, reveals to be originated most probably and mainly from the sample, due to a desorption process of chemisorbed water or even to a recombination process of sorbed oxygen and hydrogen; other water releases find their probable origin in the inner surfaces of the oven or in the gas-abduction pipes. The typical peak of CO_2 at 600 °C has been confirmed as in the other experiments. The water gas reaction becomes dominant at high temperatures, caused by an external[252] water source that provided different amounts of water vapour along the experiment.

[248] This is due to the working principle of the mass spectrometer: the molecules are ionized and fragmented by electron impact, so for water there will be a signal at mass 18, 17, 16, 2. (only 18 and 2 are here measured due to the overlapping with other fragments)
[249] Since the water was not stable the equilibrium reaction rates was not reached in every step. These observations are in line with the study of H.S. Hinnsen, K. Kühn, R. Moorman, B. Schlögl, M. Fechter, M. Mitchell, "*Oxidation experiments and theoretical examinations on graphite materials relevant for the PBMR*", Nucl. Eng. And Design 238 (2008) 3018-3025
[250] Previous works stated that the reaction rate ln(R) is proportional to 1000/T up to 830 °C and the slope varies with the graphite shape due to the different surface area. For T>830 °C the influences of shape do not exist due to the superficial penetration depth (
[251] L. Xiaowei, R. Jean-Charles, Y. Suzuan, "*Theoretical analysis of mass transfer and reaction in a porous medium applied to the gasification of graphite by water vapour*", Nucl. Eng. and Design 236 (2006), 938-947
[252] "External" is intended with reference to the sample.

8.4.3 Experiment "AVR Heat Step 02" under Argon atmosphere

Sample

Dimensions	H20Ø8 mm
Weight Initial	1.7489 g ± 0.1 mg
Weight Final	1.7465 g ± 0.1 mg
Mass Loss	2.4 mg (0.137%)

Parameters:

Argon flow	3.6 l/h
Relative Pressure	1 bar
Heating rate	5 °C/min
Maximum Temp.:	1300 °C
Holding time at High Temp:	steps of 100 °C holding for 3 hours each step

Notes about the experiment

This experiment is identical to the "AVR heat step 01". It was performed to check the repeatability of the results and, referring to the excessive water emissions observed in the previous treatment, by flushing for longer time the treatment chamber.

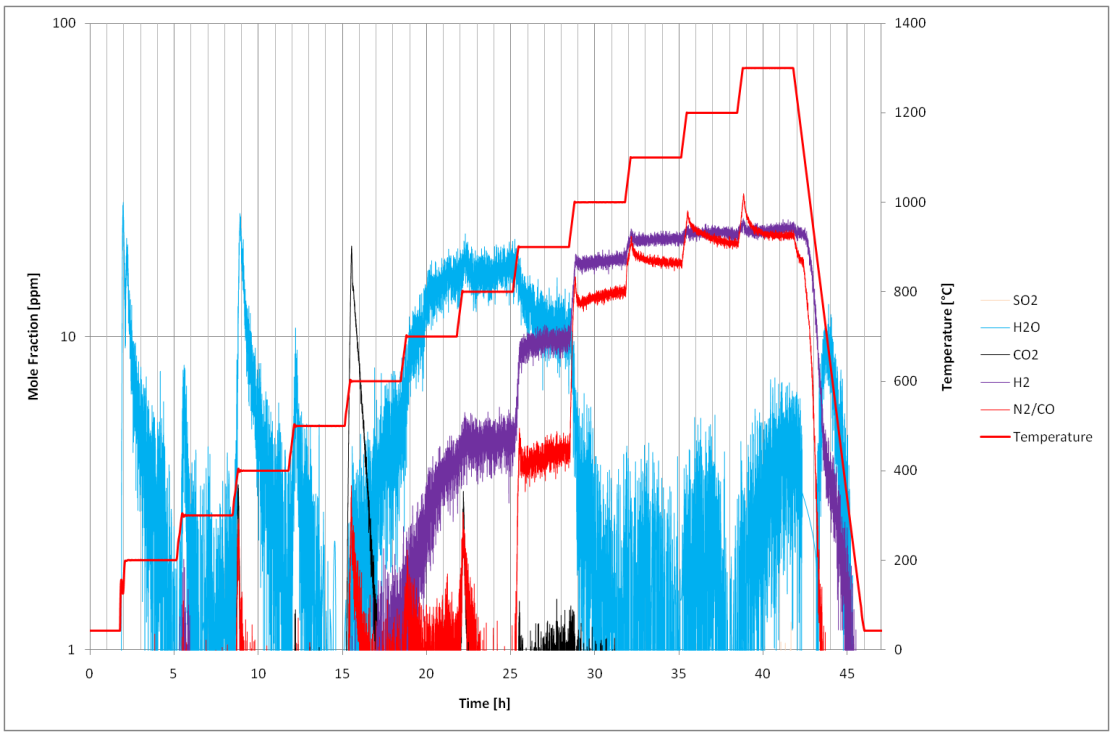

Figure 8.4.7: On-line gaseous emissions from AVR graphite, sample "CR 02", semilog plot

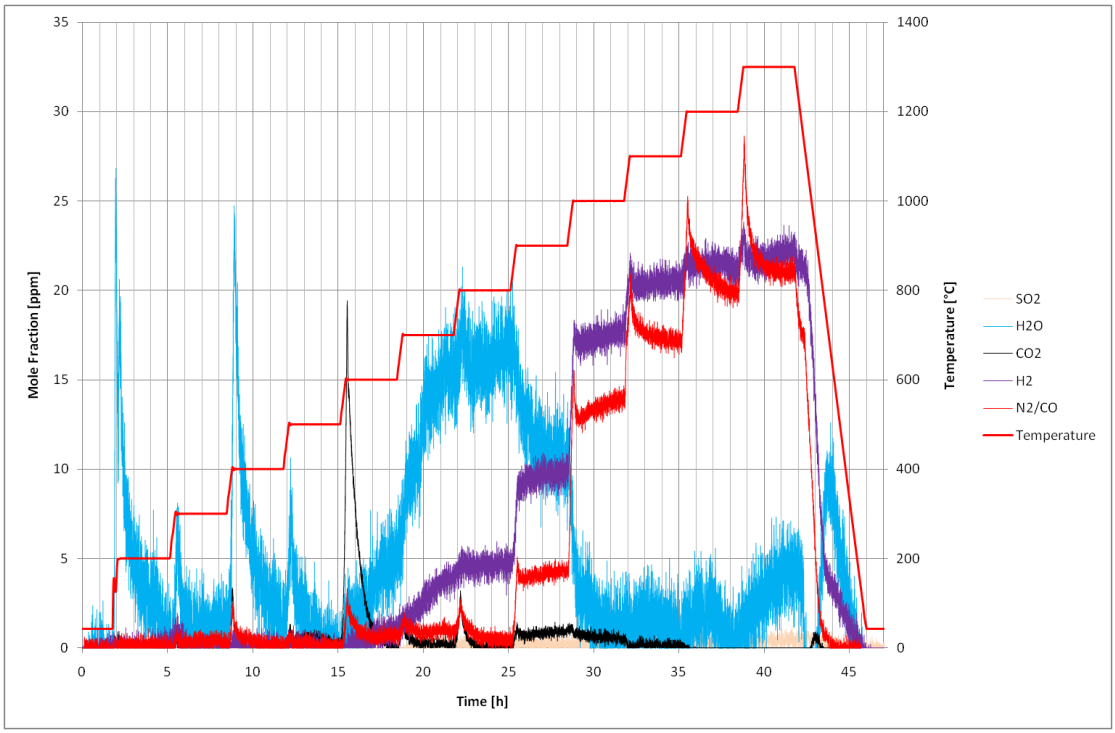

Figure 8.4.8: On-line gaseous emissions from AVR graphite, sample "CR 02", linear plot

8.4.3.1 Interpretation of the results

This experiment, identical to the "AVR Heat Step 1", was performed to check the repeatability of the results. It started immediately after the former treatment was finished: the TGA was opened and the sample was replaced by a new one. This fact could explain the lower general measured values (see figs. 8.4.7-8). However, all the peculiar emissions are observed here too. In particular, the water peaks at the first heating step (up to 200 °C) and the ones at 300 °C and 400 °C are quite marked, even showing half of the maximum values observed in the experiment "AVR Heat Step 01". As the temperature of 600 °C is reached, the typical CO_2 peak is measured here too, slightly lower than the former one, compatible with statistical fluctuations. At high temperatures, the dominating reaction is again the water-gas one. The mass loss, measured by weighing the sample before and after the experiment, revealed to be 0.137% against 0.152% for the former experience: this difference underlines the influence of the water source on the emissions and the mass loss. In future experiments more attention will be necessary to eliminate all the external sourced, which are affecting the results.

Concerning sulfur dioxide, it was detected in very low values (around 1ppm), comparable with the detection limit of the mass spectrometer, due to the very small sample. Methane was not detected.

In conclusion, the presence of oxidizing species, originally embedded in the graphite matrix, has been confirmed. This fact explains the higher release rates during the first steps of the thermal treatment. Many secondary emissions were observed because of external sources, but the comparison of similar experiments performed with different equipment allowed to confirm the previous statement. A parallelism with radionuclide release experiments and observations found in literature permitted the interpretation of the removal mechanism of tritium and radiocarbon, getting closer to the development of an industrial purification method. Future experiments should focus on irradiated graphite in order to have a confirmation of what has been measured and interpreted here.

9. SIMS analysis before and after thermal treatment

In this section several SIMS analyses will be shown and discussed. The purpose of such analysis is to study the depth profile of many elements in the AVR graphite and to compare the differences after a high temperature thermal treatment. The distribution of many impurities and oxidants is of fundamental importance to understand their removal mechanisms and to correlate it to the radioactive species, in order to develop a proper purification process.

9.1 Generalities on Secondary Ion Mass Spectrometry

SIMS spectrometry consists on a bombardment of a sample surface with a primary ion beam, followed by mass spectrometry of the emitted secondary ions. The detection limit is very low, i.e. $1 \cdot 10^{10-16}$ atoms/cc. The SIMS primary ion beam can be focused to less than 1 μm in diameter. During SIMS analysis, the sample surface is slowly sputtered away. Continuous analysis while sputtering produces information as a function of depth, called "depth profile". When the sputtering rate is extremely slow, the entire analysis can be performed while consuming very few atomic layers. This slow sputtering mode is called static SIMS in contrast to dynamic SIMS used for depth profiles. Shallow sputtering minimizes the damage done to organic substances present on the sample surface. The resulting ion fragmentation patterns contain information useful for identifying molecular species. Only dynamic SIMS will be treated in this work.

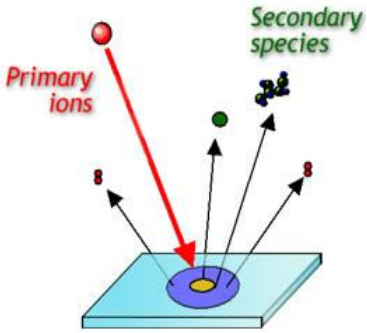

Figure 9.0: Schematic working principle of SIMS

The bombarding primary ion beam produces monoatomic and polyatomic particles of sample material, along with electrons and photons. The secondary particles carry charges and they have kinetic energies that range from zero to several hundred eV. Primary sources normally used are Cs+, O_2+, Ar+, O+, with energies between 1 and 30 keV. Sputter rates are typically in the range of 0.5 to 5 nm/s, strongly dependent on the beam intensity, the sample material and the crystal orientation.

One of the main important factors that affect the ionization efficiency in SIMS is connected with the primary beam used. For example, oxygen bombardment increases the yield of positive ions while cesium bombardment increases the yield of negative ions. In particular, C, N, O, S, Cl and H show higher yield as negative secondary ions together with Cs+ primary source. On the other hand, Li, Ca, Na and many others show higher yields as positively charged ions using O_2+ primary beam.

9.2 Results and Discussion

Two AVR virgin graphite samples were investigated, cut from the inner part of a massive cylinder of graphite. The sample "AVR square 0" was not treated; the sample "AVR square 1" was treated in the TGA, as described in section 8.4.1. Here are reported some sample's parameters.

Sample "AVR square 0"

Weight	ca. 1.4 g
Treatment:	none

Sample "AVR square 1"

Weight Initial	1.3376 g ± 0.1 mg
Weight Final	1.3362 g ± 0.1 mg
Mass Loss	1.4 mg (0.105%)
Parameters:	
Argon flow	3.6 l/h
Relative Pressure	1 bar
Treatment	Thermal treatment under argon at 1300 °C
Heating rate	5 °C/min
Holding time at High Temp.	6 hours
Equipment used:	TGA (without weighing)

SIMS parameters

Investigated area	ca. 100x100 μm^2
Primary Ion	Cs+
Energy	2 keV
Sputtered area	ca. 300x300 μm^2

After 4 hours from the thermal treatment a very first SIMS analysis was performed for each sample, showing some interesting results. A second series of SIMS measurement have been

performed about one month later in order to check the results, during which time the sample was stored in ambient air. Taking into account that graphite is absolutely not homogeneous, some SEM images were taken to have a closer look to the investigated area (300x300 μm).
Before every experiment, vacuum was established for many hours in order to get an inert environment for measuring.

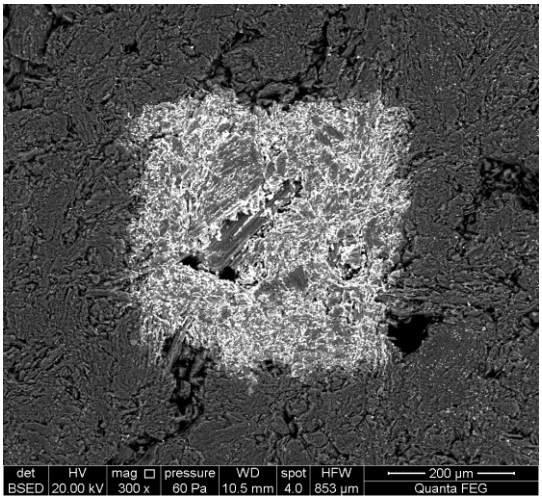

Figure 9.1: AVR virgin square 1 baked

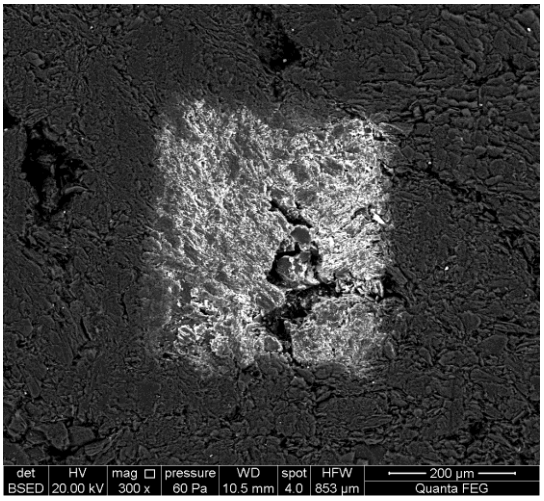

Figure 9.2: AVR virgin square 0 not baked

The real area interested by the measurement was about 100x100 μm, in the middle of the crater, to avoid edge effects. Looking at fig. 9.1 it can be deduced that the measurement interested partially a filler particle and partially the binder phase; fig. 9.2 shows a less clear structure because of the presence of some holes. In the present study no sufficient information are available in order to separate the measured values by considering the filler or the binder phase, so the obtained data will be compared without doing such distinction.

Considering the background fluctuations of the mass spectrometer used for the SIMS analysis, a direct comparison among different measurement is not advisable. Then it has been assumed, hypothesis confirmed also from the analysis, a homogeneous distribution of ^{13}C with the depth; actually the very first layers are less rich of ^{13}C, but it has been considered only its mean counts value in order to "normalize" with it all the measurements and to do in such way a more realistic comparison. The first 50 measured dots have been omitted in order to analyze reliable values. Results obtained from one of the analyses showed high fluctuations, so it was decided to omit them.

The elements of interest are: Sulfur, Chlorine, Nitrogen, Oxygen, Calcium, Lithium, and Hydrogen. These elements have been measured as ions in the mass spectrometer, respectively

as CN-, S-, Cl-, O-, Ca-[253], LiO-[254], H-. In the following, all the results are presented divided by element of interest, to have a clearer comparison between the profiles before and after the thermal treatment. Some results are very clear, some others need further investigations.

The results are shown in two ways: the one is an integral profile, the other is a three dimensional profile.

Considering as first the integral profile, it represents the total measured counts versus time. To obtain a depth profile from that, a proper calibration time-to-depth is necessary, since the speed of excavation of the cesium ion-beam depends strongly on the nature of the specimen. Graphite is a strongly inhomogeneous material and a calibration is not simple. However, it was assumed a total depth at the end of the experiment of about 7±3 μm, with a further assumption that the variation of the crater depth is a linear function of the time.[255] The integral profiles are plotted versus the measurement time here, since the uncertainties on the real depth are considerable. The above-cited value is used only to give a rough estimation of the real depth.

It was chosen to build a 3D profile due to some uncertainties in the interpretation of some results. In fact, assuming a non-homogeneous distribution of a certain element, i.e. hot spots, the integral profile could lead to wrong interpretations, since the total amount is not representative of the effective structure of that particular element. In particular, a general 3D profile is built by stacking the different 2D distributions obtained for every measurement over the time. In that way a similar-cube shape is obtained, with dimensions of about 100x100x100 μm. Actually, the depth is only apparent, but necessary to have a clear view of the distribution of a certain element: the real depth is about 15 times smaller.

[253] The polarity and primary source for this ion is the wrong one: the Cs+ ion beam will result in very low yield of Calcium ions
[254] Same consideration as above
[255] It is mainly true, except for the first seconds of the measurement.

9.2.1 Sulfur before and after thermal treatment

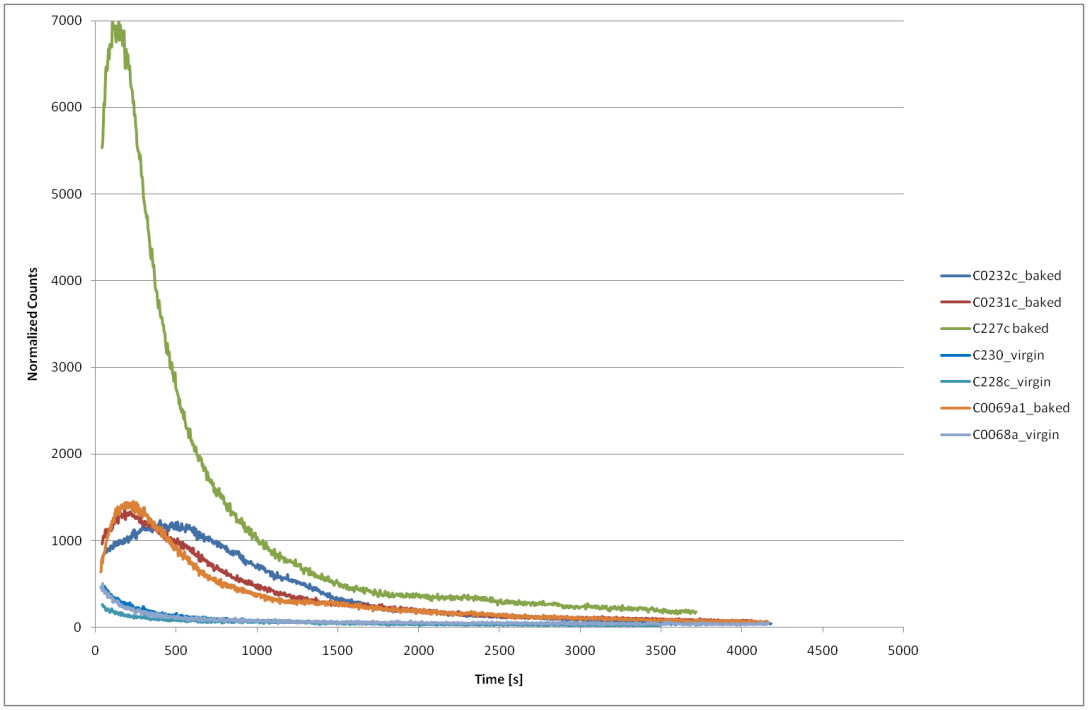

Figure 9.2.1: Comparison among normalized SIMS depth profiles of sulfur as S-, linear plot

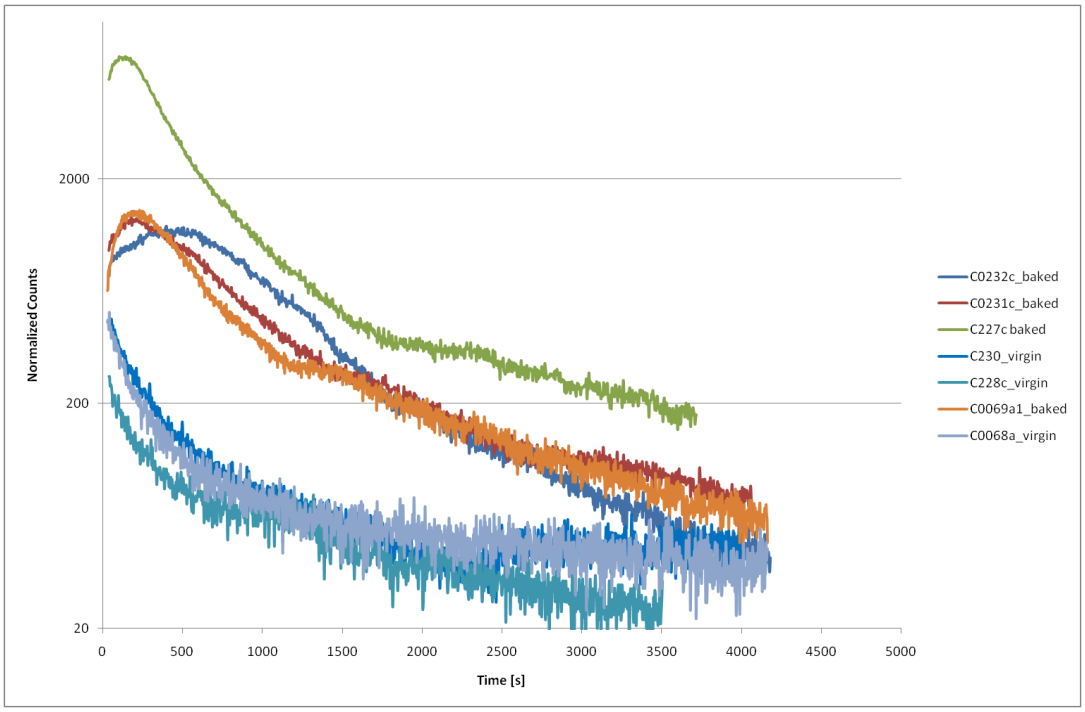

Figure 9.2.2: Comparison among normalized SIMS depth profiles of sulfur as S-, semilog plot

Sulfur was measured for the first time during the experiments with on-line gaseous measuring through a mass spectrometer. Following that, SIMS analyses have been performed to check the hypothesized removal model:[256] the first step of such model is the migration of sulfur from the bulk to the sample surface by thermal treatment. In fact, referring to figs. 9.2.1-2, it can be noticed a consistent increase in the surface concentration of sulfur after the thermal treatment. The result is reproducible, although the inhomogeneous nature of graphite. A clearer vision of this can be performed looking at the 3D depth profiles reported in fig 9.2.3: it can be noticed that sulfur is present mainly as hot spots near the untreated sample surface; during the treatment a migration occurred from the bulk of the graphite, resulting in a high superficial concentration. However, the distribution of the migrated sulfur seems to be a superimposition of hot spots and a spread distribution.

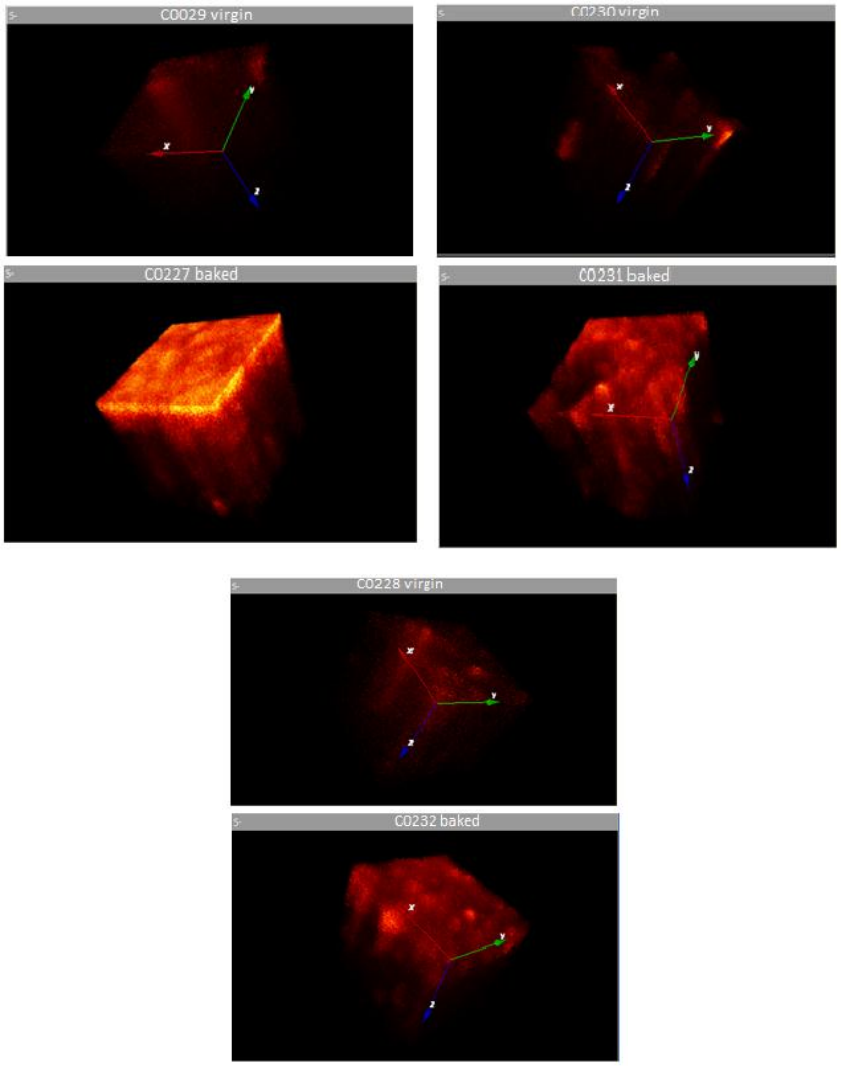

Figure 9.2.3: Comparison among SIMS 3Ddepth profiles of sulfur (S-)

[256] See section 8.3.2

This result has been confirmed by two other observations:

- A consistent amount of sulfur and especially calcium was found on the Al_2O_3 thermal shielding inner surface exposed directly to the sample, in the induction oven;[257]
- Some tens of ppm of SO_2 were measured in the gaseous emissions from the massive sample in the induction oven:[258]
- Small amounts of sulfur were measured on the surface of the graphite sample, thermally treated in the experiment "CR02", through SEM;[259]

Considering that part of the sulfur (S-34) is a precursor of Cl-36, its removal before using the graphite in a reactor will result in lower amounts of activated product and, consequently, in an easier handling and storage. However, other experiments should confirm that fact, but the last step that will validate the theory is the study of an irradiated graphite sample under thermal treatment.

9.2.2 Chlorine before and after thermal treatment

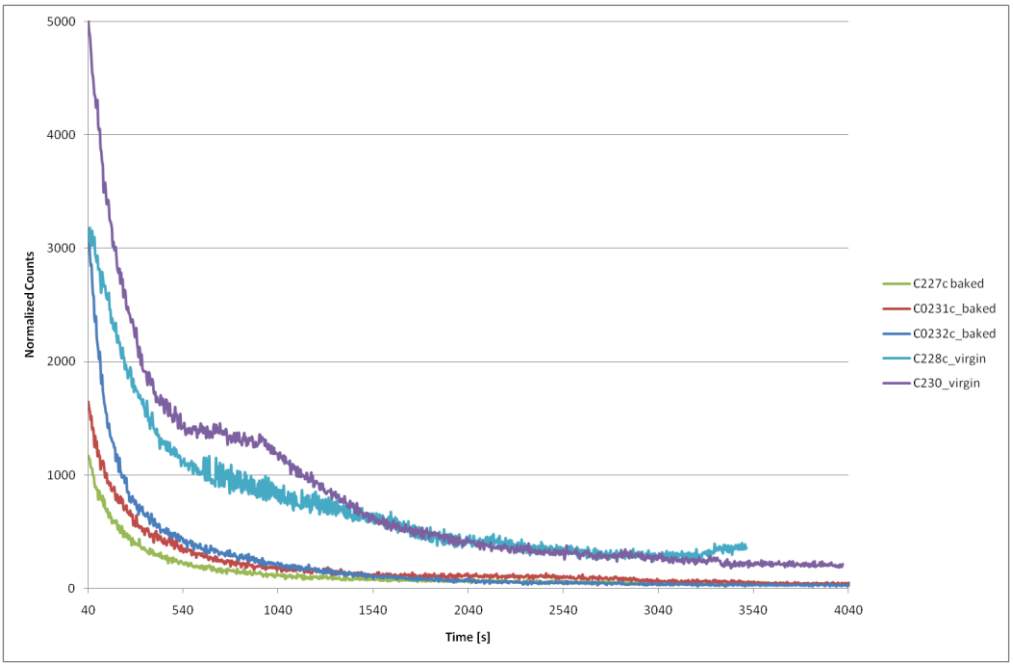

Figure 9.2.4: Comparison among normalized SIMS depth profiles of chlorine as Cl-, linear plot

[257] See section 11.3
[258] See section 8.3.1.1-5
[259] See section 11.2

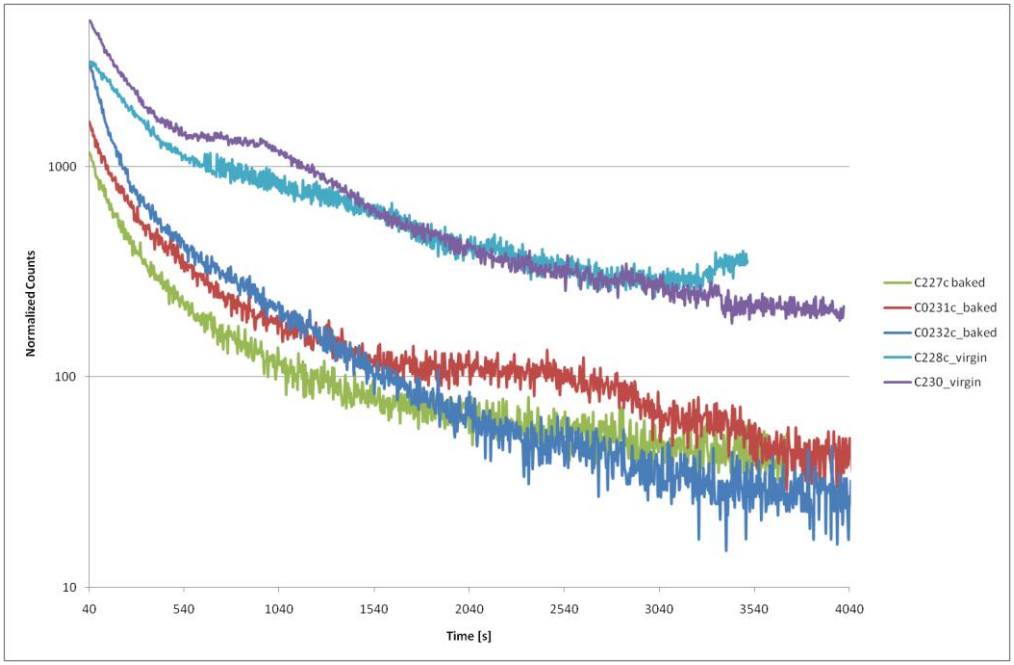

Figure 9.2.5: Comparison among normalized SIMS depth profiles of chlorine as Cl-, semilog plot

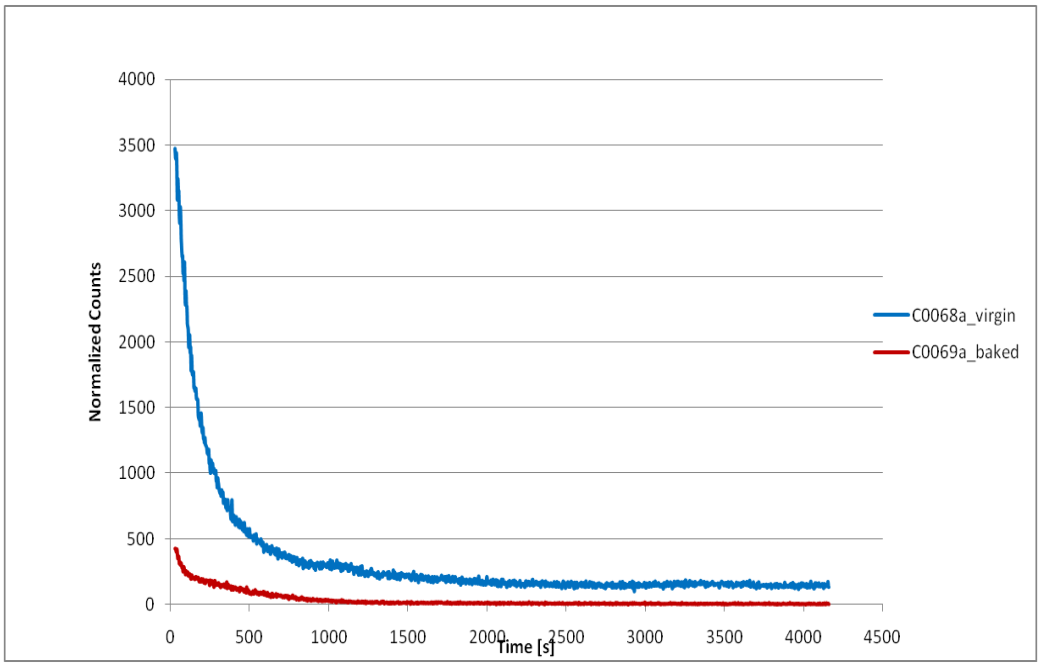

Figure 9.2.6: Comparison among normalized SIMS depth profiles of chlorine as Cl-, linear plot

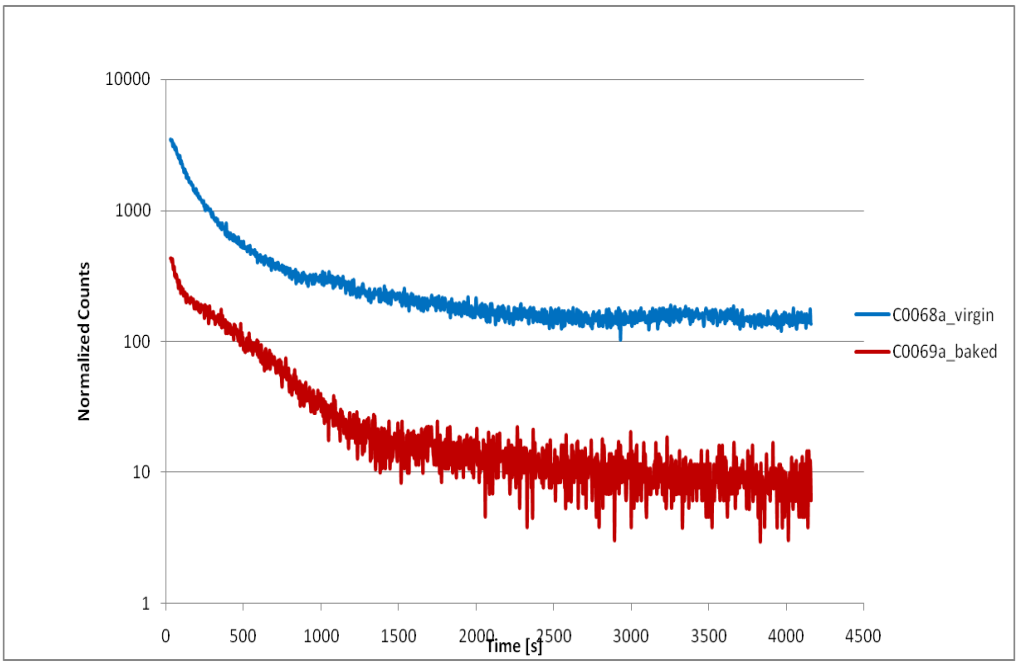

Figure 9.2.7: Comparison among normalized SIMS depth profiles of chlorine as Cl-, semilog plot

Because of a strong variation in the background of the mass spectrometer, it was chosen to show the results obtained from the different measurements separately: figs. 9.2.4-5 show the values obtained by the most recent analysis; figs. 9.2.6-7 show the results of the first analysis.

Looking at figs. 9.2.4-7 it can be noticed an important integral decrease of the chlorine concentration, mostly at the surface, after the baking process. It is confirmed by all the measurements. This result was partially unexpected because Chlorine is present normally as hot spots and the investigated surfaces were artificial ones. One reason of that could have been the presence of a contamination by NaCl, but Natrium was investigated too and it was present in all measurement in negligible amounts compared to Chlorine. On the other hand, however, considering the working principle of SIMS and considering the primary ion beam used in the present case, the presence of NaCl cannot be excluded.[260] The AVR graphite was not chemically purified during its manufacture, then the other possible origin stands on the raw materials.[261] Further investigations are needed to understand the source of the measured Chlorine. Considering the present analysis, it is not possible to determine the chemical form, so further analyses are necessary.

[260] Indeed the usage of Cs+ as primary ion beam is resulting in very low yields for Na and high yields for Cl, which could explain the different values among the two measured elements.
[261] See chapter 3,7

Previous experiments of Vaudrey et al.[262] showed that chlorine is mainly present as hot spots: looking at the 3D depth profiles such observation is confirmed also for the AVR graphite but, differently from the literature results, the typical dimension of an hot spot is meanly 10μm in diameter.[263] Moreover, Vaudrey found that chlorine is present mainly in organic form with a relative fraction of about 70%; the other fraction was hypothesized to be bound with oxygen. Thermal treatments at temperatures up to 1000 °C showed that the organic part was completely removed, at least from the sample surface (first few nanometers). In the present case, considering the integral profile, it resulted a total mean removal of about 64%. For a better comparison with values obtained in literature[264], by considering the very first values connected with the first superficial layers, it resulted a mean removal efficiency of 71%.

Sample	**Mean value on surface [counts]**	**Mean integral value [counts]**
Not treated	3627	677140
Treated	1053	242202
Removed fraction	71%	64%

Table 9.2.1: Fractional removal of chlorine, superficial and integral

The obtained results are not in accordance with the ones found in literature. However it can be explained through the presence of many variables: the graphite grade investigated by Vaudrey was a different grade (SLA2) and, in addition, the treatments of Vaudrey experienced maximum temperatures of about 1000 °C, while here 1300 °C were used for 6 hours. Moreover, it is possible that in the AVR graphite chlorine is mainly present in the organic form. More investigations in the future should clarify this point.

A clearer vision of different surface concentrations can be performed looking at the 3D depth profiles of Chlorine from SIMS analysis (fig 9.2.8): the high fractional removal is visually notable. It has to be underlined, however, that the high removal is related to the first micrometers in depth from the sample surface. More investigations are necessary to evaluate the release efficiencies from the bulk graphite.

When future investigations will confirm the results obtained here also for i-graphite, a high temperature thermal treatment could represent a good solution for chlorine removal in an efficient way. For what concerns modern graphite, chlorine is present normally in much lower amounts, also due to the fact that the purification processes, performed during the

[262] C.E. Vaudrey, C. Gaillard, N. Toulhoat, N. Moncoffre, M.L. Schlegel, L. Raimbault, "*Chlorine speciation in nuclear graphite studied by X-Ray Absorption Near Edge Structure*", J. Nucl. Mat. 418 (2011)

[263] Vaudrey observed spots with a mean diameter of 5 μm

[264] Vaudrey used XPS analyses to check the effective removal of Chlorine, analyses focused on the first nanometers from the surface of the sample

manufacture, are normally implying fluorinates[265]. From this point of view, an efficient method for chlorine removal will find most of the applications in the old-grade graphite.

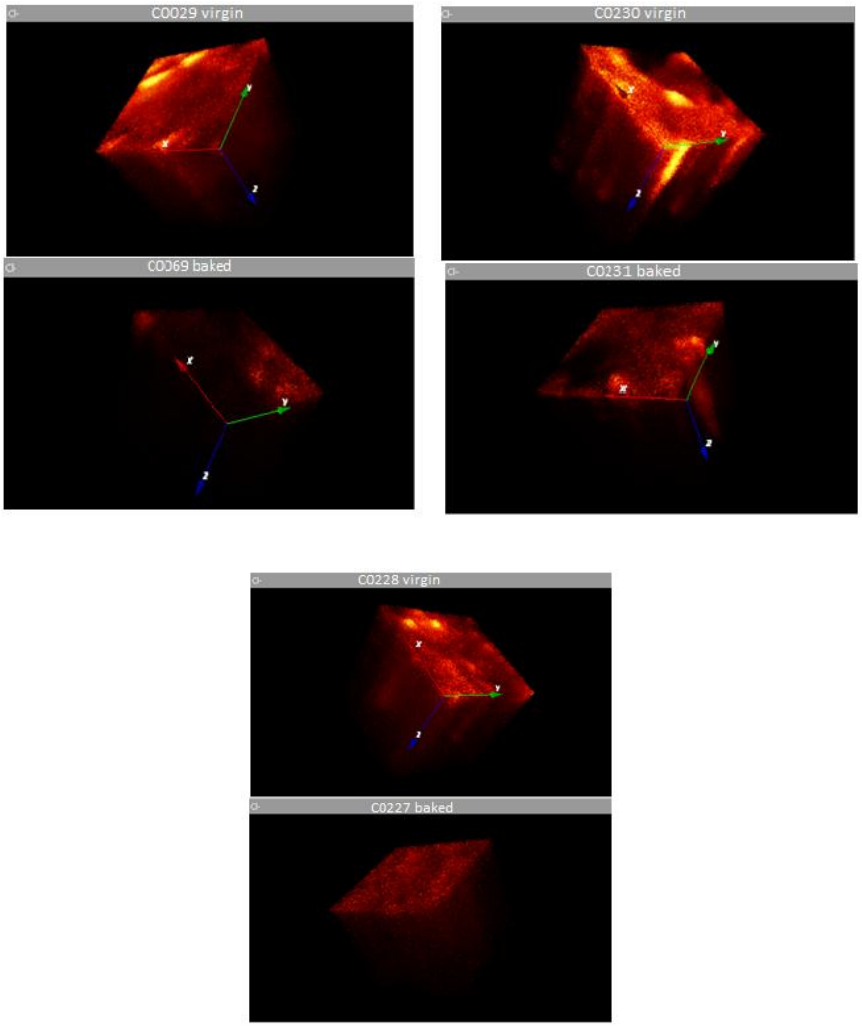

Figure 9.2.8: Comparison among SIMS 3D depth profiles of chlorine as Cl-, untreated (upper pictures) and treated (lower pictures)

[265] See chapter 5

9.2.3 Nitrogen before and after thermal treatment

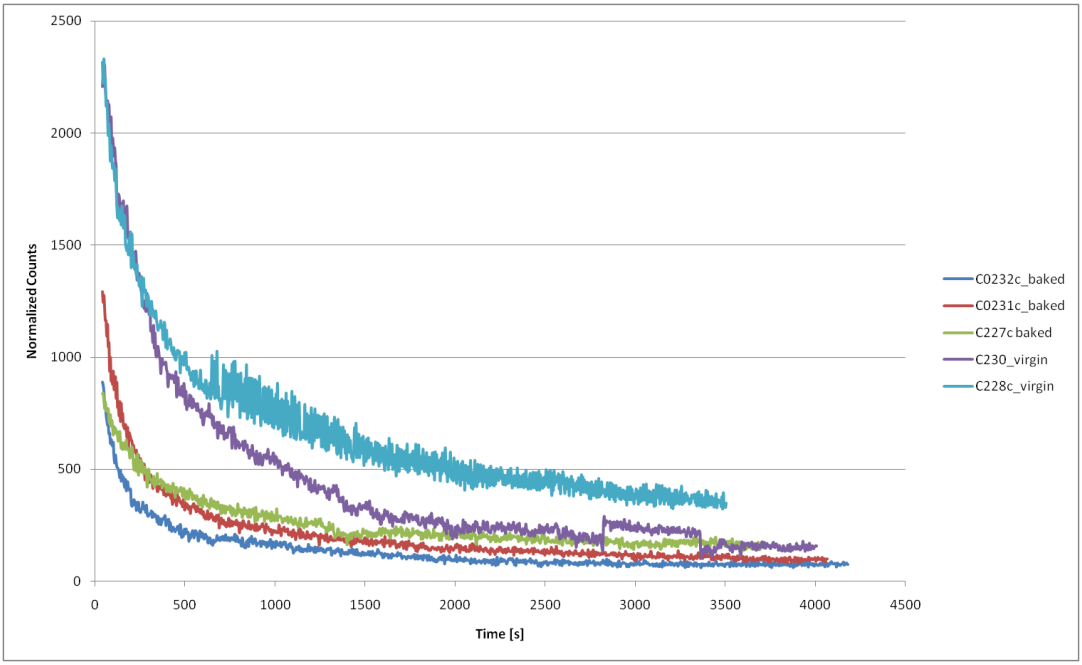

Figure 9.2.9: Comparison among normalized SIMS depth profiles of nitrogen as CN-, linear plot

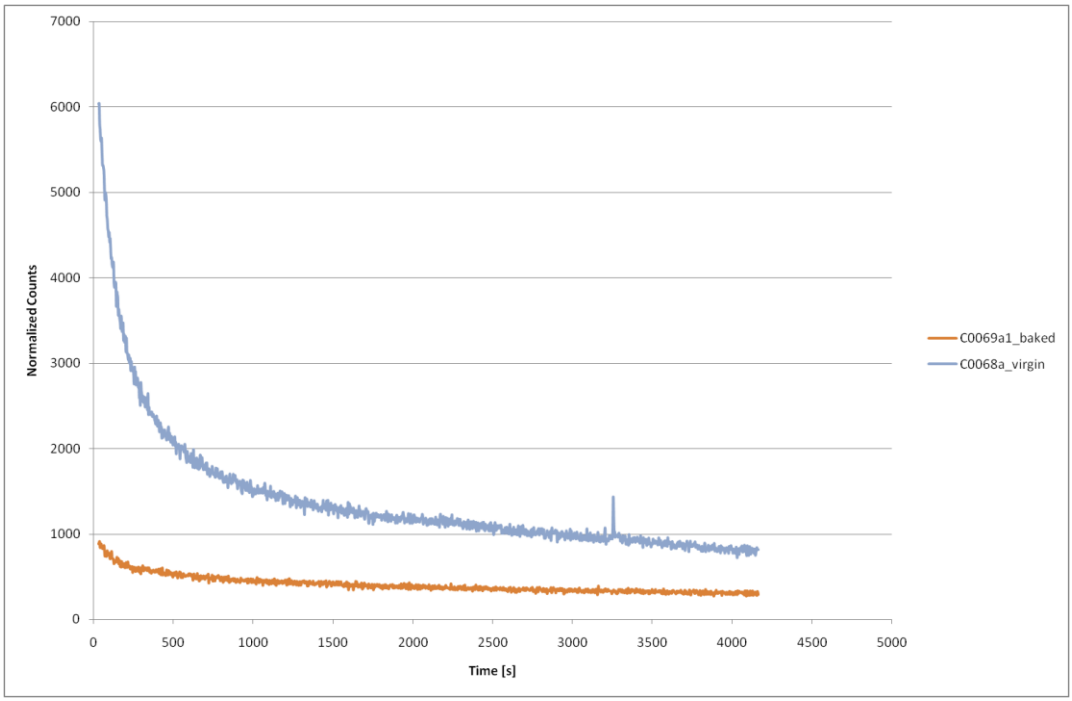

Figure 9.2.10: Comparison among normalized SIMS depth profiles of nitrogen as CN-, linear plot

Due to a strong variation in the background of the mass spectrometer, it was chosen to analyze separately the results obtained from the different measurements: figs. 9.2.9 shows the values obtained by the most recent analysis; fig. 9.2.10 shows the results of the first analysis.

By observing figs. 9.2.9-10 it can be noticed that all the performed measurements show a removal of nitrogen, more marked near the surface, after the thermal treatment. As

mentioned in chapters 3-4, nitrogen can originate from the raw materials, the manufacture process and the long exposure of the sample to ambient air.

Linking to previous experiments of Takahashi,[266] the results here presented are similar, but the lacking of a precise depth calibration cannot lead to precise results. However, to give a range of values, the high concentration of nitrogen near the sample surface is estimated to extend in depth between 300 nm and 1 μm. Since nitrogen is mainly concentrated on the surface of virgin AVR graphite, it is believed that after its neutron activation the C-14 distribution will be similar: considering that the range of a recoiled C-14 after its generation is at maximum in the order of the micrometer, the above mentioned hypothesis seems to be validated. A first experimental confirmation of that has been obtained by some experiments of Dr. Vulpius,[267] shown in fig. 9.2.11.

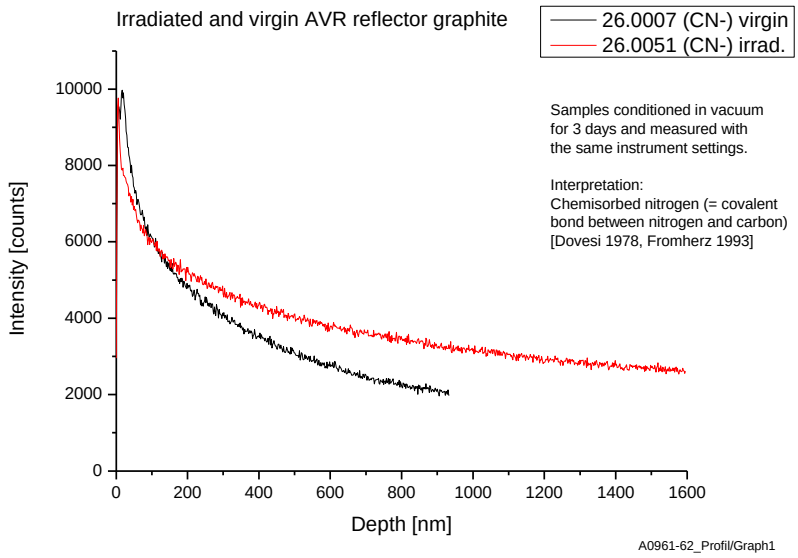

Figure 9.2.11: Comparison among SIMS depth profiles of CN- of virgin and irradiated AVR graphite

If C-14 shows a similar depth profile as N-14, considering that the thermal treatment has removed part of the superficial nitrogen, it is possible to have found an effective removal method. Considering previous works with thermal treatments,[268,269] it was hypothesized that C-14 was mainly concentrated on the sample surfaces and released by slight oxidation: this hypothesis seems to be confirmed by the present work. Indeed, looking at chapter 8.3, the on-line gaseous emissions showed a very marked CO_2 peak, likely correspondent to the mobile

[266] R. Takahashi, M. Toyahara, S. Maruki, H. Hueda, T. Yamamoto, "*Investigation of morphology and impurity of nuclear grade graphite, and leaching mechanism of carbon-14*", p.7
[267] Dr. Vulpius, Forschungzentrum Juelich
[268] T. Podruzhina, "*Graphite as radioactive waste: corrosion behaviour under final repository conditions and thermal treatment*", Juel 4166, 2004
[269] M. Florjan, "*Dekontamination von Nucleargraphit durch thermische Behandlung*", Juel-4322, 2009

part of graphite removed by a slight oxidation of the surfaces: that peak will be presumably one of the most important carriers of C-14 since it is released as first, so it is likely to come from the nitrogen (and successively C-14) enriched surfaces.

Another interesting result stands on the validation of a reasonable hypothesis assumed in chapter 4, i.e. the C-13 distribution is homogeneous: it revealed to be true for all specimens, with the exception of the first superficial layers (see fig. 9.2.12).

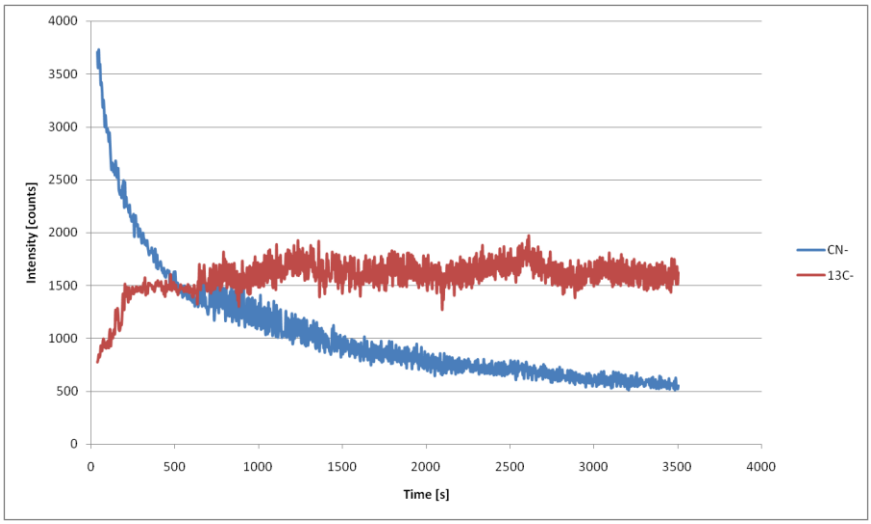

Figure 9.2.12: Comparison among SIMS depth profiles of CN- and ^{13}C- of virgin AVR graphite

Keeping in mind what has been discussed about the relation between C-14 and N-14, in the following the fractional removal factors will be calculated. Two different calculations are performed: the first one is related to the superficial removal, i.e. the first SIMS measurements are considered; the second one is related to the integral removal of nitrogen, considering the entire integral depth profile of every measurement. Indicative values are listed in table 9.2.2.

Sample	**Mean value on surface [counts]**	**Mean integral value [counts]**
Not treated	2300 (900)	1122704
Treated	1033 (250)	451356
Removed fraction	55%-72%	60%

Table 9.2.2: Fractional removal of nitrogen, superficial and integral, indicative values

However, in this case some values are really scattered, so it was decided to build a Gaussian curve from the data of all the experiments (see figs. 9.2.13-14). By considering only the second experiment, it result a mean integral fractional removal of 58%; taking into account also the first one, it results a mean of 60%. For what concerns the superficial values, strong differences were observed between the two experiments, so the relative values had been kept separately,

result in 72% and 55% respectively for the first and the second experiment. More experiments would be necessary to have a confirmation of such values.

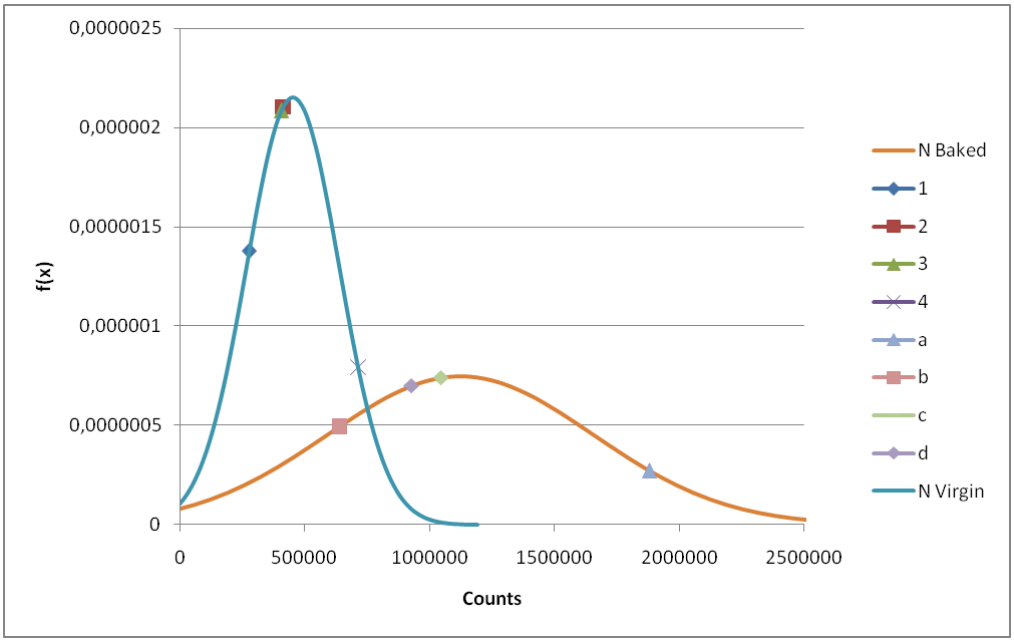

Figure 9.2.13: Gaussians distribution of the (nitrogen) whole available data from the two SIMS experiments

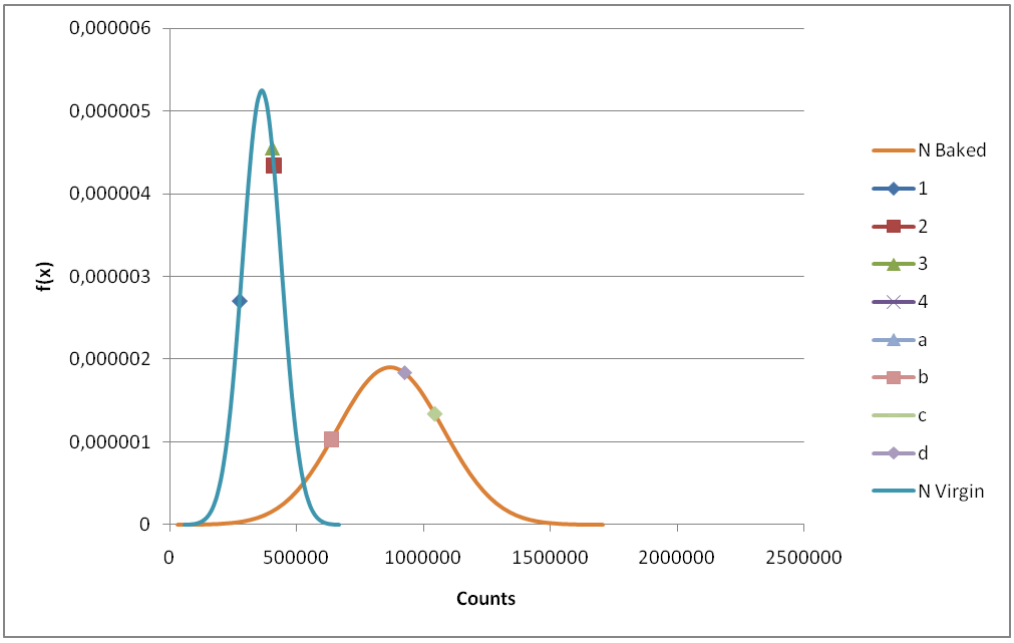

Figure 9.2.14: Gaussian distributions of the (nitrogen) results from the second SIMS experiment

A better comprehension on the thermal treatment effects can be evinced from the 3D profiles of nitrogen (figs. 9.2.15). In the virgin material, nitrogen is present both as hot spots, with a mean diameter of 10μm, and as a spread distribution over the surface, with an evident inhomogeneous character. Comparing the profiles before and after thermal treatment the removal effect is not very marked but, excluding the results from sample c0321, it can be

noticed a trend in the direction of a partial nitrogen removal, with lower removal efficiencies than the ones for chlorine.

In conclusion, a general removal of nitrogen occurs during the thermal treatment, with a removal factor in the order of 50%. Considering that the radiocarbon is concentrated the more on the surfaces, it can be stated that the treatment is efficient only for that fraction: a HTTT[270] under argon atmosphere can be used to improve the leaching behaviour by depleting the most mobile part of radiocarbon with a fractional removal up to some tens of percentage, as observed in previous experiments by Florjan.[271]

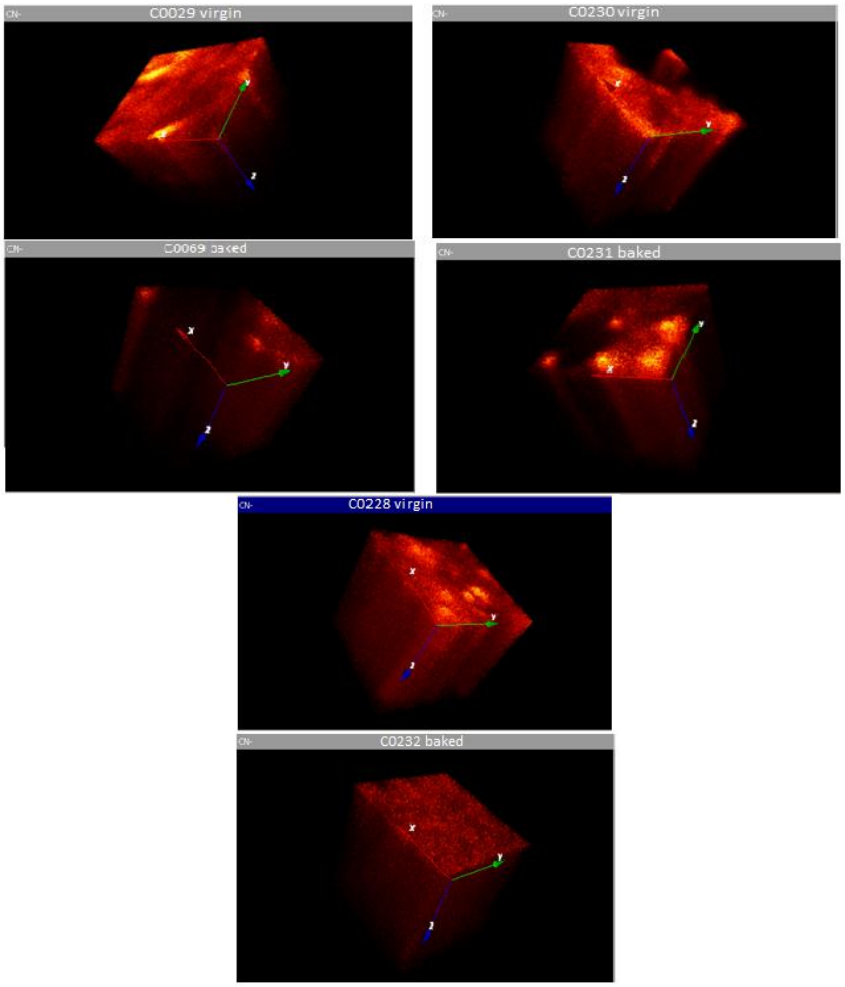

Figure 9.2.15: Comparison among SIMS 3D depth profiles of nitrogen as CN-, untreated (upper pictures) and treated (lower pictures)

[270] High Temperature Thermal Treatment

[271] M. Florjan, "*Dekontamination von Nucleargraphit durch thermische Behandlung*", Juel-4322, 2009

9.2.4 Oxygen before and after thermal treatment

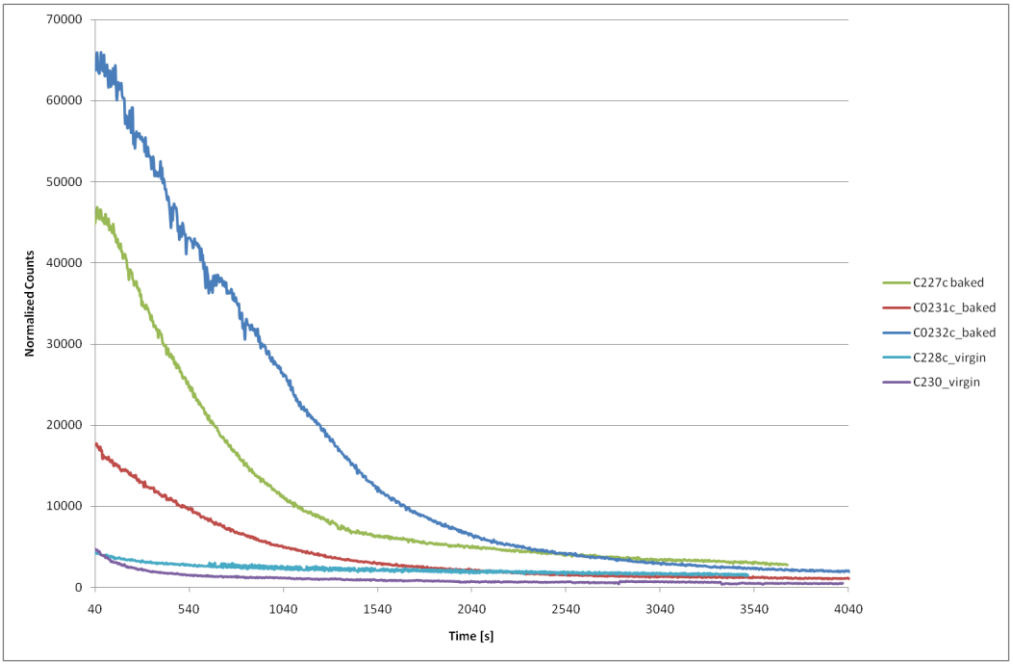

Figure 9.2.16: Comparison among normalized SIMS depth profiles of oxygen as O-, linear plot

All the measurements showed a high increase of the oxygen concentration after thermal treatment, in particular on the outer layers of the specimen (see fig. 9.2.16).

A hypothesis to explain that consists on a higher surface area after the treatment: the higher the available surface, the more the adsorbed (chemisorbed) oxygen. Indeed, looking at SEM images[272], taken before and after thermal treatment, one can observe real structure changes, with partial exfoliation of the graphite layers or even disappearance of some graphitic structures. If this was the case, one should expect, in line of principle, an increase in the amount of the adsorbed nitrogen, coming from air; this is not the case. It is necessary to investigate the more on the oxygen and nitrogen bonds and adsorption/desorption mechanism to come to a conclusion.

Another hypothesis, linked to the origin of such oxygen increase, could be related with the boundary conditions during the thermal treatment (see section 8.4.1): through the usage of a mass spectrometer it was discovered a considerable amount of water from an external source; at high temperatures (1300 °C), the established regime is the "mass transfer" one, so all the reactions are taking place at the sample surface. Following these considerations, it is expected to find higher amounts of oxygen after the thermal treatment, since a fraction of the oxidized graphite is likely to be not removed from its structure at the end of the treatment: considering a Langmuir-Hinselwood reaction scheme, before being released to the gas phase the chemical

[272] See section 11.2

species react on the surface, but a decrease in the temperature could freeze the release, resulting in higher amounts of graphite oxide found on the surface. So the water-presence explanation seems to be the more reasonable.

An analysis of the 3D profiles (fig. 9.2.17) reveals again a very marked increase of oxygen, mainly near the surface.

Considering virgin graphite, oxygen was found to be present as a superimposition of hot spots (identified as impurities) and a spread distribution over the surface (most probably chemisorbed oxygen, present in slightly higher amounts on surface). This leads to the conclusion that oxygen is already present inside the graphite, and even though its amount is limited, it is likely to be one of the responsible for graphite oxidation and species removal under inert atmosphere. In particular, it is believed that the embedded oxygen (both sorbed on the micro or macro structure) is causing a slight oxidation of the graphite inner and outer surfaces, leading to a depletion of the surface-enriched radiocarbon. These conclusions are in accordance with all the experiments, performed in the past by Podruhzina and Florjan, showing a steep initial release of radiocarbon during thermal treatment under inert atmosphere. More in detail, a particular experiment of Florjan[273] consisted in several treatments on the same sample, under inert gas, with intermediate exposure to air: it was observed a steep release of radiocarbon during the first treatment steps, in decreasing values in every treatment but with similar emissions. It is possible that after the first treatment the small amount of chemisorbed oxygen on the surfaces was the responsible of the steep release. The conclusion that the radiocarbon release is not temperature dependent but is correlated with superficial oxidation of graphite surfaces seems to be validated.[274]

[273] See section 7.2 fig. 7.2.1
[274] See section 8.3 experiment AVR3T

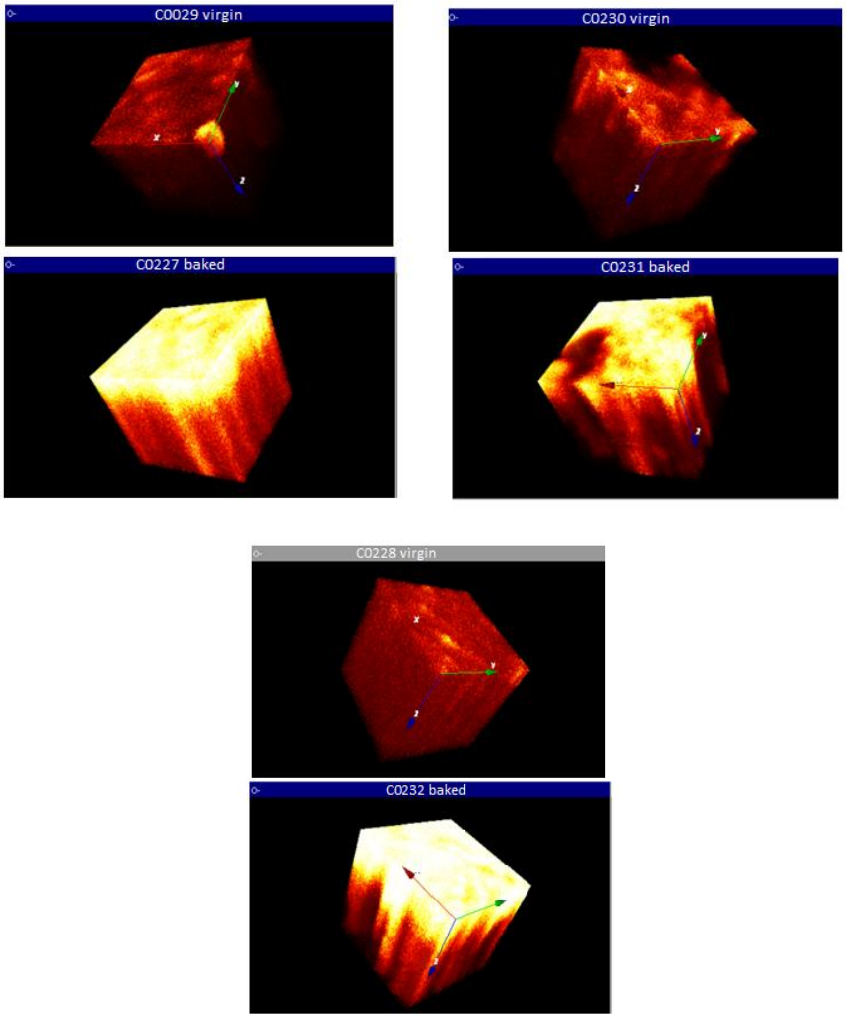

Figure 9.2.17: Comparison among 3D SIMS depth profiles of oxygen as O-, untreated (upper pictures) and treated (lower pictures)

9.2.5 Hydrogen before and after thermal treatment

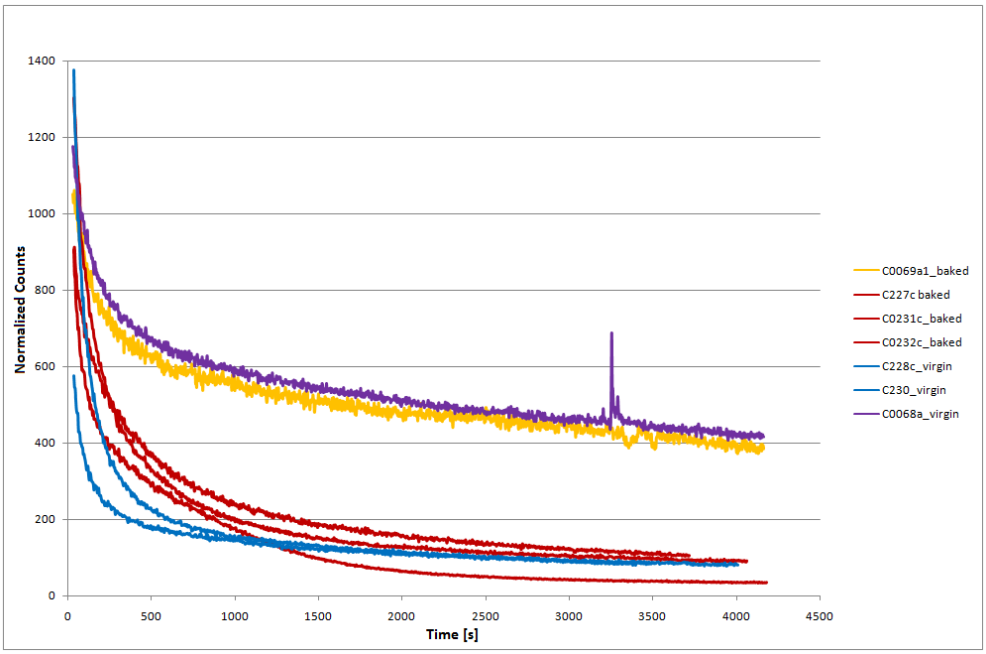

Figure 9.2.18: Comparison among normalized SIMS depth profiles of hydrogen as H-, linear plot

Because of the different background of the mass spectrometer between the first experiment and the second, the profiles comparison is kept separated. In particular, considering fig. 9.2.18, the first measurement provided the yellow and violet line while the second provided all the others: there is no significant difference among the profiles, considering the ones taken during the same experiment. This finding supports the reaction of graphite with water, since the generated hydrogen is released into the gas phase while the oxygen bonds the available carbon atoms. However, it is believed that small amounts of hydrogen are present as H- or OH- functional groups, but different analyses are necessary to measure them. As an example, a PGNAA (Prompt Gamma Nuclear Activation Analysis) showed 74 ppm_w of hydrogen present inside the graphite specimen.[275]

[275] Zsolt Révay, PGNAA, December 2010, Nuclear Research Department, Institute of Isotopes, HAS, Budapest, Konkoly-Thege Miklosutca 29-33. 1121 Hungary

9.2.6 Lithium Oxide before and after thermal treatment

Lithium oxide has been investigated too. However, the yield of LiO- is very low due to the usage of Cs+ as a primary ion beam in the SIMS analyses. Some information are anyway obtainable from the 3D depth profiles (fig 9.2.19). It can be noticed a nearly homogeneous distribution of LiO- in form of hot-spots. It seems that after the baking process the concentration is increased, but it is most likely due to the higher oxygen content, as showed before.

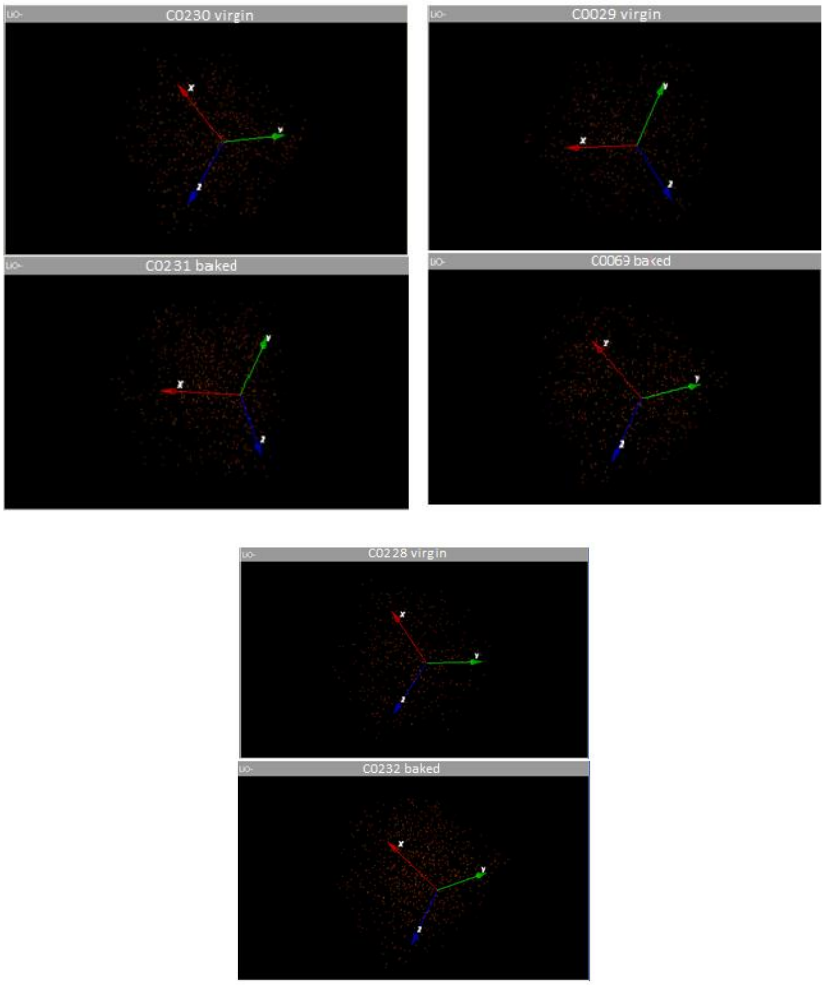

Figure 9.2.19: Comparison among 3D SIMS depth profiles of LiO-, untreated (upper pictures) and treated (lower pictures)

9.2.7 Calcium as CaO- and CCa- before and after thermal treatment

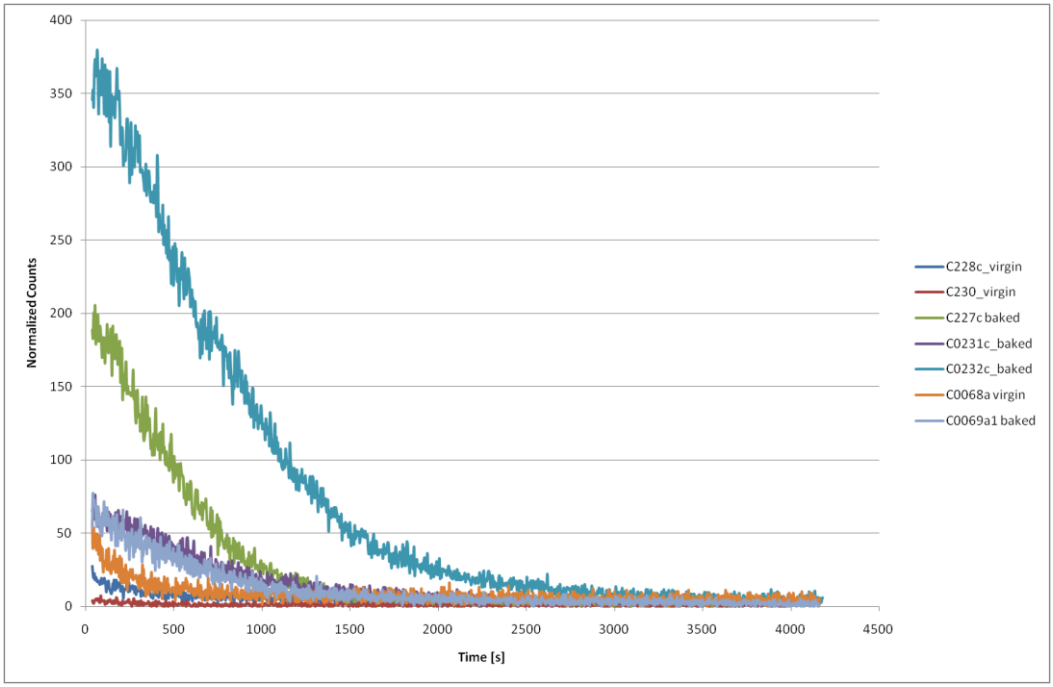

Figure 9.2.20: Comparison among normalized SIMS depth profiles of calcium as CaO-, linear plot

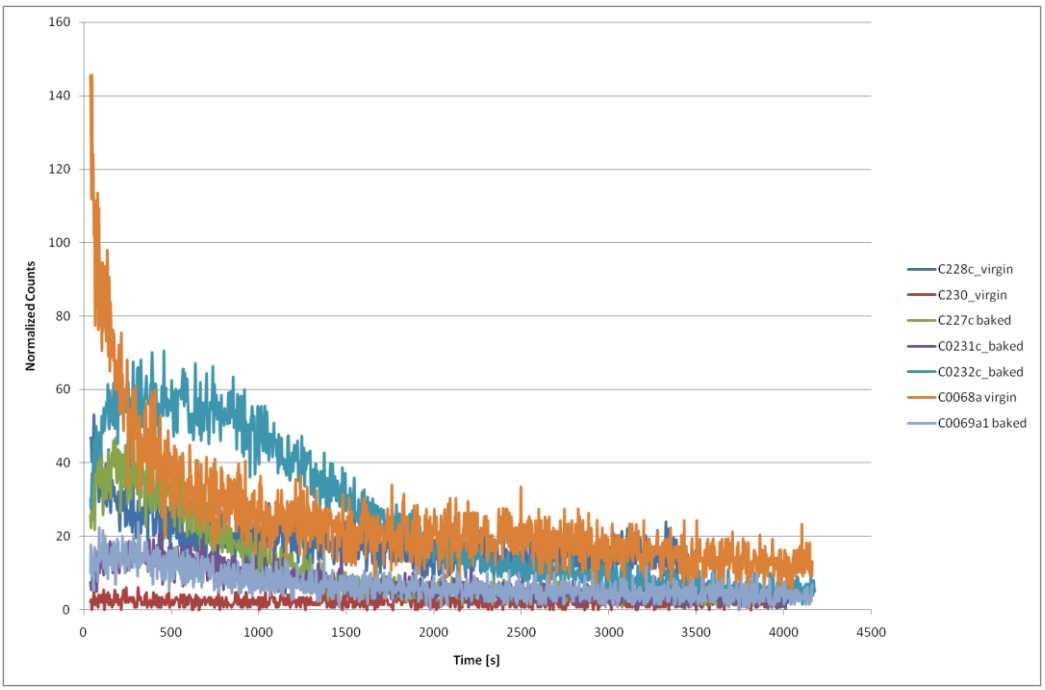

Figure 9.2.21: Comparison among normalized SIMS depth profiles of calcium as CaC-, linear plot

Previous SEM + XRF investigations [276] showed high concentration of Calcium, not homogenously distributed, on the thermally treated sample surfaces. Some crystallized calcium sulfate has been observed by SEM + XRF analysis also in the Al_2O_3 thermal shielding placed around the sample during the thermal treatment. Starting from that it was expected a

[276] See secion 11.2

similar result from SIMS analyses. Indeed, looking at fig. 9.2.20, it is clear that the concentration of CaO- on the sample surface increased due to the thermal treatment. Such increase shows different magnitudes because of the not homogeneousness of Calcium, but a general trend can be noticed. Differently, looking the CCa- profiles in fig. 9.2.21, the treatment effect is not very clear, since the differences are not significant as for CaO-. The reasons of that could be:

- Small differences are due to the not homogeneousness of the sample, so measured profiles are normally different in graphite: there is not a real thermal treatment effect for CCa-.
- As underlined by the SEM images of SIMS-interested areas, choosing the "white area"[277] for the baked sample was not possible because of the rough pointing equipment provided with SIMS, so even though there was a net effect on CCa- due to the thermal treatment it was not measured because of the chosen SIMS areas.

Elemental Calcium was observed in negligible amounts, most probably due to the fact that Cs+ was used as primary beam, which generally gives low yields of Calcium ions. More considerations about possible routes of calcium removal are reported in section 11.3.

Looking at the 3D profiles, the thermally treated graphite shows a general increase in the superficial concentration. Less clear are the results for CCa-. (see figs. 9.2.22-23).

In conclusion Calcium revealed to have migrated to the sample surface during the thermal treatment. Some SEM images confirmed this observation.

The removal of calcium was never observed before, so further analyses are necessary to confirm what has been observed here. Linking the discovery to the AVR i-graphite, it has to be reminded that Ca-41 is present in significant quantities (see chapter 4), even if much lower than C-14 or H-3. The present results could represent a step in the removal of radioactive calcium, for example by mechanically removal of the sample graphite surfaces, enriched of Calcium after the thermal treatment.

[277] Calcium was found to be spread over many inhomogeneous areas on the sample surface. Refer to SEM chapter for more details;

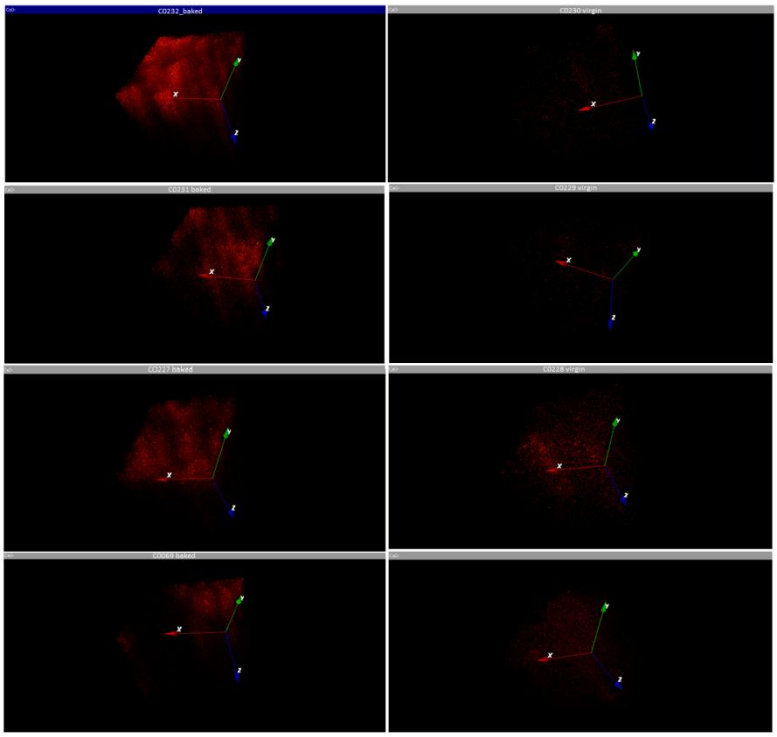

Figure 9.2.22: Comparison among 3D SIMS depth profiles of calcium as CaO-, after (left) and before (right) thermal treatment

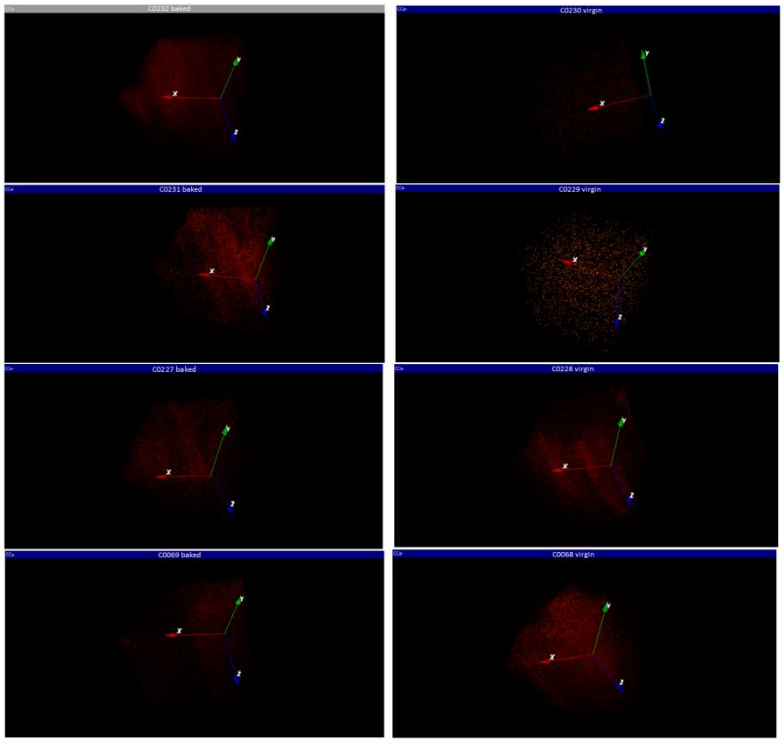

Figure 9.2.23: Comparison among 3D SIMS depth profiles of calcium as CCa- after (left) and before (right) thermal treatment

Conclusions for SIMS analyses

High temperature thermal treatments have shown a real influence on many impurities, evident for sulfur, chlorine, calcium and in a lower extent on nitrogen. Lithium Oxide was measured inside the graphite matrix in a nearly homogeneous distribution of hot spots. Sulfur and calcium diffused to the outside graphite surfaces because of the thermal treatment, while chlorine and nitrogen were removed, even though in different ratios. The reason for the very high oxygen concentration originates in the presence of the water-gas reaction at high temperatures. The finding here exposed are in agreement with what has been hypothesized in the past, in particular the C-14 distribution showed to be similar to the nitrogen one and its removal by slight oxidation of the porous structure of graphite can reasonably be correlated with the nitrogen removal.

10. XPS Analysis before and after thermal treatment

10.1 Generalities on X-Ray Photoelectron Spectroscopy

X-ray Photoelectron Spectroscopy (XPS), also known as Electron Spectroscopy for Chemical Analysis (ESCA), is used to determine quantitative atomic composition and chemistry. It is a surface analysis technique with a sampling volume that extends from the surface to a depth of approximately 5-10nanometers. XPS is an elemental analysis technique that is unique in providing chemical state information of the detected elements.

The sample is irradiated with mono-energetic X-rays (1.5 keV) causing photoelectrons to be emitted from the sample surface. An electron energy analyzer determines the photoelectrons' binding energies, which are characteristic of the elements within the sampling volume. From the binding energy and intensity of a photoelectron peak the elemental identity, chemical state, and quantity of an element are determined.

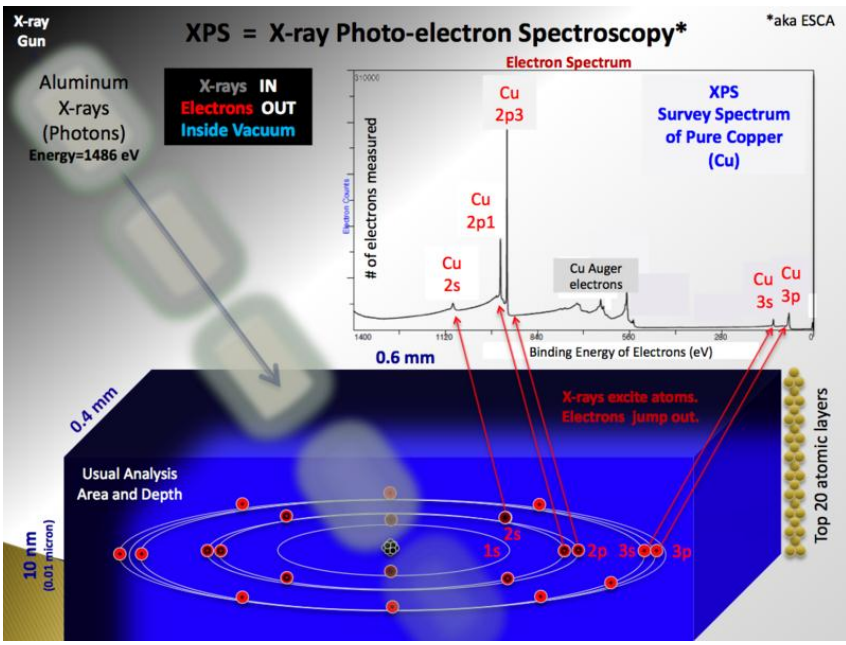

Figure 10.1.0: Schematic working principle of XPS

All elements are detectable except for H and He, due to the too small diameter of their orbital. Detection limits depend on element, for most of them they are in the 0.01-0.1 % at. range.

XPS instruments normally use a highly focused beam of monochromatic aluminum Kα X-rays (1486 eV). Ultra High Vacuum (UHV) is required to perform the analysis (pressure in the order of 10^{-9} mbar). The measured spot is about 800-1000 μm^2.

Because the energy of a X-ray with particular wavelength is known, the electron binding energy of each of the emitted electrons can be determined by using:

$$E_{binding}=E_{photon}-(E_{kinetic}+\phi)$$

where $E_{binding}$ is the binding energy (BE) of the electron, E_{photon} is the energy of the X-ray photons being used, $E_{kinetic}$ is the kinetic energy of the electron as measured by the instrument and ϕ is the work function.[278]

9.2 Results and Discussion

The investigated samples are the same used in the SIMS analyses (see chapter 9), one was untreated while the other went through a high temperature thermal treatment (see section 8.4.1). The XPS analyses have been chosen to have an ulterior confirmation of the results obtained by SIMS[279] and to look for the bindings of some elements in the superficial layers of the graphite sample, before and after the thermal treatment.

Two measurements for each sample were performed to compare repeatability and to take into account the non-homogeneous nature of the specimen: even by naked eyes it was possible to distinguish different zones on the sample's surface, so the first measurement was taken in a “light spot”, the second one in a “dark spot”. Indeed, many more measurements would be necessary to do statistical considerations: the reported values have to be considered only for a first approach. However, the results hereby presented could confirm or not some inferred observations resulting from previous experiments.

The investigated components in the XPS spectra were: C1s, N1s, S2p, Ca2p3, Na1s, O1s and Li1s.

---

[278] The work function is the minimum energy that must be given to an electron to liberate it from the surface of a particular substance. In the photoelectric effect, electron excitation is achieved by absorption of a photon. If the photon's energy is greater than the substance's work function, photoelectric emission occurs and the electron is liberated from the surface. Excess photon energy results in a liberated electron with non-zero kinetic energy. The photoelectric work function is $\Phi=h\ f_0$ where h is Planck's constant and f_0 is the minimum (threshold) frequency of the photon required to produce photoelectric emission.

[279] It has to be reminded that XPS is related only to the very first nanometers of the sample, while SIMS interested the first micrometers;

The following elements have been excluded after the interpretation of the electronic spectra: CaO, $CaCO_3$, Na_2CO_3, $Na_2C_2O_4$, NaN_3, CN_2, Na_2O, Cl, S, Li. Moreover O-H bond (normally measured between 531 and 532 eV) were not detected.
The obtained spectra were interpreted and the possible chemical bondings and relative bonding energies were identified via software through a deconvolution of the individual peaks into Gaussian fits. All the percentages were calculated at FWHM, taking as a reference the peak C1s. It was necessary, however, to shift the spectra to fit with reference values of about 0.28 eV.

Analyzing the C1s spectra, it results that each one consists of one major peak centered near 284.7 eV with an asymmetry on the high binding energy side, indicating the presence of carbon atoms with three different binding energies. Due to the availability of a dedicated software it was possible to decompose the spectra, obtaining two well defined peaks (centered respectively near 284.7 eV and 285 eV) and a very small/broaden one (not considered).

The most abundant element is, of course carbon, mainly present as C-C (sp^2 hybridized) and in a minor part as C-C (sp^3 hybridized), with slightly different values between the two measured spots. The broadening of the sp^2 peak is presumably related to the not perfect lattice, possibly distorted by vacancies or deformations also due to the presence of interstitials atoms. C-O is present in the range of 3%, nearly double than a typical graphite of reference. From the analysis of the N1s spectra it was found that low amounts of nitrogen are present in the graphite surface; however, the values are close to the limit detection of the analyser, so 700 ppm are reported but the uncertainty on this value is high. In the first measurement ("AVR#0 light spot") it was possible to identify a peak of sodium,[280] but it was not possible to assign a certain bonding. Probably the sodium is present as hot spot together with other impurities. Concerning the O1s spectra of the untreated sample ("AVR square 0"): it was possible to identify a peak around 532.9 eV, after having slightly shifted the spectra. The assigned bonding resulted in an ether structure C-O-C.
A summary of the calculated values and assigned bonding are reported in table 10.1 (the unassigned peaks are denoted with "*").

[280] Sodium was also detected in a former PGNAA analysis with a mass fraction of 64 ppm.

AVR#0 light spot

Element	Peakname	EB/eV	Konz./At.-%	Elementkonz./At.-%
C	C-C sp2	284,7	83,27	97,75
	C-C sp3	285,0	11,94	
	C-O	286,2	2,54	
N	N*	399,7	0,07	0,07
Na	Na*	1072,4	0,04	0,04
O	C-O-C	532,9	2,13	2,13

AVR#0 dark spot

Element	Peakname	EB/eV	Konz./At.-%	Elementkonz./At.-%
C	C-C sp2	284,6	81,57	97,87
	C-C sp3	285,0	13,25	
	C-O	286,1	3,05	
N	N*	399,2	0,07	0,07
O	C-O-C	532,9	2,06	2,06

Table 10.1: Results from XPS analysis of untreated AVR graphite sample

Concerning the treated sample, the results are reported in table 10.2.

AVR#1 light spot

Element	Peakname	EB/eV	Konz./At.-%	Elementkonz./At.-%
C	C-C sp2	284,7	78,36	97,28
	C-C sp3	285,0	11,83	
	C-O	286,0	7,09	
O		532,4	1,10	2,72
	C-O-C	533,7	0,92	
	O*	535,6	0,29	
		537,7	0,41	

AVR#1 dark spot

Element	Peakname	EB/eV	Konz./At.-%	Elementkonz./At.-%
C	C-C sp2	284,6	76,37	92,43
	C-C sp3	285,0	8,87	
	C-O	285,9	7,19	
Ca	Ca*	348,7	1,31	2,39
		353,6	1,08	
O		532,1	0,81	5,19
	C-O-C	533,4	2,94	
	O*	536,4	0,46	
		538,3	0,98	

Table 10.2: Results from XPS analysis of an thermal-treated AVR graphite sample

Without going too deep in detail in the description of the calculated values for the treated sample, a comparison with the former analysis is performed. The results obtained before and after the treatment (tabs. 10.1-2) show marked variation of the relative concentrations. In particular, for what concerns the C-C sp^2-bond it was measured a decrease of 4-6%, leading to the conclusion that a less ordered superficial structure has been created. An important difference can be seen also in the C-O values, increased of about 4%, together with the appearance of C-O-C ether structures in the order of 1%. The total oxygen concentration increased up to 5% (it was 2% in the virgin sample), comprehensive of some not identified bonding.

The nitrogen peak, already small in the previous measurement, disappeared completely, or at least has become smaller than the detection limit of the equipment.

An important observable peak reveals the presence of calcium, but it was not possible assigning it a specific bonding. The fact that calcium has been measured only in one spot can lead to think that it is not homogeneous on the surface, but more investigations would be necessary. However, linking to SEM measurements (see chapter 11), this assumption seems to be confirmed.

The interpretation of the results did not allow identifying the bonding of nitrogen and calcium. This is due to the fact that electron bonding energies are very close to each other. For what concerns nitrogen, the small amount has increased the difficulties in the interpretation, since a not very pronounced peak was measured (especially in the dark spot). In the virgin sample it was measured 399.7eV (light spot) and 399.2eV (dark spot): the latter value is particularly uncertain due to the very broad peak, so it is not considered here. The other value does not allow a precise assignment, but considering that the C-N bond has a bonding energy of about 399.4 eV it can be excluded. Reference bonding energies for C=N and C≡N are respectively 399.8 eV and 399.6 eV, so it is possible that nitrogen is present as a combination of these two bonding. However, it has to be underlined that high uncertainties are affecting these results, so more precise investigations are needed to obtain clearer results.

It can be found, anyway, a parallelism with the results obtained with other analysis, for example with SIMS (chapter 9). For what concerns the untreated specimens, the presence of bonded oxygen is confirmed (as C-O and C-O-C), at least for the first nanometers of the sample. This fact could be explained in three ways:

- Oxygen and nitrogen are already embedded in graphite, due to the manufacture process;
- Oxygen and nitrogen are coming from the sample preparation procedure: the examined specimens were prepared by dry cutting, experiencing so high local temperatures, especially on the surface; being such preparation a sort of treatment in air, it is possible that the specimen has been influenced, revealing during the analysis higher concentrations of oxygen and nitrogen than the ones originally present in the graphite;
- Oxygen and nitrogen come from the prolonged exposure of the sample to the ambient air;

Considering PGNAA analysis, the nitrogen content in graphite was about 120 ppm,[281] but that measurement was referred to the total specimen without considering an eventual inhomogeneous distribution in the porous matrix. Takahashi[282] reported that nitrogen is concentrated the more in the superficial layers, confirmed also by the SIMS analysis (Chapter 9).

Regarding the results of thermal treatment at high temperatures in argon (with low amounts of water), it was noticed in SIMS a strong increase in the oxygen superficial concentration and, on the other side, a partial removal of nitrogen from the surface, results confirmed also from the presented XPS results, even though in a less precise way. Taking into account these considerations, it can be stated that:

- It is not possible to exclude the fact that nitrogen is coming from the sample preparation in air, but it can be affirmed that the thermal treatment has succeeded on its partial removal, at least from the superficial layers of the graphite;
- It is not possible to exclude that nitrogen originates from the sample exposure to ambient air: on the contrary, following former experiences and observations,[283] a long time exposure to air is likely to cause chemisorption of many gases on the graphite surfaces;
- It is possible that nitrogen, at last, originated also during the cooling down step of the graphite manufacture

In conclusion, further studies are necessary to better understand the nitrogen bonding with the graphite.

---

[281] Mole fractions from Zsolt Révay, PGNAA December 2010, Nuclear Research Department, Institute of Isotopes, HAS, Budapest, Konkoly-Thege Miklosutca 29-33. 1121 Hungary

[282] R. Takahashi, M. Toyahara, S. Maruki, H. Hueda, T. Yamamoto, "*Investigation of morphology and impurity of nuclear grade graphite, and leaching mechanism of carbon-14*", p.7

[283] M. Okada, T. Sogabe, "*Behaviour of gas desorption and gas permeability of carbon materials*",

Concerning oxygen, after the thermal treatment it was measured a consistent increase on the surface concentration. In particular the already present C-O-C ether structure did not increased but, on the other side, appeared C-O-C epoxy structure together with unknown bonded oxygen. This fact is confirmed by SIMS analysis and by the thermal treatment boundary conditions: in particular the reaction of graphite with water is believed to be the responsible of what has been observed. An interesting fact is that some measurements on AVR fuel pebble graphite showed the presence of COC epoxy structure with the same order of magnitude without being thermally treated; after the exposure to neutron radiation an increase of such structure was observed, in concomitance with a depletion of C-C sp^2. It can be interpreted in the way that the neutron radiation is damaging the graphite structure, creating so a less ordered lattice with many defects and increasing the number of active sites able to bond oxygen and other gases. On the other hand, the neutron irradiation could induce high local temperatures and implant the already superficially-adsorbed gases.

In conclusion, XPS analyses have confirmed the effective removal of nitrogen after the thermal treatment, even if the uncertainties were high; the presence of bonded oxygen on the surface has been proven, with a consistent increase as a consequence of the treatment conditions; some impurities as calcium were detected after the thermal treatment, supporting the findings of SIMS analyses.

More investigations are necessary, however, to better understand the bonding of some elements as calcium and nitrogen.

11. Scanning Electron Microscope Investigations

11.1 Generalities on Scanning Electron Microscopy

The scanning electron microscopy produces high quality and highly magnified images by scanning the sample with an electron beam based on raster scanning. The signals produced are various: backscatter electrons, secondary electrons, characteristic X-Rays and visible light. Secondary electrons and backscatter electrons are commonly used for imaging samples: secondary electrons are most valuable for showing morphology of the samples, since they originate within the first nanometers from the sample surface; backscatter electrons are most valuable for illustrating contrasts since they are reflected for elastic scatter out of the specimen. Due to the fact that heavier elements reflect more electrons than the lighter ones, they appear brighter in the resulting image. Characteristic X-rays are generated when an energetic beam of electrons interacts with the inner shell electrons by inelastic scattering with enough energy to excite inner shell electrons to outer shell orbitals, leaving inner-shell vacancies. As outer-shell electrons fall to the various inner shell orbitals, characteristic amounts of energy are generated as a function of the target element and the type of orbital decay. The X-rays are used in the X-Ray Fluorescence Spectroscopy, to perform elemental analyses.

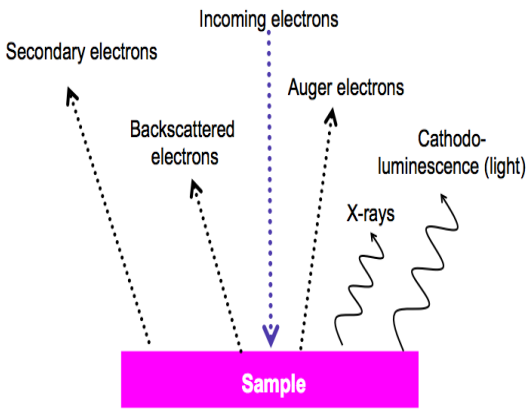

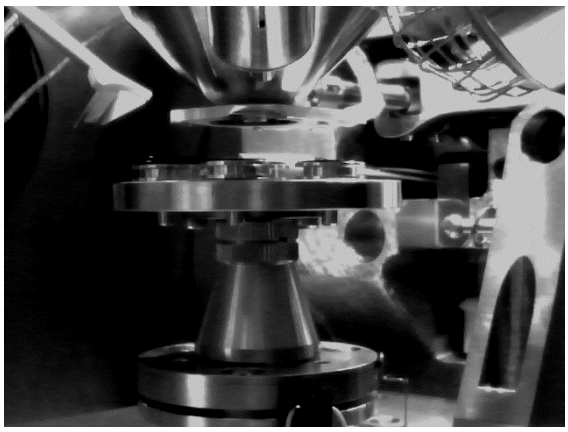

Figure 11.1.0: Scheme of the different signals produced in a SEM (left) and inner view of the SEM installed at FZJ (right)

11.2 Investigations on the superficial morphology of AVR graphite, before and after a thermal treatment

The purpose of the analyses here exposed was to investigate the effect of high temperature thermal treatments on the graphite structure change and on the possible migration of some impurities from the bulk graphite to the surface.

The first specimen which is going to be presented has been treated in the experiment "AVR square 1", discussed in section 8.4.1. The maximum temperature was 1300 °C and the treatment lasted 6 hours, under argon and small amounts of water vapour. In figs. 11.2.1a-b is reported an overview of the sample surface, at a magnification of 300x-1200x: it can be noticed the inhomogeneous nature in addition to the presence of small white spots (impurities). After the treatment the surface revealed consistent differences (see figs. 11.2.2-4): even at relatively low magnification it is possible to observe a massive appearance of impurities over the sample's surface. To be more precise, not all the surface was covered by superficial impurities but macroscopic white areas were observable nearly with naked eye. At higher magnifications (2400x) it is possible to see a needle-like form of the impurities. Taking advantage of the EDXRF (Energy Dispersive X-Ray Fluorescence analysis) provided with the SEM equipment, several points were measured in order to identify the nature of the impurities: they revealed to be mostly calcium, together with smaller amounts of oxygen and, at last, sulphur. The emission of sulphur was already observed in gaseous form during the experiments with the induction oven (see section 8.3) and it was measured in high concentrations near the graphite surface by SIMS (see chapter 9). Considering calcium, it was found with SIMS analyses too, but its chemical form seemed to be mainly correlated with oxygen more than with carbon. The present results confirm that observation (see fig. 11.2.5). From the point of view of impurities removal, it has been proven then a sulphur and calcium migration from the bulk graphite to the surface. Moreover, sulphur showed to be removed by oxidation and measured in the gaseous phase, but calcium is likely to stay on the graphite surface or in the vicinity of the sample. Further investigations on the sample holder have been performed in order to understand whether calcium was removed from the surface: the melting point of calcium is about 842 °C, so it is possible that, because of the gravity, it was partially removed from the sample. This will be discussed in section 11.3.

Because of the consistent amount of impurities on the treated graphite surface, an evaluation of the superficial structure was not possible. It was decided then to perform further investigations on samples treated for shorter time at high temperatures: the choice

fell on the specimens designated for the "AVR Heat Step 02", treatment performed under argon (with involuntary small amounts of water) for about 42 hours with temperature steps of 100 °C, each hold for 3 hours up to 1300 °C. The shorter exposure of the sample to high temperature was hypothesized to have removed lower quantities of calcium (among the other impurities), in order to perform a better comparison. In addition, it was thought to investigate the very same spot before and after thermal treatment, in the way to have a clearer view of the treatment effects.

In figs. 11.2.6-7 are reported images respectively before and after the thermal treatment. As hypothesized, the impurities migrated to the surface are in lower amounts. In addition, some structural changes are observable. For a better comparison higher magnification images are reported in figs. 11.2.8-9. At a magnification of 12000x a layer destruction after the treatment is notable: some structures are completely disappeared while stacked planes seem to be exfoliated. These structural changes are due to the reactions occurring at high temperatures, both due to external oxidants and to embedded ones.

For a better understanding of the treatment effects under considerable oxidizing gases see figs. 1.12.10-11: the graphite reported here is a different grade one (DIDO), treated under argon with about 1000 ppm of oxygen. An enhanced structural change is observable, in the same way as it was observed before but more marked in this case.

In conclusion, temperature and oxidants have a significant impact on the graphite surface and on the impurities removal, so an optimization of the treatment parameters and a precise control of the gases have to be considered in order to develop an industrial purification process.

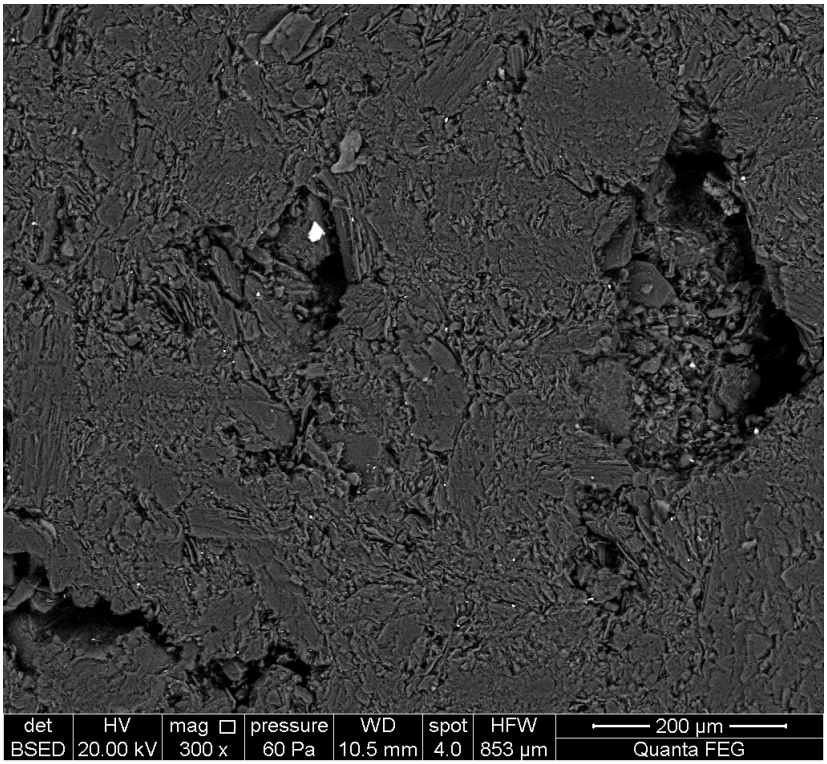

Figure 11.2.1a: Overview of AVR graphite surface, untreated, magnification 300x

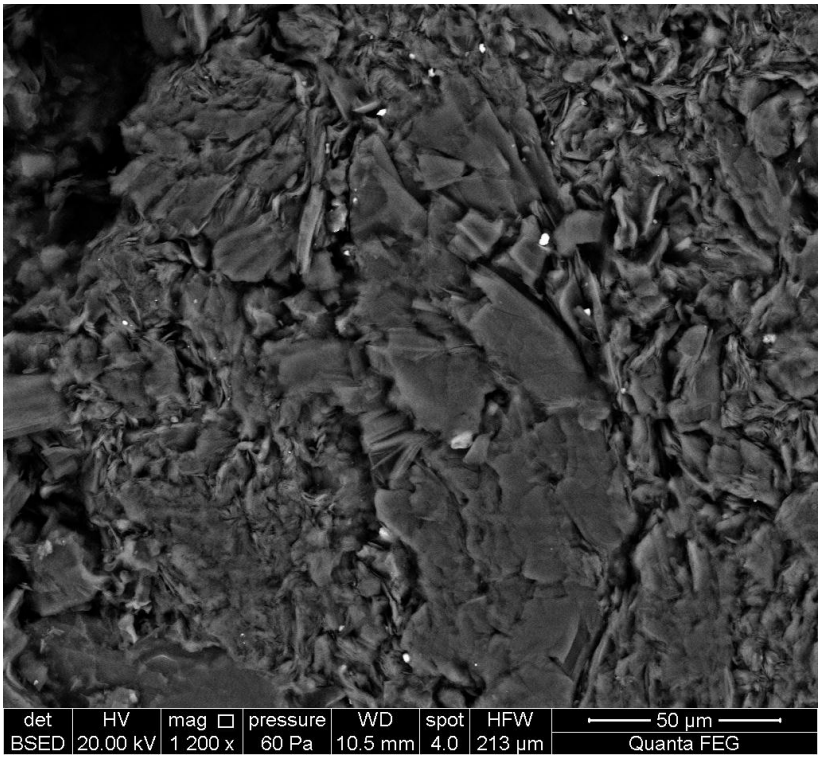

Figure 11.2.1b: Overview of AVR graphite surface, untreated, magnification 1200x

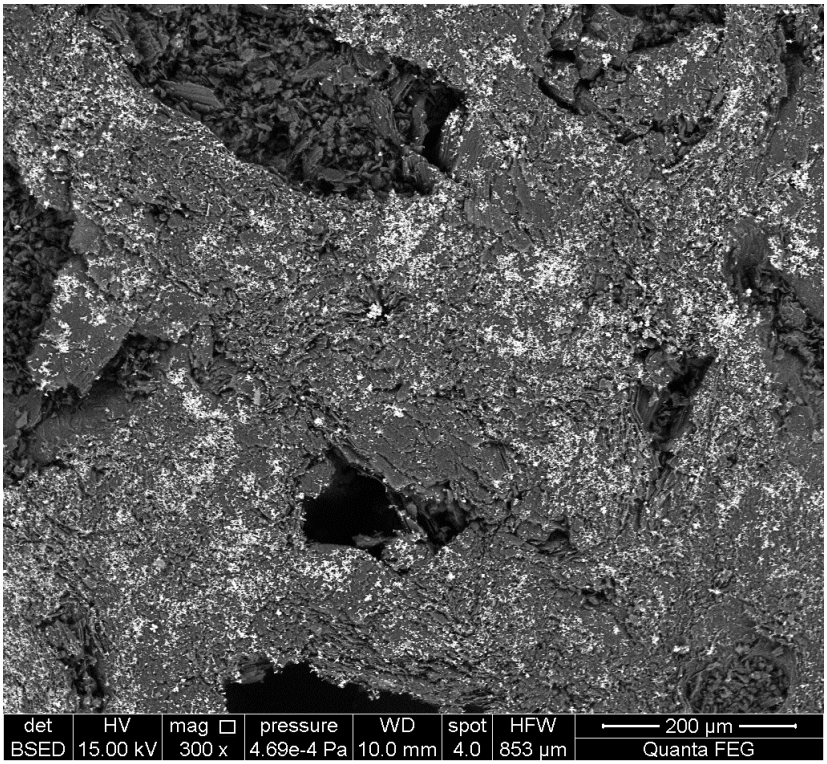

Figure 11.2.2: Overview of AVR graphite surface, treated in experiment "AVR square 1", mag. 300x

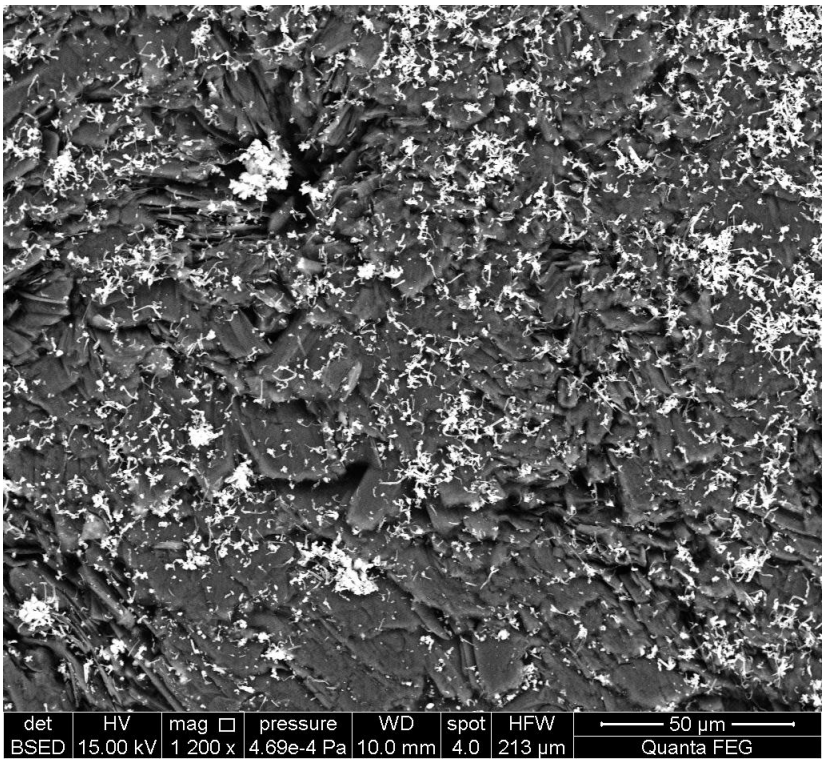

Figure 11.2.3: Overview of AVR graphite surface, treated in experiment "AVR square 1", mag. 1200x

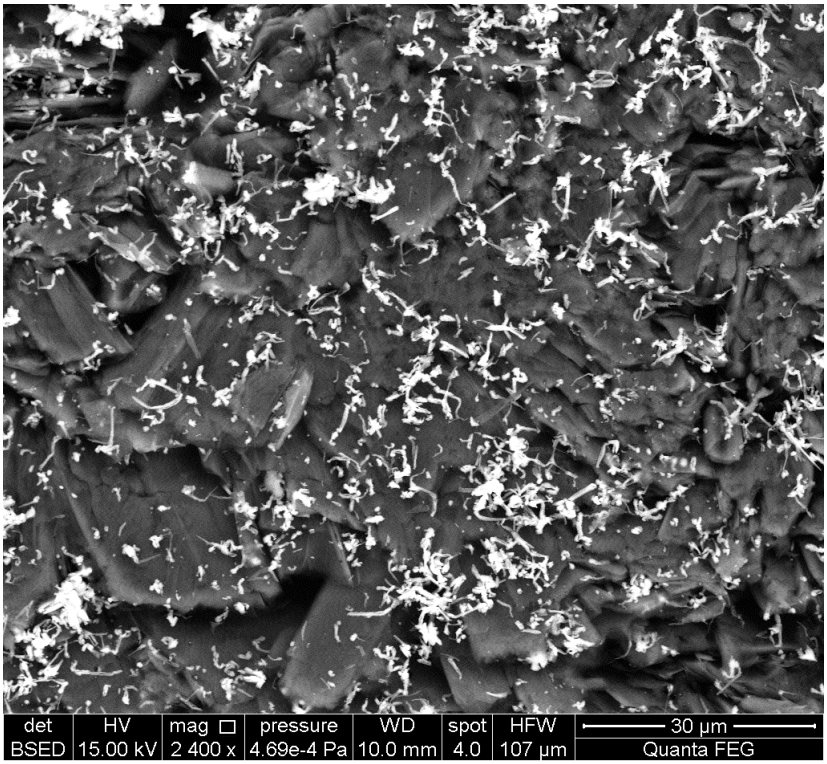

Figure 11.2.4: Overview of AVR graphite surface, treated in experiment "AVR square 1", mag. 2400x

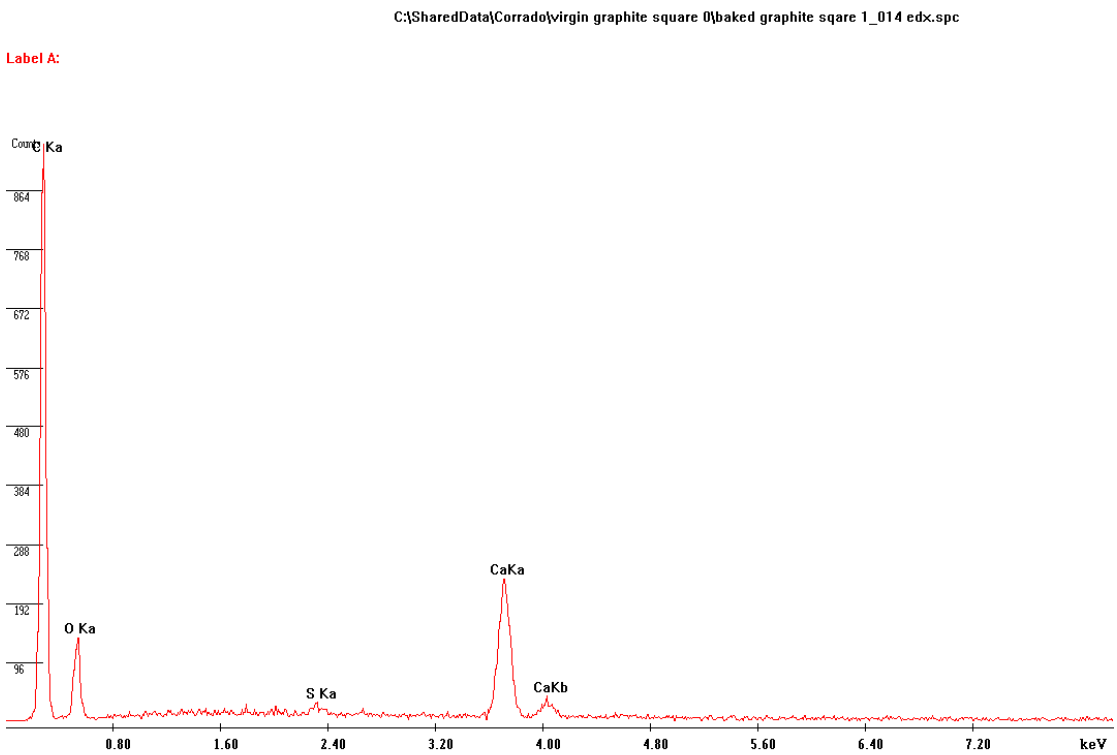

Figure 11.2.5: Exemplary EDXRF spectra performed with the sample "AVR square 1"

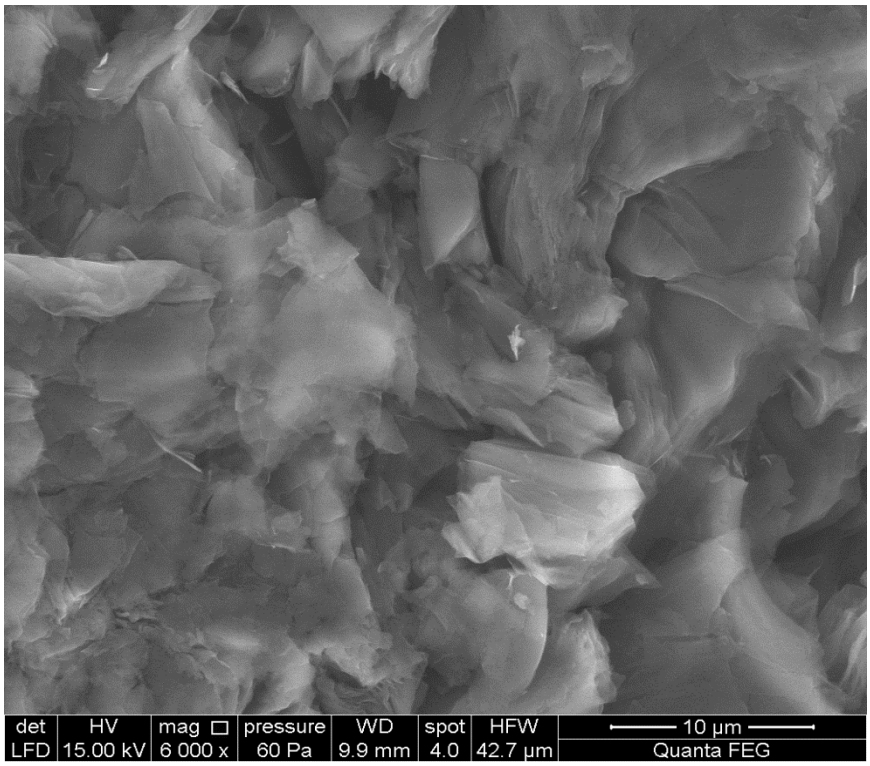

Figure 11.2.6: Overview of "AVR heat step 2" graphite surface, untreated,mag.6000x

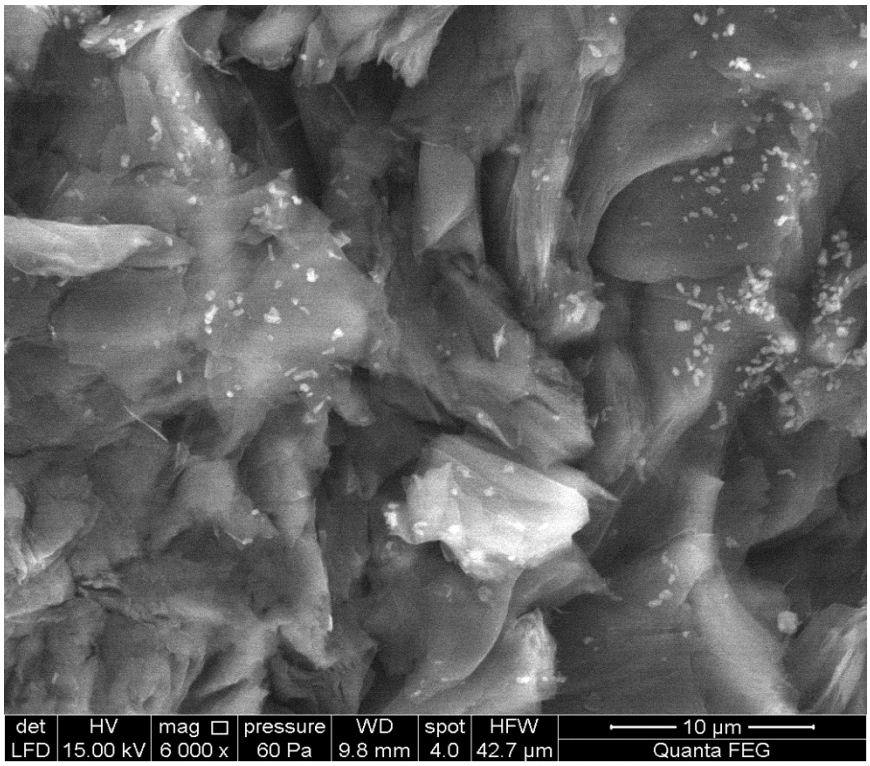

Figure 11.2.7: Overview of AVR graphite surface, treated in experiment "AVR heat step 2",mag.6000x

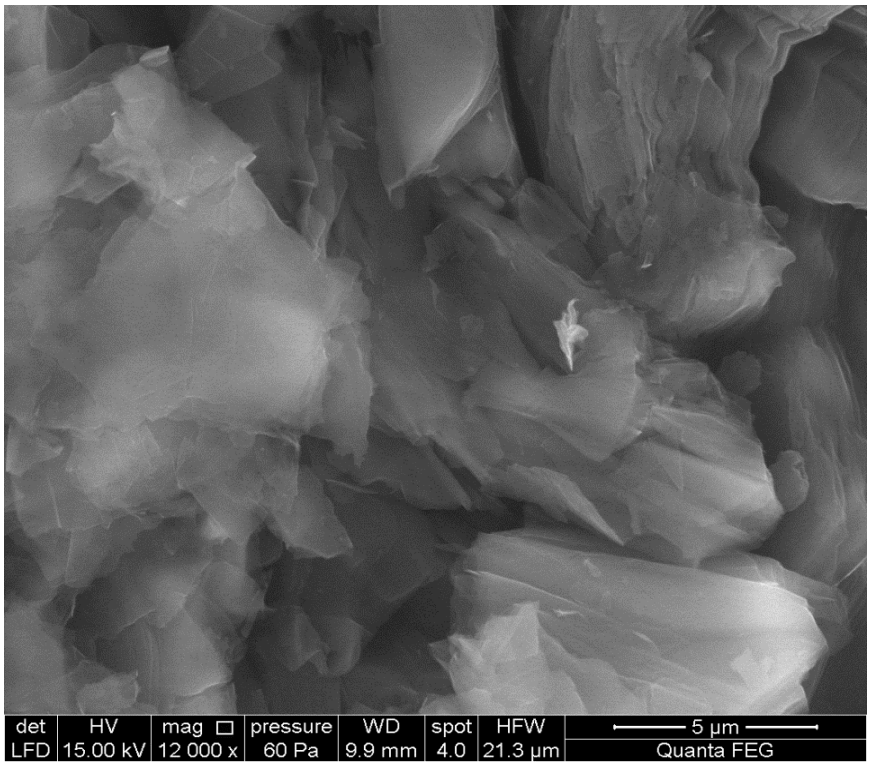

Figure 11.2.8: Overview of AVR "heat step 2" graphite surface, untreated, mag.12000x

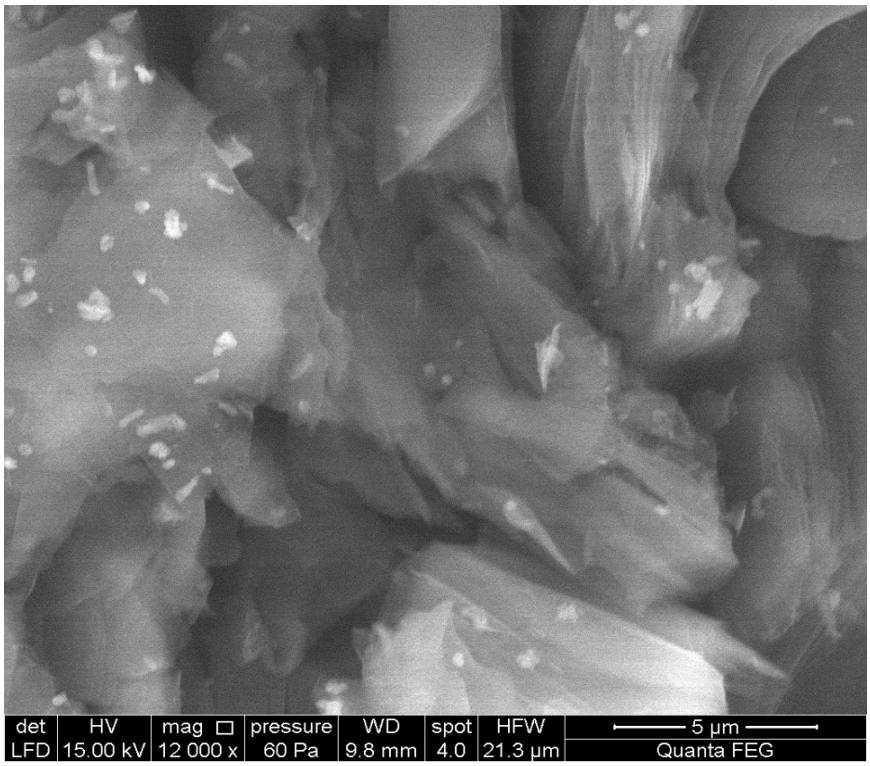

Figure 11.2.9: Overview of AVR graphite surface, treated in experiment "AVR heat step 2",mag. 12000x

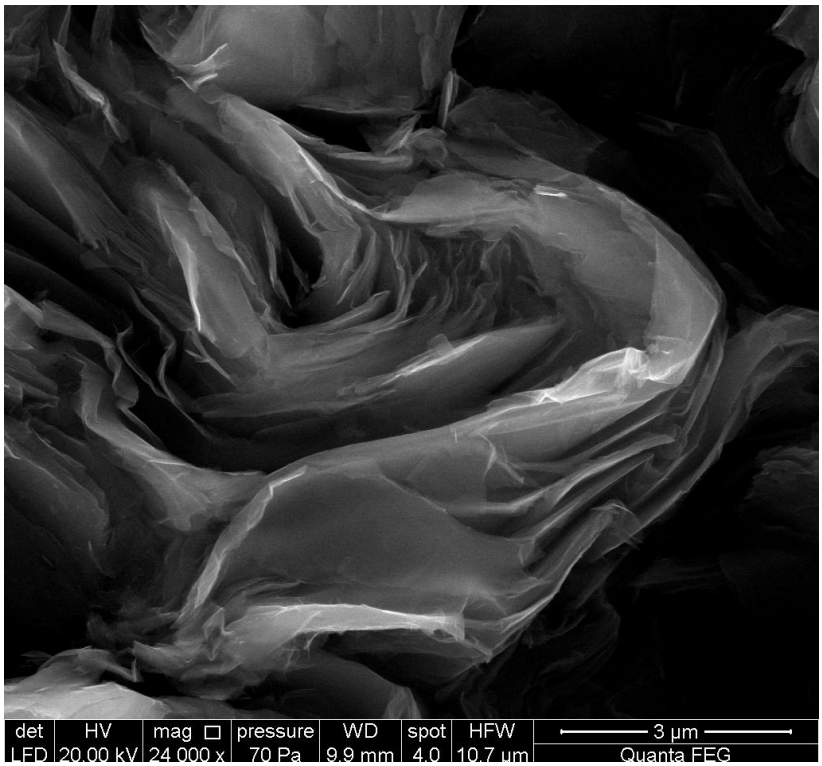

Figure 11.2.10: Overview of DIDO graphite surface, untreated, mag. 24000x

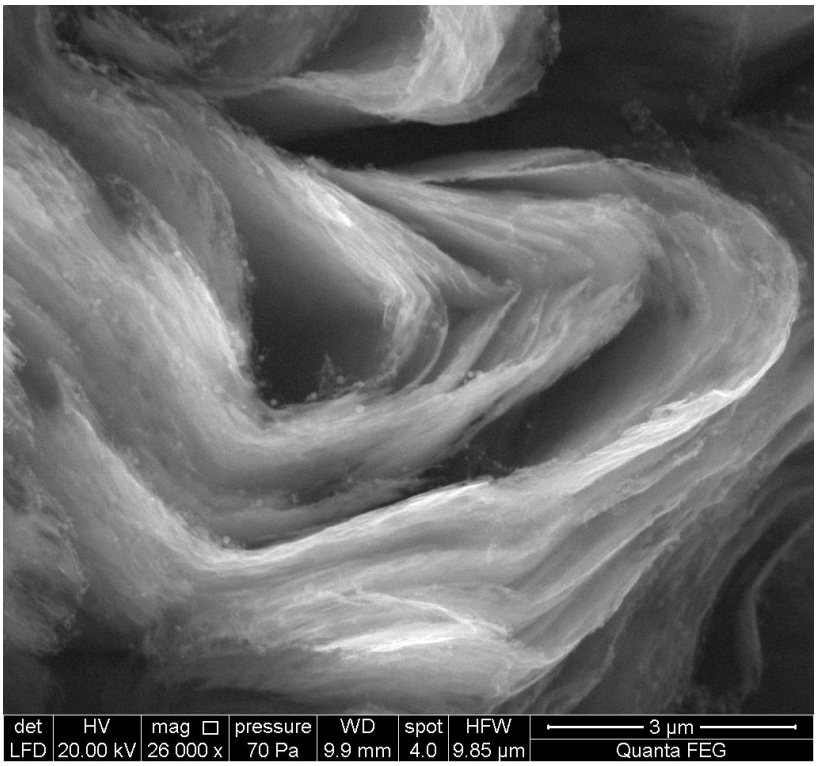

Figure 11.2.11: Overview of DIDO graphite surface, treated at high temperature,mag. 26000x

11.3 Investigations on the sample holder

Calcium was found on the sample's surface after thermal treatment in amounts directly connected with the temperature and the treatment time. Assuming that it was in the elemental form and considering that the melting point of calcium is about 842 °C, it is reasonable to think that it left the sample surface due to the action of gravity, in a liquid form. On the other hand, previous EDX analyses showed that calcium is likely to be bound with oxygen, probably also in form of CaO. Considering that calcium oxide has a melting point of about 2572 °C, this would lead to state that such impurity is likely to be not removed by thermal treatment.

Before doing further discussions, the SEM investigations on the sample holder are presented.

In figs. 11.3.1-2 a shield of Al_2O_3 thermally treated under oxygen and the same one used in the induction oven, in touch with the graphite sample, are shown respectively. It can be noticed that the second is covered with superficial impurities. Some tests have been performed to understand the origin of such impurities and the only explanation was found in the graphite sample. Several EDX measurements (fig. 11.3.3) focused on the impurities revealed the contemporary presence of magnesium, calcium and sulphur, already observed in other analyses on the graphite surface after thermal treatment.

Further investigations on the bottom part of the sample holder revealed consistent amounts of calcium, present both on elements in direct contact with the sample and on elements posed on its bottom (see figs. 11.3.4-5). More in detail, the form of the impurities found in the bottom of the sample holder revealed mostly shapes like solidified-drops: the impurities present here were measured by EDX (fig. 11.3.6), revealing again calcium, oxygen (coming probably from the Al_2O_3 holder), sulphur and silicon.

In conclusion, following the observations here performed, it is probable that in the AVR graphite part of the calcium is present in the elemental form or, in any case, in a low melting point form, since it was found on the surfaces in touch with the sample and on its bottom after thermal treatment at 1300 °C. In addition, considering the fraction found on the sample surface, it can be hypothesized the contemporary presence of two (or more) chemical forms of calcium, with markedly different melting points. Assuming that, the removal mechanism of calcium is likely to occur in two different steps: the first one consists on the migration of the impurity from the bulk graphite to the sample surface; the second step is probably the partial removal due to dropping or the reaction with oxygen, which will stabilize the impurity on the sample surface. For what concerns this last fraction, a

superficial thickness removal could represent a solution to obtain an impurity-enriched material, which is likely to contain activated nuclides (as Ca-41) in the case of i-graphite.

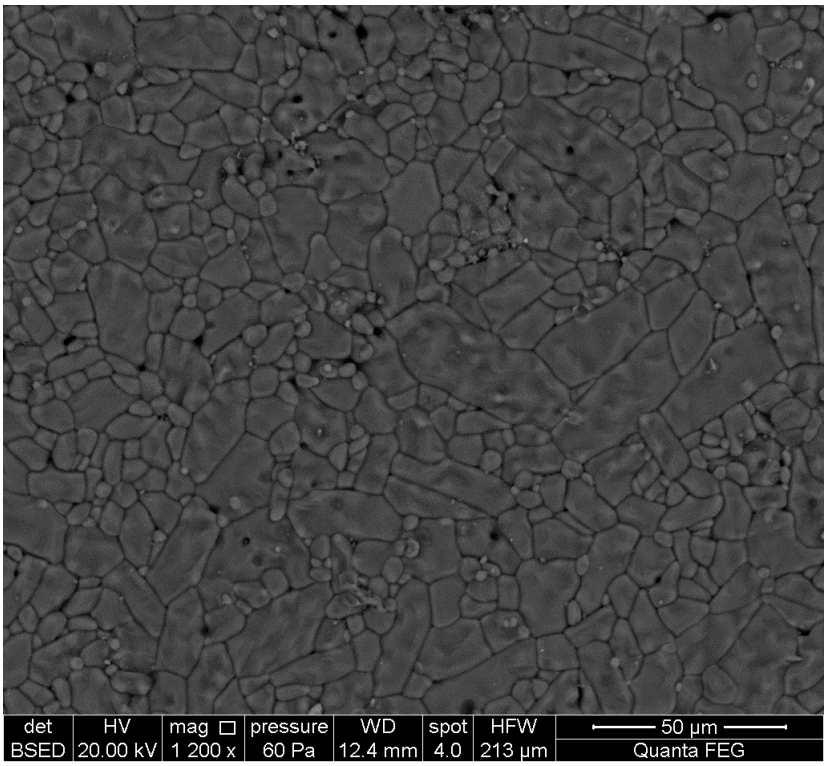

Figure 11.3.1: Overview of Al2O3 shielding thermally treated alone under oxygen

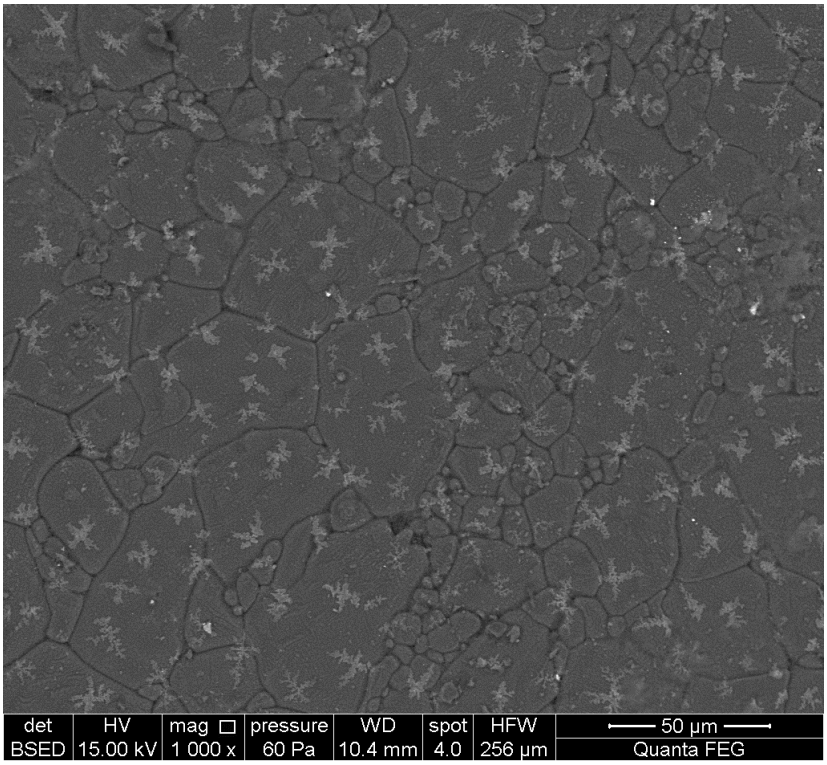

Figure 11.3.2: Overview of Al_2O_3 shielding used in the induction oven, become in touch with the graphite sample

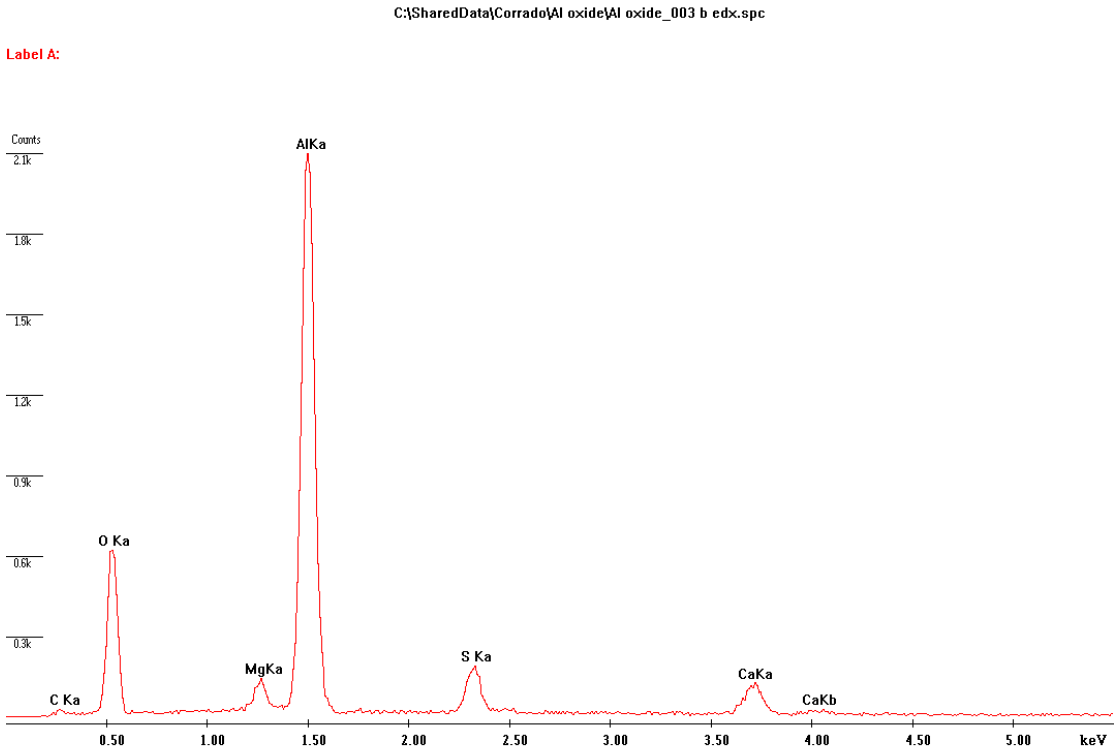

Figure 11.3.3: EDX spectra of the Al_2O_3 thermal shield, after being used in the induction oven

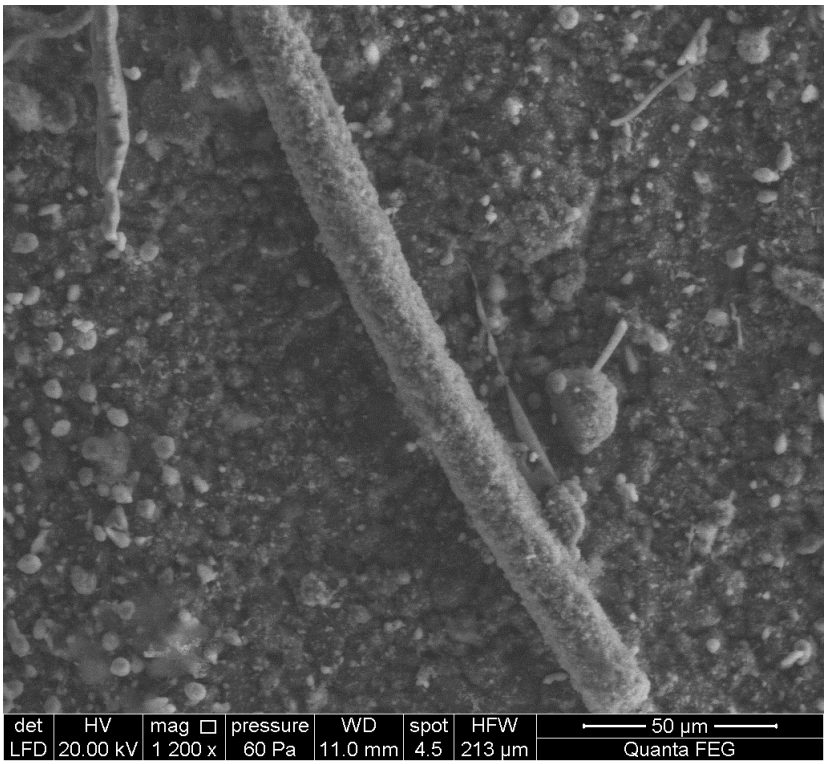

Figure 11.3.4: SEM image of the bottom part of the sample holder, not directly in contact with the graphite, after being used in the induction oven

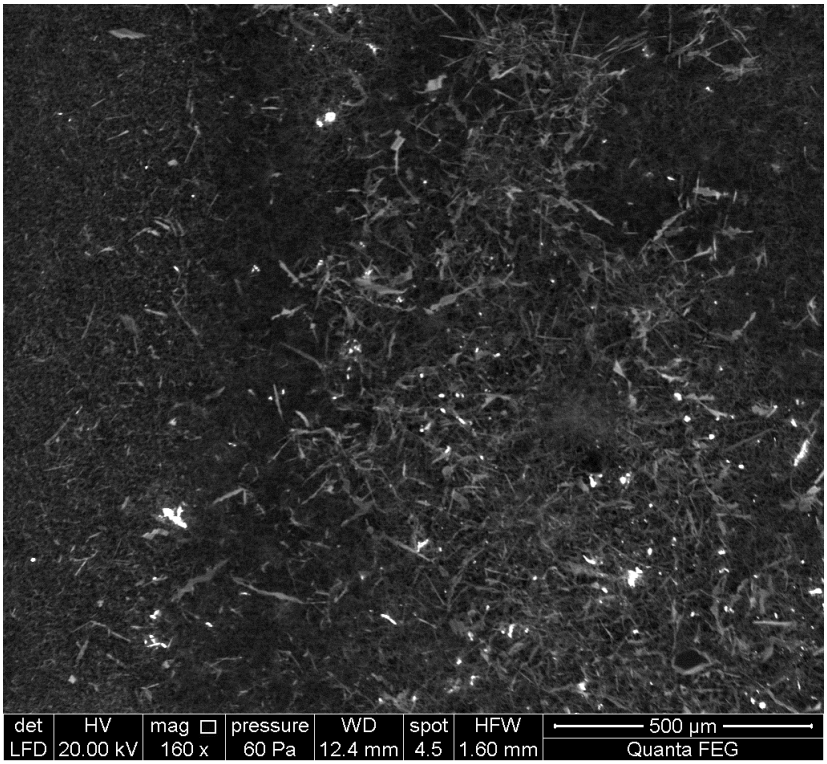

Figure 11.3.5: SEM image of the bottom part of the Al_2O_3 sample holder, not directly in contact with the graphite, after being used in the induction oven

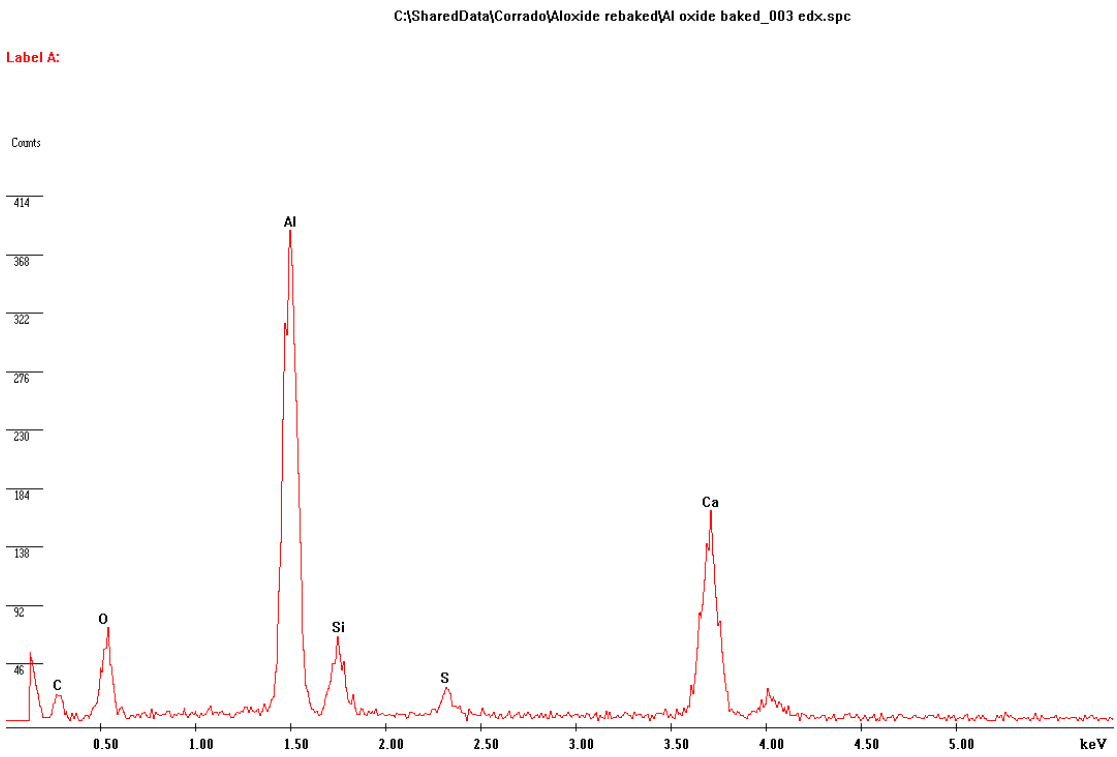

Figure 11.3.6: EDX spectra of the of the bottom part of the Al_2O_3sample holder, not directly in contact with the graphite, after being used in the induction oven. Focused on impurity of fig. 11.3.4

Summary and Outlook

The disposal of i-graphite is a consistent problem from the point of view of volume and especially of leaching of radionuclides. The requirements for conditioning and treatments are generally governed by the waste acceptance criteria of the specific designed repository. In particular the Konrad repository is the one designated for low and intermediate level waste disposal (like irradiated carbonaceous materials) in Germany. Many treatment options are under study to separate in a selective way some important radionuclides as ^{3}H, ^{14}C and ^{36}Cl: their removal from the graphite matrix will result in an easier and safer disposal, other than in substantial savings due to the restrictions imposed by the Konrad waste acceptance criteria.

Among the possible decontamination options, a promising process concerns high temperature thermal treatments. Many investigations have been performed in the past in order to understand the effects of different temperatures and different atmospheres on radionuclides selective release. Together with a contemporary development of many models in the scientific community, experiments performed in the past allowed to obtain in a selective way consistent removal of tritium and lower extraction of radiocarbon from i-graphite. Despite that, many questions have been left unanswered since the removal mechanisms are still not fully understood, in particular the ones for radiocarbon, while others are nearly unknown, as the ones for chlorine-36 and for calcium-41. The purpose of this work was to contribute on the understanding of such mechanisms, especially the ones connected with the precursors of the relevant activation products and oxidizing species adsorbed and/or originally embedded in the graphite structure during manufacturing. In particular, assuming the hypothesis that the governing physical-chemical removal mechanisms for impurities are the same for virgin and i-graphite, several thermal treatments have been applied to virgin samples of AVR graphite. After having identified the main radionuclides precursors, together with their possible origin and location, several investigations have been focused on the thermal treatment effects on such species.
Both massive and small samples have been used with different equipment, in order to achieve reproducibility and to confirm the obtained results on different scales.

In particular, massive samples tested in an induction oven showed on-line emissions during thermal treatments which were not observable with small ones, used in a thermo gravimetric analyser: methane and sulphur dioxide in small quantities have been measured.

The intention of thermal treatments was to operate under argon atmosphere, in order to measure the outgases and to connect their release with the embedded species and with temperature. Perfectly inert conditions were not achievable with any of the used equipment, but the comparison of multiple on-line measurements have allowed to reveal the effective presence of oxidizing species and different volatile chemical compounds in the graphite structure. Their release, in particular, has been proven to occur during the first steps of the treatment.

Several comparisons of the emissions, measured with the TGA and the induction oven, with results obtained in the past allowed to link the removal of some nuclides with the outgases measured here. More in detail, water (steam) was found to be released from the sample even at relatively high temperatures, during the initial treatment step: tritium release curves observed in the past have been confirmed by such observation, leading to the conclusion that most of it is probably released in form of water.

It seems to be confirmed that the removal of radiocarbon occurs because of a slight oxidation of the graphite surfaces, assuming its superficial enrichment. During the initial heating step, a well-defined peak of CO_2 was measured in all the experiments at relatively low temperatures, followed by a marked peak of CO at higher temperatures. In previous experiments it was observed a steep initial release even under inert atmosphere, linked to a partial oxidation probably caused by embedded oxidizing species: that hypothesis has been confirmed.

Methane was observed to be released from massive samples, resulting from the pyrolysis of embedded hydrocarbons, during the heating up step: it is probable that during treatments of i-graphite small amounts of tritium and radiocarbon will be released in form of methane, in all the possible combinations.

At last, sulphur was measured as SO_2 in small quantities, mostly during the high temperature step, probably due to a small income of oxygen: since it is one of the precursors of ^{36}Cl, its removal before implying graphite in a NPP would result in lower activation products.

A repeated thermal treatment on the same sample showed considerably lower emissions in the first steps, together with a reduced mass loss, compared to the one measured in the first treatment. This observation confirms the effective presence of many chemical species inside the graphite matrix, main responsible of the gaseous emissions during treatments under inert gases. On the other hand, the lower amounts of outgases can be linked to a probable improved behaviour of the thermally treated i-graphite under repository conditions. Further studies on i-graphite could confirm such hypothesis.

Concerning other radionuclides, in particular ^{36}Cl and ^{41}Ca, few studies have been established in the past. Considering the respective main precursors, i.e. ^{35}Cl and ^{40}Ca, some investigations with SIMS have been performed, focusing also on other species like nitrogen, the main precursor of ^{14}C. The results confirmed an effective removal of some species from the first micrometers in depth from the sample surface, with high efficiencies for chlorine (up to 70%), and lower removal efficiencies for nitrogen. Nitrogen removal was confirmed also by XPS analysis, but future investigations are necessary in order to prove what has been measured here.

For what concerns calcium, its migration from the graphite bulk to the surface was observed through SEM images, XPS, XRF and SIMS. Most of the calcium on the surface was found to be bound with oxygen through XRF and SIMS analyses. However, part of the calcium coming from the sample was found also on the bottom part of the sample holder, with a completely different structure, together with sulphur. It is probable that calcium, after having migrated to the sample surface, had reacted with oxygen and also sulphur, forming at least two different compounds with different melting points. It has been confirmed by visual inspections with SEM analyses. Calcium was found on the sample surface in higher amounts after longer exposures to high temperatures.

Superficial structure changes and impurity migration have been observed via Secondary Electron Microscope analyses, with a marked effect on the structure when oxygen was used in the process gases.

In conclusion, high temperature thermal treatments revealed to affect graphite in many ways, removing many impurities and causing the migration of others. The presence of oxidizing species, originally embedded but also chemisorbed on the graphite surfaces, has been proven. The connection with previous experiments has confirmed some observations and hypothesis, in particular correlated with the removal mechanism of radiocarbon and tritium.

Concerning the development of an industrial-scale purification process, it is necessary to develop a multi-step treatment, where the thermal one could be used as first in order to remove part of the volatile radionuclides, especially tritium and radiocarbon. At the present state, a high temperature thermal treatment with optimized parameters and well controlled boundary conditions seems to be advisable only for graphite pre-conditioning: the most mobile nuclides are likely to be removed, showing so an improved leaching behaviour under repository conditions. Further investigations are necessary to prove, quantify and interpret

what has been measured, focusing in particular also on the effective removal efficiency of chlorine and calcium through thermal treatment.

At last, future investigations should be focused also on carbon bricks, since the activity arising from the activation products present in such material is order of magnitudes higher than the one in i-graphite.

Appendix 1

A.1.1 Temperature Calibration of the Induction Oven

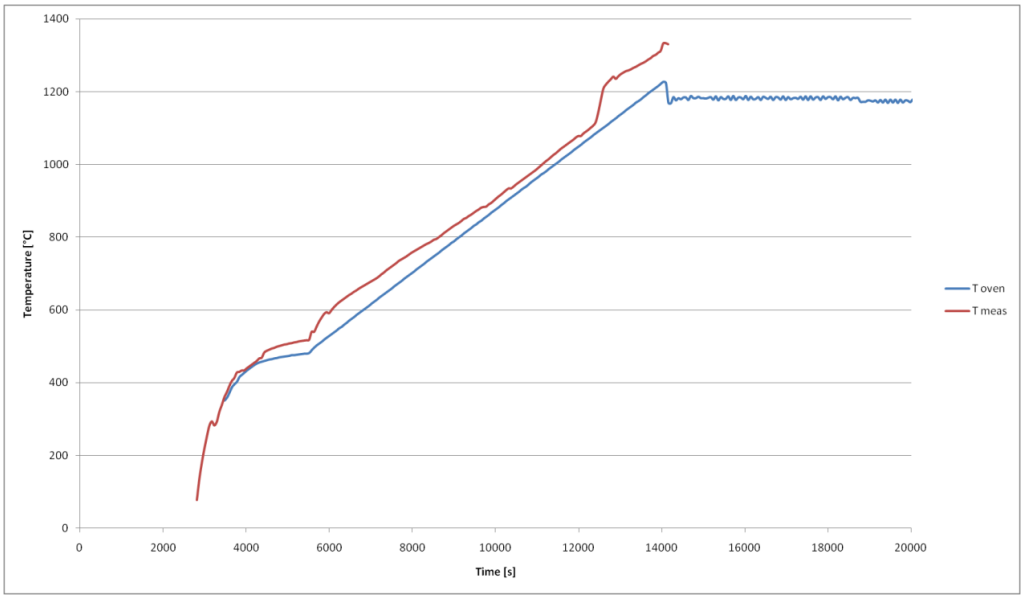

Figure A.1.1.1: Comparison between real temperature (red) and pyrometer's one (blue)

The displayed temperature (red line A.1.1.1) was obtained with a pyrometer, installed in the induction oven facility to measure indirectly the temperature.[284] Previous experiments showed that the measured temperature was affected by some fluctuations/imprecisions. For that reason a calibration through the usage of a thermocouple has been performed. The used thermocouple was a type-K one (NiCr-Ni) from Roessel Messtechnik, Ø 1.5 mm mineral-insulated metal sheathed (MIMS), able to operate in both oxidizing and reducing environment up to temperatures of 1280 °C (1300°C for short time). Results of the calibration are reported in fig. A.1.1.1: the blue line refers to the signal from the pyrometer, the red one is from the thermocouple. Temperature measurement confirmed to be not very precise, mostly at low and high temperatures: the minimal measurable designed value was about 350 °C but, as the oven reached that value, the programmed-linear heating curve was not faithfully followed. However, the malfunctioning of the equipment was shown especially at high temperatures: starting from about 900 °C it was discovered a high measurement error up to 100 °C. At the regime temperature (1300 °C) the thermocouple (type K) was destroyed because of the unbearable heat, so data is available only for the heating up step. Due to this calibration it was possible to correct the regime temperature to perform further experiments (see magenta line in fig. A.1.1.1). The temperature during the heating and cooling step has been extrapolated through the above-mentioned calibration. However, the uncertainties on the temperature values are considerable due to the oven instabilities, estimated up to 30 °C.

[284] A description of the device is reported in section 8.1

A.1.2: Delay time corrections of the Measured Values

It has to be considered that there is a “delay time” between the emissions occurring at the sample side and their measurement in the mass spectrometer, due to the connection line and the relatively large volume of the oven. This fact has to be kept in mind before connecting directly the measured temperature at a certain time with the emissions occurring at the same time. Water emission and temperature fluctuations in the experiment "AVR 1" have permitted to shift the temperature curve of about 400 seconds to well fit together (see fig. A.1.2.1). The same shifting has been applied also to the other experiments. In fig. A.1.21 the delay is shown clearly: the pink line is the corrected temperature, the blue line is the measured one.

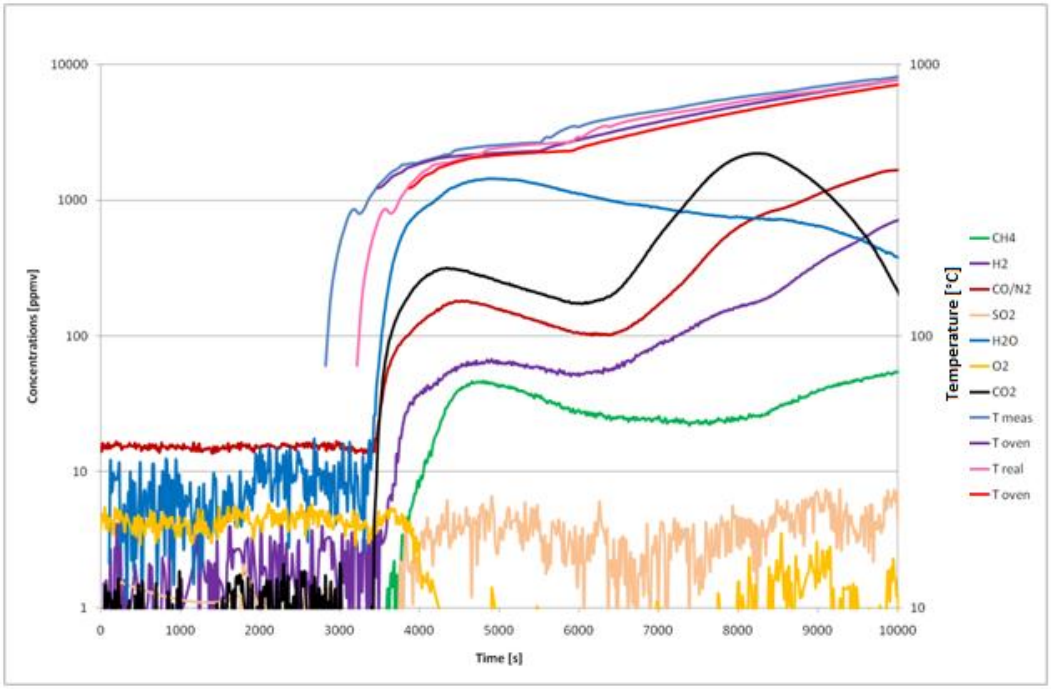

Figure A.1.2.1: Comparison among temperature signals before (cyan) and after (magenta) time-delay corrections, among gaseous measurements

Because of the above-listed reasons, temperature values have a relatively high uncertainty, so calculations referred to temperature cannot be precisely performed. Probably the pyrometer was defective because more than 100 °C error at high temperatures seems to be unacceptable.

A.1.3 Purification/Regeneration of the Al_2O_3 Sample Holder

After having performed every experiment in the induction oven, in order to establish the same conditions for every successive experiment and to remove the particles reacted on the Al_2O_3 shielding, a "re-generation" method has been developed. It consisted of annealing the alumina shielding/holder in an electric oven under air, in order to allow the reaction of the carbon particles with the oxygen and to be released in form of CO or CO_2. After some trials, the method revealed to be successful for annealing temperatures of 1300 °C for at least 4 hours. In addition, it has to be kept in mind that alumina is manufactured by using water and oil, which are likely to react when the material is warm enough. The above-described method has been used also for the new made materials and not only for the used ones. Unfortunately, the treatment revealed to produce a more reactive alumina, when posed in touch with carbon: this can be observed in the experiments AVR2 and AVR3 in sections 8.3.1.2-3 respectively. In figs. A.1.3.1-2 two photos are reported to give a better idea of the result of the purification process. However, for future applications, another material has to be chosen, in order to not produce secondary emissions that overlap the real gases coming from the sample.

Figure A.1.3.1: Alumina holder and thermal shield before the purification process

Figure A.1.3.2: Alumina holder and thermal shield after the purification process

A.1.4 Mass Calculations from the on-line Gaseous Measurements

To perform calculations with the aim of obtaining the masses relative to every compound, starting from on-line emissions measurement in the MS, some assumption have been adopted. First of all, it must be considered that, for all measured gases, there is an inevitable residence time inside the MS. This is varying depending on the considered emission and the total gas flow so, even though a certain gaseous emission had stopped, many minutes are necessary to remove it from the measuring system.

The MS system provides Ion Currents for each m/e fragment which, due to a proper calibration through "calibration gases"[285], are converted into partial pressures and, then, to mole fractions according to Dalton's law.

$$p_{tot} = \sum p_i$$

$$x_i = \frac{p_i}{p_{tot}} = \frac{n_i}{n_{tot}}$$

Unfortunately, due to many secondary emissions during the experiments, precise calculations on the sample mass loss were not performable. However, the total mass loss has been measured directly by weighing the samples, so that can be considered as a true reference.

The assumed hypotheses to calculate the relative mass from gaseous emissions are:

- Ideal gases
- Gas flow approximated to pure argon flow, since all the other emissions have been measured in very low values (<0.5% mole fraction)

The molar flow rate is approximated with:

$$\dot{n} = \dot{V} \cdot \frac{P}{RT} \left[{}^{mol}/_{h} \right]$$

where it has been considered $\dot{V}$ volumetric flow [m^3 h^{-1}], M_{mol} molar mass [g mol^{-1}], R= 8.314 [J $mol^{-1}K^{-1}$], P argon pressure [Pa], T temperature [K].

With values of 2 bar pressure, $6 \cdot 10^{-3}$ m^3/h argon flow rate, 25 °C temperature, it results:

$$\dot{n} = 48.43 \cdot 10^{-2} \left[{}^{mol}/_{h} \right]$$

With values of 2 bar pressure, $3.6 \cdot 10^{-3}$ m^3/h argon flow rate, 25 °C temperature, it results:

$$\dot{n} = 29.06 \cdot 10^{-2} \left[{}^{mol}/_{h} \right]$$

Considering, as assumed in the hypothesis, the total moles of argon representative of the total gas mixture moles, the mass for each compound can be found by multiplying $\dot{n}$ for the molar mass (M_i) and the area (Ai) obtained as in fig. A.1.4.1.

[285] Refer to Appendix A1.5 for further details on MS calibration

The formula to calculate the mass is then:

$$m_i = M_i \cdot \frac{\dot{n}}{3600} \cdot A_i \cdot 10^{-6}\ [g_i]$$

Two gaseous emissions are normally measured with a time interval in between of about 10 seconds, due to the set values of the MS. Such settings were chosen in the way to get a good precision with a relative short-time measurement. Shorter measurements showed to be more imprecise; longer measurements were more accurate, but the time interval was too high to see short-lasting emissions.

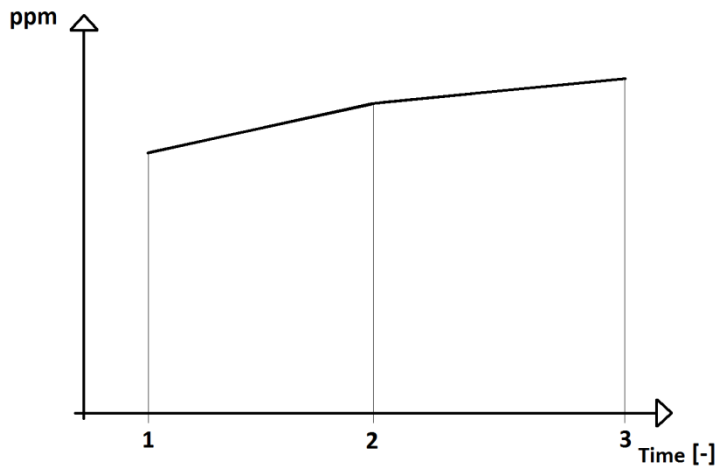

Figure A.1.4.1: Representation of Trapezi formula to calculate the area between successive measurements

A.1.5 Calibration of the Mass Spectrometer

Ionisation is the part of the procedure for analysing neutral particles which has the greatest effect upon the sample gas. A small fraction of the atoms or molecules present in the gas phase are converted into an ionised state by bombarding them with low energy electrons. These produce singly and multiply charged positive ions. The energy of the collision electrons has a strong effect on the number and on the type of ions that are produced (see fig. A.1.5.1). The ionisation process of the neutral particles starts at a minimum energy (the "appearance potential") of the electrons. The number of ions produced increases rapidly with increasing electron energy, reaching a maximum at 50 – 150 eV depending on the type of gas, then falling slowly again as the energy is further increased. The yield of ions – and therewith the sensitivity – should be as great as possible, therefore electron energies in the range 70 – 100 eV are used in most cases. In the present case, the chosen electron energy was 70 eV.

The mass spectrometer provides then ion currents, proportional to the partial pressure of every gaseous species. For the ionisation of molecules, the number of possible kinds of ions

increases rapidly with increasing complexity of the molecules. Fragment ions appear in addition to singly and multiply charged molecular ions.

$$
\begin{aligned}
ABC + e^- \longrightarrow\ & ABC^+ + 2e^- \\
& ABC^{++} + 3e^- \\
& AB^+ + C + 2e^- \\
& BC^+ + A + 2e^- \\
& A^+ + BC + 2e^- \\
& C^+ + AB + 2e^- \\
& B^+ + A + C + 2e^-
\end{aligned}
$$

For that reason and also because the mass spectrometer is not an absolute instrument, many calibrations are necessary in order to obtain directly at the output the molar fractions for each measured gas. This procedure is necessary because many ions, generated from different molecules, could present the same m/e.[286]

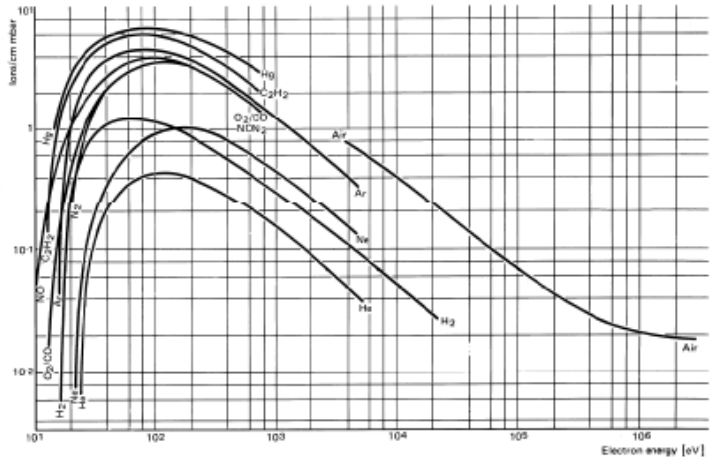

Figure A.1.5.1: Ionization produced by electron impact, as a function of the electron energy

In particular, the calibration gases, with certified gas mixtures, were:

1: Ar + SO_2 (8700ppm)
2: Ar+ N_2 (50%) +O_2 (20%)
3. Ar + CO_2 (30%)
4. Ar+ H_2(5%)+ CO (10%)
5. Ar + CH_4 (10%)

Every calibration gas mixture contains the so-called internal standard, a not overlapping gas which is used during the calibration as reference to calculate the concentration of the other gases.

The m/e values chosen for the measurements have taken into account the resolution of the instrument and the software furnished with the equipment (see tab. A.1.5.1).[287] Due to a not

[286] This problem is more marked in this case since the resolution of the mass spectrometer is about 0.1 m/e

[287] The NIST library was used for reference to choose the proper fragments

proper response of the software, together with many overlapping peaks, it was chosen not to measure nitrogen directly, but to measure it together with the carbon monoxide.

Compound	H_2	H_2O	O_2	CO	CH_4	SO_2	CO_2
m/e	2	2,18	32	28	15,13,2	64,32	44,28

Table A.1.5.1: m/e fragments considered for the calibration of the mass spectrometer

A.1.6 Design of the new Sample Holder

The original sample holder was made of two parts:

- The part in contact with the sample was made of porous Al_2O_3
- The lower part was made by several layers of graphite wool, insulated on the top in order to avoid the establishment of an axial flux

Figure A1.6.1: Upper part of the original sample holder

Figure A1.6.2: Components of the lower part of the original sample holder

The main reasons that led to abandon such holder are listed in the following:

- Inefficient fluid dynamics
- Porosity: gas and water adsorption are favoured. In this way a secondary emissions of these gases could occur at high temperatures, overlapping so the real emissions of the sample
- Pyrolysis at high temperatures: it could lead to products or carbon particles emitted during the treatment

Because of the above listed reasons, a thermo-fluid dynamic simplified simulation was performed, with the purpose of building a new, more inert, sample holder.

The key-features of the new holder, used to choose the proper material and geometry, were:

- Improved fluid dynamics
- High temperature resistance
- Inert as much as possible, both in reducing and oxidizing ambient
- Thermal shielding, in order to reduce the thermal radiation of the inner oven surfaces, made of fused quartz
- Maximum costs/benefits ratio

The chosen material was Al_2O_3 Alsint(R) 99.7%. Due to economic reasons and difficulty in manufacturing the holder, the bottom part was designed in a special-grade steel (Iconel(R) alloy 617) able to bear up to 1000 °C and the geometry of the holder has been simplified as much as possible, considering the requested features.

In figs. A1.6.3-4 are shown the results of the simplified thermodynamic simulation, performed with the following hypothesis:

- Geometry 2D, axial symmetry
- Steady State
- Irradiative heat exchange between the sample and the inner walls of the oven (assumed ε_{walls}=0.7 andε_{sample}=1)
- Conduction in the fused quartz walls
- Adiabatic top and bottom of the treatment chamber
- External walls with irradiative heat exchange with the environment ε_{walls}=0.7
- Air flow 7 l/h
- Sample temperature of 1100 °C (maximum advised temperature without a thermal shield)

For what concerns the CFD simulation, the following assumptions have been considered:

- Geometry 2D, axial symmetry
- Steady State
- Low inlet gas velocity (0,1 m/s)
- Sample holder not porous

The CFD simulation results are reported in fig. A1.6.5.

The performed simulations allowed the design of an improved sample holder (figs. A1.6.6-7) together with a thermal shielding, able to operate at temperatures higher than 1100 °C (up to 1600°C by design). A comparison between the old and new holder, installed in the induction oven, is shown in figs. A1.6.8a-b).

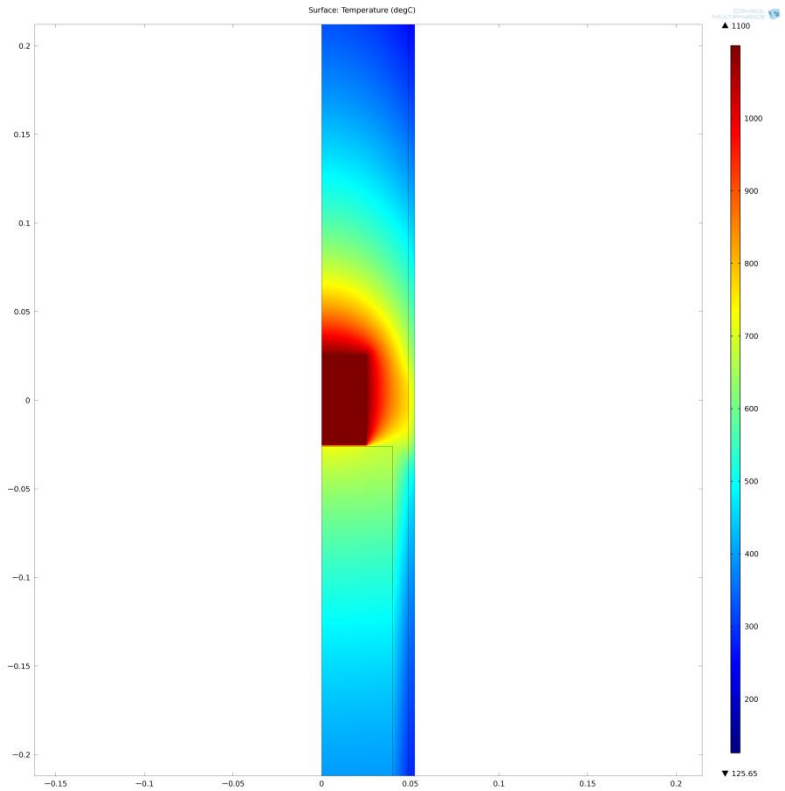

Figure A1.6.3: Thermodynamic simulation of the original sample holder

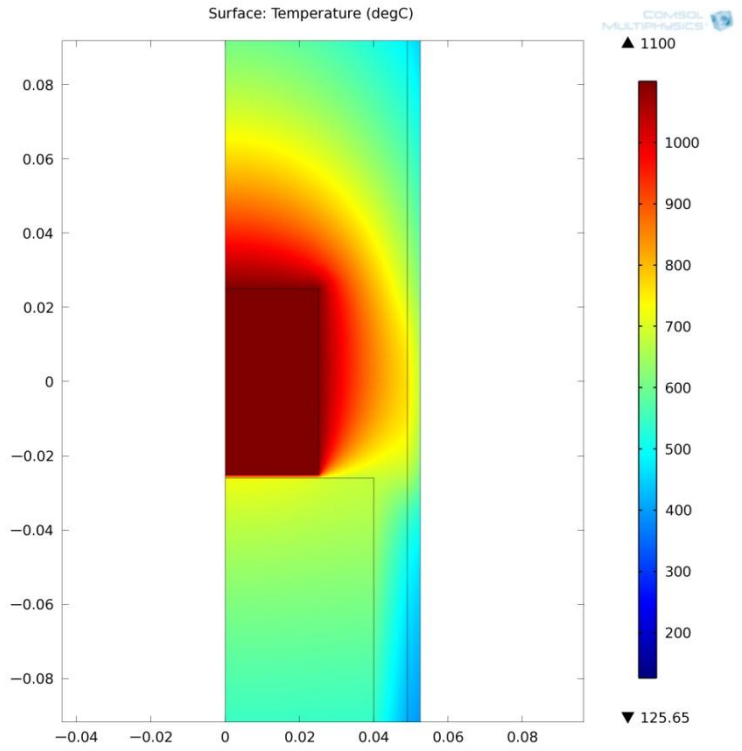

Figure A1.6.4: Thermodynamic simulation of the original sample holder, zoomed

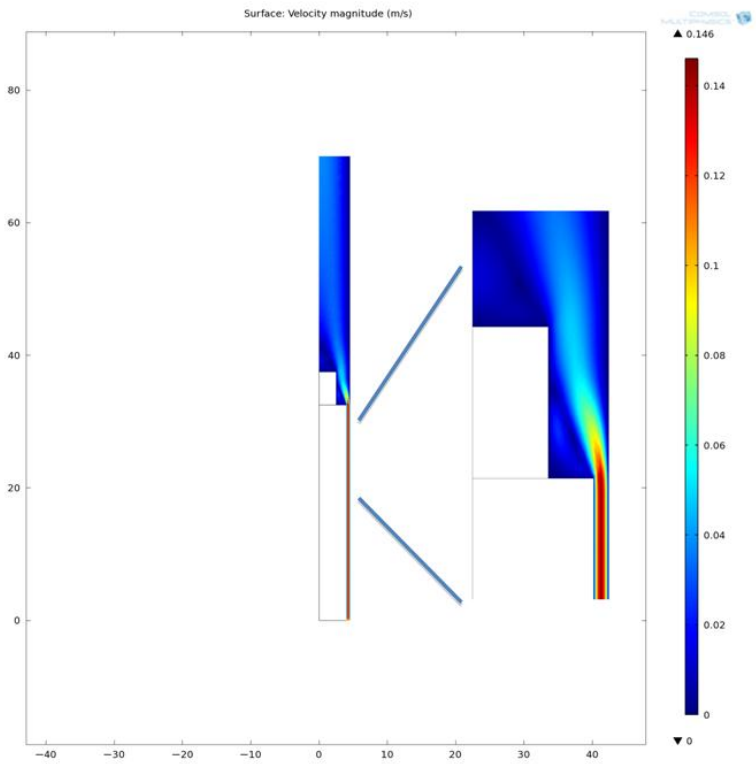

Figure A1.6.5: Fluid dynamic simulation of the original sample holder

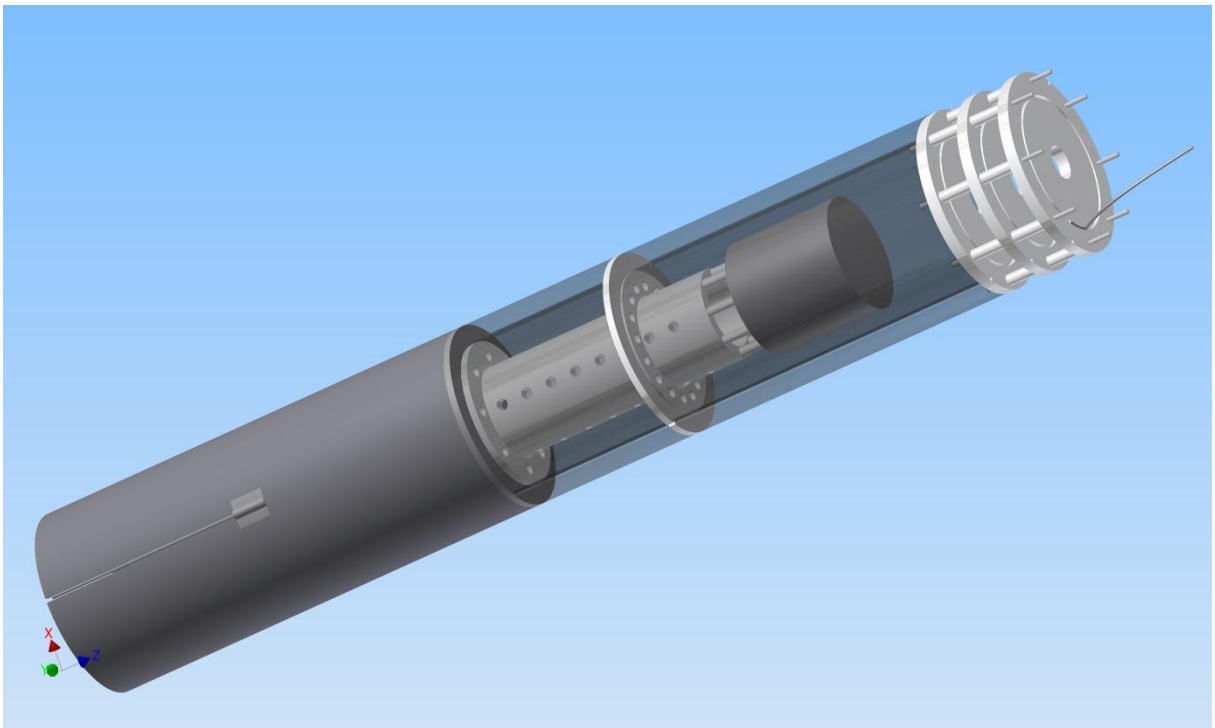

Figure A1.6.6: New sample holder with thermal shielding, overview

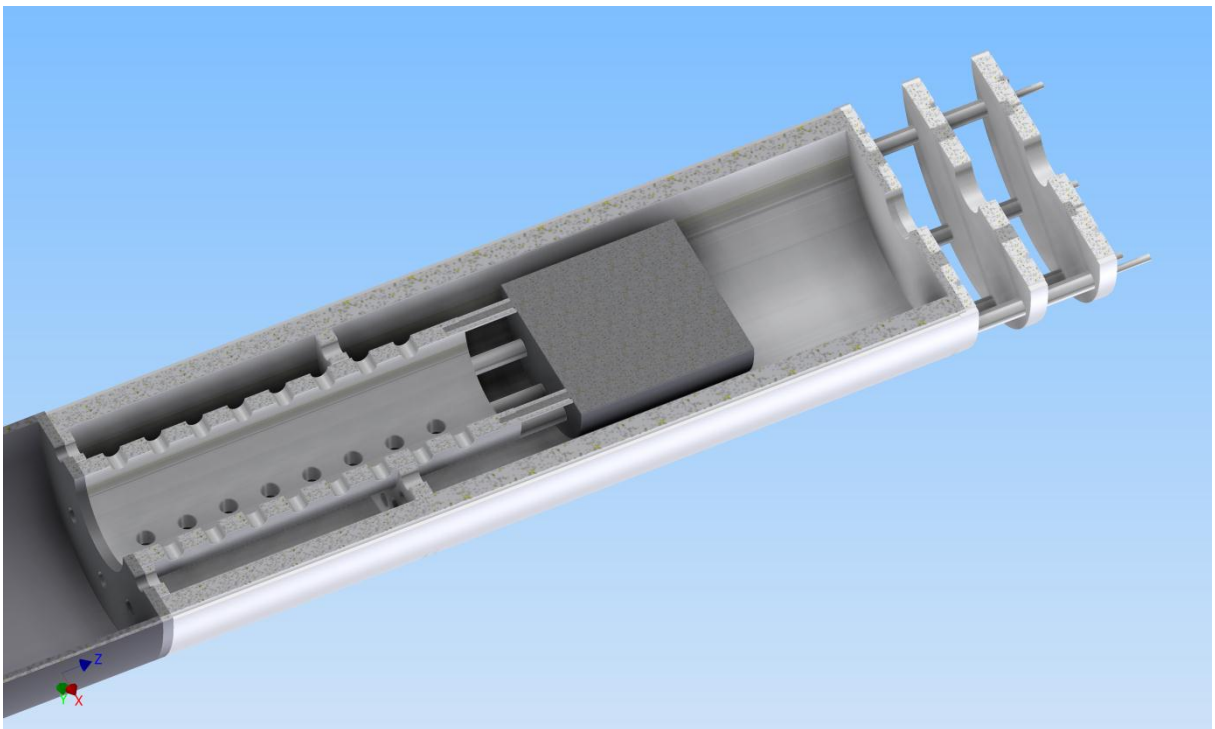

Figure A1.6.7: New sample holder with thermal shielding, section view

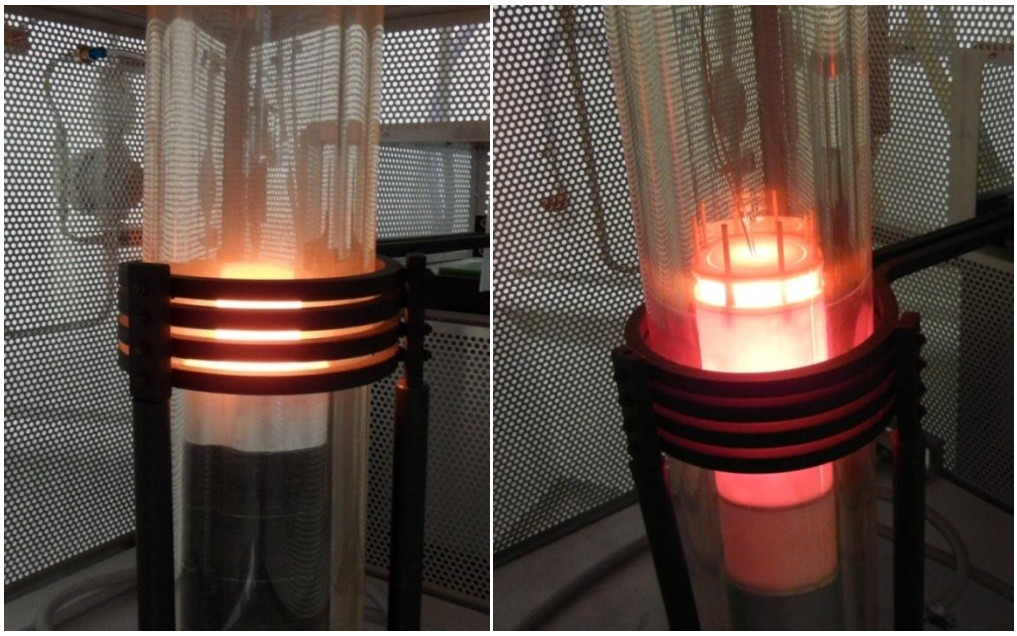

Figure A1.6.8.a-b: Comparison between the old (left) and new (right) sample holder, installed in the oven

References

Ashida K., Watanabe K., "*Diffusion costants of tritium in graphites and compensation effect*", J. Nucl. Mat. 183, 1991

Association of German Engineers (VDI) - The society for energy technologies (PUBL.), "*AVR - Experimental High Temperature Reactor 21 years of successful operation for a future energy technology*", VDI Verlag, Düsseldorf 1990

Atsumi H., J. Nucl. Mat., 307-311 (2002)

Atsumi H., J. Nucl. Mat. 313-316 (2003)

Atsumi H., S. Tokura, M. Miyake, J. Nucl. Mater. 155-157 (1988)

Atsumi H., Tauchi K., "*Hydrogen absorption and transport in graphite materials", Journal of alloys and compounds*", 356, 2003

Atsumi H., Tanabe T., Shikama T., "*Hydrogen behaviour in carbon and graphite before and after neutron irradiation - Trapping, diffusion and the simulation of bulk retention*", J. Nucl. Mat. 417, 2011

Bethe A., 1950, Rev. Mod. Phys., 22, 213

Bisplinghoff B., Lochny M., Fachinger J., Bruecher H., "*Radiochemical characterisation of graphite from Juelich experimental reactor (AVR)*", Institut fuer Sicherheitforschung und Reaktortechnik, FZJ, 1999

Blacard A., "*The Thermal Oxidation of graphite*", 2000

Blow S., J. Phys. D., Appl. Phys. 4 (1971)

Brenneke P., *"Anforderungen an endzulagernde radioaktive Abfälle (Vorläufige Endlagerbedingungen"*, Stand: April 1990 in der FassungvomOktober 1993) - Schachtanlage Konrad - 1993. BfS-ET-3/90-REV-2.

Brown J.G., Glynn P.D., *"Kinetic dissolution of carbonates and Mn oxides in acidic water: measurement of in situ field rates and reactive transport modeling"*, Applied Geochemistry, Vol.18 n.8, 1225, 2003

Carbowaste Project: "*www.carbowaste.eu*"

Clayton A.M., Harper A., Wheatley C.J., AEA Technology, "*Behaviour of chlorine in nuclear graphites*", UK NIREX report, 1996

Coltman R.R., Klabunde C.E., McDonald D.L., Redman J.K., "*Reactor Damage in pure materials*", J. of Appl. Physics 33, 3509, 1962

Delle W., Koizlik K., Nickel H., "*Graphitische Werkstoffefürden Einsatz in Kernreaktoren*", München, Karl Thiemig AG 1983

Dundey N.D., "*Review of low mass-atom-production in Fast Reactors*", 1968

El-Genk Mohammed S., Tournier J.M., "*Development and validation of a model for the chemical kinetics of graphite oxidation*", J.Nucl. Mat. 411 (2011)

El-Genk M.S., Tournier J.M., "*Proceedings of the 2010 International Congress on Advances in NuclearPowerPlants* (ICAPP '10)", Paper No. 10159, 2010

Fachinger J., von Lensa W., Prodruhzina T., "*Decontamination of nuclear graphite*", Nuclear Engineering and Design 238 (2008)

Fischer P.G., "*Verhalten von tritium in Reaktorgraphiten*", 1975

Florjan M., "*Dekontamination von NukleargraphitdurchthermischeBehandlung*", FZJ-4322, 2009, valuereported to year 2012

Fromherz T., Mendoza C., Ruette F., "*Chemisorption of atomic H,C, N and O on a cluster-model graphitesurface*", 1993

Gray W.J., "*A study of the oxidation of graphite in liquid water for radioactive waste storage application, Radioactive Waste Management*" , Vol.3 n.2, 137, 1982.

Haas E.W., Hofmann R., Richter F., "*Errors in activation analysis by nuclear recoil", Journal of Radioanalytical Chemistry"*, Vol. 69, 1982

Haasz A.A., Franzen P., Chiu S., Pitcher C.S., Journal of Applied Physics, 77, 1995

Hinssen H.K., Kuehn K., Moormann R., Schloegl B., Fechter M., Mitchell M., "*Oxidation experiments and theoretical examinations on graphite materials relevant for the PBMR*", J. Nucl. Engineering and Design 238, 2008

IAEA, "*Application of the Concepts of Exclusion, Exemption and Clearance"*, IAEA Safety Standards Series No.RS-G-1.7, Vienna (2004).

IAEA, *"HTR-PM Project Status and Test Program",* TWG-GCR-22

IARC Monographs Volume 79

ICEM 2007, Proceedings of the 11th International Conference on environmental Remediation and Radioactive waste Management, "*The AVR (HTGR) decommissioning project with new strategy"*

Jiang W., Nadeau G., Zaghib K., Kinoshita K., "*Thermal analysis of the oxidation of natural graphite - effect of particle size*", Thermochimica Acta 351, 2000

Karaca F., Morgan T.J., George A., Bull I.D., Herod A.A., Millan M., Kandiyoti R., "*Molecular mass ranges of coal tar pitch fractions by mass spectrometry and size-exclusion chromatography*", Rapid Commun. Mass Spectrom. 2003; 23: 2087-2098

Katayama K., Nishikawa M., "*Release behaviour of tritium from graphite material*", 2001

Keim W., Behr A., Schmitt G., "*Grundlagender Industriellen Chemie*", 1986

Marsden B. J., *"Nuclear Graphite for High Temperature Reactor"*, IAEA Technical Committee Meeting on "Gas Turbine Power Conversion Systems for Modular HTGRs", Palo Alto, California, November 2000

Moormann R., "*A safety Re-Evaluation of the AVR", ForschungszentrumJülich*", Jül-4275

Moorman R., *"Fission product transport and source terms in HTRs: Experience from AVR pebble bed reactor"* (2008)

Nic M., Jirat J., Kosaba B., "*Rhombohedral graphite*", IUPAC Compendium of Chemical Technology

Nightingale R.E., *"Nuclear Graphite"*ed. 1962,New York and London: Academic Press

Nomura S., Imai H., Fujii K., Shindo M., "*Relation between gasification rates and gas desorption behaviour with metallic impurities of carbon and graphite materials for the HTTR*"

Okada M., Sogabe T., "*Behaviour of gas desorption and gas permeability of carbon materials*"

Podruzhina T., "*Graphite as radioactive waste: corrosion behaviour under final repository conditions and thermal treatment*", Juel 4166, 2004

Pokrovsky O.S., Schott J., *"Processes at the magnesium-bearing carbonates solution interface. II. Kinetics and mechanism of magnesite dissolution"*, Geochimica et Cosmochimica Acta, Vol.63 n.6, 881, 1999.

Polovina M., Babic B., "*Carbon*" vol. 35, 1997

Priggen R., "*Die beinahe Atom-Katastrophe in inhaerent sicheren Reaktor in Juelich*"

Printz R.J., Quade U., Wahl J., "*Packaging requirements for graphite and carbon brick from the decommissioning of the AVR in consideration of the german final disposal regulations*"

Révay Zsolt, “*Prompt Gamma Nuclear Activation Analysis for ForschungszentrumJuelich*”, December 2010, Nuclear Research Department, Institute of Isotopes, HAS, Budapest, Konkoly-ThegeMiklosutca 29-33. 1121 Hungary

Saeki M., "*Effects of pyrolitic carbon structure on diffusivity of tritium*", J. Nucl. Mat. 131, 1985

Schmidt P.C., "*Alternativen zur Verminderungder C-14 emission bei der Wiederaufbereitung von HTR-Brennenelement*", Juel-1567, 1979

Sheppard S.C., Johnson L.H., Goodwin B.W., Tait J.C., Wuschkle D.M., Davidson C.C., "*Waste Manage*",16 (1997)

Shouyin Hu; Ruipian Wang; Zuying Gao (2004), "*Safety Demonstration Tests on HTR-10*", proceedings of the conference on High Temperature Reactors (Beijing, China)

Stainmard J.W., "*Graphite oxidation - A literature Survey*", 1990

Sterner H., Crossand M.T., Rodriguez A.; “*Decommissioning of gas-cooled reactors*”. Kerntechnik 70 (2005)

Szentmilklòsi L., “*PGNAA Analysis for ForschungzentrumJuelich*“, 2011

Takahashi R., Toyahara M., Maruki S., Hueda H., Yamamoto T., "*Investigation of morphology and impurity of nuclear grade graphite, and leachingmechanism of carbon-14*"

Telling R.H., Heggie M.I., "*Radiationdefects in graphite*", Philosophical Magazine, Vol. 87, 2007

Thomas J.M., "*Chemistry and Physics of Carbon, vol. 1*", 1965

Thrower P.A., Mathew G.K., McGinnis N.J., "*Carbon 20*", 1982

Thurlbeck A., "*Summarised Compatibility Review of Reactor materials for CO2-cooled Graphite moderated Reactors*", TRG Report 267 (1962)

Toulhoat P., "*Scientific bases for nuclear waste management*", Mat. Res. Soc. Symp.Proc., 2007

Vaudey C., Toulhoat N., Moncoffre N., Bérerd N., "*Chlorine speciation in nuclear graphite: consequences on temperature release and on leaching*", Radiochim. Acta 98, 2010

Vaudey C.E., Toulhoat N., Moncoffre N., "*Thermal Behaviour of chlorine in nuclear graphite at a microscopic scale*", J. Nucl. mat. 395 (2009)

Vaudrey C.E., C. Gaillard, N. Toulhoat, N. Moncoffre, M.L.Schlegel, L. Raimbault, "*Chlorine speciation in nuclear graphite studied by X-Ray Absorption Near Edge Structure*", J. Nucl. Mat. 418 (2011)

Wang L., Jones L.E., "*X-Ray Diffraction of Nuclear Graphite*"

Warrier M., "*Multi-scale modelling of hydrogen isotope transport in porous graphite*", PhDDissertation, University of Greisfswald, Germany, 2004

Wenzel U., Hertz D., Schmidt P., "*Determination of 14C in spent HTGR fuel elements*", Journal of Radioanal. Chem. 53, 1979

Woerner J., Botzem W., S.D. Preston, "*Heat treatment of graphite and resulting tritium emissions*"

Xiaowei Luo, Jean-Charles R., Suyuan Yu, "*Effect of Temperature on graphite oxidation behavior",* INET Tsinghua University, Beijing, China; CEA Cadarache, France; 2003

Xiaowei Luo, Jean-Charles R., Suyuan Yu, "*Theoretical analysis of mass transfer and reaction in a porous medium applied to the gasification of graphite by water vapour*", Nucl. Eng and Design 236 (2006) 938-947

Graphite properties:

http://invsee.asu.edu/nmodules/carbonmod/point.html

http://en.wikipedia.org/wiki/Mohs_scale_of_mineral_hardness

http://www.substech.com/dokuwiki/doku.php?id=graphite

http://www.carbonandgraphite.org/

Repository Konrad:

www.endlager-konrad.de/cln_153/nn_1272768/EN/Subjects/Preface

www.endlager-konrad.de/cln_153/nn_1996290/EN/Subjects/Origins

Repository Asse:

www.bfs.de/en/endlager/asse/grundlagen/geschichte.html

List of Tables

Table 1.1: Main parameters of AVR reactor

Table 3.1: Typical impurities in raw petroleum coke

Table 3.2: Typical constituents of coal-tar pitch binders

Table 3.3: Metallic impurities in calcined petroleum coke

Table 3.4: Comparison among different impurities of AVR carbon brick and a modern coal-tar pitch

Table 4.1: Estimation of main contaminants of primary systems (basis 2004)

Table 4.2: Estimation of the activity distribution in the AVR plant (basis 2004)

Table 4.3: Radionuclide inventory estimation in AVR graphite and Carbon Brick

Table 4.4: Exemplary results of a graphite sample and a carbon brick sample

Table 4.5: Main neutron-activation reactions leading to C-14 production

Table 4.6: Nuclear parameters for neutron activation production of ^{3}H from some precursors and their contribution

Table 4.7: Some neutron activation reactions leading to H-3 production

Table 4.8: Nuclear parameters for neutron activation production of ^{3}H from some precursors and their contribution

Table 4.9: Some neutron activation reactions leading to Cl-36 production

Table 4.10: Nuclear parameters for neutron activation production of ^{36}Cl from some precursors and their relative contribution

Table 4.11: Some neutron activation reactions leading to Cl-36 production

Table 4.12: Main neutron reactions and relative precursors

Table 5.1: Recoil energies of the C-14 nucleus after gamma emission

Table 6.3.1: Representative impurity levels of three classes of graphite

Table 6.3.2: Comparison among different purification treatments of carbonaceous materials

Table 6.3.3: Comparison among different carbonates properties

Table 8.3.1: Comparison among measured mass losses from the experiments in the induction oven

Table 8.3.2: Ratio among different gases released during thermal treatment of sample "AVR 1"

Table 8.3.3: Ratio among different gases released during thermal treatment of sample "AVR 2"

Table 8.3.4: Ratio among different gases released during thermal treatment of sample "AVR 3"

Table 9.2.1: Fractional removal of chlorine, superficial and integral

Table 9.2.2: Fractional removal of nitrogen, superficial and integral, indicative values

Table 10.1: Results from XPS analysis of untreated AVR graphite sample

Table 10.2: Results from XPS analysis of an thermal-treated AVR graphite sample

Table A.1.5.1: m/e fragments considered for the calibration of the mass spectrometer

List of Figures

Figure 0.1: Carbowaste Project's Work Package Scheme

Figure 1.1: Scheme of a Pebble Bed Nuclear Reactor

Figure 1.2: View of the reactor vessel and its internal structure

Figure 1.3: Internal structure of the core and heat exchanger's chamber

Figure 1.4: Barriers structure of AVR

Figure 1.5: Fuel structure and TRISO particles

Figure 1.6: AVR in 1978

Figure 1.7: AVR today

Figure 1.8: Reactor pressure vessel extraction within the new material lock

Figure 2.1: Ideal crystal structure of graphite (left) and Carbon hybridized orbital present in graphite (right)

Figure 2.2: Turbostratic structure of graphite

Figure 2.3: Influencing parameters characterizing graphite grades

Figure 3.1: Scheme of the extrusion process

Figure 3.2: Scheme of a classical moulding (not used anymore)

Figure 3.3: Block of AVR Carbon Brick

Figure 3.4: Typical time-temperature cycle for a large graphitizing furnace

Figure 3.5: View of an Acheson furnace

Figure 3.6: General scheme of the graphite manufacture process

Figure 3.7: Comparison among some impurities of AVR reflector virgin graphite, a modern coal-tar pitch and values found in literature

Figure 3.8: view of a massive sample of AVR graphite

Figure 3.9: view of an unknown-grade graphite

Figure 3.10: Impurities in AVR reflector graphite, Modern Pitch and Carbon bricks of two formulations

Figure 3.11: View of a massive sample of AVR carbon brick

Figure 4.1: Radioactive decay of the AVR reflector inventory referred to table 4.3

Figure 4.2: Radioactive decay of the AVR reflector inventory referred to table 4.3

Figure 4.3-a: Cross sections of the above-listed reactions for C-14 production

Figure 4.3-b: Cross sections of the above-listed reactions for C-14 production at high neutron energies

Figure 4.4: Theoretical C-14 production in an HTGR as a function of the fluence and the nitrogen content

Figure 4.5: Theoretical H-3 production rate in some HTGR: in the AVR H-3 is reaching the constant rate after longer time due to the higher amount of Li-6 impurity

Figure 4.6: Cross section versus incident neutron energy of three reactions of oxygen isotopes leading to C-14 production

Figure 4.7: Cross section versus incident neutron energy of three oxygen isotopes reactions leading to C-14 production, zoomed at high neutron energies

Figure 4.8: Cross section versus incident neutron energy of three reactions of nitrogen isotopes leading to C-14 production

Figure 4.9: Cross section versus incident neutron energy of three nitrogen isotopes reactions leading to C-14 production, zoomed at high neutron energies

Figure 4.10: Cross section versus incident neutron energy of the neutron reaction of C-13 leading to C-14 production

Figure 4.11: Cross section versus incident neutron energy of the neutron reaction of C-12 leading to C-13 production

Figure 4.12: Cross section versus incident neutron energy of the main reactions leading to H-3 production

Figure 4.13: Cross section versus incident neutron energy of the reaction of H-1 leading to deuterium production

Figure 4.14: Cross section versus incident neutron energy of some reactions of N-14 leading to H-3 production

Figure 4.15: Cross section versus incident neutron energy of some reactions leading to Cl-36 production

Figure 4.16: Cross section versus incident neutron energy of some reactions leading to Cl-36 production, zoomed at high neutron energies

Figure 4.17: Cross section versus incident neutron energy of the S-34 reaction leading to S-35 production

Figure 4.18: Cross section versus incident neutron energy of the Ca-40, Ca-42, Ca-43 reactions leading to Ca-41 production

Figure 4.19: Prompt fission neutron energy spectrum from thermal fission of ^{235}U

Figure 5.1: Scheme of the three typical regimes occurring in reactions with graphite

Figure 5.2: Edge configurations of a graphite basal plane

Figure 5.3: Scheme of the gamma-ray emission from an excited C-14 atom

Figure 5.4: decay scheme of C-14 from thermal neutron capture of C-13. Energies are in keV and the intensities (in brackets) are referred to 100 neutron captures

Figure 5.5: Hydrogen trapping sites and transport in a graphite material

Figure 6.1.1: Scheme of the three-classes waste classification system compared to the heat-generating classification

Figure 6.3.3: Flowchart of the SiC formation method

Figure 7.1.1: Scheme of different histories of a nuclear-grade graphite

Figure 7.2.1: ^{14}C release vs time during former thermal treatments

Figure 7.2.2: ^{14}C release vs 12C% release during former thermal treatments

Figure 7.2.3: ^{14}C% fractional release vs time during former thermal treatments under nitrogen

Figure 7.2.4: ^{3}H% release vs^{12}C% release during former thermal treatments under different conditions

Figure 7.2.5: ^{3}H% release time during former thermal treatments under nitrogen atmosphere

Figure 8.1.1: Overview of the experimental set up with the induction oven

Figure 8.1.2: Overview of the Induction Oven Facility

Figure 8.1.3: Front view of the control and power supply unit

Figure 8.1.4: Overview of the cooling unit

Figure 8.1.5: Overview of the Induction Oven

Figure 8.1.6: Inside view of the Induction Oven

Figure 8.1.7: Schematic representation of the pyrometer feedback action

Figure 8.1.8: Scheme of the Mass Spectrometer System

Figure 8.1.9: View of the Mass Spectrometer (left) next to the Induction Oven (right)

Figure 8.1.10: SETSYS Evolution from SETARAM (exterior view)

Figure 8.1.11: TGA Oven (left) together with the Mass Spectrometer (right)

Figure 8.1.12: SETSYS Evolution from SETARAM (oven)

Figure 8.2.1: Coarse material before being cut in smaller samples. Left: Carbon Brick, middle: Unknown grade graphite, right: AVR grade graphite

Figure 8.2.2: Massive samples of AVR graphite, H50Ø50 mm

Figure 8.2.3: Small sample used both in the TGA and the small electric oven, H20Ø8 mm

Figure 8.3.1: On-line gaseous emissions from AVR graphite, massive sample "AVR 1", semi-log plot

Figure 8.3.2: On-line gaseous emissions from AVR graphite, massive sample "AVR 1", linear plot

Figure 8.3.3: On-line gaseous emissions from AVR graphite, massive sample "AVR 2", semi-log plot

Figure 8.3.4: On-line gaseous emissions from AVR graphite, massive sample "AVR 2", linear plot

Figure 8.3.5: On-line gaseous emissions from AVR graphite, massive sample "AVR 3", semi-log plot

Figure 8.3.6: On-line gaseous emissions from AVR graphite, massive sample "AVR 3", linear plot

Figure 8.3.7: On-line gaseous emissions from AVR graphite, massive sample "AVR 3T", semi-log plot

Figure 8.3.8: On-line gaseous emissions from AVR graphite, massive sample "AVR 3T", linear plot

Figure 8.3.9: On-line gaseous emissions from AVR graphite, massive sample "AVR FT", linear plot

Figure 8.3.10: Rough interpretation of the mass loss dependence with treatment time

Figure 8.3.11: Cumulative release of water from different massive samples during thermal treatments in the Induction Oven, linear plot (indicative values)

Figure 8.3.12: Cumulative release of water from different massive samples during thermal treatments in the Induction Oven, semilog plot (indicative values)

Figure 8.3.13: Cumulative release of CO from different massive samples during thermal treatments in the Induction Oven, linear plot (indicative values)

Figure 8.3.14: Cumulative release of CO from different massive samples during thermal treatments in the Induction Oven, semilog plot (indicative values)

Figure 8.3.15: Cumulative release of CO_2 from different massive samples during thermal treatments in the Induction Oven, linear plot (indicative values)

Figure 8.3.16: Cumulative release of CO and $CO_2$from different massive samples during thermal treatments in the Induction Oven, linear plot (indicative values)

Figure 8.3.17: Cumulative release of CH_4 from different massive samples during thermal treatments in the Induction Oven, linear plot (indicative values)

Figure 8.3.18: Cumulative release of CH_4 from different massive samples during thermal treatments in the Induction Oven, semilog plot (indicative values)

Figure 8.3.19: Release of H_2 from different massive samples during thermal treatments in the Induction Oven, linear plot (indicative values)

Figure 8.3.20: Release of H_2 from different massive samples during thermal treatments in the Induction Oven, semilog plot (indicative values)

Figure 8.3.21: Release of SO_2 from different massive samples during thermal treatments in the Induction Oven, semilog plot (indicative values)

Figure 8.3.22: Release of SO_2 from different massive samples during thermal treatments in the Induction Oven, semilog plot (indicative values)

Figure 8.3.23: Comparison among the cumulative water emissions during successive treatments AVR3 and AVR3T of the same sample, semilogplot (indicative values)

Figure 8.3.24: Comparison among the cumulative water emissions during successive treatments AVR3 and AVR3T of the same sample, linear plot (indicative values)

Figure 8.3.25: Comparison among the cumulative CO emissions during successive treatments AVR3 and AVR3T of the same sample, semilog plot (indicative values)

Figure 8.3.26: Comparison among the cumulative CO emissions during successive treatments AVR3 and AVR3T of the same sample, linear plot (indicative values)

Figure 8.3.27: Comparison among the cumulative CO_2 emissions during successive treatments AVR3 and AVR3T of the same sample, semilog plot (indicative values)

Figure 8.3.28: Comparison among the cumulative CO_2 emissions during successive treatments AVR3 and AVR3T of the same sample, linear plot (indicative values)

Figure 8.3.29: Comparison among the cumulative H_2 emissions during successive treatments AVR3 and AVR3T of the same sample, linear plot (indicative values)

Figure 8.3.30: Comparison among the cumulative H_2 emissions during successive treatments AVR3 and AVR3T of the same sample, linear plot (indicative values)

Figure 8.3.31: Comparison among the cumulative CO and CO_2 emissions during several treatments, linear plot (indicative values)

Figure 8.3.32: View of the sample bottom: the reacted areas are the dark cycles, corresponding to the Al_2O_3 supports

Figure 8.4.1: On-line gaseous emissions from AVR graphite, sample "AVR Square 1", semilog plot, water signal is indicative

Figure 8.4.2: On-line gaseous emissions from AVR graphite, sample "Square 1", linear plot, water signal is indicative

Figure 8.4.3: Comparison among the relative cumulative emissions of CO and CO_2 from the TGA and the Induction oven (indicative values)

Figure 8.4.4: On-line gaseous emissions from AVR graphite, sample "CR 01", semilog plot

Figure 8.4.5: On-line gaseous emissions from AVR graphite, sample "CR 01", linear plot

Figure 8.4.6: On-line weight measurement of AVR graphite, sample "CR 01", TGA

Figure 8.4.7: On-line gaseous emissions from AVR graphite, sample "CR 02", semilogplot

Figure 8.4.8: On-line gaseous emissions from AVR graphite, sample "CR 02", linearplot

Figure 9.0: Schematic working principle of SIMS

Figure 9.1: AVR virgin square 1 baked

Figure 9.2: AVR virgin square 0 not baked

Figure 9.2.1: Comparison among normalized SIMS depth profiles of sulfur as S-, linear plot

Figure 9.2.2: Comparison among normalized SIMS depth profiles of sulfur as S-, semilog plot

Figure 9.2.3: Comparison among SIMS 3Ddepth profiles of sulfur (S-)

Figure 9.2.4: Comparison among normalized SIMS depth profiles of chlorine as Cl-, linear plot

Figure 9.2.5: Comparison among normalized SIMS depth profiles of chlorine as Cl-, semilog plot

Figure 9.2.6: Comparison among normalized SIMS depth profiles of chlorine as Cl-, linear plot

Figure 9.2.7: Comparison among normalized SIMS depth profiles of chlorine as Cl-, semilog plot

Figure 9.2.8: Comparison among SIMS 3D depth profiles of chlorine as Cl-, untreated (upper pictures) and treated (lower pictures)

Figure 9.2.9: Comparison among normalized SIMS depth profiles of nitrogen as CN-, linear plot

Figure 9.2.10: Comparison among normalized SIMS depth profiles of nitrogen as CN-, linear plot

Figure 9.2.11: Comparison among SIMS depth profiles of CN- of virgin and irradiated AVR graphite

Figure 9.2.12: Comparison among SIMS depth profiles of CN- and ^{13}C- of virgin AVR graphite

Figure 9.2.13: Gaussians distribution of the (nitrogen) whole available data from the two SIMS experiments

Figure 9.2.14: Gaussian distributions of the (nitrogen) results from the second SIMS experiment

Figure 9.2.15: Comparison among SIMS 3D depth profiles of nitrogen as CN-, untreated (upper pictures) and treated (lower pictures)

Figure 9.2.16: Comparison among normalized SIMS depth profiles of oxygen as O-, linear plot

Figure 9.2.17: Comparison among 3D SIMS depth profiles of oxygen as O-, untreated (upper pictures) and treated (lower pictures)

Figure 9.2.18: Comparison among normalized SIMS depth profiles of hydrogen as H-, linear plot

Figure 9.2.19: Comparison among 3D SIMS depth profiles of LiO-, untreated (upper pictures) and treated (lower pictures)

Figure 9.2.20: Comparison among normalized SIMS depth profiles of calcium as CaO-, linear plot

Figure 9.2.21: Comparison among normalized SIMS depth profiles of calcium as CaC-, linear plot

Figure 9.2.22: Comparison among 3D SIMS depth profiles of calcium as CaO-, after (left) and before (right) thermal treatment

Figure 9.2.23: Comparison among 3D SIMS depth profiles of calcium as CCa-

after (left) and before (right) thermal treatment

Figure 10.1.0: Schematic working principle of XPS

Figure 11.1.0: Scheme of the different signals produced in a SEM (left) and inner view of the SEM installed at FZJ (right)

Figure 11.2.1a: Overview of AVR graphite surface, untreated, magnification 300x

Figure 11.2.1b: Overview of AVR graphite surface, untreated, magnification 1200x

Figure 11.2.2: Overview of AVR graphite surface, treated in experiment "AVR square 1", mag. 300x

Figure 11.2.3: Overview of AVR graphite surface, treated in experiment "AVR square 1", mag. 1200x

Figure 11.2.4: Overview of AVR graphite surface, treated in experiment "AVR square 1",mag. 2400x

Figure 11.2.5: Exemplary EDXRF spectra performed with the sample "AVR square 1"

Figure 11.2.6: Overview of "AVR heat step 2" graphite surface, untreated, mag.6000x

Figure 11.2.7: Overview of AVR graphite surface, treated in experiment "AVR heat step 2", mag.6000x

Figure 11.2.8: Overview of AVR "heat step 2" graphite surface, untreated, mag.12000x

Figure 11.2.9: Overview of AVR graphite surface, treated in experiment "AVR heat step 2",mag. 12000x

Figure 11.2.10: Overview of DIDO graphite surface, untreated, mag. 24000x

Figure 11.2.11: Overview of DIDO graphite surface, treated at high temperature, mag. 26000x

Figure 11.3.1: Overview of Al2O3 shielding thermally treated alone under oxygen

Figure 11.3.2: Overview of Al_2O_3 shielding used in the induction oven, become in touch with the graphite sample

Figure 11.3.3: EDX spectra of the Al_2O_3 thermal shield, after being used in the induction oven

Figure 11.3.4: SEM image of the bottom part of the sample holder, not directly in contact with the graphite, after being used in the induction oven

Figure 11.3.5: SEM image of the bottom part of the Al_2O_3 sample holder, not directly in contact with the graphite, after being used in the induction oven

Figure 11.3.6: EDX spectra of the of the bottom part of the Al_2O_3sample holder, not directly in contact with the graphite, after being used in the induction oven. Focused on impurity of fig. 11.3.4

Figure A.1.1.1: Comparison between real temperature (red) and pyrometer's one (blue)

Figure A.1.2.1: Comparison among temperature signals before (cyan) and after (magenta) time-delay corrections, among gaseous measurements

Figure A.1.3.1: Alumina holder and thermal shield before the purification process

Figure A.1.3.2: Alumina holder and thermal shield after the purification process

Figure A.1.4.1: Representation of Trapezi formula to calculate the area between successive measurements

Figure A.1.5.1: Ionization produced by electron impact, as a function of the electron energy

Figure A1.6.1: Upper part of the original sample holder

Figure A1.6.2: Components of the lower part of the original sample holder

Figure A1.6.3: Thermodynamic simulation of the original sample holder

Figure A1.6.4: Thermodynamic simulation of the original sample holder, zoomed

Figure A1.6.5: Fluid dynamic simulation of the original sample holder

Figure A1.6.6: New sample holder with thermal shielding, overview

Figure A1.6.7: New sample holder with thermal shielding, section view

Figure A1.6.8.a-b: Comparison between the old (left) and new (right) sample holder, installed in the oven

Acknowledgments

I would like to thank sincerely all the staff of Forschungszentrum Juelich involved in the Carbowaste project, in particular Dr. Von Lensa, Dr. Vulpius and K. Baginski for their supervising, their support and the precious advices, M. Gungor for the support in the laboratory, M. Klinkemberg for the SEM analyses, Dr. Breuer for the SIMS analyses, A. Neumann for the XRD analyses, C. Fischer for the TGA analyses, K. Hinssen and B. Schögl for their help and advices for every experiment and all of them for their assistance. I would like to thank also all the IEK-6 staff that shared with me an unforgettable experience in the past year at the FZJ. Heartfelt thanks to my professors Mostacci and Dr. Scherer for their assistance during the last year. I want to thank also my beloved parents, that supported me both economically and emotionally. At last, I owe a special thank-you to my beloved Anna Maria, always by my side, always ready to give me advices and pushing me to learn german.